

STRENGTH AND BEHAVIOUR
OF
REINFORCED CONCRETE SPANDREL BEAMS

STRENGTH AND BEHAVIOUR
OF REINFORCED CONCRETE SPANDREL
BEAMS

A Thesis Submitted for the Degree of
DOCTOR OF PHILOSOPHY
of the
UNIVERSITY OF EDINBURGH
by
ANIS A. MOHAMAD ALI
B.Sc., M.Eng.

Department of Civil Engineering and Building Science

May 1983



To my family.

DECLARATION

This thesis is the result of research work for the degree of Doctor of Philosophy undertaken in the Department of Civil Engineering and Building Science, University of Edinburgh.

It is declared that all the work and results in this thesis have been carried out and achieved by the author himself and the thesis has been composed by him under the supervision of Dr. D.R. Fairbairn, unless otherwise stated.

Edinburgh, May 1983

Anis A. Mohamad Ali.

ACKNOWLEDGEMENTS

I wish to thank Dr. D.R. Fairbairn, for his supervision, counsel and encouragement throughout this investigation. Thanks are owed to Professor A.W. Hendry for the provision of facilities within the department.

Thanks are also due to the technical staff for their assistance in conducting the experimental investigation and to Miss Gillian Erskine for her careful typing of this thesis.

The financial assistance of University of Basrah, Iraq is gratefully acknowledged.

Encouragement and support of my wife is highly appreciated.

Thanks are due to Mrs. V. Thomson the librarian for tracing most of the references.

ABSTRACT

The strength and behaviour of a reinforced concrete floor-spandrel beam assembly was investigated experimentally and analytically. Tests were carried out on a total of eighteen specimens simulating a typical floor-spandrel beam assembly which are divided into five groups, to evaluate the ultimate flexural, torsional and deformation capacities under the effect of various parameters. The main parameters examined were - loading arrangement, the amounts of longitudinal and transverse steel in the spandrel beams and the concrete strength.

The stress block parameters were evaluated at the inelastic stage for a section under flexural compression. The approach adopted was extended to include the effect of the confinement provided by the lateral reinforcement in the section.

Analytical and empirical approaches were adopted to establish a procedure to evaluate the cracking and ultimate torsional strength of the reinforced concrete spandrel beams.

The influence of test variables on the deformation response of test specimens was discussed and evaluated. The experimental results are compared with the computed values obtained on the basis of a direct analysis of the sections.

The torsional stiffness was defined and evaluated for two stages, prior to cracking and after cracking as well as the corresponding angles of twist. Some other aspects of the problem were discussed and some suggestions have also been made for further research.

C O N T E N T S

	<u>Page</u>
Acknowledgements	i
Abstract	ii
Contents	iii
Notations	vii
CHAPTER 1 : INTRODUCTION	1
1.1 General Introduction	1
1.2 Review of Literature	2
1.2.1 Spandrel Beam	2
1.2.2 Floor Beam	8
1.2.3 Floor-Spandrel Beam Joint	11
1.2.4 Floor-Spandrel Beam Assembly	14
1.3 Scope of the Investigation	17
1.4 Outline of the Investigation	18
CHAPTER 2 : TEST PROGRAMME	21
2.1 Introduction	21
2.2 Design Analysis	21
2.2.1 Proportioning of Test Specimens	22
2.2.2 Design of Test Specimens	22
2.3 Material and Fabrication	27
2.4 Test Set-Up and Instrumentation	29
2.4.1 Simulation of Conditions at Cut-Off Points	29
2.4.2 Loading Arrangements	30
2.4.3 Measurements of Deflections and Rotations	31
2.4.4 Strain in the Steel Bars and Concrete	32
2.5 Test Procedure	33

	<u>Page</u>
CHAPTER 3 : GENERAL BEHAVIOUR AND MODES OF FAILURE	35
3.1 Introduction	35
3.2 General Behaviour of Specimens	35
3.2.1 Floor Beams (F.B.)	35
3.2.2 Spandrel Beams (S.B.)	37
3.3 Modes of Failure	40
3.3.1 Floor Beam Failure	41
3.3.2 Spandrel Beam Failure	42
3.4 The Observed Effect of the Variables on the Failure Mechanism of the Test Specimens	45
3.4.1 Load Application	45
3.4.2 Longitudinal Steel	46
3.4.3 Transverse Steel	47
3.4.4 Length of the Spandrel Beam	48
3.4.5 Concrete Strength	49
3.4.6 Joint Detailing	49
CHAPTER 4 : ANALYTICAL FORMULATION FOR FLEXURAL ULTIMATE STRENGTH	52
4.1 Introduction	52
4.2 Section Under Flexural Compression	52
4.2.1 Stress Strain Relationship for Concrete	53
4.2.2 Initial Modulus of Elasticity	61
4.2.3 Strain at Maximum Stress	63
4.2.4 Ultimate Strain at Failure	64
4.2.5 Comparison of Various Stress-Strain Relationships	65
4.3 Stress Block Parameters for a Section Under Flexure	66

	<u>Page</u>
4.4 Flexural Strength of Confined Section	71
4.5 Biaxial Stress-Strain Relationship for Concrete	76
4.6 Flexural Resistance Prior to Cracking	78
 CHAPTER 5 : ANALYTICAL FORMULATION FOR ULTIMATE TORSIONAL STRENGTH	 81
5.1 Torsional Strength Prior to Cracking	81
5.1.1 Strength of a Concrete Section in Pure Torsion	81
5.1.2 Strength of a Concrete Section Subjected to Bending and Torsion	91
5.1.3 Comparison with Test Results	93
5.2 Ultimate Torsional Strength of a Rectangular Beam with Longitudinal and Transverse Steel	95
5.2.1 Analysis	102
5.2.2 Deformation Conditions and Failure Criteria	108
5.2.3 Simplified Method for Predicting the Ultimate Torsional Strength	113
5.2.4 Strength in Shear Compression Mode	114
5.2.5 Discussion	119
 CHAPTER 6 : MOMENT CURVATURE CHARACTERISTICS OF FLEXURAL SECTION	 126
6.1 Introduction	126
6.2 Moment Curvature Relationship	126
6.2.1 Analysis at Cracking Stage	128
6.2.2 Analysis at Yield Stage	129
6.2.3 Analysis at Ultimate Stage	135
6.3 Moment Curvature Relationship for Confined Section	140
6.4 Experimental Evaluation of Curvature	144

	<u>Page</u>
CHAPTER 7 : TORQUE-TWIST CHARACTERISTICS	145
7.1 Torsional Stiffness	145
7.1.1 Precracking Stiffness	145
7.1.2 Postcracking Stiffness	150
7.1.3 Comparison and Discussion	156
7.2 Deformation Response	157
7.2.1 Rotational Behaviour	158
7.2.2 Ductility	162
CHAPTER 8 : DISCUSSION AND CONCLUSION	164
8.1 Introduction	164
8.2 Effect of Variables	164
8.2.1 Longitudinal Steel	164
8.2.2 Transverse Steel	166
8.2.3 Concrete Strength	167
8.2.4 The Joint	168
8.2.5 Behaviour at Service Load	168
8.3 Conclusions	169
8.4 Suggestion for Further Research	172
References	174
Appendix	183

NOTATIONS

ad	depth of compressive reinforcement from compressive face of the section = d'
A	concrete cross sectional area = $b.h$
A_c	effective area of concrete
A_{sc}	area of compression steel
A_{sl}	area of longitudinal steel provided to resist torsion
A_{ss}	area of top and bottom steel bars in tension only
A_{st}	area of tension reinforcement
A_s, A_v, A_w	area of one leg of a stirrup
b	width of beam section
b_l	smaller dimension of the closed stirrup
b_f, b_s	width of floor and spandrel beam
C	ratio of modulus of rupture to tensile strength of concrete = f_r/f_t
C, C_c	compressive force in concrete
C_u	total compressive force in concrete at ultimate
C_{cs}	compressive force in steel in compression

d	effective depth of beam section
$d_f \cdot d_s$	effective depth of floor and spandrel beam section
E_c	initial modulus of elasticity of concrete
E_o	second modulus of elasticity at strain, $\epsilon_o = f_o/\epsilon_o$
E_s	modulus of elasticity of steel
E_t	modulus of elasticity of concrete in uniaxial tension
f	stress at any fibre
f_{av}	average stress in compressive block
f_{av}''	average stress in compressive block for bound concrete
f_c'	cylinder strength of concrete
f_c''	cylinder strength of bound concrete analogous to f_c'
f_{cu}	characteristic cube strength of concrete
f_s	stress in tension steel
f_s'	stress in compression steel
f_{sy}	specified yield strength of main reinforcement
f_{sy}'	specified yield strength of compression reinforcement
f_{su}	stress in the steel at ultimate
f_t	tensile strength of concrete related to modulus of rupture tests

f_{wy}	yield stress of a stirrup
f_o	maximum compressive strength of concrete prism expressed by the cylinder strength = f_c'
$\bar{g}d$	distance from extreme compressive fibre to the resultant of the compressive force
G	shear modulus of elasticity
GK	torsional rigidity
h	overall depth beam section
h_1	larger dimension of closed stirrup
h_f, h_s	overall depth of floor and spandrel beam section
I	second moment of area
K	torsional constant
k	a coefficient (with appropriate subscripts)
L_f, L_s	length of floor and spandrel beam
L_p	spread of peak curvature or plastic length over which plastic rotation occurs with constant curvature
m	modular ratio E_s/E_c
M	applied moment
M_{cr}, M_y, M_u	cracking, yield and ultimate moment

M_u'	flexural resistance of concrete section prior to cracking
M_{b1}	pure flexural strength in positive bending
M_{b2}	pure flexural strength in lateral bending
M_{b3}	pure flexural strength in negative bending
P, Q	applied load
P	reinforcement ratio (with appropriate subscripts)
P_s	tensile reinforcement ratio = A_{st}/bd
P'	compressive reinforcing ratio = A_{sc}'/bd
P''	binding ratio defined in section 4.4
P_b	balanced tensile reinforcement ratio
P_t	total volume of reinforcement including longitudinal steel and stirrups expressed as a percent of concrete volume
P_w	web reinforcement ratio = $(0.85 A_w/bd) (b_1/s)$
q	mechanical percentage of reinforcement = $P_s \cdot f_{sy}/f'_c$
q''	parameter referring to the effectiveness of the transverse reinforcement
R	ratio E_c/E_0
R	ratio M_{b3}/M_{b1}

R	ratio of forces in bottom and top steel = $A_{st} f_s / A_{sc} 'f_s'$
r	ratio of reinforcement defined in equation 5.52
S	torsional stiffness (with appropriate subscripts)
s	spacing of stirrups
T	total tensile force in main reinforcement in a beam section
T	torque (with appropriate subscripts)
T_c, T_s	torque resisted by concrete and steel
T_{cr}, T_u	cracking and ultimate torque of reinforced concrete beam
T_e, T_p	elastic and plastic torque
T_{eq}	equivalent torque necessary to produce the same shearing stress as that produced by the flexural shear at the critical section
T_u'	ultimate torsional strength of unreinforced concrete section in pure torsion
T_{un}	ultimate torsional strength in bending and torsion
T_{us}	failure torque in shear compression mode
V	shear force
V_{cr}, V_u	cracking and ultimate shear force

v_c, v_s	shear stress resisted by concrete and steel
V_c, V_s	shear force resisted by concrete and steel
V_u'	shear resistance of the concrete where $T = 0$, $M \neq 0$
V_u	ultimate force transferred from the floor beam to spandrel beam
v_o	ultimate shear stress defined in section 5.2
u	ductility index = Δ_u/Δ_y
x_d	distance of neutral axis from compression face
$x_u d$	distance of neutral axis from compression face at ultimate
$\bar{y}d$	distance of centre of compressive block from neutral axis
Z	distance between section of maximum moment and an adjacent section of zero moment
α	ratio h/b
α	ratio f_{av}/f_c'
α	ratio of principal stress in orthogonal direction to principle stress in direction considered
α, β, λ	constants depend on ratio h/b

β, θ	cracking angles
ϵ	strain in concrete (with appropriate subscripts)
ϵ_0	strain in concrete at maximum stress f_0
ϵ_u	strain in concrete at ultimate failure
ϵ_s	strain in steel
ϵ_{sy}	strain in steel at yield
ϵ_{su}	strain in steel at ultimate
ϵ_t	strain in concrete in tension
θ	rotation of beam (with appropriate subscripts)
θ	angle of twist (with appropriate subscripts)
Δ	deflection (with appropriate subscripts)
μ	poisson's ratio
τ	torsional shearing stress
τ_0	ultimate torsional shearing stress defined in section 5.2
ψ	ratio M/T
δ	ratio V/T
Ω	slope of T_u vs $b_1 h_1 A_w f_{wy}/s$ curve

CHAPTER 1 : INTRODUCTION

1.1 General Introduction

1.2 Review of Literature

1.2.1 Spandrel Beam

1.2.2 Floor Beam

1.2.3 Floor-Spandrel Beam Joint

1.2.4 Floor-Spandrel Beam Assembly

1.3 Scope of the Investigation

1.4 Outline of the Investigation

1.1 General Introduction

The floor-spandrel beam assembly is an important and critical part of the overall structure. The strength and behaviour of the spandrel beam is often governed by the floor beam. Figure 2.1 shows how a floor-spandrel beam assembly forms part of the structural frame.

A knowledge of the internal forces and deformations of each individual member will enable a more efficient design. In the actual structure however the interaction between the floor and spandrel beam makes the situation more complicated and quite different. The behaviour and strength of floor and spandrel beams are very much correlated in determining the final mode of failure.

Three possible types of failure can be recognised, namely:

1. Floor beam failure.
2. Spandrel beam failure.
3. Joint failure.

The joint should be designed to be stronger than the members framing into it as well as exhibiting a certain degree of ductility. The joint region is subjected to a complex stress distribution due to the effect of multi-directional forces such as axial load, bending, torsion, and shear which are transferred from the beam members as a result of the applied design load.

Spandrel beams are often employed along the external edge of the structure to transfer load into the columns. In transferring load from the slab to the supporting edge column, the spandrel beams are subjected to a combination of torsion, bending moment and shear.

The nature of the failure of a reinforced concrete spandrel beam under combined stresses is also complex and the essential conditions resulting in such failures are not fully understood.

This is not the case with the floor beams since the behaviour of flexural members is well understood.

Figure 1.1 shows the most common types of spandrel beams which are used in practice.

The present study is limited to the strength and behaviour of a floor-spandrel beam assembly as shown in Figure 2.1 where the effect of the slab is not included.

1.2 Review of Literature

A considerable amount of information is available on the behaviour and strength of individual members under pure torsion or bending. However very little is available on the behaviour of the floor-spandrel beam assembly as a part of reinforced concrete frame.

Although it is not intended to review the large amount of information available regarding torsion or flexure, some more relevant papers will be reviewed and discussed if necessary.

1.2.1 Spandrel Beam

Until the late 1960's, the development of a recommended design process for reinforced concrete beams subjected to torsion in addition to bending and shear had been very slow. The American Concrete Institute "Building Code Requirements for Reinforced Concrete" [1], current during this period, stated that torsional stresses should be

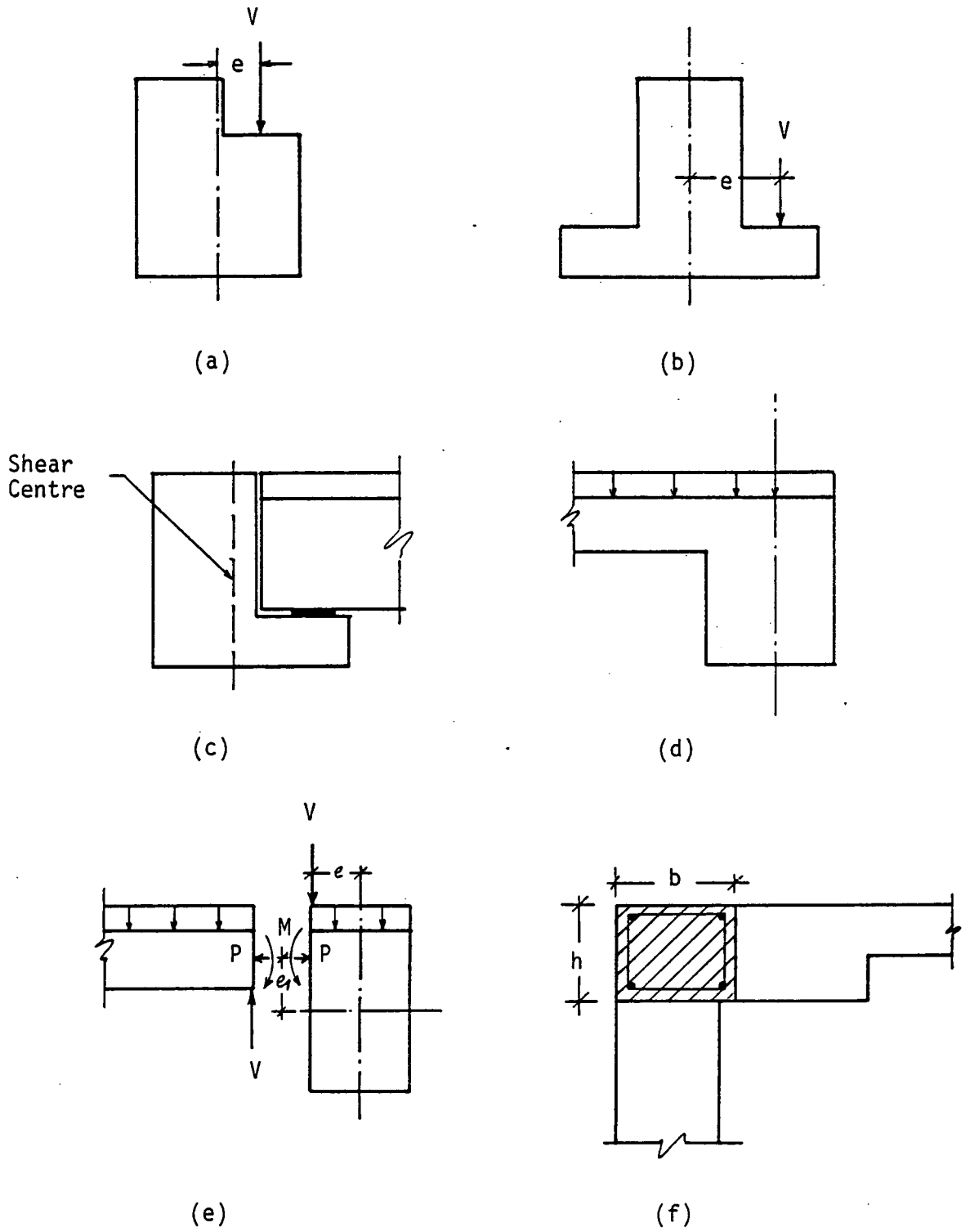


Figure 1.1 Spandrel Beams

considered in the design but gave no provision for allowable stresses nor did it include a procedure for the determination of torsional stresses in indeterminate structures. The first guide to designers became available in 1969 [2]. The ACI Committee 438, recommended that torsion should be neglected if the ultimate shear stress due to torsion was less than $0.11 \sqrt{f_c'}_c$. The justification was that this stress corresponded to about 25 percent of the pure torsion strength of a member without web reinforcement, and that it had been shown in a beam without stirrups that a torsional moment equal to 30 percent of the pure torsional strength caused no reduction in the flexural strength and only a 5-15 percent reduction in the shear strength. In a beam with stirrups, the stress of $0.11 \sqrt{f_c'}_c$ would correspond to a torsional moment less than 25 percent of the pure strength, which would again reduce the flexural strength by only a few percent, and the shear strength by less than 15 percent. For a section where τ_u was greater than $0.11 \sqrt{f_c'}_c$ the strength of the concrete was to be shared between the needs of torsion and shear, the contribution to each being given by τ_{ca} and v_{ca} respectively,

$$\text{where } \tau_{ca} = \frac{\tau_c}{\sqrt{1 + (3 v_u / \tau_u)^2}}$$

$$v_{ca} = \frac{v_c}{\sqrt{1 + (\tau_u / 3 v_u)^2}}$$

and v_u = ultimate flexural shear stress. Stirrups were to be designed as the sum of those required to resist the remaining torque and those necessary to resist the remaining shear, and were to be the closed type of stirrups since diagonal cracks due to torsion would appear on

all faces. In addition further longitudinal steel reinforcement equal in volume to that of the closed stirrups was to be distributed around the beam. No reference was made to stiffness requirements.

The recommendations of the ACI Committee 438 were incorporated into the ACI Code of 1971 [3] and the value of τ_u was given by $\tau_u = 3 T_u / b^2 h$. The recommendations could only be readily applied if the torsional moment (T) was known. Marshall [4] discussed the problem of torsion in concrete with reference to the British CP110-1972. Goode [5] compared the two codes of practice, ACI 318-71 and B.S. CP110-72.

When discussing the design of reinforced concrete beams to resist torsional loads, two different types of torsion must be distinguished:

- (a) Equilibrium torsion: A torsion necessary to maintain equilibrium in a structure.
- (b) Compatibility torsion: The twist required to maintain compatibility in a structure. A given load will produce a compatibility torsion in an indeterminate structure if the torsion can be eliminated by releasing redundant restraints. Statically determinate structures are subject only to equilibrium torsion. In this case the torsion moment must be fully designed for and sufficient reinforcement is to be provided as required by statics.

The ACI Code of 1971 and CP110-72 have adequate design rules based on a large amount of research which enabled engineers to suitably proportion the reinforcement for this case.

The spandrel beam being a part of a monolithic building frame is

subject to both types of torsion, i.e. the compatibility condition is required as well as statics in order to determine the torsional requirements. What is now required from the members is a twist and not torque since the magnitude of the torsion is dependent on the value of torsional stiffness of the member. For this case the solution given by the codes of practice is that the torsional moment in the spandrel beam is obtained by elastic analysis and the calculation of torsional stiffness is based on the uncracked section [6].

This philosophy was highly questionable as it was known after cracking that the torsional stiffness of reinforced concrete decreases significantly [7]. Using the code approach, an unrealistic high torsion would result and if under a given load the member did not crack, the torsional reinforcement would be virtually unstressed. On the other hand, after cracking the torsional stiffness would be reduced drastically, resulting in a redistribution of forces which would lead to a reduction in the torsion in the member. The required amount of torsional reinforcement would therefore be reduced.

There have been relatively few studies on post-cracking torsional stiffness. Lampert [8] derived an expression to calculate the post-cracking torsional rigidity of rectangular cross-sections. The torsional rigidity was given as a function of the percentage of steel. A new concept of post-cracking shear modulus was used and the theory is applicable to any arbitrary cross-section including rectangular and circular sections. Giving the post-cracking rigidity as a function of the amount of steel provided large values can be expected when using the conventional elastic method.

The concept of post-cracking shear modulus was employed by Hsu [9]

to derive a method of determining the post-cracking torsional rigidity of reinforced concrete sections. However the method is more efficient when it is applied to members under pure torsion. The effect of combined torsion, bending and shear must be studied before the method can be applied.

Ramakrishnan and Rangan [10] derived an equation to predict the torsional rigidity at any stage as a function of the initial torsional rigidity of the uncracked beam under pure torsion. Pandit and Warwaruk [11] introduced the effect of bending moment on the initial torsional stiffness of reinforced concrete rectangular beams under combined loading of torsion and bending. Secant and tangential stiffness can also be predicted in terms of the initial torsional stiffness based on the assumption that the relationship between torque and twist is a curve and not a straight line [12].

Pandit [13] considered the effect of combined torsion, bending and shear on the torsional stiffness, and suggested expressions by which the torsional stiffness can be predicted at the pre-cracking and post-cracking stage. The proposed expressions are given in terms of the initial torsional stiffness of uncracked beams under pure torsion. In fact those expressions are very simple to use and the corresponding angles of twist can be easily calculated. By definition the torsional stiffness is the torque required to produce a unit angle of twist per unit length.

Hsu [7] proposed an empirical equation to calculate the cracking angle of twist for reinforced concrete beams under pure torsion. The effect of reinforcement was taken into account and the cracking angle of twist was given as a function of the angle of twist at failure of

a plain concrete member. Hsu also proposed another empirical equation to calculate the angle of twist at ultimate torque of a reinforced concrete member. The proposed equation was given as a function of the total percentage of reinforcement, ratio of height to width of the cross-section and the width of the cross-section.

Information and methods are available to predict the torsional strength at cracking and at ultimate. A large number of beams have been tested under different conditions by various investigators.

Zia [14,15] reviewed the available torsion theories for concrete members and the problems associated with; most theories can be categorised as under:

1. Elastic theory.
2. Plastic theory.
3. Semi-plastic theory.

However Hsu [16] employed a new failure criteria to explain the experimental excessive strength unaccounted by the elastic theory. Hsu, using motion picture equipment, was able to observe the failure process of unreinforced concrete beams under pure torsion. Crack propagation and final mode of failure were observed very clearly.

Skew bending theory has been employed by many investigators to predict the ultimate torsional strength of reinforced concrete beams. This theory was first developed by Collins [17]. Rangan and Hall [18] further modified and applied the theory to determine the strength of rectangular prestressed concrete beams subjected to combined torsion, bending and shear.

Three modes of failure are defined by the Skew bending theory

depending on the location of the compression zone. In mode 1 the compression zone lies at the top of the beam cross-section. In modes 2 and 3 the compression zone lies at the side and the bottom of the cross-section respectively. The type of failure, whether it is mode 1, 2 or 3 is directly dependent on the ratio of bending moment to twisting moment or the ratio of shear force to twisting moment and the geometry of the section. For beams under pure torsion, modes 1, 2 and 3 are not defined by the torsion vector and the beams fail about an axis for which the bending strength is least.

Collins [17] also defined a fourth mode of failure to allow for the effect of shear forces. The experimental results of Mukherjee and Warwaruk [19] and Henry and Zia [20] were used by Rangan and Hall [18] to test the validity of the approach used by Collins to define the strength in a shear compression mode.

Rangan et al [21] subsequently modified the Skew bending theory and the modified theory can be used to predict the complete behaviour of reinforced concrete beams subjected to pure torsion as well as beams under combined torsion and bending. The theory can also predict the type of failure of over-reinforced or under-reinforced beams. The balanced steel ratio, below which the reinforcement will not yield can be determined with reasonable accuracy. Therefore steel quantities can be determined to ensure the ductility of beams under load. Rangan et al also proposed a simplified version of the theory for design purposes. The Skew bending theory is further discussed in Chapter 5.

1.2.2 Floor Beam

Prediction of the ultimate flexural strength requires the evaluation

of the stress block parameters for a section under flexure. For this purpose many idealized stress distributions have been proposed. A trapezoidal stress distribution was proposed by Jensen [22], a rectangular stress distribution was proposed by Whitney [23] and a universally accepted rectangular idealized stress distribution was proposed by Hognestad [24] who also reviewed many proposed idealizations.

An ultimate strength theory based on an equivalent rectangular stress distribution was further suggested by Mattock et al [25]. However a more exact design theory can be developed by employing the actual stress-strain relationship for the concrete in the analysis.

The behaviour and load-deformation characteristics of flexural members are well defined and established.

The load-deformation behaviour of reinforced concrete floor beams under pure flexure has a great influence on the ductility requirements. For this purpose analytical investigations have been carried out on the moment force deformation of reinforced concrete frames and the individual members, which are directly related to this study to provide information on ductility behaviour and hence on analytical approach.

Roy and Sozen [26] studied the effect of square ties on the load-deformation characteristics of members subjected to axial loads. Szulczynski and Sozen [27], Bresler and Gilbert [28] and Pfisher [29] also studied experimentally the effect of ties in reinforced concrete members subjected to different types of loading. The conclusion that can be drawn in this respect is that ties provide a significant improvement in the deformation capacities of concrete though the carrying capacity may not be increased.

The moment-curvature characteristics of reinforced concrete members

were studied by Mattock [30]. Tests were carried out to study the rotational capacity of hinging regions, and the equations derived were based on the concept of compatibility of strains and equilibrium of forces to evaluate the rotational capacity of the hinging regions of reinforced concrete members. The influence of the amount of steel and concrete on moment and rotation capacity was considered by these equations.

Corley [31], using his own test results and employing the same compatibility and equilibrium principles as Mattock, derived expressions to predict the inelastic rotation and spread of plasticity. Size of beam and the confinement of the concrete in compression were considered as the main parameters. It was found that the spread of inelastic deformations along the beam beyond a distance $d/2$ from the point of maximum moment is a function of the geometry of the member. Size of the beam was found to be of no significant influence on the magnitude of the maximum concrete compression strain. Corley's work may be considered as an extension to Mattock's work.

Experimental and analytical investigations were carried out by Chan [32] to study the ultimate strength and deformation of plastic hinges in reinforced concrete frames. He compared the assumption of plastic hinges concentrated at a point and the actual spread of plasticity and found that larger plastic rotations are developed in under-reinforced sections. The stress-strain capacity of concrete is increased by the lateral binding.

Pfrang, Siess and Sozen [33] presented an analytical study and a simplified method to relate axial load, moment and curvature for reinforced concrete cross-sections. In this method simplified

assumptions for the stress-strain relationships for concrete and reinforcement were adopted. The axial forces were calculated from the normal stresses and the curvature from the stress distribution.

Roy and Sozen [34] discussed the effect of rectangular ties on the load-deformation characteristics of concrete. Ductility was also studied as a factor governing the rotation capacity of the section and then moment distribution in a structure. Similarly the effect of the reinforcement on the ductility of the concrete was studied by Shah and Rangan [35].

An important contribution to the analysis of reinforced concrete members is provided by Cohn and Ghosh [36]. They presented an analytical analysis on the ductility of the reinforced concrete sections. Ductility and the factors which have a great influence on ductility for a wide range of geometrical, material and loading variables were well defined and investigated.

1.2.3 Floor-Spandrel Beam Joint

The resistance of the joint depends on the capacity of the concrete to withstand the torsion and shear forces, also on the yield strength of the tension and web reinforcement. In general the joint should satisfy the following requirements [37]:

1. The joint should be able to resist at least the failure moment of the floor beam. It is preferable for the flexural failure to occur outside the joint.
2. The joint should have sufficient ductility to allow redistribution of the forces in the frame as well as

avoiding any brittle failure.

3. The joint should be sufficiently reinforced to transmit the load from the floor beam to the spandrel beam and to resist any shear in addition to that taken by concrete.
4. The joint should provide sufficient anchorage for the flexural steel in the floor beam.
5. The joint should be simply reinforced and easy to fabricate. Extra stirrups should be avoided.

It is important to consider the joint properties in designing a joint in a frame. The joint should be over-designed so that plastic hinge formation will occur outside the joint with the joint having a specific yield capacity.

The following five different modes of joint failure have been reported in literature [38]:

1. The most common failure is by diagonal tension cracks in the joint itself when reinforcement can no longer resist the tensile stresses caused by the applied moment.
2. Splitting crack failure due to high tensile stresses occurring perpendicular to the direction of the reinforcing bar. This kind of failure is possible in all joints with inclined reinforcing bars.
3. Failure may primarily be caused by yielding of the reinforcement in the joint. A secondary diagonal tension crack occurs.

4. Anchorage failure occurs when the necessary interaction between concrete and reinforcement fails or when the reinforcement crushes the concrete by local crushing at bends in the reinforcement.
5. The fifth reported failure is due to crushing of the concrete in the joint.

The points mentioned above are related to concrete joints in general. The floor-spandrel beam joint has not yet been investigated thoroughly. However for design considerations, Collins and Lampert [39] designed the floor-spandrel beam joints using Leonhardt's recommendations by placing closely spaced stirrups to ensure full transmission of the reaction from the floor beam to the spandrel beam.

Hsu and Burton [40] tested specimens designed to fail in the joint by not providing shear or torsional reinforcement in the spandrel beam. In this way it was possible to see the failure surface at the joint. They concluded that in order to prevent joint failure it is necessary to provide stirrups within the failure surface. The total number of stirrups provided should carry the reaction from the floor beam.

From the investigations reviewed, the following points can be concluded:

1. Most of the investigations carried out to date on the strength and behaviour of the spandrel beam and floor beam have been based upon individual beams.
2. With reference to 1 above, some modifications are required

to make the analysis applicable to reinforced concrete frames.

3. The main factors affecting the strength and behaviour of reinforced concrete individual members and therefore frames, are: the applied load, concrete strength, amount of tension and lateral reinforcement, spacing of stirrups, confinement of the joint and the detailing of the reinforcement.

1.2.4 Floor-Spandrel Beam Assembly

Very little theoretical and experimental information is available regarding the behaviour and strength of a reinforced concrete floor-spandrel beam assembly.

Saether and Prachand [41] presented a theoretical approach to establish the interaction between the torsional deformation of the spandrel beam and the flexural bending in the adjoining slab and the supporting columns. The approach is based on the analysis of a simplified structure consisting of closely spaced independent beams monolithically framed into the spandrel beams which in turn are monolithically cast with the supporting columns. Charts were produced to determine the torsional moments in the spandrel beams.

Collins and Lampert [39] experimentally investigated the behaviour and strength of spandrel beams. The work carried out by Collins and Lampert can be divided into parts. Firstly they examined the design procedure of the ACI Code of 1971, in which they concluded that if gross stiffness values were used then an over estimation of reinforcement

would result. Also accurate values of torques could be predicted if cracked values were used, though this led to a cumbersome trial and error design method. Secondly they suggested that as the torsional stiffness of the beam decreases significantly after cracking, and because compatibility is involved in the analysis, zero torsional stiffness can be assumed. However minimum torsional steel in the form of stirrups should be provided to ensure ductility and limit crack propagation.

Onsongo and Collins [42], studied the behaviour of longitudinally restrained reinforced concrete beams under torsion. The results of two series of tests were reported. The first series of tests were carried out on beams tested in pure torsion while longitudinally restrained and the second series were carried out on a floor-spandrel beam assembly with the spandrel beams fully restrained longitudinally. Specimens of both series were designed by assuming zero torsional stiffness for the spandrel beam. They concluded that longitudinal restraint for beams subjected to torsion can be considered as being equivalent to additional longitudinal reinforcement. Using this concept the truss analogy formulae can be used to give a satisfactory prediction of the post-cracked stiffness values and ultimate torque. The restrained specimens behaved in a very similar way to the unrestrained specimens reported by Collins and Lampert [39] indicating that longitudinal restraint is a secondary effect.

The major contribution to the analysis of reinforced concrete spandrel beams was provided by Hsu and Burton [40]. A total of 10 specimens were tested under two types of loading, viz concentrated and uniformly distributed. Hsu and Burton also examined the ACI-1971

method and concluded as Collins and Lampert; that the ACI code method of design is safe but uneconomical. They examined the limit design concept and assigned a torsional moment to the spandrel beam by means of a specified shear stress due to torsion ($\tau_u = 0.33 \sqrt{f_c}$). It was assumed that the spandrel beam would resist twist infinitely under the assigned torque until flexural failure occurred at the midspan of the floor beam. They also examined the failure surface at the joint. Finally they concluded that using the limit design concept and assuming ($\tau_u = 0.33 \sqrt{f_c}$) would result in safe and economic design. This method was incorporated by the ACI 318-77 code later.

Phillai and Bhargaran [43] noted that the pre-cracking stiffness is not significantly affected by a variation in the reinforcement and they assumed that the post-cracking torsional stiffness is negligible in relation to the pre-cracking stiffness. From their experimental results they concluded that the method of limit analysis may be extended to the analysis of indeterminate structures having members subjected to torsion. The cracking torque was calculated on the basis of the plastic theory and reinforcement should be provided so that members have adequate twisting capacity. Finally they proposed that the maximum torque developed in the torsional member will be limited to the cracking torque, and from the strength considerations it is sufficient to provide reinforcement only to resist a maximum torque equal to the cracking torque.

Hsu and Hwang [44] employed limit design in designing spandrel beams. They examined the ACI Code recommendations (ACI 318-71 and ACI 318-77). Their alternate approach was originally suggested by Collins and Lampert in that the torsional stiffness of the spandrel

beams was assumed zero. However an expression was proposed to calculate the minimum torsional web reinforcement to be provided to ensure ductility.

As a result of the research work undertaken and subsequently published, the ACI Building Code was amended in 1977 [45] with a new design procedure based on the work of Hsu and Burton [40], that is, critical sections were required to resist a specified torsional shear stress of $\tau_u = 0.33 \sqrt{f'_c}$.

Mansur and Rangan [46] carried out a comparative study in which five methods of design were compared; viz the conventional elastic method, three limit design methods and the method put forward by Hsu and Hwang [44]. They concluded that the new ACI procedure [45] proposed by Hsu and Burton [40] using the concept of limit design is satisfactory and desirable as it provides an economic design. Also this method may be applied to statically indeterminate reinforced concrete structures in which a reduction in torsion can occur due to distribution of internal forces after cracking.

As a result of Mansur and Rangan's experimental investigation Hsu and Hwang put forward another expression to calculate the minimum amount of torsional steel in the form of longitudinal steel [47].

1.3 Scope of the Investigation

The main objective of this study is to carry out an experimental investigation on the strength and behaviour of a reinforced concrete floor-spandrel beam assembly.

The strength of the spandrel beam is to be evaluated under two types of loading arrangements using two different lengths. Also the

strength and behaviour of the assembly is to be evaluated using two different scales, viz full scale specimens and one-third scale models. The influence of the amount of tension and lateral reinforcement and spacing of the stirrups is to be studied. The effect of the test variables on the failure mechanism and deformation behaviour is also investigated.

It is also intended to establish an analytical approach for the evaluation of the ultimate flexural and torsional strength of the floor and spandrel beam respectively and to define a moment-curvature relationship for the floor beam and a torque-twist relationship for the spandrel beam.

The study is limited to the structural behaviour of a cast in-situ reinforced concrete floor-spandrel beam assembly under static loading. Reinforcement detailing is not considered as a variable and the effects of shrinkage, creep and temperature changes are excluded from this investigation.

1.4 Outline of the Investigation

Tests were carried out on a total of eighteen specimens which can be divided into two main series:

1. Eight full scale specimens.
2. Ten one-third scale models.

The main variables were:

1. Two types of loading arrangement:
 - (a) One concentrated load at midspan of the floor beam.

- (b) In addition to (a) another concentrated load at the joint.
2. Length of the spandrel beams:
 - (a) Length of the spandrel beam equal to the length of the floor beam.
 - (b) Length of the spandrel half the length of the floor beam.
 3. Two different beam depths were used. However in all cases the depth of the floor beam is equal to the depth of the spandrel beam.
 4. Longitudinal steel:
 - (a) Spandrel beams provided with longitudinal steel due to torsion.
 - (b) Spandrel beams provided with no longitudinal steel due to torsion.
 5. Type of concrete - three grades of concrete were used, viz 30, 35 and 40 N/mm².

The measuring technique was kept the same in each test. Further details of the test specimens are shown in Table 2.1.

The investigation consisted of both experimental and analytical phases. Detailed particulars of the design specimens, properties of material, testing procedure and instrumentation are reported in Chapter 2. Chapter 3 describes the general behaviour of the test specimens, failure mechanism, and possible modes of failure.

A generalized stress-strain relationship for concrete under

compression is analytically established and simplified on the basis of the test results in Chapter 4.

The simplified relationship is adopted as a representation of inelastic stress distribution and computations are made for the stress block parameters for a confined section on the basis of certain basic relationships suggested by other investigators. The simplified relationship is also adopted in the skew bending theory in Chapter 5.

In Chapter 5 an analytical approach is adopted to determine the torsional strength of reinforced concrete beams prior to cracking as well as the ultimate torsional strength. Chapter 6 and 7 describe the moment-curvature and torque-twist characteristics. Expressions are proposed to predict the cracking and ultimate angle of twist. Comparison is made between computed and measured results. The deformation response of the test specimens and then rotation capacity are also discussed.

The influence of various parameters on various aspects of the specimen's behaviour are discussed in Chapter 8. The general conclusion drawn from this study are also summarised in Chapter 8, and some suggestions are made for further research in the field.

CHAPTER 2 : TEST PROGRAMME

2.1 Introduction

2.2 Design Analysis

2.2.1 Proportioning of Test Specimens

2.2.2 Design of Test Specimens

2.3 Material and Fabrication

2.4 Test Set Up and Instrumentation

2.4.1 Simulation of Conditions at Cut-Off Points

2.4.2 Loading Arrangements

2.4.3 Measurements of Deflections and Rotations

2.4.4 Strain in the Steel Bars and Concrete

2.5 Test Procedure

2.1 Introduction

The main object of the test programme was to study the behaviour and the failure mechanism of a floor-spandrel-beam assembly under two different loading arrangements and different design parameters.

Indeed, it would be extremely difficult and costly to test three-dimensional frames in order to study the behaviour of the floor-spandrel beam system, shown in Figure 2.1. Alternatively therefore T-shaped in plan specimens are tested. In this chapter the design of the test specimens, material properties, a description of the test programme, test arrangement, instrumentation and the procedure are all discussed. The following parameters were kept constant in conducting the test programme: type of steel, the detailing of the reinforcement and the section properties in the full scale specimens.

2.2 Design Analysis

Figure 2.2 shows the bending moment diagram for the floor-spandrel-beam assembly when the floor beam is loaded by the load (P) at some point. At each of the points of the inflection (I.P.), the bending moment is equal to zero. It is possible then to use the T-shape (in plan) structure between the three points of inflection as a test specimen; provided that the existing conditions at the cut sections are simulated by appropriate hinges and restraints when the specimen is being tested.

The ends of the spandrel beam are torsionally fixed. This condition of total torsional fixity may not be an exact simulation of the framed structure but it is adopted for the purposes of testing to greatly simplify the analysis and the test procedure.

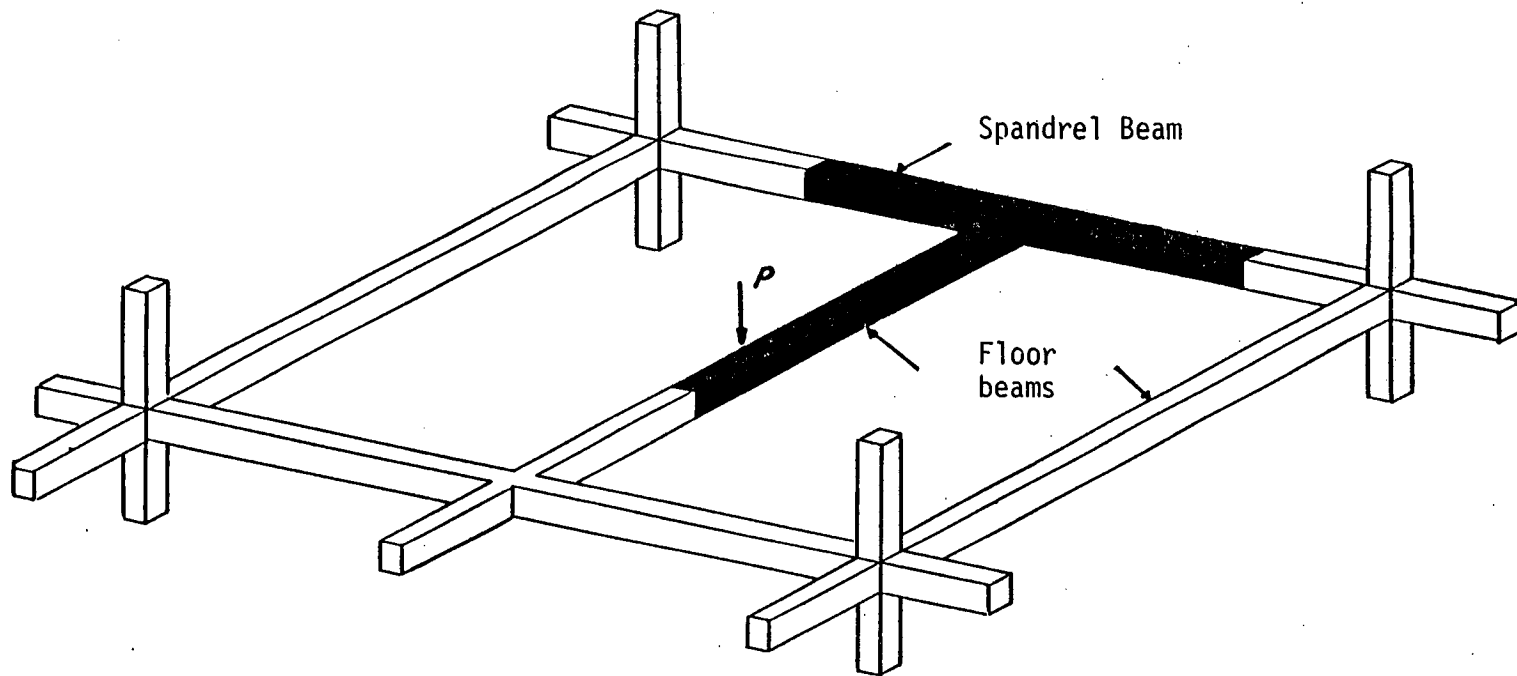
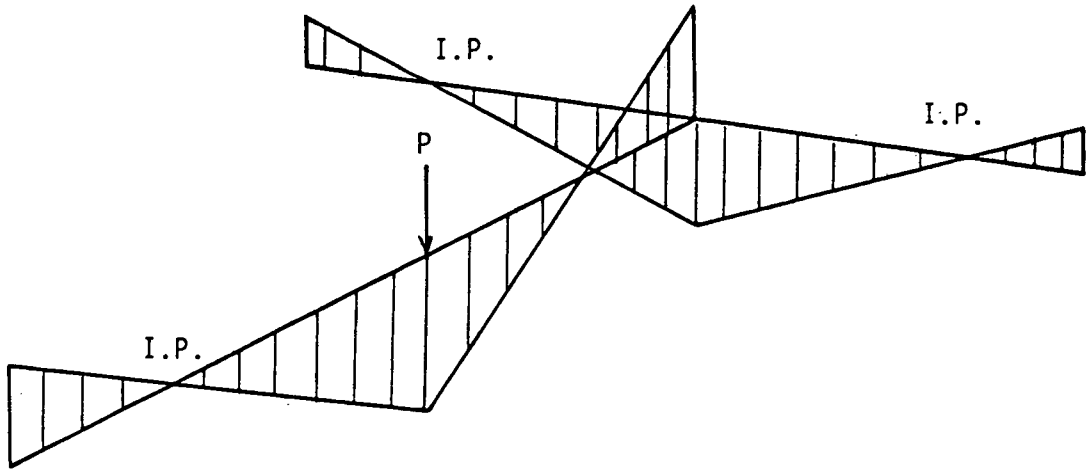


Figure 2.1 Spandrel Beam Within a Structural Frame



I.P. = Inflection Point

Figure 2.2 Bending Moment Diagram for the Floor-Spandrel Beam Assembly Under Load, P .

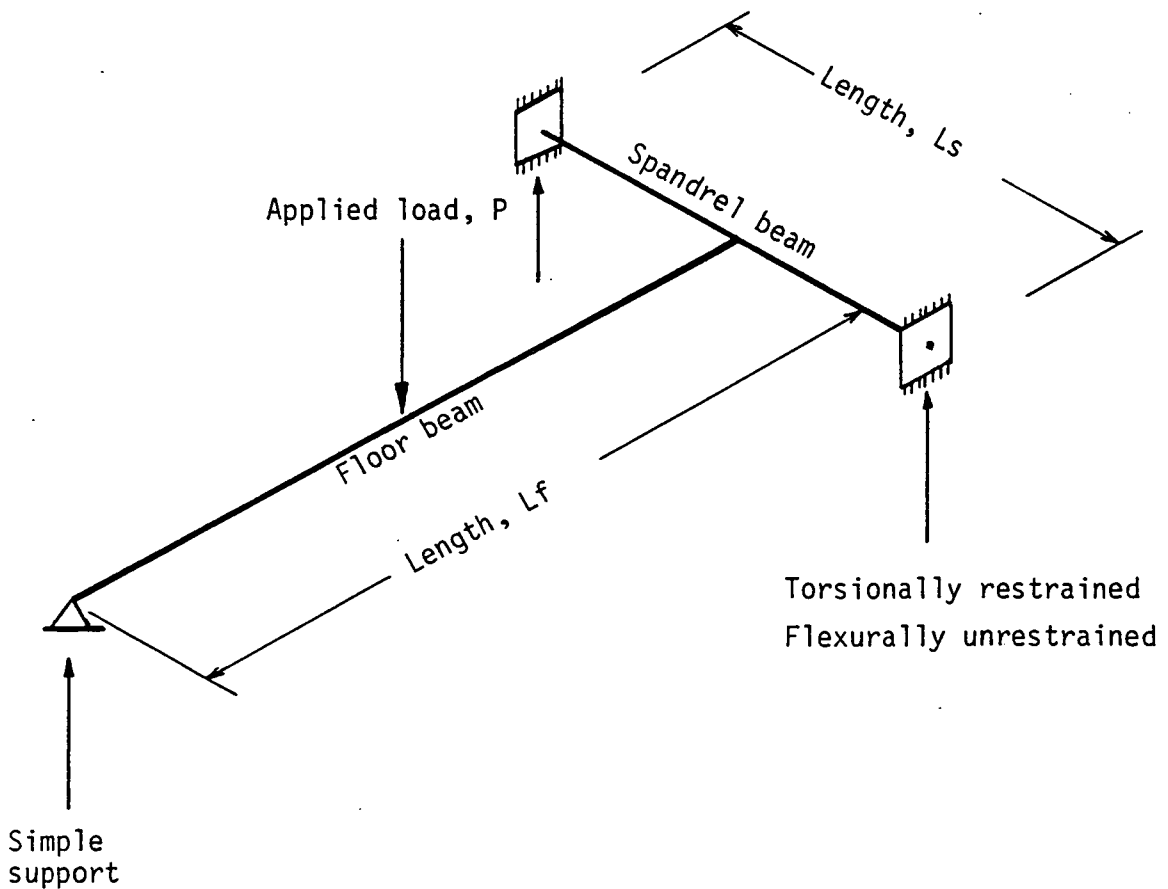


Figure 2.3 The Structural Frame Being Investigated

The structural model in Figure 2.3 is statically indeterminate to one degree. A restraining moment $(= 2 T_U)$ at the joint will be produced due to the floor beam loading and because of symmetry will be transmitted equally into the two parts of the spandrel beam. Therefore, the torsional moment in the spandrel beam is equal to (T_U) . If the value of the torsional moment (T_U) is known, the frame is thus reduced to a statically determinate one; bending moments and shear forces can then be found by statics as shown in Figure 2.4.

The design of the test specimens was carried out using different design methods under the provision of the ACI Code of 1971 and CP110-1972 where necessary.

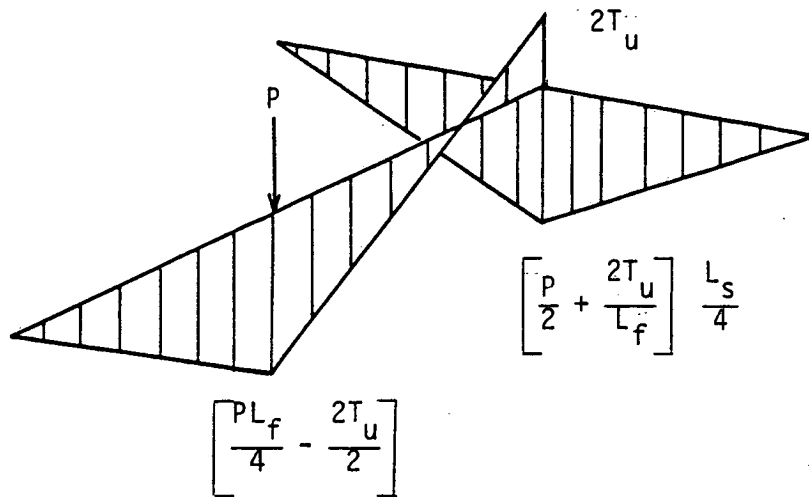
2.2.1 Proportioning of Test Specimens

The dimensions and details of the test specimens are shown in Table 2.1. The dimensions of the spandrel beams and floor beams which are commonly used in reinforced concrete building frames, provide guidance for selecting the dimensions of the test specimens. For this purpose a brief survey was carried out which revealed that the beam span in reinforced concrete multi-storey frames varies between 2.0 to 20 metres, in general. Slender beams were avoided in order not to further complicate the behaviour of the beam and its failure mechanism.

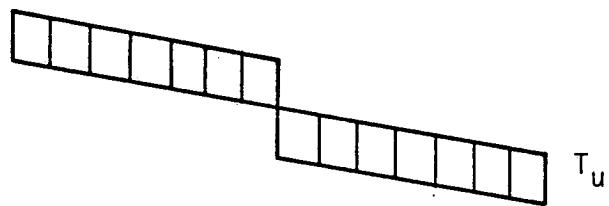
The actual length of the test specimens were increased by (150 mm) to provide an adequate support at each of the three cut-off points.

2.2.2 Design of the Test Specimens

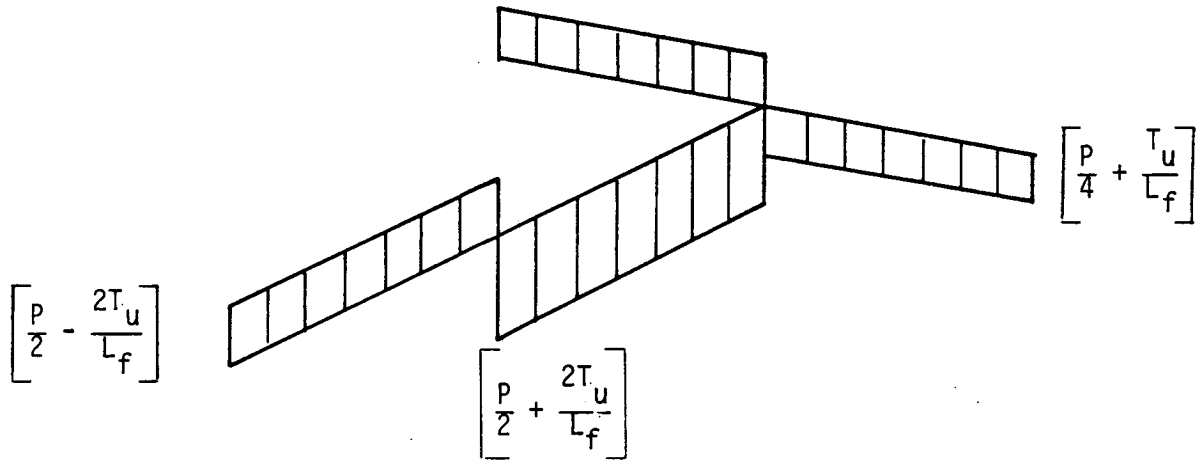
Collins and Lampert (1971) and Mansur and Rangan (1978), studied



(a) Bending Moment Diagram



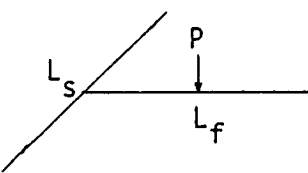
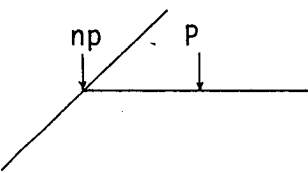
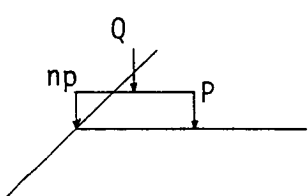
(b) Torsional Moment



(c) Shear Force Diagram

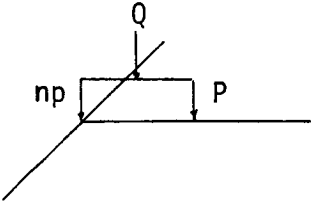
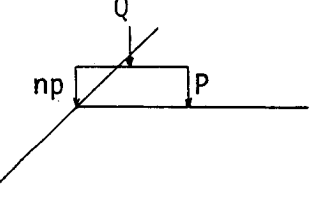
Figure 2.4 Distribution of Torsional and Flexural Moments

Table 2.1 Details of Test Specimens

Group No.	No. of Specimens	Details
GR1	4, B1 B2 B3 B4	 <p>* $L_f = L_s = 2700$ mm ** $h_f = h_s = 300$ mm $d_f = d_s = 280$ mm $b_f = b_s = 150$ mm</p> <ul style="list-style-type: none"> - No longitudinal steel for torsion was provided in the spandrel beams. - Floor beams were equally reinforced.
GR2	4, B5 B6 B7 B8	 <p>$n = 0.5$ $L_f = 2 L_s = 2700$ mm $h_f = h_s = 300$ mm $d_f = d_s = 280$ mm $b_f = b_s = 150$ mm</p> <ul style="list-style-type: none"> - No longitudinal steel due to torsion was provided in the spandrel beam. - Floor beams were equally reinforced, identical to GR1 - floor beams.
GR3	4, A1 A2 A3 A4	 <p>$Q = (1 + n) P$ $n = 0.5$ $L_f = L_s = 800$ mm $h_f = h_s = 200$ mm $d_f = d_s = 180$ mm $b_f = b_s = 75$ mm</p>

continued/...

Table 2.1 (continued)

Group No.	No. of Specimens	Details	
GR4	4 , B1 B2 B3 B4		$Q = (1 + n) P$ $n = 0.5$ $L_f = L_s = 800 \text{ mm}$ $h_f = h_s = 150 \text{ mm}$ $d_f = d_s = 130 \text{ mm}$ $b_f = b_s = 75 \text{ mm}$
GR5	2 , C1 C2		- Similar to GR3. - No stirrups were provided in the spandrel beams.

* L_f = length of the floor beam

L_s = length of the floor spandrel

h_f = overall depth of the section of the F.B.

h_s = overall depth of the section of the S.B.

b_f = breadth of F.B. section

b_s = breadth of S.B. section

d_f = depth of the F.B. section

d_s = depth of the S.B. section

**s and f are subscripts for the spandrel and floor beams respectively.

conclusively spandrel beams designed by a conventional elastic method using uncracked stiffness values. Although this method was not employed in the test programme, a brief discussion is relevant.

By equating the flexural end rotation of the floor beam to the torsional rotation at the centre of the spandrel beam, the restraining moment, ($2 T_u$) can be calculated using the following equation:

$$2 T_u = \frac{PL_f \left[3 - \frac{1}{2} \left(\frac{L_s}{L_f} \right)^3 \frac{EI_f}{EI_s} \right]}{\left[16 + \left(\frac{L_s}{L_f} \right)^3 \frac{EI_f}{EI_s} + 12 \left(\frac{L_s}{L_f} \right) \left(\frac{EI_f}{GK_s} \right) \right]} \quad (2.1)$$

where: EI = Flexural stiffness of the beam

L = Length of the beam

GK = Torsional stiffness of the beam

s , and f = are subscripts for the spandrel and floor beams respectively.

It can be seen from equation 2.1 that the restraining moment is extremely sensitive to changes in the stiffness of the spandrel beam. If it is infinitely stiff, i.e. $EI_s = \infty$, $GK_s = \infty$, the restraining moment is equal to $\frac{3 PL_f}{16}$ viz the value for a propped cantilever. If, on the other hand, the spandrel beam has zero torsional stiffness ($EI_s = 0$), the restraining moment is equal to zero. When the beams crack the torsional stiffness decreases drastically. Consequently the restraining moment and thus the torsional moment in the spandrel beam will decrease also. It is obvious then that the reinforcement provided to resist

torsion will be unnecessarily high. The conclusion that is therefore made is that the method produces an adequate design from an ultimate load point of view but it can be considered too uneconomical.

A more reasonable approach can be made by using the post-cracking stiffness values; the following expression is given by Lampert (1971):

$$GK_{cr} = \frac{E_s (b_o d_o)^2 A_h}{2 (b_o + d_o) s} (1 + m) \quad (2.2)$$

where: A_h = cross-sectional area of the hoop bar,

b_o, d_o = dimensions between the corner bars of the hoop,

s = spacing of the hoops,

m = ratio of the volume of longitudinal steel to the volume of hoop steel.

The stiffness calculated by equation 2.2 is a function of the transverse steel and accordingly larger values can be expected using the conventional elastic method. Also regions of low tensile stress remain virtually uncracked accounting for additional stiffness in the spandrel. Nevertheless the expression gives fairly good predictions.

Collins and Lampert (1971) showed that an accurate indication of torque could be obtained using cracked stiffness, but before the cracked stiffness can be calculated, the reinforcement must already be designed. In order to do that, the magnitude of the torque must be known. This demands the use of cracked stiffness properties, resulting in a lengthy trial and error design procedure.

The effect of the torsional moment on the web steel of the spandrel beam is significantly great and therefore must be fully design for. However the longitudinal steel in the spandrel beam due to torsion was

considered as a variable. For the spandrel beams of groups GR1 and GR2, no provision was made for longitudinal steel whereas beams of groups GR3 and GR4 longitudinal steel due to torsion was provided as shown in Table 2.2.

Spandrel beams in all groups were designed according to labelled methods A, B and C with assumed torsional stresses of $0.44 \sqrt{f_c'}$, $0.33 \sqrt{f_c'}$ and $0.25 \sqrt{f_c'}$ respectively. The fourth design method labelled D originally was that proposed by Collins and Lampert (1971) using zero torsional moment. They also proposed that the joint should be provided with closely spaced stirrups to provide 100% hang up of the load transferred from the floor beam. Hwang and Hsu (1977) used the same method ($T_u = 0$) and proposed an equation for the minimum torsional steel to be provided in the spandrel beam as web steel.

To design a spandrel beam using method (D) with zero torsional stiffness and torsional moment, none of the previously mentioned recommendations can be satisfied practically and the design is too conservative. Therefore it is suggested that the spandrel beams designed by method (D) should be provided with nominal stirrups based on the ACI 318-71 recommendations with maximum stirrup spacing not greater than $(d/2)$. The design torsional moments are shown in Table 2.3.

The spacing of the stirrups which was determined by the shear stresses due to shear and torsion expected in the beams and the shear resisted by the concrete, were computed according to ACI-ASCE committee 352 recommendations. The corresponding spacing of the stirrups given by CP110 are smaller. However the design torsional stresses are within the recommended values for ultimate torsion shear.

Table 2.2 Effect of Torsion on the Longitudinal Steel of the Spandrel Beam

Specimen	Required bottom long. steel when torsional moment is considered (mm ²)	Bottom long. steel when torsional moment is not considered	
		Required (mm ²)	Provided (mm ²)
GR1 - B1	526	339	339
- B2	448	353	364
- B3	411	324	339
- B4	252	252	287.5
GR2 - B5	500	319	339
- B6	451	317	339
- B7	420	315	339
- B8	310	310	339

Table 2.3 Details of the Design Methods

Design Method	Specimen	f_c' (N/mm ²)	Torsional Moment	Notes
A	GR1 - B1	30	$T_u = 0.44 \sqrt{f_c'} \frac{b^2 h}{3}$	Limit design
	GR2 - B5	40		
	GR3 - A1	30		
	GR4 - B1	40		
B	GR1 - B2	40	$T_u = 0.33 \sqrt{f_c'} \frac{b^2 h}{3}$	Limit design, ACI method, proposed by Hsu and Hwang (1974)
	GR2 - B6	30		
	GR3 - A2	40		
	GR4 - B2	40		
C	GR1 - B3	30	$T_u = 0.25 \sqrt{f_c'} \frac{b^2 h}{3}$	Limit design
	GR2 - B7	30		
	GR3 - A3	40		
	GR4 - B3	40		
D	GR1 - B4	35	$T_u = 0$	Zero torsional stiffness, using the uncracked stiffness values, originally proposed by Collins and Lampert (1971). Also proposed by Hwang and Hsu (1977) as limit design with provision of minimum torsional reinforcement.
	GR2 - B8	40		
	GR3 - A4	40		
	GR4 - B4	40		
	GR5 - C1	40		
	GR5 - C2	40		

The floor beams in the test specimens are designed by the same method using the following equation:

$$\frac{Mu}{bd^2 f_c'} = q (1 - 0.59 q)$$

$$\text{where } q = \left(\frac{A_{st}}{bd}\right) \left(\frac{f_{sy}}{f_c'}\right) = p_s \frac{f_{sy}}{f_c'}$$

According to the ACI 318-71 recommendations, beam reinforcement should not be less than $p_{s \min} = \frac{200}{f_{sy}}$ and not more than $0.75 p_b$, where p_b is the balanced reinforcement ratio for balanced conditions at ultimate failure and is given by:

$$p_b = \left(\frac{0.85 k_1 f_c'}{f_{sy}}\right) \left(\frac{87,000}{87,000 + f_{sy}}\right)$$

where f_c' = concrete cylinder strength (psi),

f_{sy} = yield stress of main steel (psi),

$k_1 = 0.85$, constant depending on f_c' ,

$$\therefore p_{s \max} = 0.05, \text{ and } p_{s \min} = 0.005$$

The limit of the beam reinforcement ratio given by CP110 is between 0.25% and 4%.

Since it is desirable to have a plastic hinge in the floor beam rather than in the joint, the negative steel provided was determined by the design negative moment ($2 T_u$) and was kept constant in each group of the test specimens.

The anchorage of the floor beam reinforcement into the spandrel beam was provided to satisfy the requirement of ACI 318-71 and CP110. Recommendations made by Somerville, Taylor and others are applicable for detailing the inside of the joint. The anchorage length required

by the bond stress limitations was provided by a horizontal extension of the floor beam bars into the spandrel beam through the joint, with a 90° bend of $(5 \times \phi)$ radius (ϕ is the diameter of the bar) and then vertical extension. Furthermore, the longitudinal bars of the floor beams were placed on top of the longitudinal bars of the spandrel beam at the joint.

In order to avoid local failure close to the clamping heads of the torsional arms due to stress concentration, a length of 300 mm each end of the spandrel beams was reinforced with additional stirrups.

This detailing of reinforcing bars was found to be quite efficient in transferring loads from the floor beam into the spandrel beam. Figure 2.5 shows the basic layout of the reinforcement in a test specimen. Tables 2.3 and 2.4 show full details of the design methods and a summary of the calculations for the design moments and shear forces respectively. The reinforcement and other details of the test specimens are given in Table 2.5.

2.3 Material and Fabrication

To obtain the required strength of the concrete within an acceptable time, trial mix designs were carried out having a constant cement : sand : gravel ratio with water/cement ratio varying between 0.6 to 0.7. The other factor which was considered was workability.

The same concrete mix was used in all test specimens using Ordinary Portland cement, 10 mm maximum size gravel and BS 882 grading zone 4 type sand. The concrete mix used and the concrete strength measured by testing cylinders on the day of testing, are shown in Table 2.6. Nine cylinders were cast from the same batch of concrete

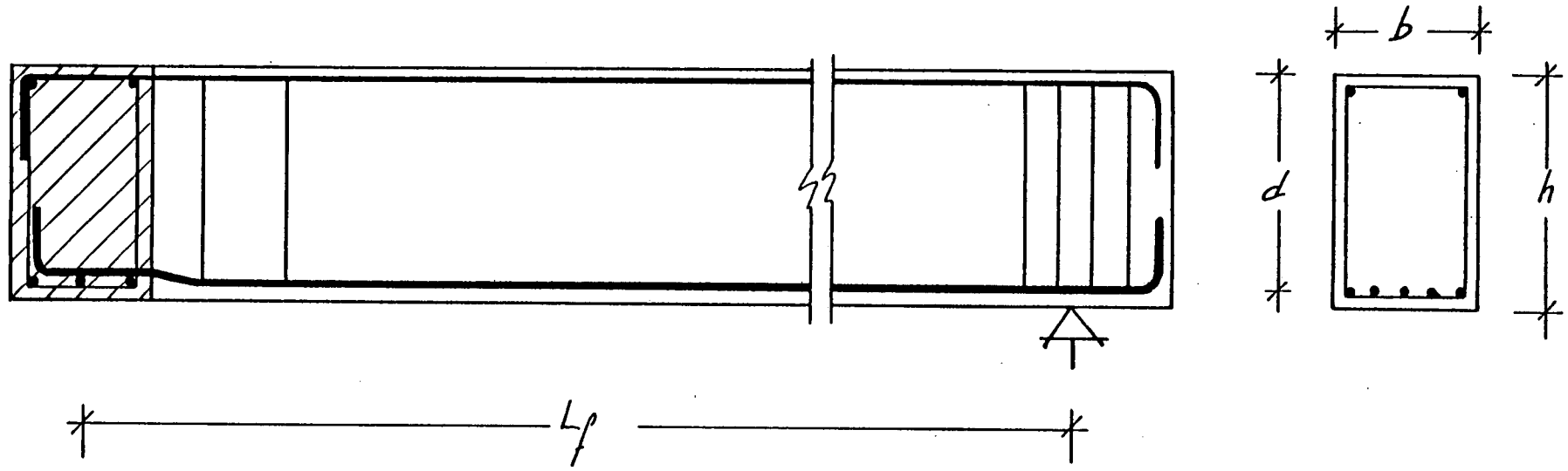


Figure 2.5 Typical Reinforcing Details (Spandrel Beam Shaded)

Table 2.4 Design Shears and Moments

Specimen	Design Method	Design Load (P _u) (kN)	Design Torque (T _u) (kN.m)	n	Design Shear (kN)		Design Moment (kN.m)		
					F. Beam	S. Beam	Floor Beam		Spandrel Beam
					$\frac{P_u}{2} + \frac{2 T_u}{L_f}$	$\frac{P_u}{4} (2n + 1) + \frac{T_u}{L_f}$	$+v_e = \left(\frac{P_u}{2} - \frac{2 T_u}{L_f}\right) \frac{L_f}{2}$	$-v_e = 2 T_u$	$\left[\frac{P_u}{4} (2n + 1) + \frac{T_u}{L_f}\right] \frac{L_s}{2}$
GR1-B1	A	70	5.42	0.0	39.0	19.5	41.8	10.84	26.32
-B2	B	70	4.7	0	38.48	19.24	42.55	9.4	25.97
-B3	C	70	3.1	0	37.3	18.6	44.15	6.2	25.1
-B4	D	70	0.0	0	35.0	17.5	47.25	0.0	23.62
GR2-B5	A	70	5.42	0.5	39.0	37.0	41.8	10.84	25.0
-B6	B	70	4.07	0.5	38.0	36.5	43.18	8.14	24.6
-B7	C	70	3.1	0.5	37.28	36.14	44.17	6.2	24.4
-B8	D	70	0.0	0.5	35.0	35.0	47.25	0.0	23.6
GR3-A1	A	45	0.904	0.5	24.76	23.63	8.10	1.81	9.45
-A2	B	45	0.783	0.5	24.46	23.48	8.22	1.57	9.39
-A3	C	45	0.595	0.5	23.99	23.24	8.52	1.19	9.30
-A4	D	45	0	0.5	22.50	22.50	9.0	0.00	9.0
GR4-B1	A	25	0.783	0.5	14.46	13.48	4.22	1.57	5.39
-B2	B	25	0.587	0.5	13.97	13.23	4.41	1.17	5.29
-B3	C	25	0.445	0.5	13.61	13.06	4.56	0.89	5.22
-B4	D	25	0.0	0.5	12.5	12.5	5.0	0.0	5.0
GR5-C1	D	25	0.0	0.5	12.5	12.5	5.0	0.0	5.0
-C2	D	25	0.0	0.5	12.5	12.5	5.0	0.0	5.0

Table 2.5 Reinforcing Details of Test Specimens

Specimen	f_c' N/mm ²	FLOOR BEAM					SPANDREL BEAM				
		Pos. Long. Steel	ρ_s	Neg. Long. Steel	ρ_s	Transverse Steel	Pos. Long. Steel	ρ_s	Top Long. Steel	ρ_s	Transverse Steel
		No. and Dia. of Bars		No. and Dia. of Bars		Dia. and Spacing of Stirrups	No. and Dia. of Bars		No. and Dia. of Bars		Dia. and Spacing of Stirrups
GR1-B1	30	5; 12 mm	1.345	2; 8 mm	0.24	6.3 mm; 140 mm	3; 12 mm	0.807	2; 8 mm	0.24	6.3 mm; 80 mm
-B2	40	5; 12 mm	1.345	2; 8 mm	0.24	6.3 mm; 140 mm	4; 10 mm + 1; 8 mm	0.866	2; 8 mm	0.24	6.3 mm; 100 mm
-B3	30	5; 12 mm	1.345	2; 8 mm	0.24	6.3 mm; 140 mm	3; 12 mm	0.807	2; 8 mm	0.24	4 mm; 100 mm
-B4	35	5; 12 mm	1.345	2; 8 mm	0.24	6.3 mm; 140 mm	3; 10 mm + 1; 8 mm	0.68	2; 8 mm	0.24	4 mm; 120 mm
GR2-B5	30	5; 12 mm	1.345	2; 8 mm	0.24	6.3 mm; 140 mm	3; 12 mm	0.807	2; 8 mm	0.24	6.3 mm; 75 mm
-B6	30	5; 12 mm	1.345	2; 8 mm	0.24	6.3 mm; 140 mm	3; 12 mm	0.807	2; 8 mm	0.24	6.3 mm; 90 mm
-B7	30	5; 12 mm	1.345	2; 8 mm	0.24	6.3 mm; 140 mm	3; 12 mm	0.807	2; 8 mm	0.24	6.3 mm; 115 mm
-B8	30	5; 12 mm	1.345	2; 8 mm	0.24	6.3 mm; 140 mm	3; 12 mm	0.807	2; 8 mm	0.24	6.3 mm; 140 mm
GR3-A1	30	2; 10 mm	1.2	2; 6 mm	0.43	5 mm; 75 mm	2; 12 mm	1.72	2; 6 mm	0.43	5 mm; 45 mm
-A2	40	2; 10 mm	1.2	2; 6 mm	0.43	5 mm; 75 mm	2; 12 mm	1.72	2; 6 mm	0.43	5 mm; 55 mm
-A3	40	2; 10 mm	1.2	2; 6 mm	0.43	5 mm; 75 mm	2; 12 mm	1.72	2; 6 mm	0.43	5 mm; 65 mm
-A4	40	2; 10 mm	1.2	2; 6 mm	0.43	5 mm; 75 mm	2; 12 mm	1.72	2; 6 mm	0.43	5 mm; 75 mm
GR4-B1	40	2; 8 mm	1.1	2; 6 mm	0.43	3 mm; 70 mm	2; 10 mm	1.2	2; 6 mm	0.43	3 mm; 30 mm
-B2	40	2; 8 mm	1.1	2; 6 mm	0.43	3 mm; 75 mm	2; 10 mm	1.2	2; 6 mm	0.43	3 mm; 40 mm
-B3	40	2; 8 mm	1.1	2; 6 mm	0.43	3 mm; 75 mm	2; 10 mm	1.2	2; 6 mm	0.43	3 mm; 50 mm
-B4	40	2; 10 mm	1.2	2; 6 mm	0.43	3 mm; 75 mm	2; 10 mm	1.2	2; 6 mm	0.43	3 mm; 75 mm
GR5-C1	40	2; 10 mm	1.2	2; 6 mm	0.43	3 mm; 75 mm	2; 10 mm	1.2	2; 6 mm	0.43	No shear or torsional
-C2	40	2; 10 mm	1.2	2; 6 mm	0.43	3 mm; 75 mm	2; 10 mm	1.2	2; 6 mm	0.43	Stirrups provided

Table 2.6 Concrete Properties

Specimen	Conc. mix	W/C Ratio	Age at testing (days)	Mean cylinder strength (N/mm ²)	Average modulus of elasticity* (kN/mm ²)
GR1 - B1	1 : 2 : 3	0.625	14	30.0	30.0
- B2	"	"	18	40.0	35.0
- B3	"	"	14	30.0	30.0
- B4	"	"	16	35.0	32.0
GR2 - B5	"	0.625	14	30.0	30.0
- B6	"	"	14	30.1	"
- B7	"	"	"	30.1	"
- B8	"	"	"	30.2	"
GR3 - A1	"	0.625	14	30.0	30.0
- A2	"	"	20	40.0	35.0
- A3	"	"	"	40.5	35.0
- A4	"	"	"	41.0	"
GR4 - B1	"	"	21	39.5	"
- B2	"	"	"	41.5	35.2
- B3	"	"	"	41.0	"
- B4	"	"	"	40.0	35.0
GR5 - C1	"	"	18	40.2	35.0
- C2	"	"	"	40.1	35.0

* Measured at (0.5×10^{-3}) strain.

as that prepared for casting a specimen. Six cylinders were stripped the following day and kept beside the specimen covered with a polythene sheet. They were tested on the same day as the testing of the specimen. The other three cylinders were cured in water and tested at 28 days.

Plain, mild steel bars of different sizes were used for the main bars and stirrups in the test programme. In order to establish the main properties of the steel bars, tests were carried out in accordance with B.S. 18 and B.S. 4449. The measured yield stresses and other properties of the reinforcing bars used in the test are given in Table 2.7. A typical stress-strain curve of a reinforcing bar is shown in Figure 2.6. The yield strain, strain hardening and the ultimate stage are denoted on the curve by letters, Y, Sh and U respectively.

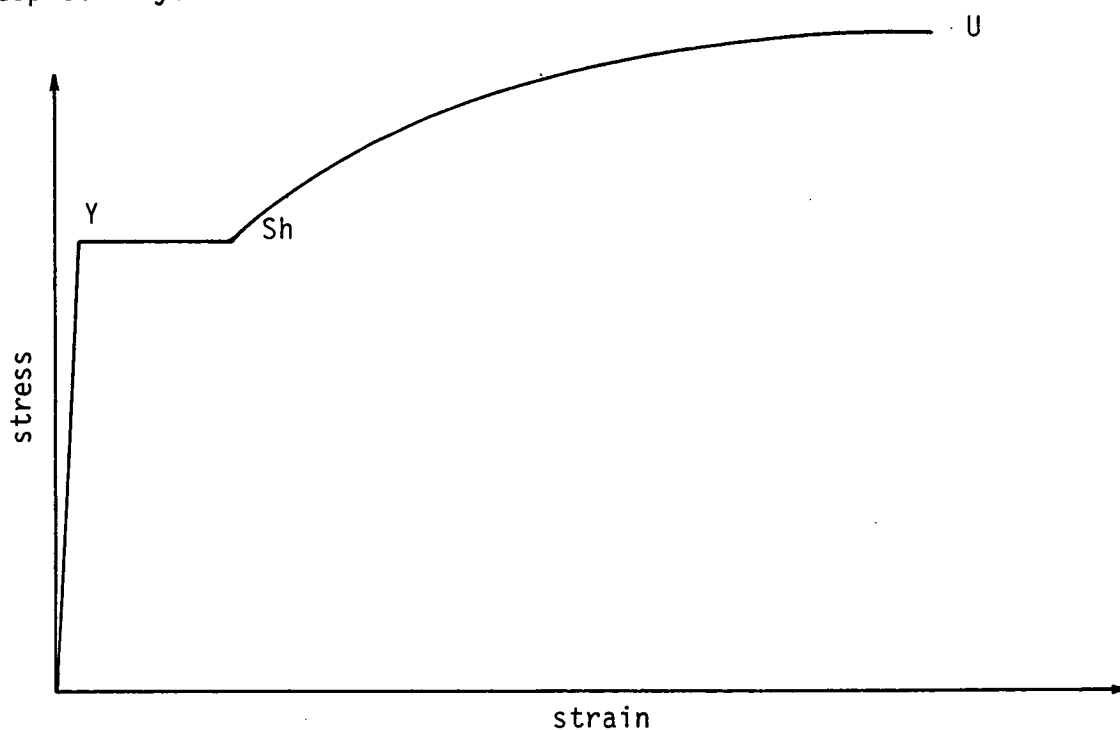


Figure 2.6 Typical Stress-Strain Curve of a Reinforcing Bar

Table 2.7(a) Steel Properties (GR1 and GR2)

Nominal Bar Dia. (mm)	Actual Bar Dia. (mm)	Actual Cross-sectional area (mm ²)	Yield Stress f_{sy} (N/mm ²)	Strain at yield $\epsilon_{sy} \times 10^{-3}$ (mm/mm)	Ultimate Strength U_2 (N/mm ²)	Modulus of Elasticity $E_s \times 10^5$ (N/mm ²)
4	4.8	18.08	332	1.65	664	2.01
6	5.945	27.74	324	1.62	495	2.00
6.3	6.03	28.54	322	1.6	578	2.01
10	10.02	78.81	305	1.5	498	2.03
12	11.89	110.97	284	1.4	451	2.03

(b) Steel Properties (GR3, GR4 and GR5)

3	3.18	7.94	530	2.6	601	2.03
5	4.7	17.35	370	1.85	604	2.0
6	5.92	27.53	563	2.8	627	2.01
8	8.20	52.81	349	1.74	595	2.00
10	9.95	77.76	346	1.73	600	2.0
12	11.99	112.91	405	2.00	650	2.02

Results are based on an average of 3 specimens of each bar.

The reinforcing cages of the floor and spandrel beams, were placed into the mould on top of steel chairs provided for the concrete cover. The heavy steel mould used was coated with lubricating oil prior to any casting operation. The entire specimen was cast in one continuous operation allowing only a short time for the concrete to consolidate and using a vibrator. After casting, the specimen was covered with a polythene sheet. The following day, the sides of the mould were removed and again covered with the polythene sheet. The specimen was finally removed on the day of testing and placed in the rig.

2.4 Test Set Up and Instrumentation

2.4.1 Simulation of Conditions at Cut-Off Points

It was intended that the cut-off points for the beams should coincide with the points of inflection (I.P.). This can be simulated using a hinge with ball bearing and when the test specimen is loaded, the hinges allow the ends of the spandrel beam to bend or to bend and twist. Under each of the ball bearings, a compression load cell is located to measure the reactions at the support at all loading stages.

The ends of the spandrel beam in the test specimen are torsionally fixed, although this is not exactly the same situation in a framed structure. Nevertheless this enables the test procedure to be made easier and the analysis to be considerably simplified. The torsional fixity of the spandrel beam is achieved by fixing an arm to the ends of the beam by means of plates and bolts as shown in Figure 2.7 and Plate 2.1. A load was applied to this torsion arm using a hydraulic

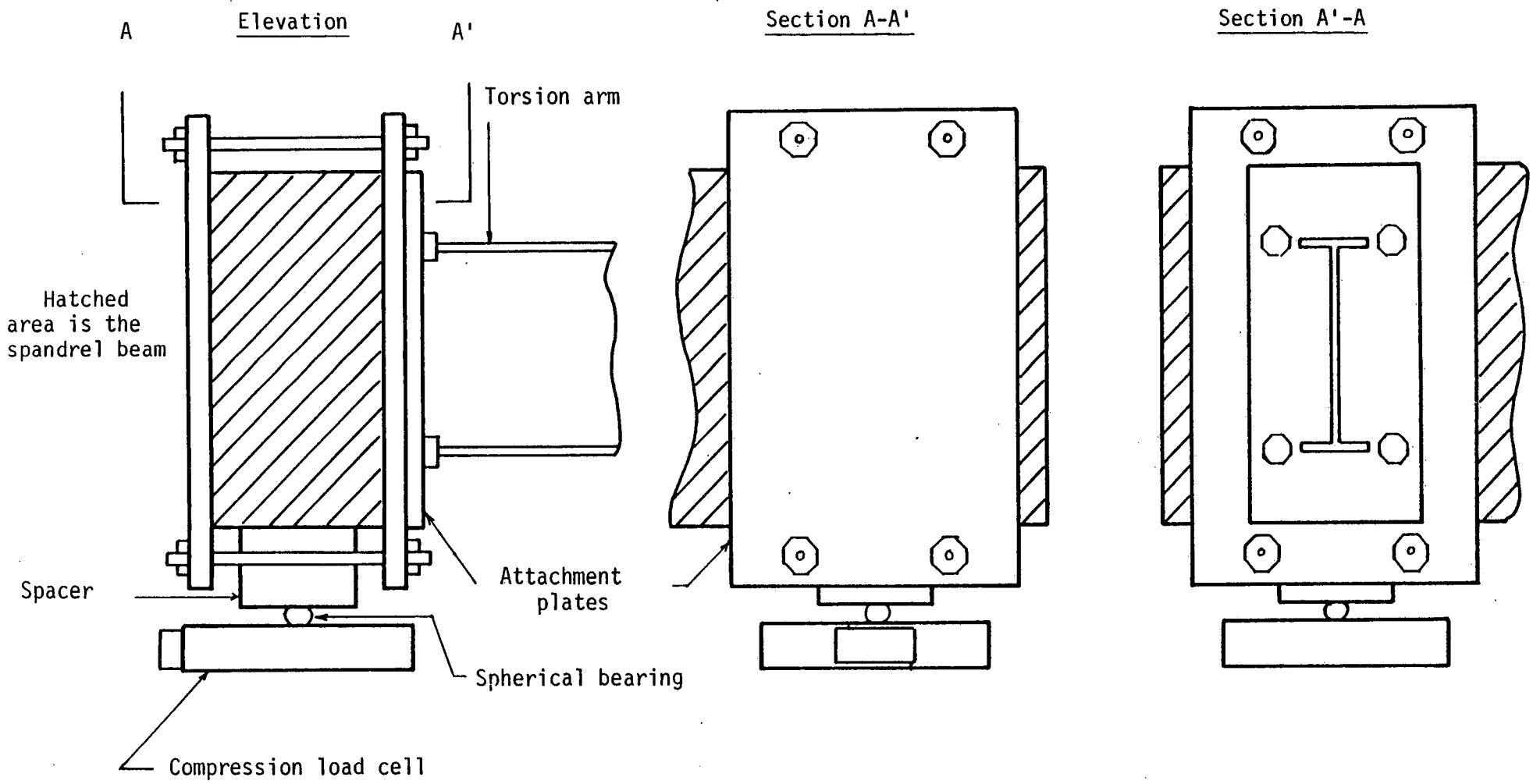


Figure 2.7 Attachment of Torsion Arm to Spandrel Beam
(not to scale)

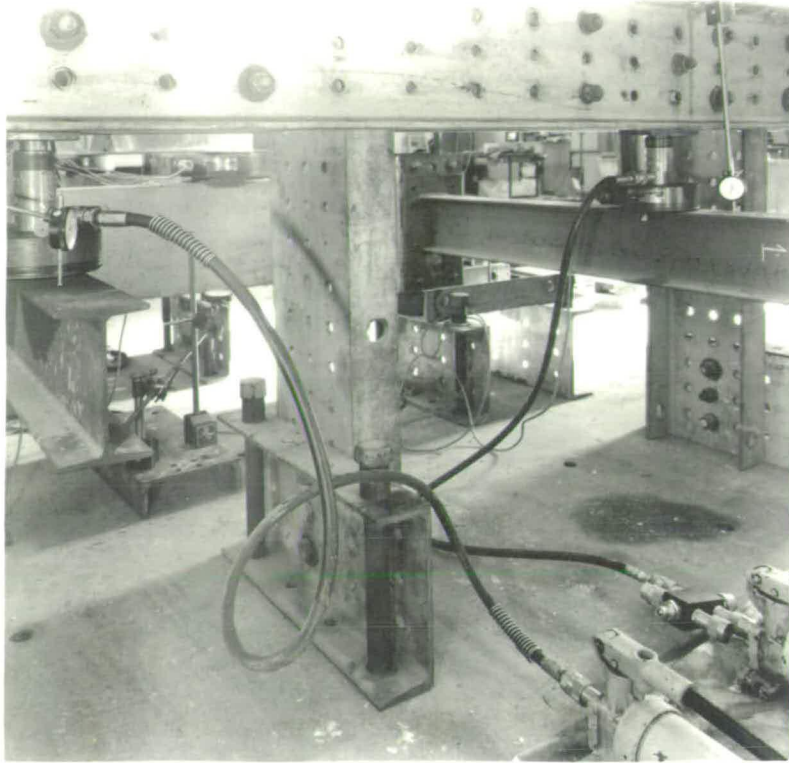


Plate 2.1 Attachment of the Torsional Arms

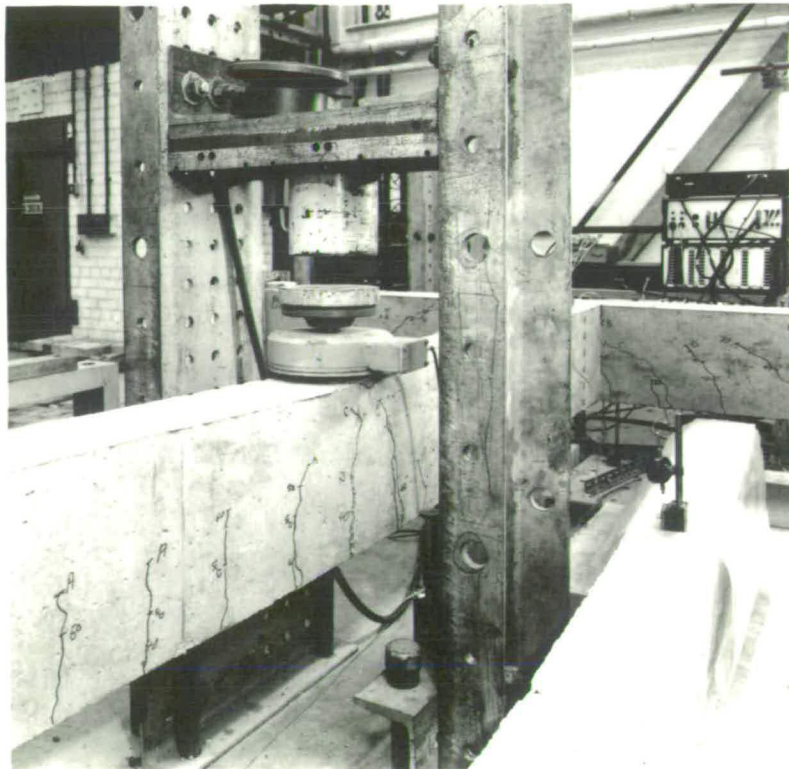


Plate 2.2 Method of Load Application

jack which was operated manually in order to keep the arm horizontal throughout the duration of the test. Compression load cells were placed between the jack and the arm to measure the load required to maintain the arm horizontal. The product of this load and the length of the arm is equal to the torsional moment in the spandrel beam. In the specimens of group GR1, a second arm was attached to each end of the spandrel beam with a dial gauge placed underneath the extreme end. Due to the applied load the ends of the spandrel beams tend to rotate torsionally; this rotation can be detected on the dial gauge. By operating the hydraulic jacks the reading on the dial gauges can be maintained constant, which means that the arm is being held in its horizontal position. For specimens in the other groups, the dial gauges were placed directly onto the torsional arms. As an additional check, a sensitive spirit level was located on each of the torsional arms.

2.4.2 Loading Arrangements

In order to simplify the test set up the effect of the floor slab was not considered and so the test specimens were subjected to concentrated loads only, even though distributed loads may not present any difficulty in the analysis.

In group GR1, the load was applied at the midspan of the floor beam using a manually operated hydraulic jack. The jack was attached to a steel cross beam bolted to two steel channels which were bolted to the floor. The method of applying the load can be seen in Plate 2.2. A load cell was placed on the beam at midspan directly beneath the jack to measure the applied load.

In the other groups two concentrated loads were applied, one at

midspan of the floor beam, the other at the joint. For this purpose a distributor beam with rollers was used. The load was applied at a distance of $2/3$ of the distributor beam length from the joint and $1/3$ from the floor beam centre so that the load transferred to the joint was half the load at the floor beam midspan. Two load cells were placed under the distributor beam at the centre of the floor beam and another one at the joint as shown in Plate 2.3(a),(b) to measure the applied load at any stage. For the specimens in groups GR3, GR4 and GR5 one load cell was used, placed on the distributor beam under the jack due to inadequate space.

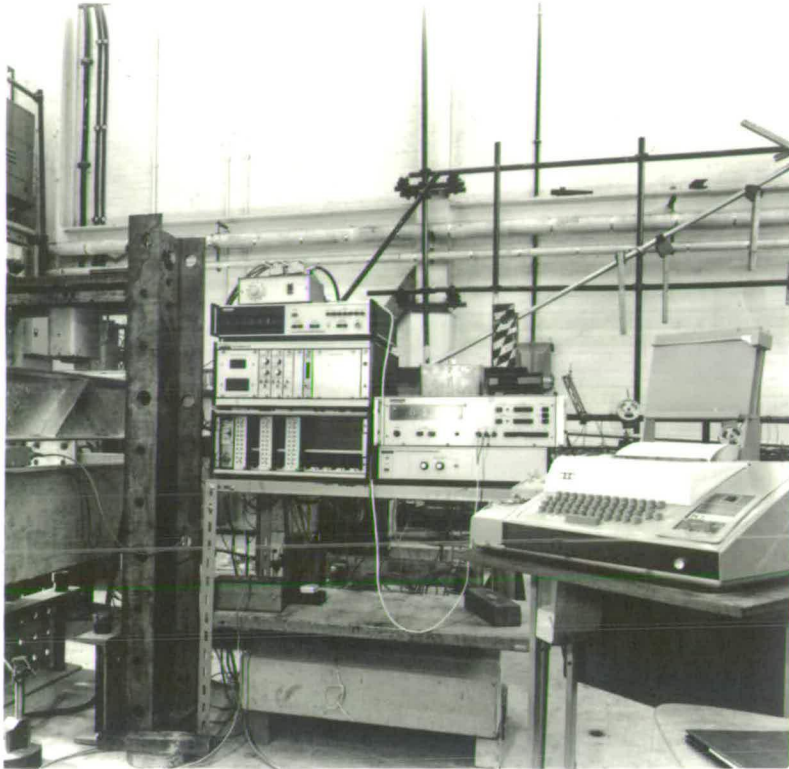
All the load cells were connected to a digital voltmeter and data logger so that a complete record of the applied loads and reactions was available at each load stage.

2.4.3 Measurements of Deflections and Rotations

The deflections at the midspan of both the floor beam and the spandrel beam were measured using dial gauges.

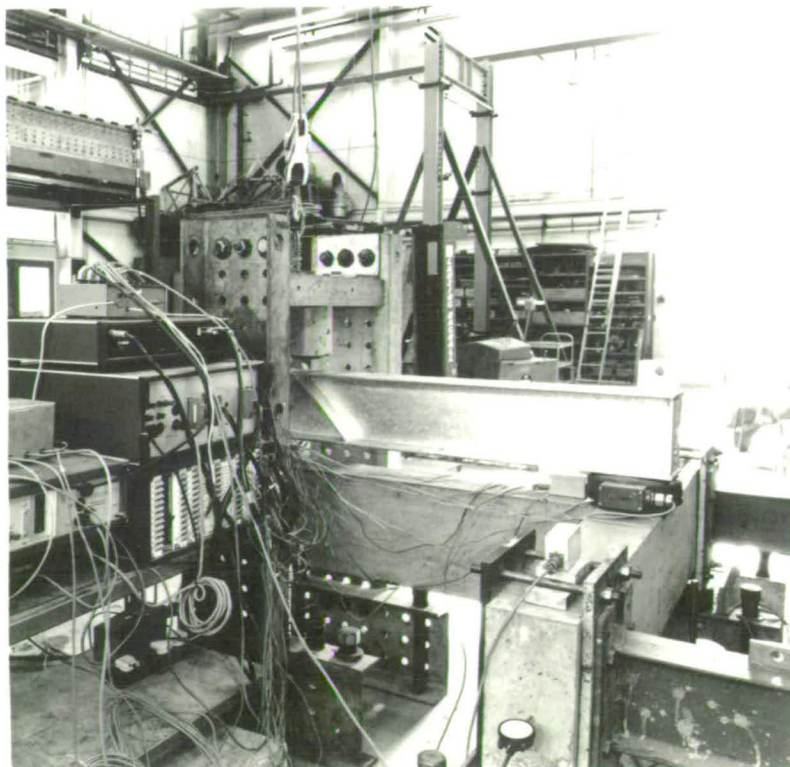
The torsional rotation of the spandrel beam was measured by the rotational arms fixed at the centre of the spandrel beam with a dial gauge underneath the extreme end. Additional inclinometers were placed at the end of the spandrel beam and the floor beam to measure the flexural rotation; one inclinometer was placed at the joint. A record of deflections and rotations was made by reading the dial gauges and the related loads at each stage.

The rotational arms measured the torsional rotations at half length of the spandrel beam. The dial gauges underneath those arms thus recorded the vertical movement of the arms as the beam twisted



(a) At the Floor Beam

Plate 2.3 Method of Load Application Using the Distributer Beam



(b) At the Joint

under torsional load. However, the spandrel beam also deflected downwards at the same time. The angle of twist can therefore be calculated from these movements.

2.4.4 Strain in the Steel Bars and Concrete

The strains in the reinforcement bars were measured using electrical resistance strain gauges. Within all specimens there were two gauges on the floor beam bottom steel at the centre, two on the floor beam stirrups near the joint, two on the floor beam top steel in the area of negative moment, two on the spandrel beam bottom steel at the joint and not less than four gauges on the stirrups of the spandrel beam; any additional gauges were also located on the spandrel beam stirrups. The type of strain gauge used was dependent on the bar diameter. Gauges of type (FLA-2-11), 2 mm in length were used for the stirrups and gauges of type (PL-10-11), 10 mm in length were used for the main bars.

The strain gauges were fixed on the steel bars and stirrups in predetermined positions and protected by Araldite glue. Waterproofing of the gauges embedded in the concrete and protecting them at the time of casting is necessary otherwise the strain readings in the data logger fluctuate over a wide range and it becomes very difficult to assess the actual strain reading. Care was taken when leading the connecting wires out of the specimens as contact with the bars would result in a loss of bond.

In order to eliminate the effect of thermal drift caused by differential heating and to couple the half circuit of the Wheatstone bridge, dummy models with the same strain gauge arrangements were used.

Although in theory dummy should be identical to the test specimen, due to the size of the specimen three small rectangular reinforced concrete beams representing the specimen members were used. The use of the dummy gauges was observed to stabilize the Wheatstone bridge so that more accurate results were obtained.

A continuous print out of the strain gauge measurements were obtained from the data printer Teletype driven by power supply unit as shown in Plate 2.3(a), (b).

Demec points were used to measure the strain in the concrete and the crack widths. These were located at the critical sections of the specimen. Demec points were fixed along the depth of the floor beam under the load at six levels and on the outside face of the spandrel beam at the centre of six levels. Demec points were also fixed on the inside face of the spandrel beam where the shear and torsional stresses are additive. On the floor beam additional Demec points were located in the area of negative movement near the joint.

2.5 Test Procedure

The specimen was first placed in the test rig then the relevant instrumentations and strain gauge connections ^{were} made. The data logger was calibrated for zero strain gauge readings and the initial readings of the load cells, strain gauges, Demec gauges, dial gauges and inclinometers readings were recorded for the no load condition. The test procedure itself was essentially the same for all specimens. Using the hydraulic jack the load was applied and once the desired value was reached, the torsional arms attached to the ends of the spandrel beam were returned to the horizontal position by operating the hydraulic

pumps attached to the jacks. All readings from the load cells, strain gauges, inclinometers and dial gauges were then recorded. The beam was closely inspected for cracks and if any were found, their propagation was marked using a black ink pen. Finally all the strain gauge, load cell and inclinometer readings were recorded again in order to reduce the effect of drift within the electrical equipment. The load was then increased to the next predetermined load level and the process repeated. The specimen was assumed to have reached failure when the applied load was observed to have decreased considerably with high deflections or twist, indicating that no further load could be sustained by the beam. Pumping of the jacks continued in order to trace further development of the cracks. Since simultaneous failure of the floor and the spandrel beams was not observed, it was found necessary to pump the jack further to fail the spandrel beam in twist in groups GR1, GR3 and GR4 and to fail the floor beam in flexure in group GR2.

Tests results are shown in Table 2.8.

Table 2.8 Test Results

Specimen	Ultimate load, P, kN		Test Design	Ultimate torque kN.m		Test Design	Moment Torque (test)	Mode of Failure
	Design	Test		Design	Test			
GR1-B1	70	50	0.71	5.42	2.85	*	6.42	A
-B2	70	80	1.14	4.7	3.75	*	7.69	A
-B3	70	80	1.14	3.13	3.96	1.26*	7.3	A
-B4	70	80	1.14	0.0	4.25	-	6.85	A
GR2-B5	70	80	1.14	5.42	7.0	1.29*	2.22	A
-B6	70	80	1.14	4.07	7.4	1.8	2.07	A
-B7	70	85	1.21	3.08	6.2	2.01	2.56	A
-B8	70	85	1.21	0.0	5.0	-	3.1	A
GR3-A1	45	70	1.55	0.904	1.7	1.88*	4.6	A
-A2	45	70	1.55	0.783	2.59	3.3 *	3.2	A
-A3	45	75	1.66	0.595	2.37	3.9 *	3.49	A
-A4	45	60	1.33	0.0	2.54	-	2.86	A
GR4-B1	25	35	1.4	0.783	1.47	1.87*	2.88	A
-B2	25	40	1.6	0.587	1.95	3.32*	2.55	A
-B3	25	40	1.6	0.445	2.24	5.03*	2.28	A
-B4	25	50	2.0	0.0	2.38	-	2.6	A

* Maximum value recorded when the floor beam failed.

A: hinge in spandrel beam and hinge in floor beam.

CHAPTER 3 : GENERAL BEHAVIOUR AND MODES OF FAILURE

3.1 Introduction

3.2 General Behaviour of Specimens

3.2.1 Floor Beams (F.B.)

3.2.2 Spandrel Beams (S.B.)

3.3 Modes of Failure

3.3.1 Floor Beam Failure

3.3.2 Spandrel Beam Failure

3.4 The Observed Effect of the Variables on the Failure Mechanism of the Test Specimens

3.4.1 Load Application

3.4.2 Longitudinal Steel

3.4.3 Transverse Steel

3.4.4 Length of the Spandrel Beam

3.4.5 Concrete Strength

3.4.6 Joint Detailing

3.1 Introduction

It is necessary to have a sufficient understanding of the general behaviour and mechanism of failure of the test specimens before developing any analytical approach for assessing the floor-spandrel beam assembly performance. This chapter provides a description of the general behaviour and modes of failure.

A total of eighteen specimens representing the spandrel-floor-beam assembly were tested. The specimens can be grouped as follows:

Group 1 (GR1) = four full scale beams (B1, B2, B3 and B4)

Group 2 (GR2) = four full scale beams (B5, B6, B7 and B8)

Group 3 (GR3) = four one third scale models (A1, A2, A3 and A4)

Group 4 (GR4) = four one third scale models (B1, B2, B3 and B4)

Group 5 (GR5) = two one third scale models (C1 and C2)

Details of each group with load arrangements are shown in Table 2.1.

3.2 General Behaviour of Test Specimens

The general behaviour of the specimens is best described by referring to the load-deflection curves, Figures 3.1(a), (b), (c) and (d), load-torque curves, Figures 3.2(a), (b), and torque-angle of twist curves, Figure 3.3(a), (b). It is evident that the behaviour of the test specimens was greatly influenced by the different test parameters. It is, therefore proposed to describe the specimens by their floor and spandrel beam behaviour.

3.2.1 Floor Beams (F.B.)

The sequence of load application is described in the test programme.

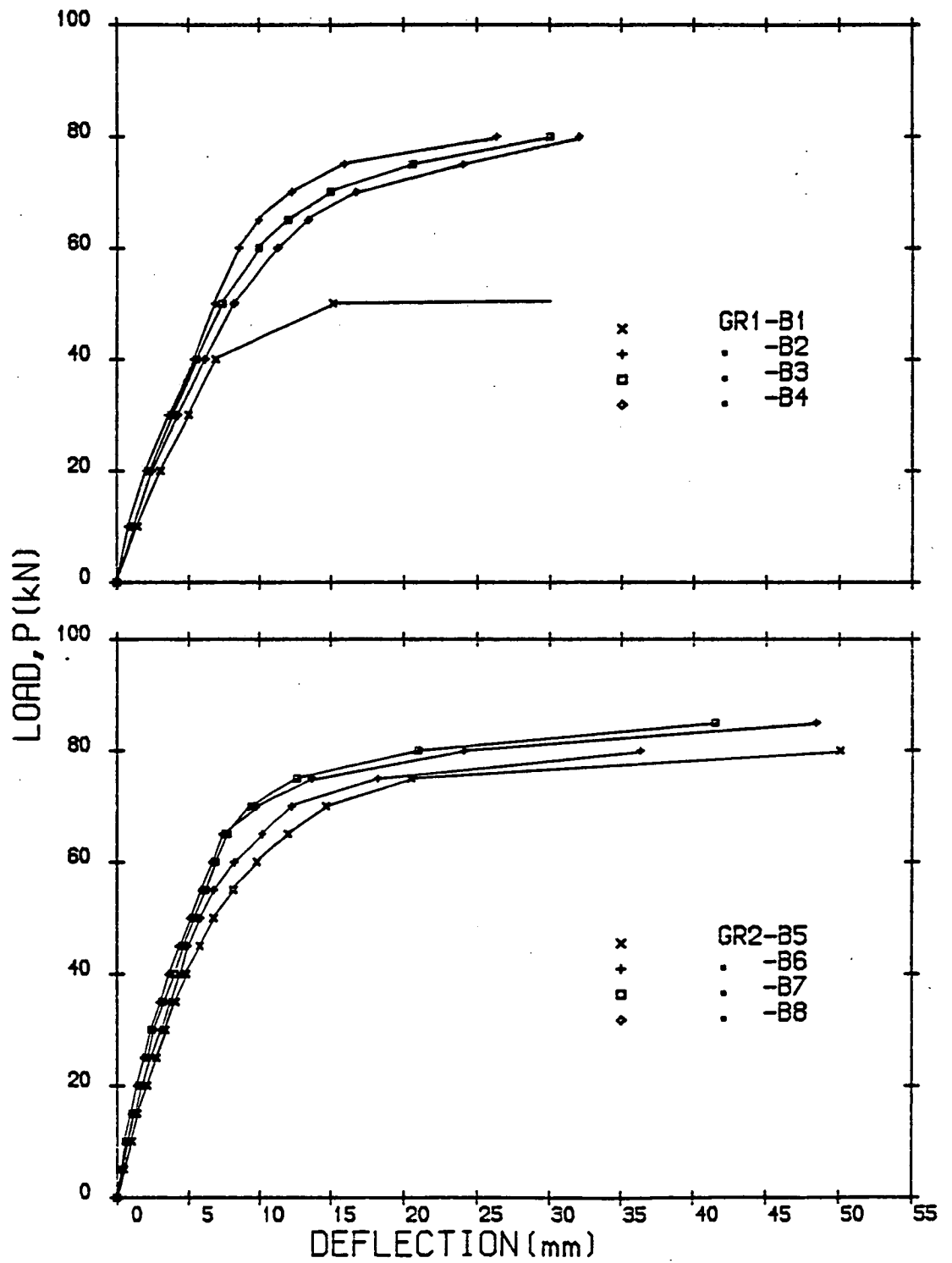


Figure 3.1(a) Load-Deflection Curves (F.B.)

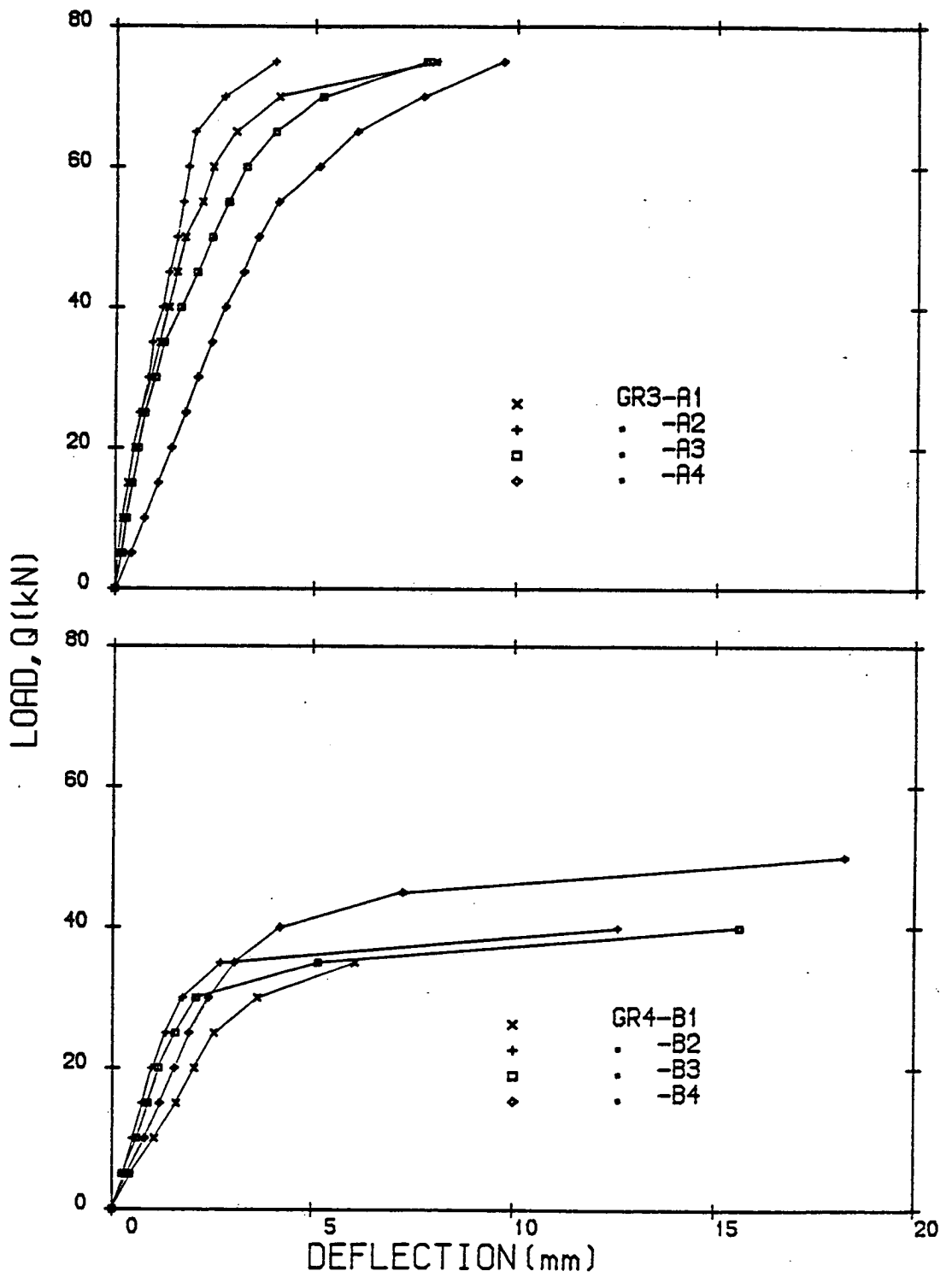


Figure 3.1(b) Load-Deflection Curves (F.B.)

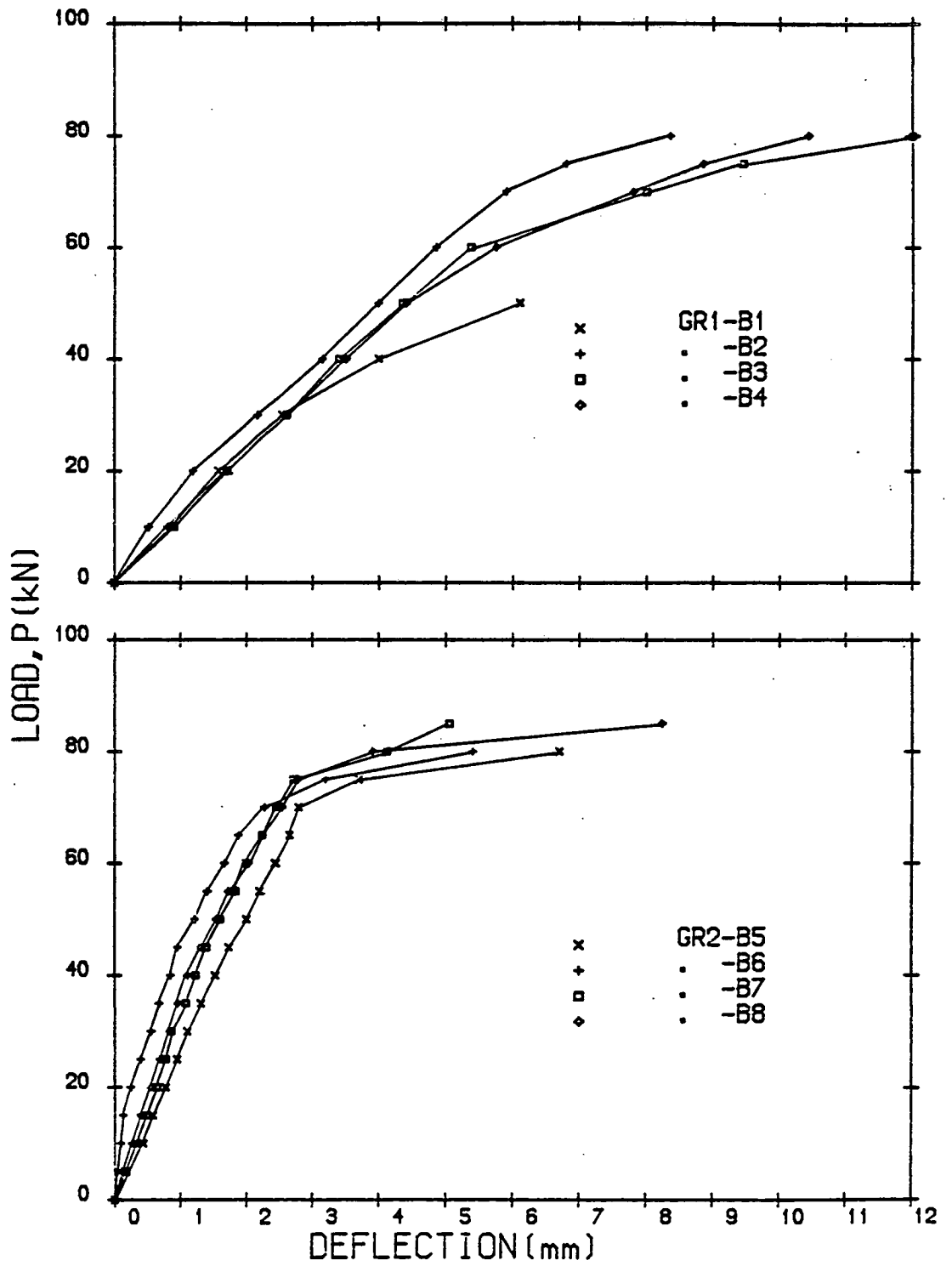


Figure 3.1(c) Load-Deflection Curves (S.B.)

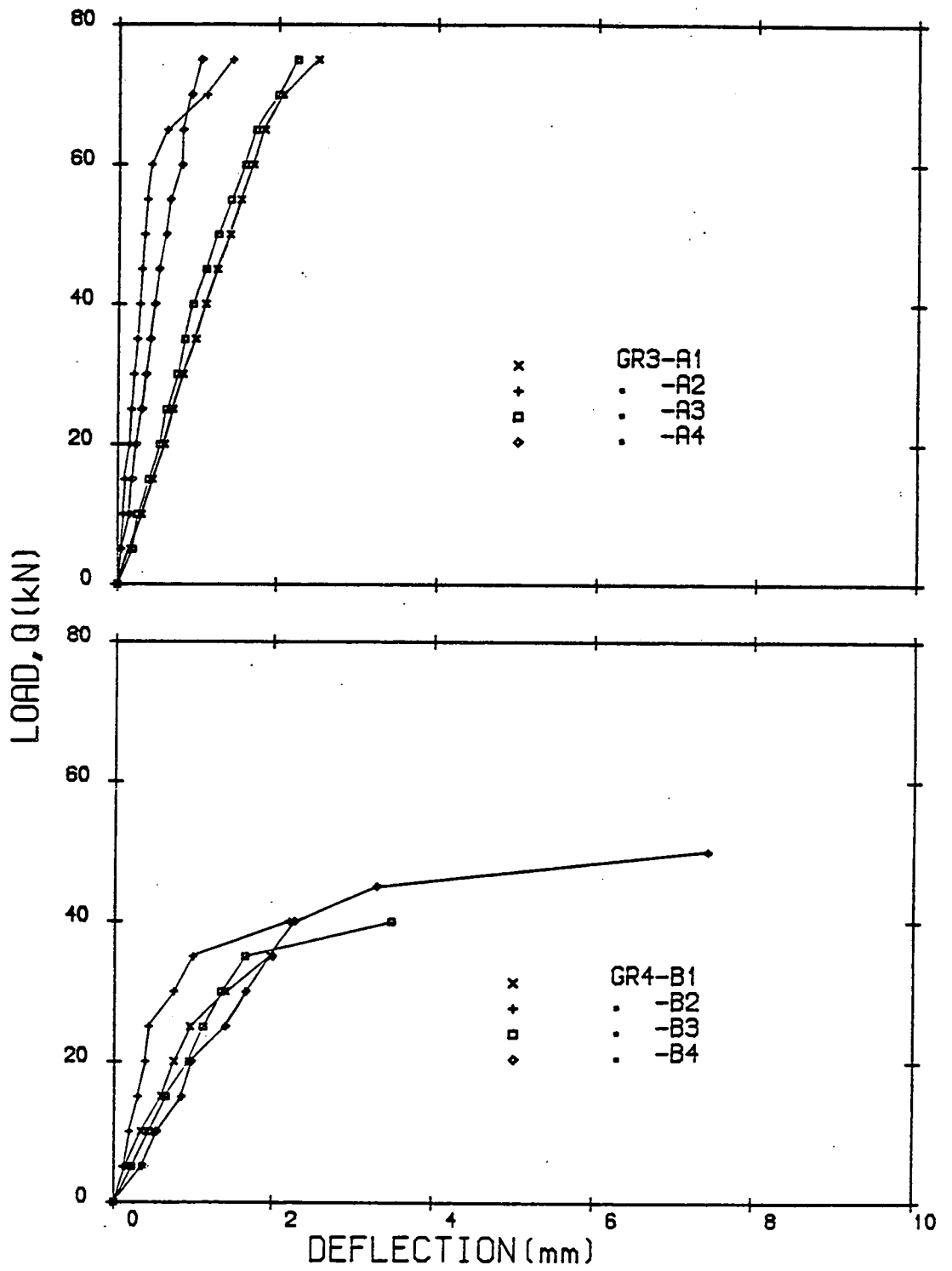


Figure 3.1(d) Load-Deflection Curves (S.B.)

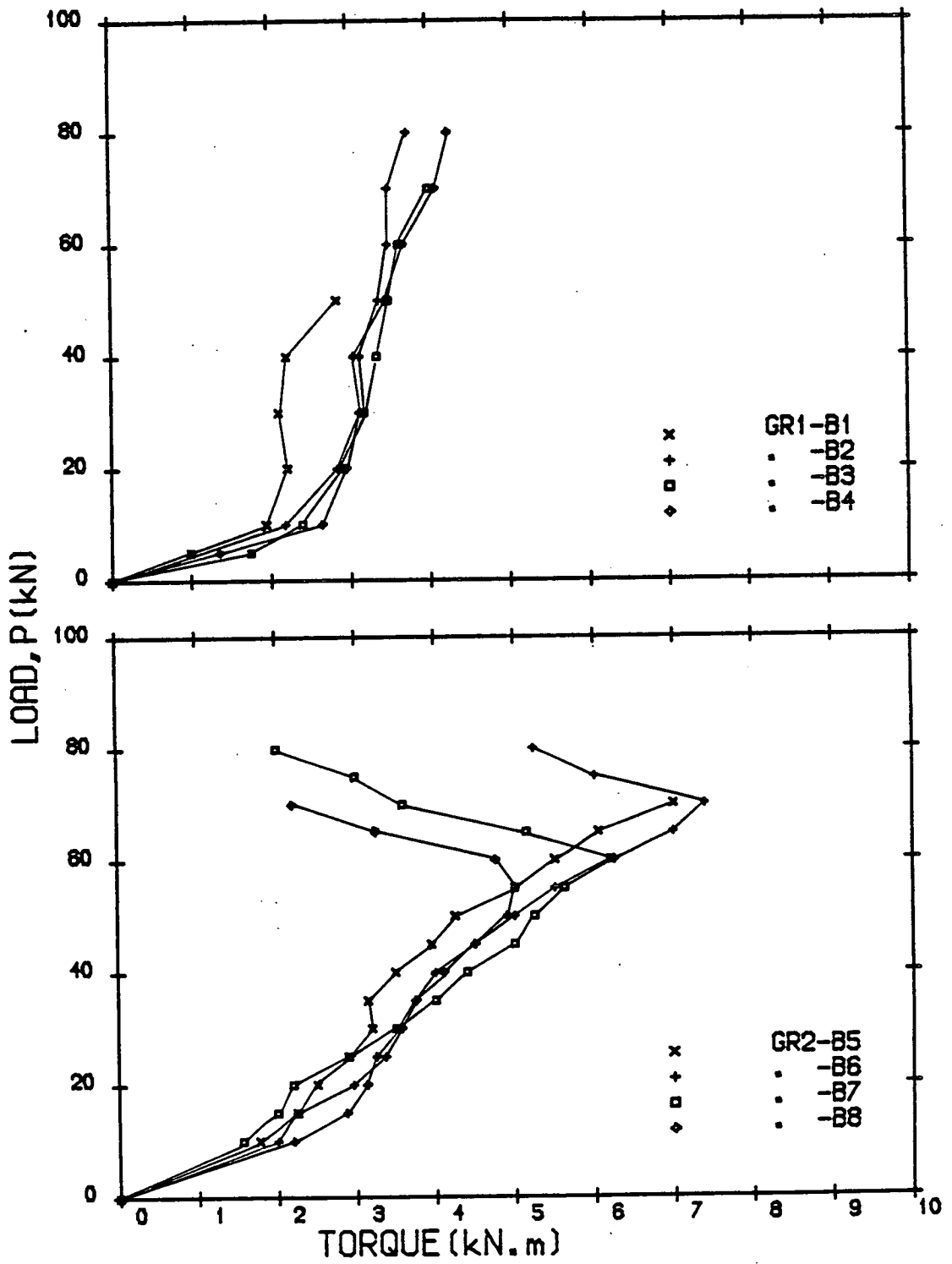


Figure 3.2(a) Load-Torque Curves

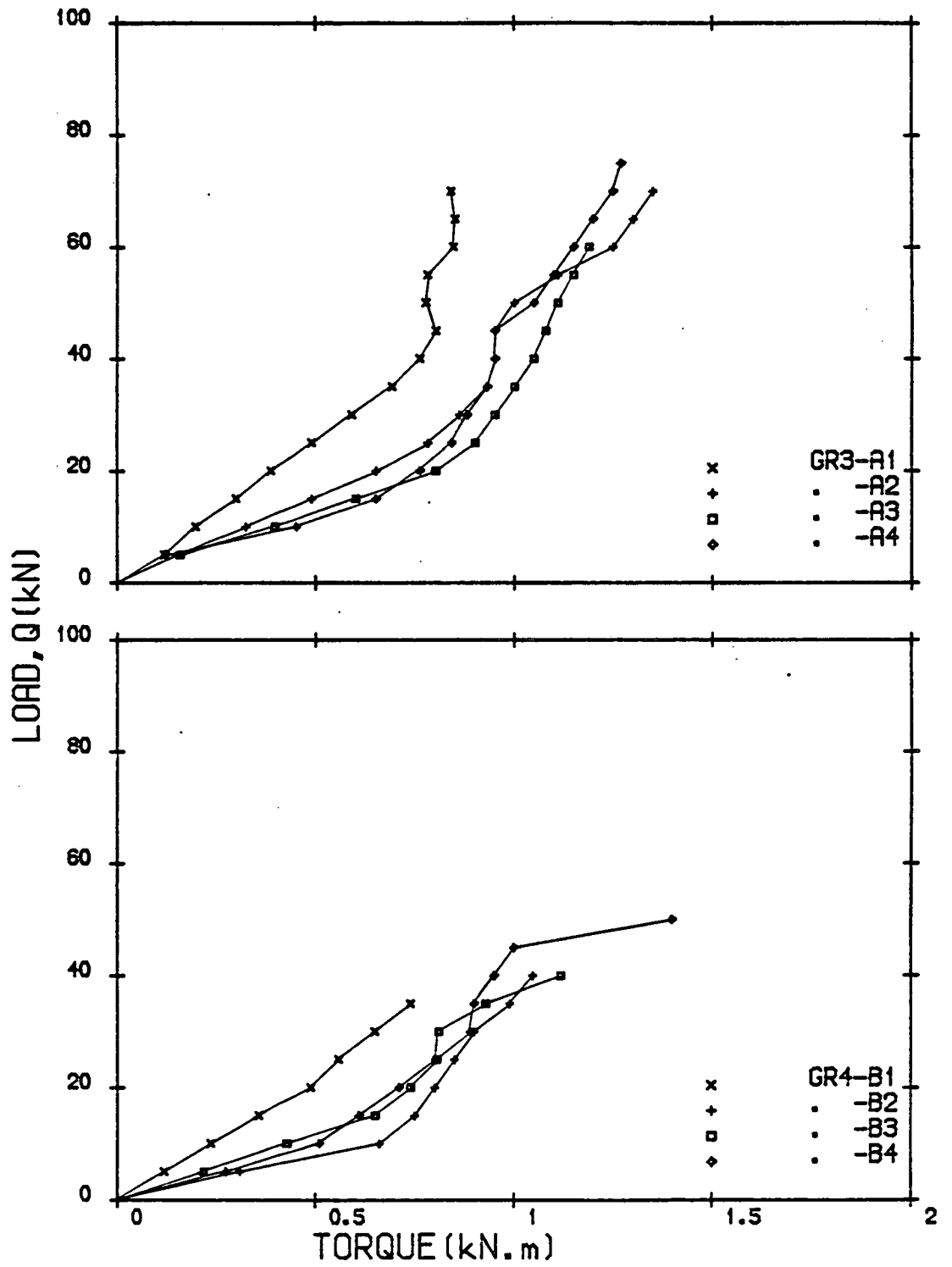


Figure 3.2(b) Load-Torque Curves

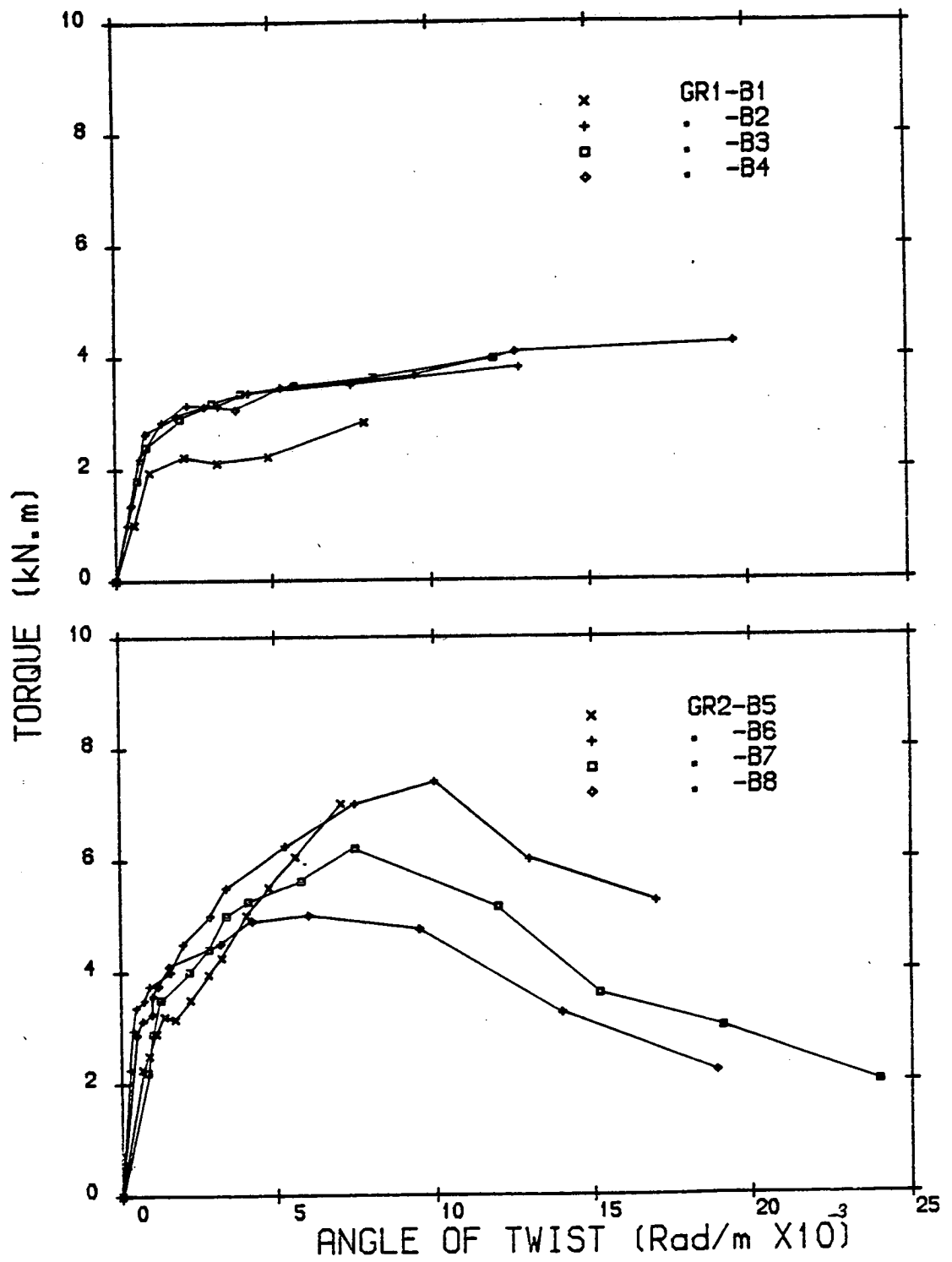


Figure 3.3(a) Torque-Angle of Twist

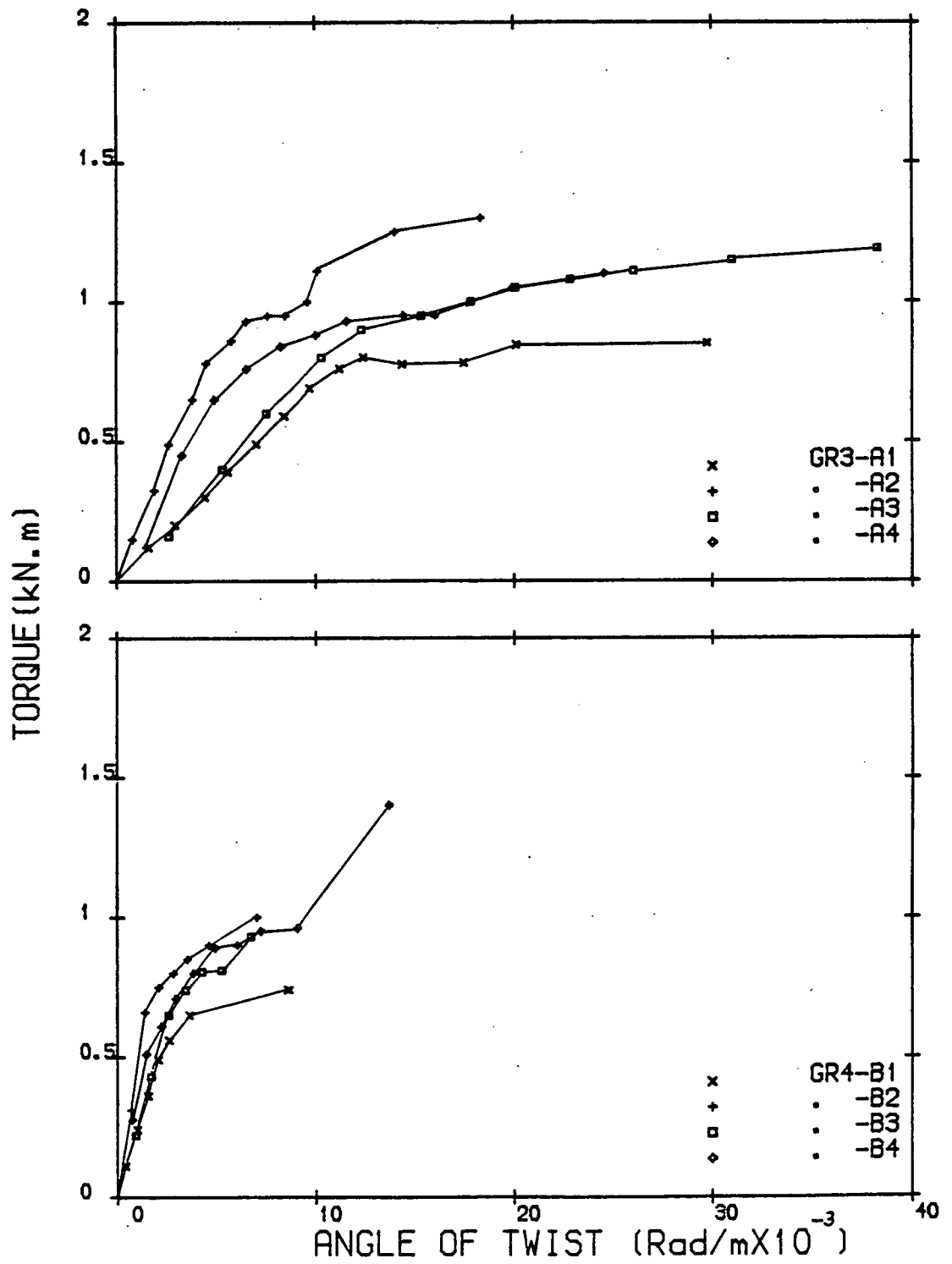


Figure 3.3(b) Torque-Angle of Twist

All floor beams in all groups had a point load at the midspan. The observed behaviour can be illustrated by referring to Figure 3.4 which shows a typical idealized load-deformation curve for the flexural section.

The first visible cracks were developed under the applied load at midspan. This stage is marked by (1) on the diagram. Concrete between 0-1 is uncracked and hence the section behaves elastically. Once, the cracks developed, point (1) was passed. The cracking load varies between 33% to 50% of the ultimate load except beam GR1-B1 which cracked at 80% of the ultimate load, as shown in Table 3.1. With increasing load, the cracks widened and extended into the beam section. Concrete and steel at this stage, defined by 1-2 on the diagram, still behaved elastically with the concrete losing a considerable amount of its tensile strength. In fact, the transition between the region of 0-1 and 1-2 is not instantaneous. It is very much dependent on the amount of steel provided in the section which controls the cracking rate towards the neutral axis (cracking rate tends to be slow with higher steel percentages).

Some of the cracks also developed away from the centre of the beam but tended to propagate towards the centre. At point (2), the steel starts to yield. This was confirmed in the test by having electrical strain gauges fixed on the longitudinal bottom steel. The crack propagation was traced using a magic marker and also using Demec points, which were fixed along the depth of the section at six levels. The crack developments could therefore be measured.

When the load was further increased, the concrete lost its tensile strength with the neutral axis moving upwards. The yield of the steel was inevitable. At this stage, represented by the

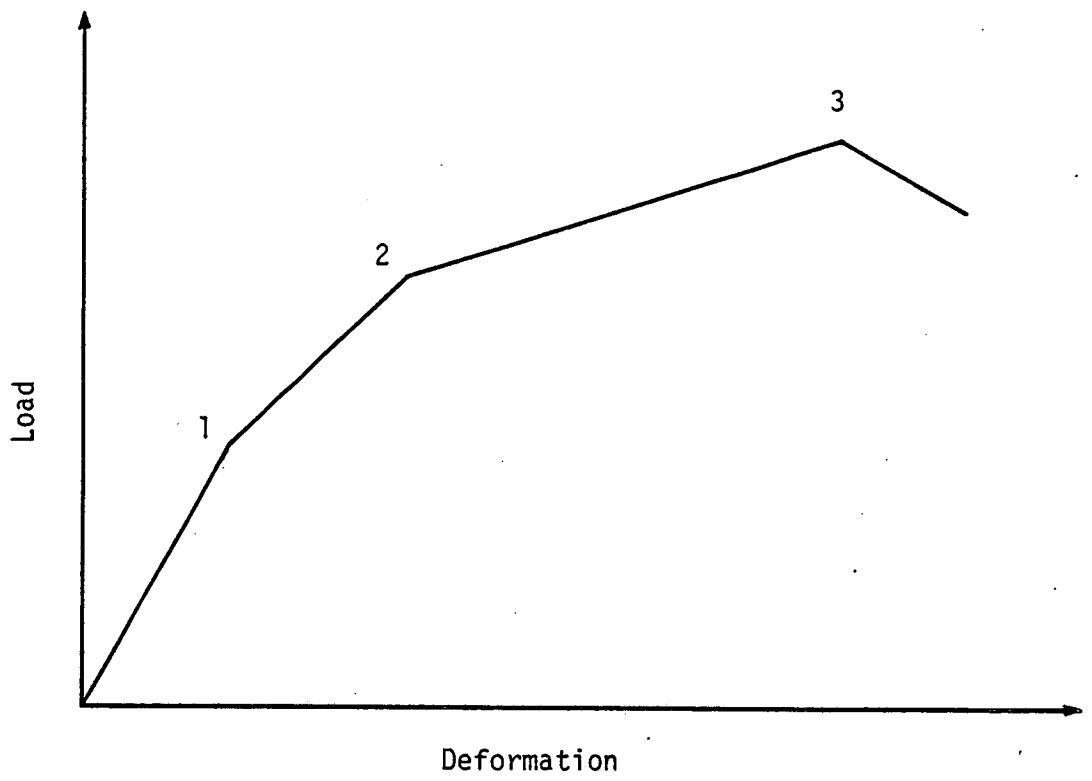


Figure 3.4 Idealized Load-Deformation Diagram

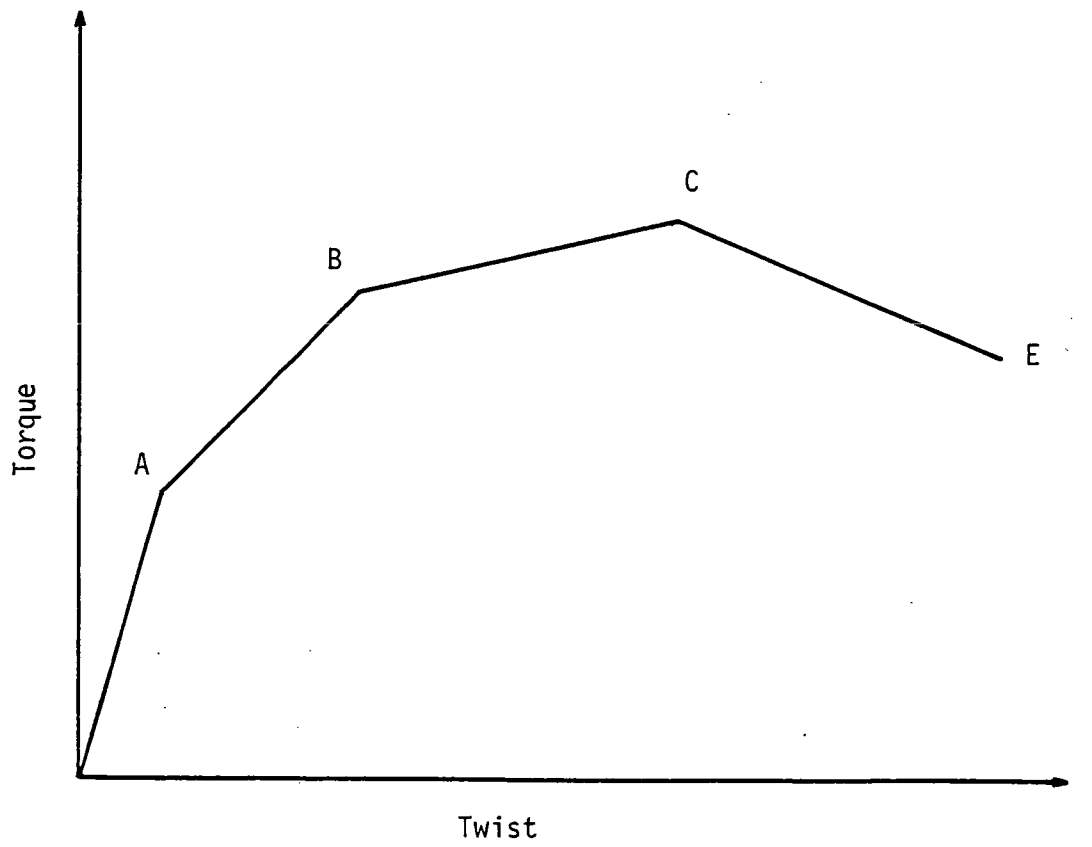


Figure 3.5 Idealized Torque-Twist Diagram

Table 3.1 Ratio of the Cracking Load to the Ultimate Load

Speciman	Flexural cracking load in F.B. ultimate load, P	Flexural cracking load in S.B. ultimate load, P	Torsional cracking load ultimate load, P
GR1-B1	0.8	1	1
B2	0.5	0.5	0.625
B3	0.5	0.5	0.5
B4	0.5	0.5	0.5
GR2-B5	0.38	0.5	0.56
B6	0.44	0.5	0.687
B7	0.41	0.41	0.65
B8	0.35	0.35	0.59
GR3-A1	0.46	0.33	0.6
A2	0.33	0.46	0.47
A3	0.33	0.66	0.66
A4	0.4	0.46	0.6
GR4-B1	0.38	0.38	0.624
B2	0.5	0.62	0.75
B3	0.5	0.5	0.62
B4	0.4	0.6	0.6

region 2-3 on the diagram, the non-linearity characteristics of concrete and steel affected the behaviour of the beam. The increase in the compressive strain of the concrete at the top of the beam was observed using Demec readings with further widening of the cracks at the bottom. The beam deflection also increased. Failure occurred by crushing of the concrete after yielding of the steel with uncontrollable deflections forming a hinge underneath the load, except for beam GR3-A4 in which the hinge was shifted away from the centre. This is represented by point (3) on the diagram. Figures 3.1(a) and (b) show load-deflection curves.

3.2.2 Spandrel Beams (S.B.)

The flexural behaviour of the spandrel beam was different from that already discussed for the floor beam. Spandrel beams were subjected to a combination of flexural and torsional loading applied at the same time. However the final cause of failure was not due to flexure. Smaller deflections were observed with the cracks developed at the centre of the beam. As the load was increased cracks tended to propagate vertically upwards and then bend away from the centre. The observed cracking loads of the spandrel beams were slightly higher than those of the floor beams i.e. between 35% to 60% of the ultimate load. Load-deflection curves of spandrel beams are shown in Figures 3.1(c) and (d).

As far as the torsional behaviour is concerned, two types of spandrel beams were recognized. The first type, was defined by the beams not reaching their ultimate torsional capacity, beams in GR1, GR3, GR4 and GR2-B5 are of this type. In the second type, the beams

reached their ultimate torsional capacity. Beams GR2-B6, GR2-B7 and GR2-B8 are of this type. After flexural cracking of the spandrel beam was detected, smaller torsional cracks on the inside face, started to develop at higher load levels of 50% to 75% of the ultimate load. They propagated vertically for a short distance and then bent towards the joint. At this stage i.e. after crack formation, the torsional stiffness decreased drastically. Also no sign of the stirrups yielding was observed in any of the specimens. With reference to Figures 3.2(a) and (b), the torque in the spandrel beam increased as the load was increased resulting in more cracks developing along with widening of the existing ones. The torque then remained nearly constant with increasing load. This allowed a redistribution of torsional moments from the spandrel beams to the floor beams. As the load was further increased, the first type of spandrel beams carried more torsion but the full torsional capacity was not reached due to flexural failure of the floor beams. The formation of the plastic hinge in the floor beam indeed accelerated the twisting of the spandrel beam and consequent failure. In other words spandrel beams of the first type failed due to twist.

The second type of spandrel beams carried more torsional moment till they reached their ultimate torsional capacity. At this stage yielding of the stirrups was observed from the strain measurements. Widening of the cracks was inevitable which at higher loads spiralled around the section. A torsional plastic hinge was formed followed by definite failure of the spandrel beam. The load was then further increased to fail the floor beam. This was achieved by forming a flexural plastic hinge under the load. Figures 3.3(a) and (b) show the torque-angle of twist curves for the spandrel beams.

The torsional behaviour can be described by referring to Figure 3.5, an idealized torque-twist diagram with points O, A, B, and C corresponding to points 0, 1, 2, and 3 in Figure 3.4 respectively. O-A on the diagram represents the elastic uncracked behaviour. A-B represents the elastic cracked behaviour. B-C represents the non-linearity characteristics of concrete and steel, which affect the behaviour of the beam. C-E represents the descending part after failure. Point (C) is the failure point. At point (A) cracking takes place; beyond this point yielding of the steel may be noticed. Strains in the stirrups and longitudinal steel were measured by electrical strain gauges. To assess the cracks in the spandrel beams, Demec points were fixed on the surface at the concrete on the inner face where the torsional and shear stresses are additive. The crack widths at mid-depth were considered to indicate the effect of torsion. Demec points were also fixed at midspan along the depth of the beam at six levels to trace the flexural cracks on the spandrel beam.

The design and behaviour of beams in group 5, however were different from the rest of the test specimens.

Two beams GR5-C1 and GR5-C2 were both designed by method (D) to carry zero torsional moment. No web reinforcement was provided to resist the torsional and shear stresses. This was to fail the specimens at the joint. Hence it was necessary to find the failure surface or the critical section within which stirrups could be provided to resist the torsional and shear stresses. The behaviour of the two specimens and failure surface were remarkably similar though beam GR5-C2 had two extra 6 mm steel bars placed with the negative steel in the floor beam in the joint, each one extending in one direction into the spandrel beam. A crack first occurred between the floor beam and spandrel beam

due to the negative moment at the end of the floor beam. The cracks then extended up to load of $Q = 44 \text{ kN}$ which caused sudden failure. Failure also caused spalling of the bottom layer of concrete along the longitudinal steel.

3.3 Modes of Failure

Failure of the floor-spandrel-beam assembly may occur in one of the following ways:

1. A hinge forms in the floor beam under the applied load; point (1), Figure 3.6.
2. A hinge forms in the floor beam in the negative area; point (2).
3. A hinge forms in the joint; failure occurs before the beams reach their ultimate capacities; point (3).
4. A hinge forms in the spandrel beam, point (4).

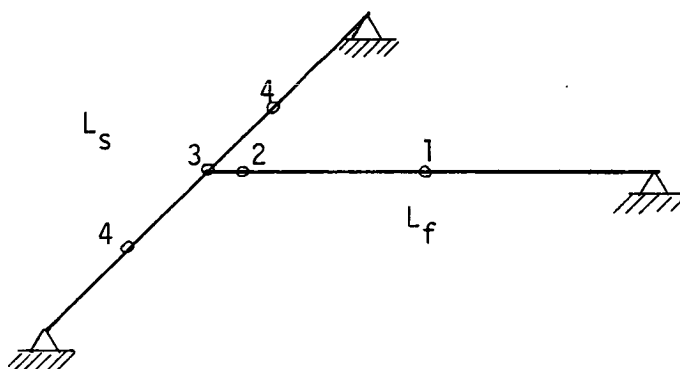


Figure 3.6 Location of Possible Hinges

The formation of any two hinges may result in the whole structure or part of it forming a mechanism with resultant collapse; possible modes of failure consist of:

- (a) Two flexural hinges 1 and 2.
- (b) Flexural hinge 1 and hinge at the joint 3.
- (c) Flexural hinge 1 and torsional hinges 4.
- (d) Torsional hinges 4 and hinge at the joint 3.

The formation of the hinges is very much dependent on the amount of steel provided. For example, hinge 2 may move to 3 when ^{an}adequate percentage of negative steel is provided.

Two types of failures were observed:

- 1. Floor beam failure.
- 2. Spandrel beam failure.

3.3.1 Floor Beam Failure

This is a flexural type of failure, with the formation of tensile plastic hinges. Those hinges obviously developed due to tension in bending causing the bottom reinforcing steel to yield sufficiently. The neutral axis was still within the section. Yielding of the bottom reinforcing steel was the main cause of the hinge rotation, since sections were under-reinforced. Failure occurred by crushing of the concrete of the compressive face.

Rotation of the flexural plastic hinge accelerated the twisting of the spandrel beam.

3.3.2 Spandrel Beam Failure

The nature of reinforced concrete failure under combined stresses is indeed complex and the essential conditions resulting in such failures are not fully understood, though the behaviour of a reinforced concrete beam under pure bending and pure torsion is well understood and established. Flexural failure has already been considered. Beams subjected to torsion must be sufficiently reinforced to avoid torsional failure which tends to be violent, destructive and usually without warning. Torsional cracking at failure is cleavage fracture caused by the principal tensile stress due to torsional shear exceeding the tensile strength of the concrete.

The final mode of failure is dependent on the applied bending and twisting moments. For beams subjected to high ratios of bending to torsion, failure results by crushing of the concrete on the compressive face. With the presence of torsion, the diagonal compression due to torsional shear stress tends to increase the direct compression caused by bending; accordingly the flexural strength is reduced; the amount of reduction depends on the amount of applied torsion. On the other hand, the compressive stress caused by bending reduces the principal tension due to torsional shear and then the torsional capacity of the beam is increased. However test data show that, high increase in the ratio of bending moment to twisting moment does not produce an increase in the torsional strength.

Where the torsional shear stress is large enough to produce a critical principal tensile strain for the cleavage fracture, is a stage before crushing of the concrete in compression and cleavage fracture in tension are reached. After the torsional cracks developed

the torsional stiffness decreased drastically, also the concrete lost most of its tensile strength and steel started to yield with considerable increase of the compressive strain; then a torsional plastic hinge was formed.

It is interesting to note that the spandrel beams exhibited inelastic deformations and as the load was increased, the torsional rotation was increased substantially compared to its value in pure torsion.

Cracks develop when the tensile stress in the tension area is greater than the tensile strength of concrete (f_t). Therefore the parameter (f_t) must be involved in any relationship which may be proposed to predict cracking.

In the past the tensile strength of concrete was neglected in most theories and codes of practice. This is due to the fact that it is small in value compared to the compressive strength. However, in a sectional analysis the tensile strength must be determined. The most common control tests which determine the tensile strength are flexural and splitting tests. It is generally believed that the modulus of rupture for concrete can be expressed as a function of its cylinder strength. Indeed the flexural test (or modulus of rupture test) is used in this study in preference to the direct tensile strength. It is a useful test; practically speaking flexural tension is more common than direct test and can be accurately measured.

The experimental results produced by Beeby [48] indicate a considerable scatter, nevertheless a number of relationships have been proposed to express the tensile strength of concrete in terms of the cylinder strength.

The tensile strength given by the ACI [49] is:

$$f_t = 0.627 \sqrt{f_c'} \quad \dots \text{ N/mm}^2 \quad (3.1)$$

where f_c' = cylinder strength of concrete.

(f_t) given by the CEB [50] is:

$$f_t = 0.272 (f_c')^{2/3} \quad \dots \text{ N/mm}^2 \quad (3.2)$$

The following relationship was suggested at the University of Illinois by Warwaruck [51]:

$$f_t = \frac{21}{3 + \frac{84}{f_c'}} \quad \dots \text{ N/mm}^2 \quad (3.3)$$

The tensile strength given by the Building Research Station [52] is:

$$f_t = K \sqrt{f_c'} \quad \dots \text{ K} = 6.2 - 10.4$$

average $f_t = 0.7 \sqrt{f_c'} \quad \dots \text{ N/mm}^2 \quad (3.4)$

Figure 3.7 shows the test results reported by Beeby [48] and the other investigators. The values of the tensile strength of concrete obtained from different formulae are shown in Table 3.2.

It can be seen from Table 3.2 that the values of (f_t) given by B.R.S. and C.E.B. are less reasonable than those given by ACI. However, the following relationship is proposed to express the tensile strength of concrete as a function of the compressive strength:

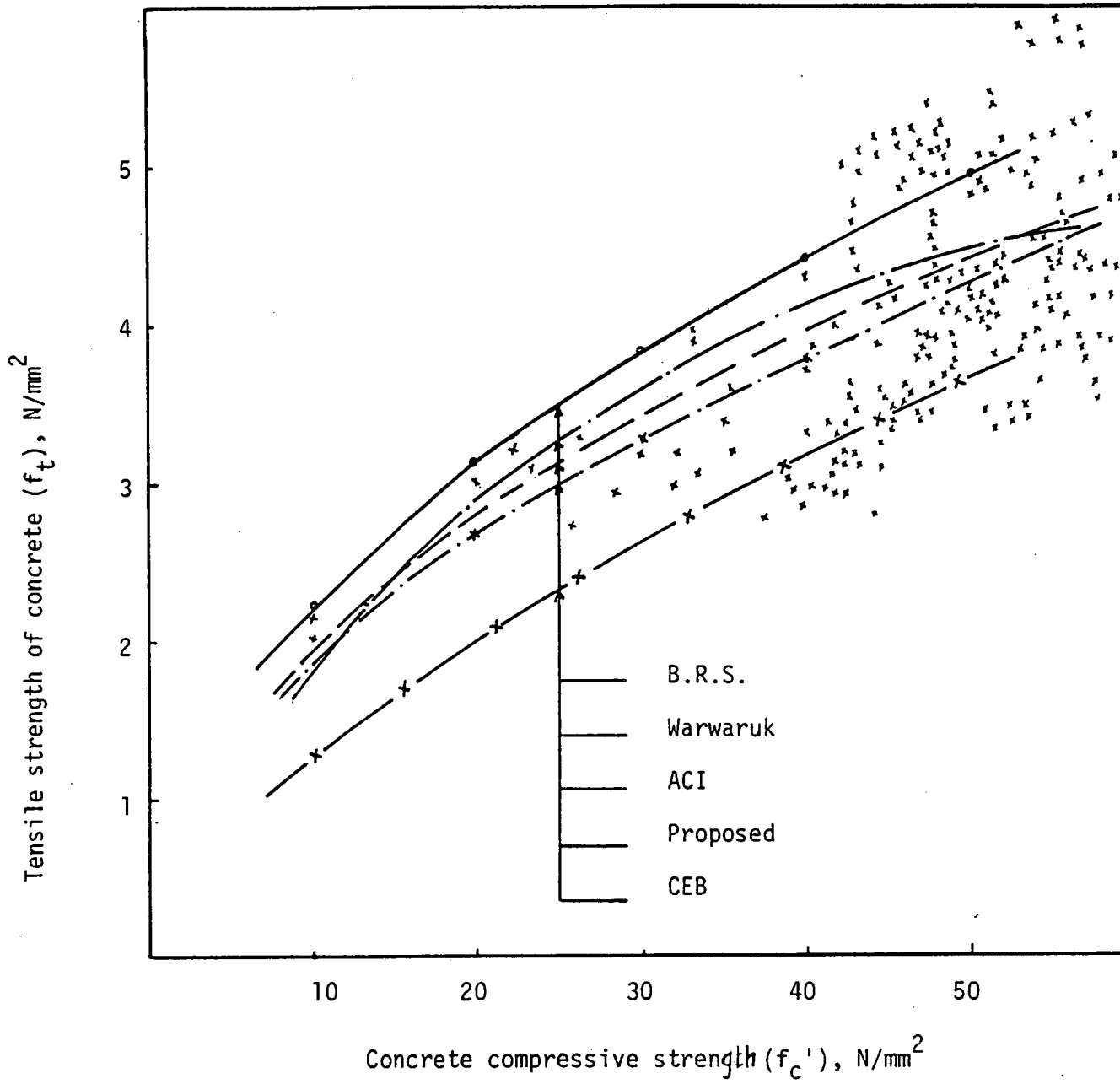


Figure 3.7 Tensile Strength Against Compressive Strength of Concrete

Table 3.2 Tensile Strength of Concrete (Expressed as Modulus of Rupture)

f'_c N/mm ²	Tensile strength f_t , N/mm ²				
	ACI eq. 3.1	CEB eq. 3.2	Warwaruck eq. 3.3	B.R.S. eq. 3.4	Proposed eq. 3.5
20	2.8	2.0	2.9	3.13	2.68
25	3.14	2.3	3.3	3.5	3.0
30	3.43	2.63	3.62	3.83	3.28
35	3.7	2.9	3.88	4.14	3.55
40	3.96	3.18	4.12	4.43	3.79
45	4.2	3.44	4.3	4.7	4.02

$$f_t = 0.6 \sqrt{f_c} \quad (3.5)$$

The above relationship has been proposed in the light of the test results which are based on flexural tests, representing the modulus of rupture of concrete.

3.4 The Observed Effect of the Variables on the Failure Mechanism of the Test Specimens

Full details of the test specimens are shown in Table 2.1. The design variables affect the distribution of internal forces in the beams which determines the failure mechanism of a particular specimen. The main variables considered in this study are:

3.4.1 Load Application

In group GR1 a point load was applied at the midspan of the floor beam only. For groups GR2, GR3, GR4 and GR5 two point loads were applied one at midspan of the floor beam, the other at the joint. This was to increase the shear effect on the spandrel beam. Since the spandrel beams of GR2 were shorter than those of group GR1, they were subjected to higher shear stresses due to torsion and shear. This may simulate an edge region of a continuous spandrel beam. Less severe shear stresses were expected in the spandrel beams of groups GR3 and GR4 since the length of the spandrel beams was equal.

The existence of high shear in spandrel beams led to wider cracks. Increasing the load and then the applied moment in the spandrel beams, increased the torsional rotation capacity as discussed earlier, this can be seen in Figures 3.8(a) and (b).

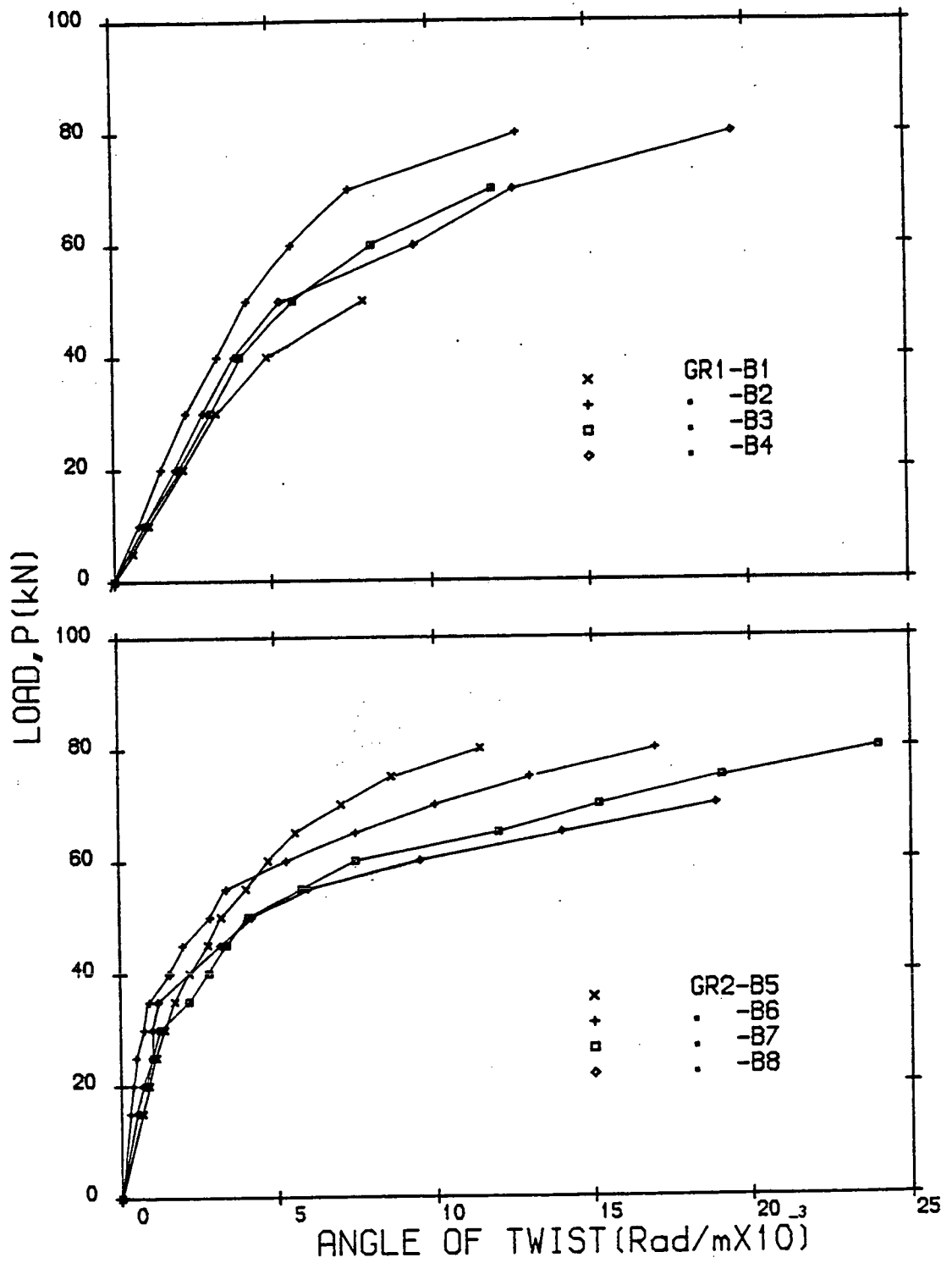


Figure 3.8(a) Load-Angle of Twist Curves

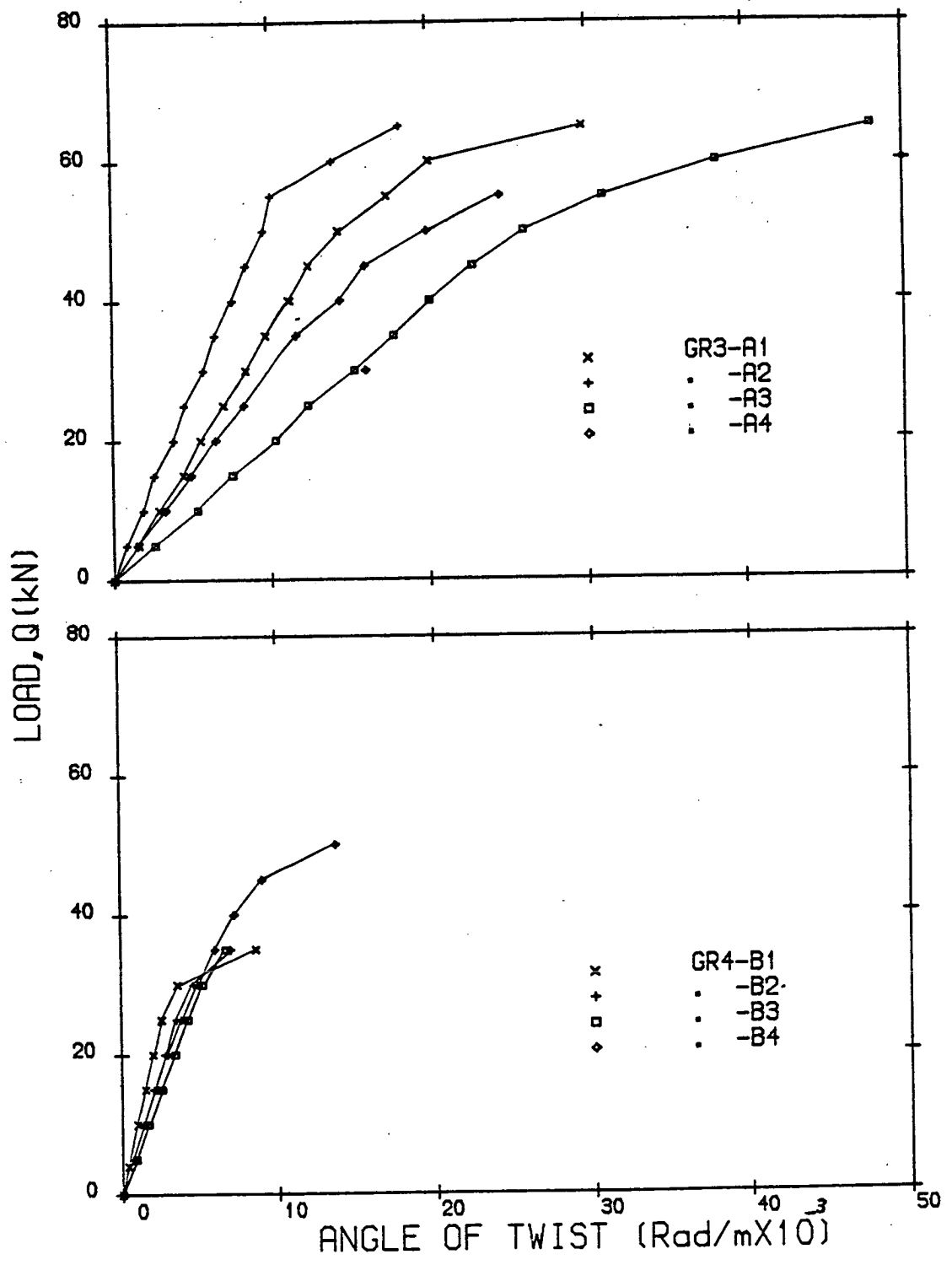


Figure 3.8(b) Load-Angle of Twist Curves

3.4.2 Longitudinal Steel

Spandrel beams in groups GR1 and GR2 were not provided with longitudinal steel due to torsion. On the other hand longitudinal steel was provided in the spandrel beams of groups GR3 and GR4. The function of the longitudinal steel is easily understood in bending, however, the observed behaviour indicated the small contribution of the longitudinal steel in the spandrel beams. No effect was observed on the ultimate torsional capacity. Specimens in groups GR1 failed in flexure in the floor beams. It was suggested that the effect may be revealed in spandrel beams of group GR2 where torsion and shear were high, also the torsional rotations were greater than those of beams in group GR1. The effect was not significant due to the fact that that beams reached their ultimate torsional capacity even where there was no provision for longitudinal steel due to torsion.

The spandrel beams in groups GR3 and GR4 were provided with longitudinal steel due to torsion; once again the effect was not pronounced since the floor beams failed long before the ultimate torsional capacity was reached.

However, the effect of the longitudinal steel was observed in controlling the crack width and counteracting the tendency of widening spiral cracks as well as anchoring the stirrups especially at the corners allowing them to develop their yield strength.

It has been suggested that the only way in which the longitudinal steel can contribute in resisting the external torsional and shear stresses is by dowel action. This is discussed in Chapter 5.

3.4.3 Transverse Steel

In order to prevent the sudden and explosive type of failure caused by torsion and shear, the spandrel beam should be sufficiently reinforced to exhibit adequate ductility. The amount and spacing of the transverse steel in the section are governed by two considerations:

1. To resist any torsional and shear stresses excessive to that resisted by concrete.
2. To provide adequate anchor^{age} for the longitudinal steel and reduce the unsupported length to prevent spalling of the bottom layer of concrete along the longitudinal steel.

The amount of web reinforcement provided in each specimen was determined by the method of design, hence the torsional moment. Accordingly specimens designed by method (A) had more stirrups than those designed by method (D). Stirrups in spandrel beams designed by method (D) were nominally spaced ($s = d/2$). Stirrups in the spandrel beams of groups GR1, GR3 and GR4 did not reach their yield point at failure, however stirrups in beams of groups GR2, did reach the yielding point before or at failure. This can be seen in Figures 3.9(a) and (b).

Test measurements show that the web steel was practically free from stress prior to crack formation and of insignificant or noticeable effect on the behaviour or strength of the spandrel beams. After crack formation, the stirrups had a significant effect in resisting the shear forces due to shear and torsion, restricting the growth of the diagonal cracks and reducing their propagation into the

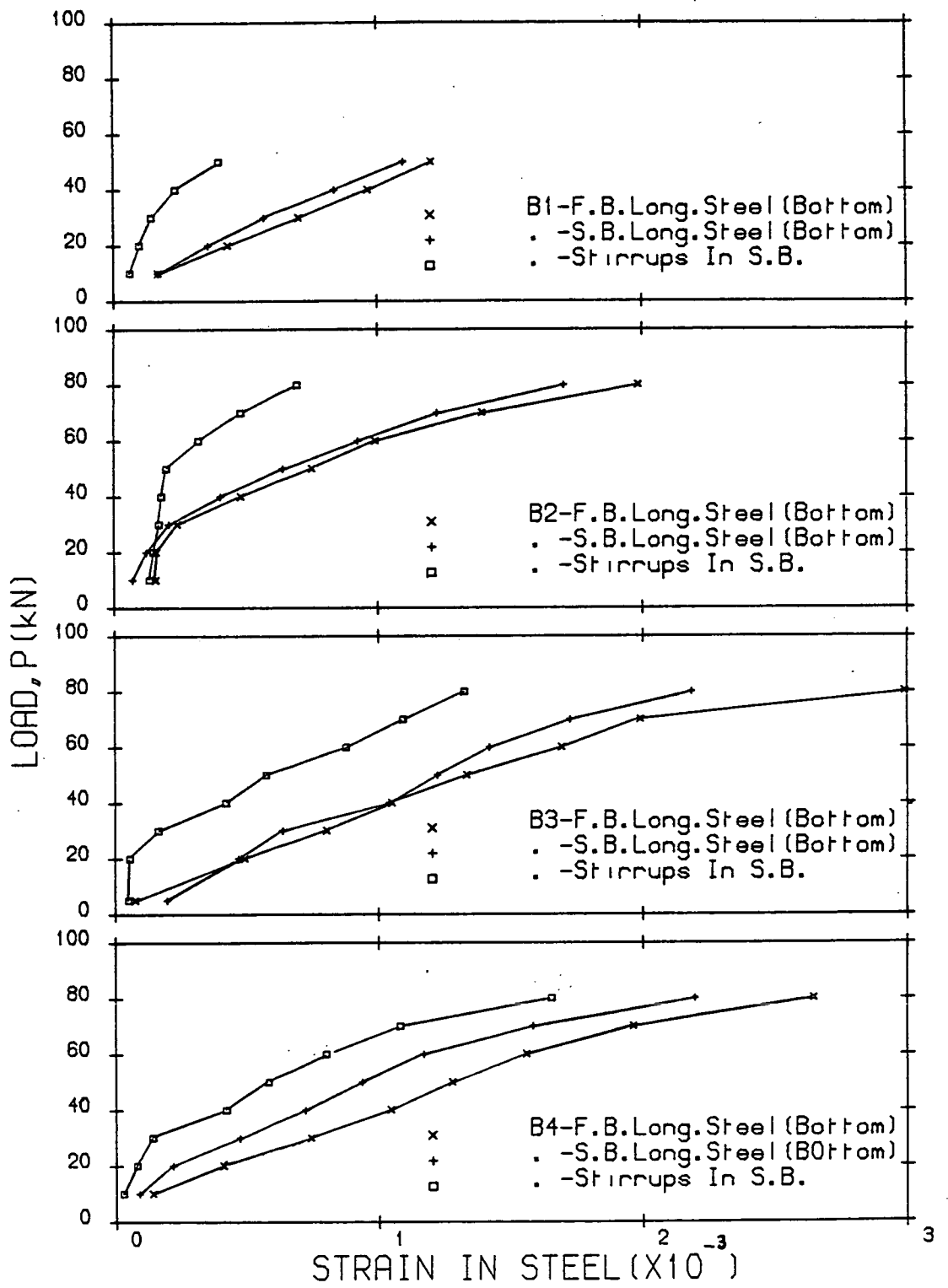


Figure 3.9(a) Load-Strain in Steel, GR1

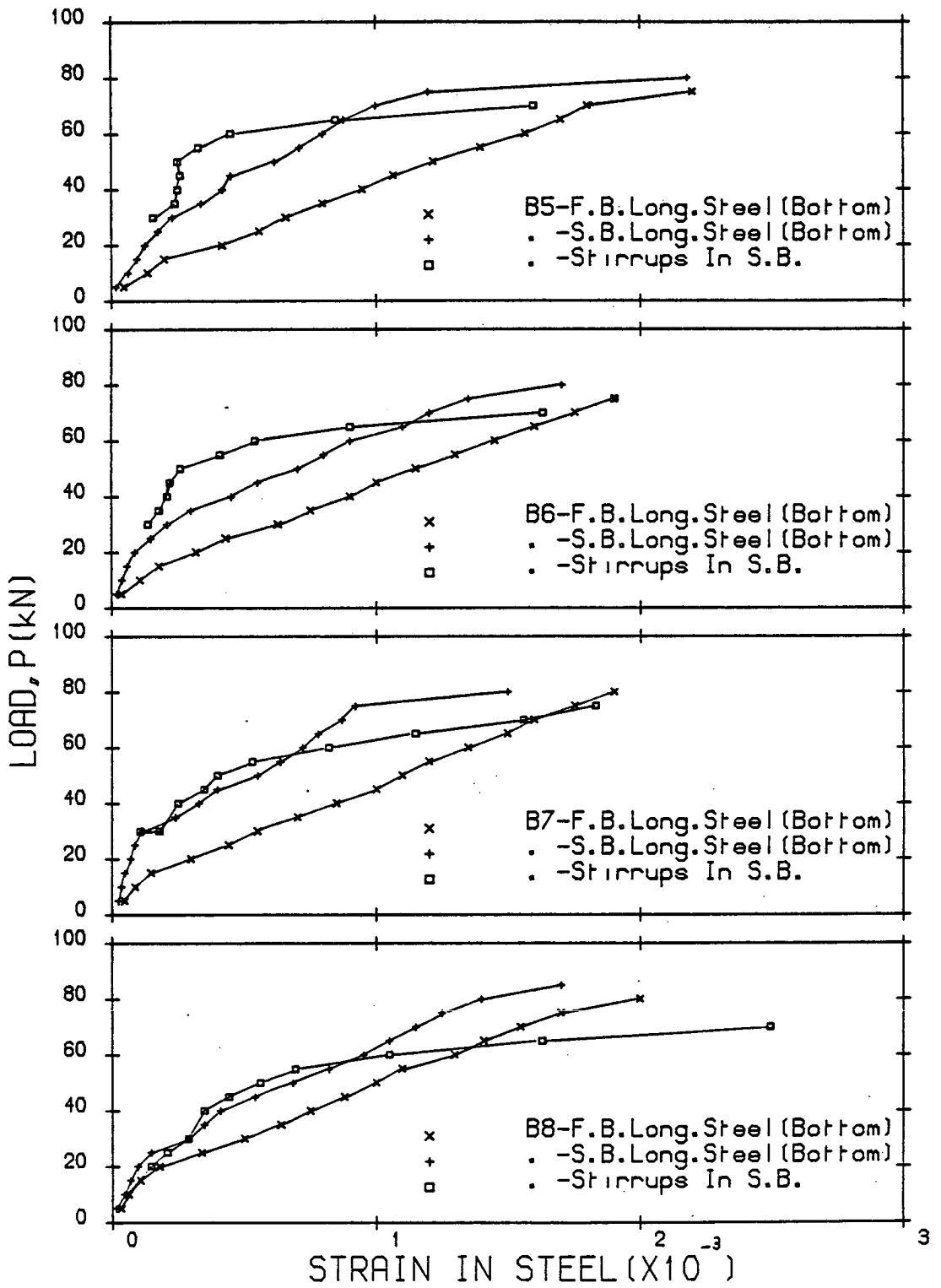


Figure 3.9(b) Load-Strain in Steel, GR2

compressive zone. Moreover stirrups are spaced to tie the longitudinal steel into the main bulk of the concrete and provide a restraint against the splitting of concrete along the longitudinal steel. The effect of stirrup spacing in the spandrel beams was observed by the occurrence of cracks. Cracking on the inner-side of the spandrel beam tended to move closer to the joint as the spacing of the stirrups was increased without effecting the joint integrity as shown in Plate 3.1.

To reach the ultimate torsional capacity stirrups must be so spaced to make sure that any failure surface will intersect a sufficient number of stirrups. However the ultimate torsional capacity may not be reached if a flexural failure in the floor beam takes place. The spandrel beam will then fail due to twist allowing the stirrups to yield sufficiently. This was true for beams under high shear and torsion.

Another significant effect of the confinement of beams sections under flexure, will be discussed in Chapter 4.

3.4.4 Length of the Spandrel Beam

The length of the spandrel beams in group GR2 was shorter than those in group GR1 (i.e. $L_s = L_f/2$).

This may simulate an edge spandrel beam in which shear and torsion are expected to be high. The test measurements confirm that cracks in beams of GR2 were wider than those of GR1, also spandrel beams of group GR2 deflected less than those in group GR1, as shown in Figure 3.1(c).

Figures 3.8(a) and (b) show the load-angle of twist curves; evidently the angle of twist for the beams in GR2 was greater than those

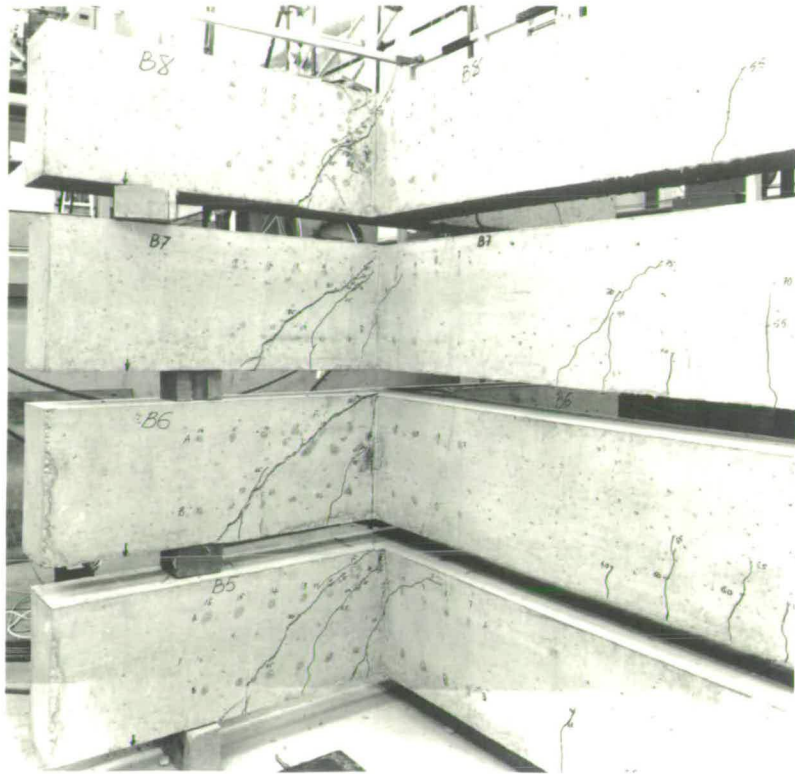


Plate 3.1(a) Spandrel Beams of Group GR2



Plate 3.1(b) Floor Beams of Group GR2

in GR1. In other words the angle of twist is larger when the ratio $\frac{L_f}{L_s}$ is large i.e. angle of twist increases as the spandrel beam length is shortened.

3.4.5 Concrete Strength

The concrete strength varied from 30 N/mm^2 to 40 N/mm^2 in the test specimens. It was observed that the concrete strength has a significant effect on the crack development. The tensile strength of concrete is very much related to the concrete strength, hence the cracking load. The ultimate strength of the beams whether in flexure or torsion is affected too. This will be discussed later.

3.4.6 Joint Detailing

In order to investigate the detailing of the reinforcing bars at the joint, two beams GR5-C1 and C2 were designed to fail at the joint. No stirrups were provided to resist torsional and shear stresses. The aim was to find the failure surface or the critical section within which stirrups could be provided to resist shear and torsional stresses, as was studied by Hsu and Burton [40].

Specimens GR5-C1 and C2 were designed by method (D) ($T_u = 0$), with the floor beam longitudinal steel placed on top of the spandrel beam longitudinal steel at the joint. The general behaviour of the test specimens is already discussed in Chapter 3; the failure surface can be seen in Plate 3.2.

After taking the necessary measurements, it was found that the failure surface consisted of a horizontal plane and two inclined planes. The total horizontal projection at the level of the bottom longitudinal steel was $(= b_f + 2 d_s)$ as shown in Figure 3.10.

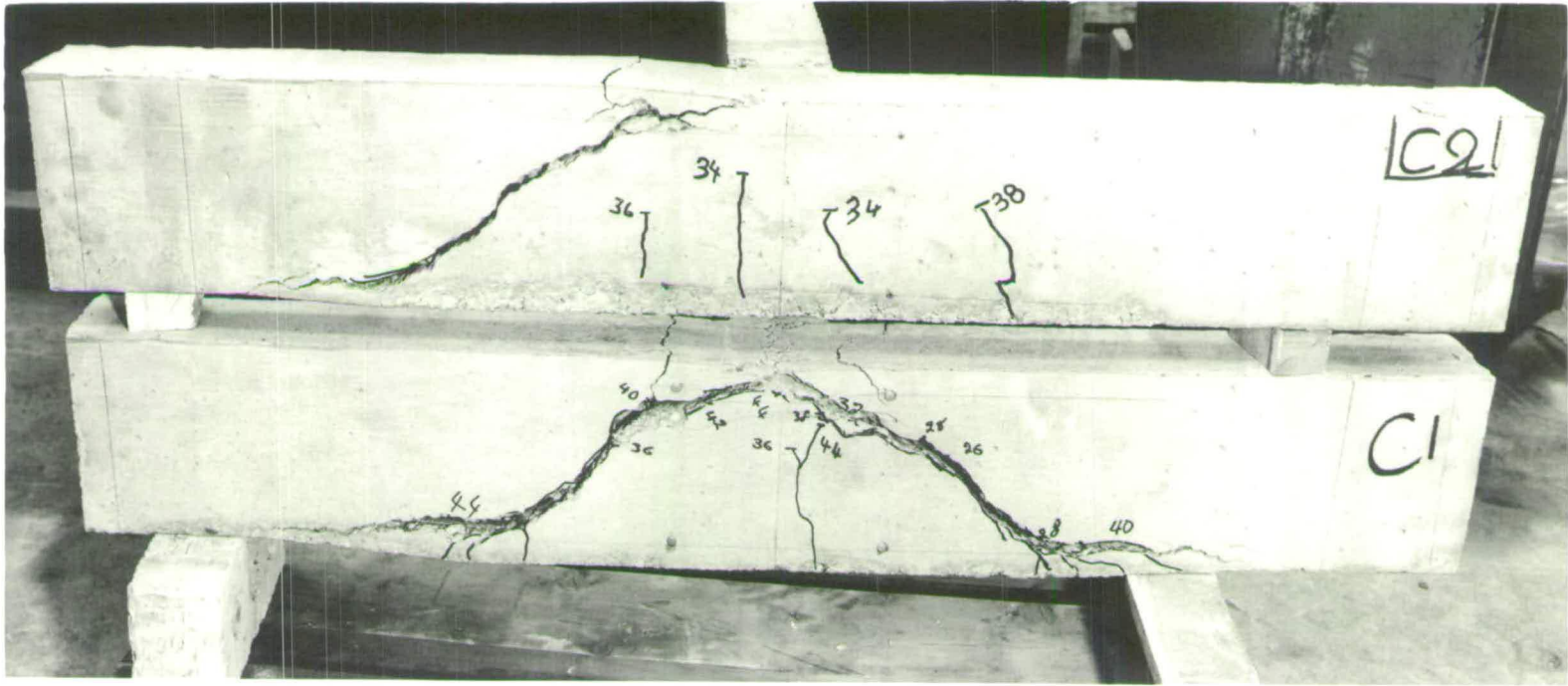


Plate 3.2 Specimens of Group GR5 (back view)

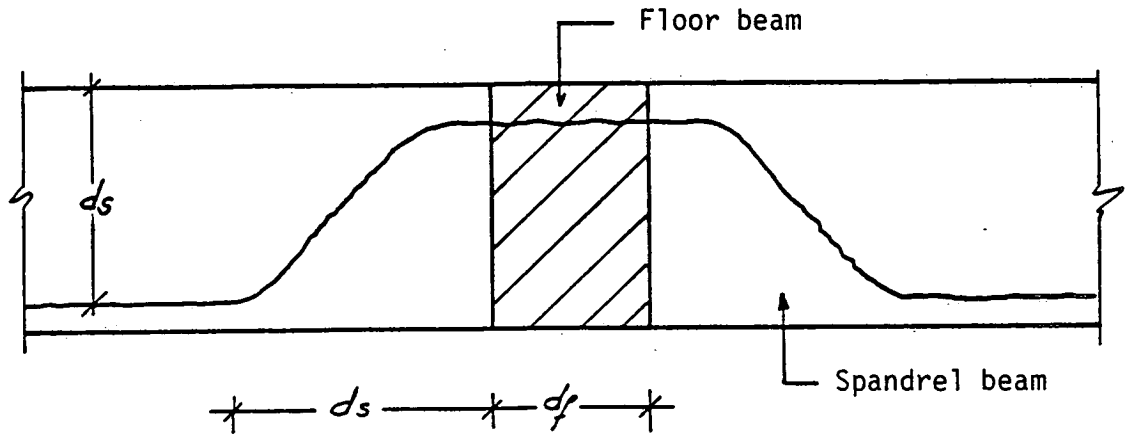
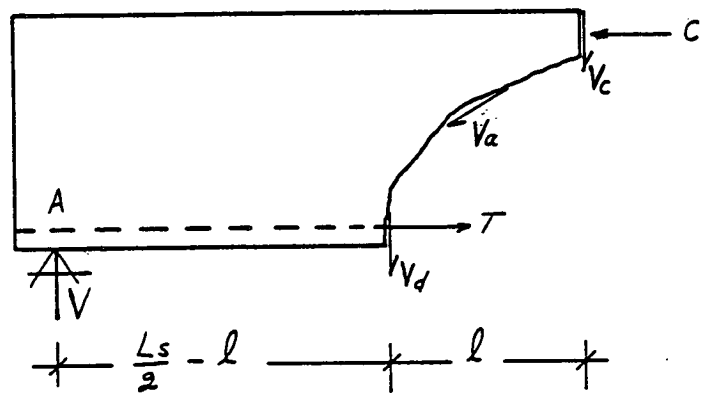


Figure 3.10 Failure Surface



$$V = V_a + V_d + V_c$$

V_c = shear in compression area

V_a = aggregate interlock

V_d = dowel action

V = reaction at A

l = half of the horizontal projection of the failure surface

L_s = length of the spandrel beam

Figure 3.11 Free Force Diagram of the Failure Surface

Specimen GR5-C2 was designed in the same manner as C1 to determine whether extra negative steel at the joint would affect the behaviour of the joint and hence the failure surface. Two extra 6 mm steel bars were provided as negative steel in the floor beam at the joint, each extending in one direction into the spandrel beam.

The failure surface and behaviour were the same as C1, as shown in Plate 3.2. To avoid ^{the} type of failure observed in GR5-C1 and C2, stirrups must be provided near the joint within the distance of (d_s) from both sides of the joint. The number of stirrups required should be sufficient to carry the reaction from the floor beam and so prevent this type of failure, i.e.:

$$\frac{b_f + 2 d_s}{s} = \frac{V_u}{2 A_v \cdot f_{wy}} \quad (3.6)$$

where b_f = width of the floor beam section

d_s = depth of the spandrel beam section

V_u = the ultimate force transferred from the floor beam to spandrel beam

A_v = area of one leg of one stirrup

f_{wy} = yield strength of a stirrup

s = spacing of stirrups.

A series of calculations were carried out to predict the length of the horizontal projection of the failure surface. Different values were taken from literature for various values of shear in the compression area, the dowel action and aggregate interlock for this purpose as shown in Figure 3.11. It was found that in all cases,

the length of the horizontal projection of the failure surface was not less than $2 d_s + d_f$ which justifies the experimental results.

It is interesting to mention here that the joint failure reported by Collins and Lampert [39] is not a joint failure in this sense. The specimens which were reported to have failed at the joint were designed according to Leonhardt's recommendations, i.e. placing as closely spaced stirrups as possible to ensure full transmission of the reaction from the floor beam. A closer examination of the specimen photographs in the report revealed that the specimen failed by shear near the joint. The joint suffered spalling of concrete because of the number of reinforcing bars used at the joint without adequate provision for bond.

Joint failure was not observed in any of the beams tested with special reference to beams GR1-B4, GR2-B8, GR3-A4 and GR4-B4 in which stirrups were nominally spaced.

At this stage a safe detailing arrangement for the reinforcing bars at the joint can be made by:

1. Placing the floor beam longitudinal steel on top of the spandrel beam longitudinal steel.
2. Satisfying equation 3.6.



CHAPTER 4 : ANALYTICAL FORMULATION FOR FLEXURAL ULTIMATE STRENGTH

- 4.1 Introduction
- 4.2 Section Under Flexural Compression
 - 4.2.1 Stress-Strain Relationship for Concrete
 - 4.2.2 Initial Modulus of Elasticity
 - 4.2.3 Strain at Maximum Stress
 - 4.2.4 Ultimate Strain at Failure
 - 4.2.5 Comparison of Various Stress-Strain Relationships
- 4.3 Stress Block Parameters for a Section Under Flexure
- 4.4 Flexural Strength of Confined Section
- 4.5 Biaxial Stress-Strain Relationship for Concrete
- 4.6 Flexural Resistance Prior to Cracking

4.1 Introduction

In this chapter the flexural strength of the floor beam is analysed and based on the assumptions that the contribution of concrete in the tension zone is not significant and the Bernoulli-Navier hypothesis that a plane section remains plane after bending and thus strain is linearly proportional to its distance from the neutral axis. The stress-strain curve for the tensile reinforcement is considered sufficient for the analysis for the zone section in tension.

4.2 Section Under Flexural Compression

In the analysis of a reinforced concrete section, an evaluation of the stress block parameters and hence the ultimate strength of the concrete section under flexural compression is required. Therefore the following factors must be considered:

1. Stress-strain relationship of concrete.
2. Modulus of elasticity.
3. Strain at maximum stress.
4. Ultimate strain at failure.

To evaluate the above factors experimentally, a series of tests were carried out on (100 x 100 x 500 mm) concrete prisms. The prisms were cast from the same batch of concrete as that already prepared for the beams, and were tested at different ages to achieve a specific strength. The concrete strength was assessed by testing six cylinders for each type of concrete.

The true strain of the concrete can be measured only over the

regions of uniform strain. The concept of strain measurement which assumes that the material composition is homogeneous can not be fully satisfied due to the fact that concrete is a multiphase material. Particle size influences its homogeneity and therefore the strain measurement. However Hanson and Kurvits [53] recommended that the strain gauge length should not be less than 3 times the maximum particle size. Thus for 10 mm maximum particle size, the minimum gauge length should be 30 mm. For this purpose electrical strain gauges, type FLA-30-11 and 30 mm in length, were fixed on two adjacent sides of the section. Demec points were also fixed on the other two sides to give an additional check on the measured strains. Loading and strain measurement were carefully controlled so that a continuous record of loads and strains was obtained up to ultimate failure using a data logger.

The maximum compressive strength of a concrete prism is represented by the cylinder strength ($f_o = f_c'$).

4.2.1 Stress-Strain Relationship for Concrete

The definition of the concrete stress-strain relationship is a basic requirement for the sectional analysis. The stress-strain relationship of concrete is influenced by a number of factors thus it may not be possible to define the relationship by one approach. Since early investigations several different hypotheses and approaches have been employed in this area, and as a result various relationships have been proposed. Some of them differ only in detail, others significantly depending mainly on how the factors affecting the stress-strain relationship of concrete can be controlled.

In the last three decades, most theories have taken into consideration the inelasticity of concrete and many expressions and curves have been proposed to define the relationship in terms of both the elastic and inelastic behaviour of concrete.

Attempts were also made to simplify the relationship and approximate the stress-strain curve to employ it in a sectional analysis. The shapes of the curve has varied between a triangle, rectangle and trapezoid and some been widely adopted by codes of practice for many countries.

The shape of the stress-strain curve is highly affected by the duration of load and rate of straining, and is associated with the mechanism of internal progressive microcracking. For stress in the region up to 30 percent of f_c' the existing cracks in concrete remain nearly unchanged. The internal energy is less than the energy required to create new microcrack surfaces. A stress level of about 30% has been proposed as the limit of elasticity [54]. At stress levels between $0.3 f_c' - 0.5 f_c'$, the stress concentration around the crack tips makes the bond cracks start to extend. At this stage the internal energy is nearly balanced by the required crack release energy. Crack lengths reach their final values and crack propagation may be considered stable as long as the applied stress is constant. At stress levels between $0.5 f_c' - 0.75 f_c'$, bond cracks continue to grow slowly and cracks at aggregate surface start to bridge in the form of mortar cracks. At this stage, while keeping the load constant the cracks continue to propagate at a decreasing rate up to their final lengths. Beyond a stress level of $0.75 f_c'$ the critical crack lengths are reached. The required crack-release energy is now less than the internal energy resulting in an increase in the crack propagation which at this stage can be considered

unstable.

The progressive failure of concrete at f_c' is caused by microcracks in the mortar, joining up with bond microcracks at the surfaces near to the aggregate and causing internal damage. Damage to material continues with increasing compressive strain. This represents the descending portion of the stress-strain curve [55]. This theory of internal crack propagation provides no more than a general description of stress-strain relationship. However this has led to a better understanding of the behaviour of the structural concrete section.

The ultimate moment capacity of a reinforced concrete section is not highly affected by the exact shape of the stress-strain curve, but the stress-strain behaviour must be accurately defined in the compatibility criteria associated with any design procedure.

The numerical approximation and the empirical formulae that have been proposed have limits of validity and acceptable degree of accuracy. Hence their application is restricted.

Hognestad [24] proposed the following stress-strain relationship for concrete under flexural compression which is still widely used by many investigators, Figure 4.1:

$$\frac{f}{f_0} = 2\left(\frac{\epsilon}{\epsilon_0}\right) - \left(\frac{\epsilon}{\epsilon_0}\right)^2 \quad \text{for } \epsilon \leq \epsilon_0 \quad (4.1a)$$

$$\frac{f}{f_0} = \frac{\epsilon_U - 0.85 \epsilon_0 - 0.15 \epsilon}{\epsilon_U - \epsilon_0} \quad \text{for } \epsilon > \epsilon_0 \quad (4.1b)$$

Sahlin [56] and Smith and Young [57] proposed the following exponential expression to represent the stress-strain relationship

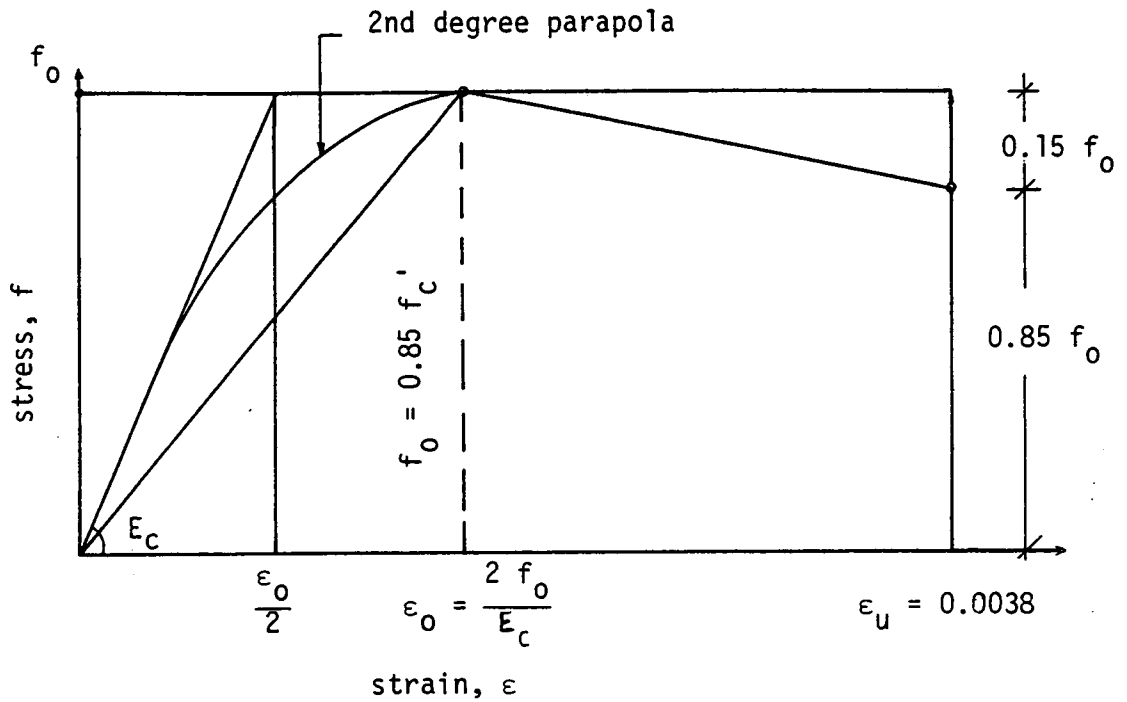


Figure 4.1 Stress-Strain Diagram in Flexure
(Hognestad) [24]

of concrete under flexural compression:

$$\frac{f}{f_0} = \left(\frac{\epsilon}{\epsilon_0}\right) e^{\left(1 - \frac{\epsilon}{\epsilon_0}\right)} \quad (4.2)$$

Sahlin used a value of 0.002 for ϵ_0 , Smith and Young assumed that $f_0 = f'_c$ and $\epsilon_0 = 0.0017$ to 0.002.

In more recent investigations into the concrete strength and deformation properties, a complete and general stress-strain relation-

ship has been emphasized. Also, the development of new testing machines has helped to obtain a complete set of stress-strain curves for a wide range of strain rates and sustained loadings.

Strain controlled and electrically programmed testing equipment was used by Rüsç [58] to obtain a complete stress-strain curve and to investigate the strength and deformation properties of concrete. It was proposed that by using the stress-strain curves of concentrically loaded concrete prisms, the stress distribution in the compressive zone in flexure can be determined.

A simple and practical stress-strain relationship was proposed and adopted by CEB [59]:

$$\frac{f}{f_0} = 2 \left(\frac{\epsilon}{\epsilon_0} \right) - \left(\frac{\epsilon}{\epsilon_0} \right)^2 \quad \text{for } \epsilon < \epsilon_0 \quad (4.3a)$$

$$f = f_0 \quad \text{for } \epsilon_0 \leq \epsilon \leq \epsilon_u \quad (4.3b)$$

where $\epsilon_0 = 0.02$, $f_0 = f_c'$ and $\epsilon_u = 0.0035$.

Another recognizable expression for the concrete stress-strain relationship is in the form of a polynomial equation, i.e.:

$$\frac{f}{f_0} = A \left(\frac{\epsilon}{\epsilon_0} \right) + B \left(\frac{\epsilon}{\epsilon_0} \right)^2 + C \left(\frac{\epsilon}{\epsilon_0} \right)^3 + D \left(\frac{\epsilon}{\epsilon_0} \right)^4 \quad (4.4)$$

where A, B, C and D are constants,

f = compressive stress at any strain,

f_0 = maximum stress in concrete,

ϵ = strain in concrete,

ϵ_0 = strain at maximum stress, f_0 .

In these polynomial forms, the maximum value of $(\frac{f}{f_0})$ occurs at $\frac{\epsilon}{\epsilon_0} = 1.1$ and since the stress block parameters are determined by integration, this may not be significant when the assumed function is compared with the experimental results. Kabaila [60] has shown that the polynomial of equation 4.4 gives a satisfactory fitting to the stress-strain curve up to a strain range of three times, ϵ_0 .

A concrete stress-strain relationship of polynomial form for different types of concrete can be obtained by evaluating the coefficients A, B, C and D in equation 4.4 from experimental results to get the best fit. The following stress-strain relationship can be proposed as an example:

$$\frac{f}{f_0} = 2.28 \left(\frac{\epsilon}{\epsilon_0}\right) - 1.76 \left(\frac{\epsilon}{\epsilon_0}\right)^2 + 0.5 \left(\frac{\epsilon}{\epsilon_0}\right)^3 - 0.04 \left(\frac{\epsilon}{\epsilon_0}\right)^4 \quad (4.5)$$

A simple form to represent the concrete stress-strain relationship was introduced by Desayi and Krishnan [61] in the following equation:

$$f = \frac{E_c \epsilon}{1 + \left(\frac{\epsilon}{\epsilon_0}\right)^2} \quad (4.6)$$

where $E_c = 2 \frac{f_0}{\epsilon_0}$ and $f_0 = f_c'$

To use equation 4.6 the value of ϵ_0 and the corresponding stress must be known. They assumed a value of $\epsilon_u = 0.003$ and a corresponding stress equal to $(7/8 f_c')$. Equation 4.6 gives a good agreement with the test results only up to a concrete strength of 40 N/mm^2 . The problems involved in the formulation of concrete stress-strain relationship were described by Saenz [62]. Two expressions were given; one which represents reasonably well the ascending portion of the curve;

the other to predict the descending portion as well. To combine the two expressions the following equation was proposed:

$$f = \frac{\epsilon}{A + B \epsilon + C \epsilon^2 + D \epsilon^3} \quad (4.7)$$

coefficients A, B, C and D were to be determined by satisfying the basic conditions of the stress-strain curve. Tulin and Gerstle [63], using their own experimental results, proposed the following equation for the concrete stress-strain relationship:

$$f = \frac{E' \epsilon}{a + \left(\frac{\epsilon}{\epsilon_0}\right)^b} \quad \text{where } E' = (a + 1) \frac{f_0}{\epsilon_0} \quad (4.8)$$

The coefficients a and b are to be adjusted to obtain the best fit of the experimental results. In their case it was found that $a = 2$ and $b = 3$.

In any mathematical model to represent the stress-strain curve of concrete under compression, the following conditions must be satisfied:

1. $f = 0$ at $\epsilon = 0$ (point of origin).
2. $\frac{df}{d\epsilon} = E_c$ at $\epsilon = 0$ (slope of the stress-strain curve at the origin equals, by definition the modulus of elasticity).
3. $f = f_0$ at $\epsilon = \epsilon_0$ (point of maximum stress, $\frac{df_0}{d\epsilon_0} = 0$).
4. As far as the descending portion is concerned the analytical curve must satisfy the experimental results and at least one experimental point must fall on the curve.

In order to propose a concrete stress-strain relationship to be used in this study, equation 4.6 may be represented by the following general form:

$$f = \frac{\epsilon}{A + B \epsilon^n} \quad (4.9)$$

Satisfying the basic conditions for the stress-strain curve, the coefficients A, B and n can be determined where

$$A = \frac{1}{E_c}, \quad B = \frac{R-1}{\epsilon_0^n E_c} \quad \text{and} \quad n = \frac{R}{R-1}$$

where $R = \frac{E_c}{E_0}$, $E_0 = \frac{f_0}{\epsilon_0}$ (secant modulus)

Thus equation 4.9 becomes:

$$\frac{f}{f_0} = \frac{R \frac{\epsilon}{\epsilon_0}}{1 + (R-1) \left(\frac{\epsilon}{\epsilon_0}\right)^n} \quad (4.10)$$

Equation 4.10 is less complicated and more suitable for practical use due to the fact that failure strain is not defined in the equation. However the ultimate strain at failure (regarding the descending portion of the curve), and the strain at maximum stress, ϵ_0 , are defined by some empirical relationships based on the experimental results.

The following equation can be derived *similarly* by satisfying the basic conditions of a stress-strain curve in the same manner as equation 4.10:

$$\frac{f}{f_0} = R \left(\frac{\epsilon}{\epsilon_0}\right) + (1-R) \left(\frac{\epsilon}{\epsilon_0}\right)^n \quad (4.11)$$

Equations 4.3(a) and 4.3(b) are special cases of equation 4.11 where $R = 2$.

4.2.2 Initial Modulus of Elasticity, E_c

A considerable amount of work has been carried out on the modulus of elasticity of concrete and a number of relationships have been proposed. Modulus of elasticity is highly dependent on the various following factors; type of aggregate, water/cement ratio, aggregate/cement ratio, curing, age and rate of loading. Similarly, those factors affect the compressive strength of the concrete, thus it is convenient to express the concrete properties as a function of the compressive strength.

The most commonly used relationships are shown below and will be compared with the one to be adopted in this study.

The value of E_c , suggested by ACI [49] is:

$$E_c = 33 \sqrt[3]{w^3 f_c'} \quad (4.12)$$

where w = density of concrete in (lb/ft³)

f_c' = cylinder strength of concrete (psi)

E_c = in (psi)

For normal weight concrete equation 4.12 becomes:

$$E_c = 57,000 \sqrt{f_c'} \quad (4.12a)$$

and in terms of the cube strength of concrete equation 4.12 becomes:

$$E_c = 50,000 \sqrt{f_{cu}} \quad (4.12b)$$

where f_{cu} = cube compressive strength of concrete in (psi). However equation 4.12b can be approximately represented as:

$$E_c = 4.78 \sqrt{f_c'} \quad (4.12c)$$

where E_c , f_c' are in kN/mm^2 and N/mm^2 respectively.

The CEB [50] suggest the following value:

$$E_c = 70,000 \sqrt{f_{cu}} \quad E_c, \text{ in (psi)}$$

f_{cu} = characteristic strength of concrete in (psi), E_c = in (psi).

This relationship can be represented in the following form with E_c in kN/mm^2 , f_c' in N/mm^2 ; the value of f_{cu} is substituted by f_c' ($f_c' = 0.78 f_{cu}$):

$$E_c = 6.58 \sqrt{f_c'} \quad (4.13)$$

Saenz [62] used another expression for E_c which can be represented by the following equation:

$$E_c = \frac{8.3 \sqrt{f_c'}}{1 + 0.07 \sqrt{f_c'}} \quad (4.14)$$

where E_c and f_c' are in kN/mm^2 and N/mm^2 respectively.

The value of E_c given in CP110, 1972 is

$$E_c = 4.5 \sqrt{f_{cu}} \quad \text{in } \text{kN/mm}^2$$

when $\rho \geq 2300 \text{ kg/m}^3$ and

$$E_c = 0.85 \rho^2 \sqrt{f_c} \times 10^{-6}$$

when (density ρ) is between $1400 - 2300 \text{ kg/m}^3$.

Some of the test results were produced by Beeby [48] and show a considerable scatter as shown in Figure 4.2. Also the relationship represented by equations 4.12, 4.13 and 4.14 are plotted in Figure 4.2.

It is clear therefore that the values of E_c given by CP110 and CEB are less reasonable than those given by ACI. On the other hand, Saenz's equation gives higher values for concrete of low strengths leading to a higher value of $R = \frac{E_c}{E_0}$. The following equation gives a reasonable presentation of the test results and as such will be adopted in this study:

$$E_c = 5.5 \sqrt{f_c} \quad (4.15)$$

The values of E_c are compared in Table 4.1.

4.2.3 Strain at Maximum Stress, ϵ_0

The position of the peak point in the stress-strain curve is highly affected by the compressive strength, loading rates and strain gradient. However by keeping the strain rate and duration of load constant the peak point may be considered stable and its coordinates can be defined in terms of the concrete strength.

Various relationships have been proposed to express the strain, ϵ_0 , at maximum stress, f_0 . These were reviewed by Popovics [64] as

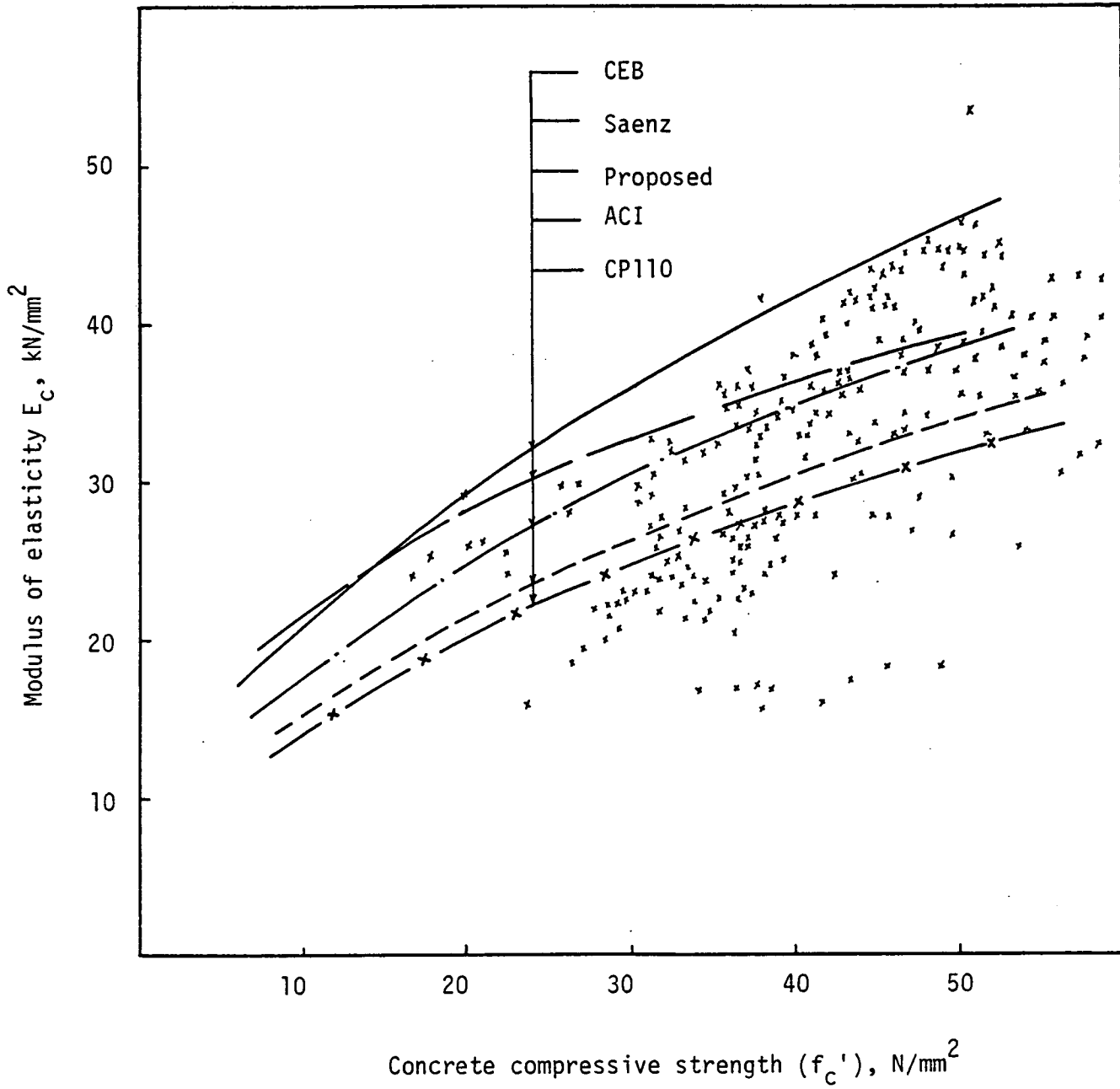


Figure 4.2 E_c , against f_c'

Table 4.1 Modulus of Elasticity, E_c

f_c' N/mm ²	E_c , kN/mm ²				
	ACI Eq. (4.12c)	CEB Eq. (4.13)	Saenz Eq. (4.14)	CP110, 1972	Proposed Eq. (4.15)
20	21.4	29.4	28.3	20.12	24.60
25	23.9	32.9	30.7	22.5	27.5
30	26.2	36.0	32.9	24.65	30.12
35	28.3	38.6	34.7	26.6	32.53
40	30.2	41.6	36.4	28.5	34.78
45	32.06	44.14	37.88	30.2	36.89

illustrated in Figure 4.3. The value of ϵ_0 is expressed by the following relationship in terms of concrete compressive strength:

$$\epsilon_0 = 0.875 \times 10^{-3} (f_0)^{\frac{1}{4}} \quad (4.16)$$

where $f_0 = f_c'$ (N/mm^2)

The values of ϵ_0 obtained by equation 4.16 are compared with experimental values in Table 4.2 and with other relationships suggested by other investigators in Figure 4.3.

4.2.4 Ultimate Strain at Failure ϵ_u

Only in 1942, complete stress-strain curves for concrete were reported by Whitney [23]. Tests were carried out on concrete cylinders; it was concluded that the flexibility of testing machines was the main cause of concrete brittle failure.

The difficulty of measuring the strain at failure experimentally has led some investigators to assume certain values for ϵ_u .

Using the testing machines available, the descending portion of stress-strain curve is indeed difficult to obtain. That is why it was necessary to test six prisms and six cylinders with continuous record of stress and strain readings during the test beyond the maximum stress until failure. The number of specimens tested may not be enough to cover the factors involved in the problem, nevertheless, they do serve the purpose.

The value of ultimate strain at failure may be obtained by the following relationship:

$$\epsilon_u = \frac{7.8 \times 10^{-3}}{(f_0)^{\frac{1}{4}}} \quad (4.17)$$

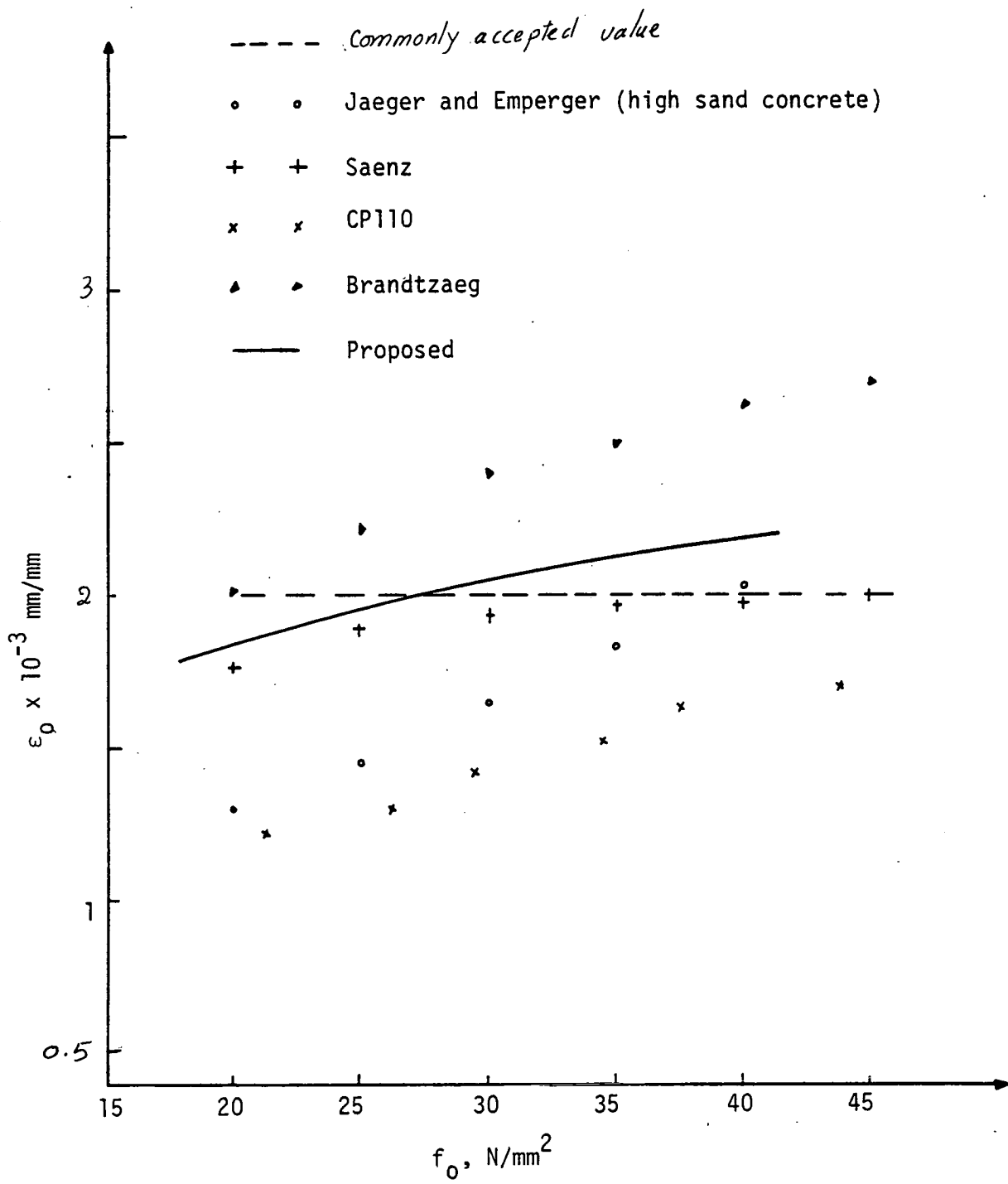


Figure 4.3 Comparison of Various Relationships for Strain at Maximum Stress

Table 4.2 Stress-Strain Parameters

f_c' N/mm ²	$\epsilon_0 = \times 10^{-3}$		$\epsilon_u = \times 10^{-3}$		$\frac{\epsilon_u}{\epsilon_0}$ Eq. (4.18)	$E_0 = \frac{f_0}{\epsilon_0}$ kN/mm ²	E_c Eq. (4.15) kN/mm ²	$R = \frac{E_c}{E_0}$
	*Experimental	Eq. (4.16)	*Experimental	Eq. (4.17)				
20	1.85	1.85	3.6	3.68	1.99	10.81	24.59	2.27
25	1.95	1.96	3.4	3.48	1.78	12.71	27.5	2.15
30	2.05	2.05	3.3	3.33	1.62	14.63	30.12	2.05
35	2.10	2.13	3.2	3.2	1.5	16.43	32.54	1.98
40	2.20	2.20	3.1	3.10	1.4	18.18	34.78	1.91

* Average of six prism tests

average R = 2.0

E_0 = secant modulus

ϵ_u = ultimate strain at failure

From equations 4.16 and 4.17:

$$\frac{\epsilon_u}{\epsilon_o} = \frac{8.9}{(f_o)^{\frac{1}{2}}} \quad (4.18)$$

$$f_o = f_c' \text{ (N/mm}^2\text{)}$$

The value of ϵ_u obtained by equation 4.17 are compared with the experimental values in Table 4.2. Stress-strain curves are shown in Figure 4.4.

4.2.5 Comparison of Various Stress-Strain Relationships

In section 4.2.1, various concrete stress-strain relationships are reported with their application and limitation as well as the factors that affect the shape of the stress-strain curve.

The stress-strain experimental results based on testing six concrete prisms and six cylinders for each type of concrete, are in Tables 4.2, 4.3 and Figure 4.4. Also the stress-strain values obtained from equation 4.10 are shown in Table 4.4.

The stress-strain curves represented by equations 4.5 and 4.10 are compared with the test results in Figure 4.5. The curve represented by equation 4.5 does not agree well with experimental results especially the ascending portion; in fact this is due to the difficulty of finding a polynomial equation that would fit all the curves, as it is very easy to fit a particular curve for a particular type of concrete.

It is obvious now, that the curve represented by equation 4.10 is in good agreement with the test results; therefore the stress distribution in concrete under flexural compression can be represented by adopting equation 4.10.

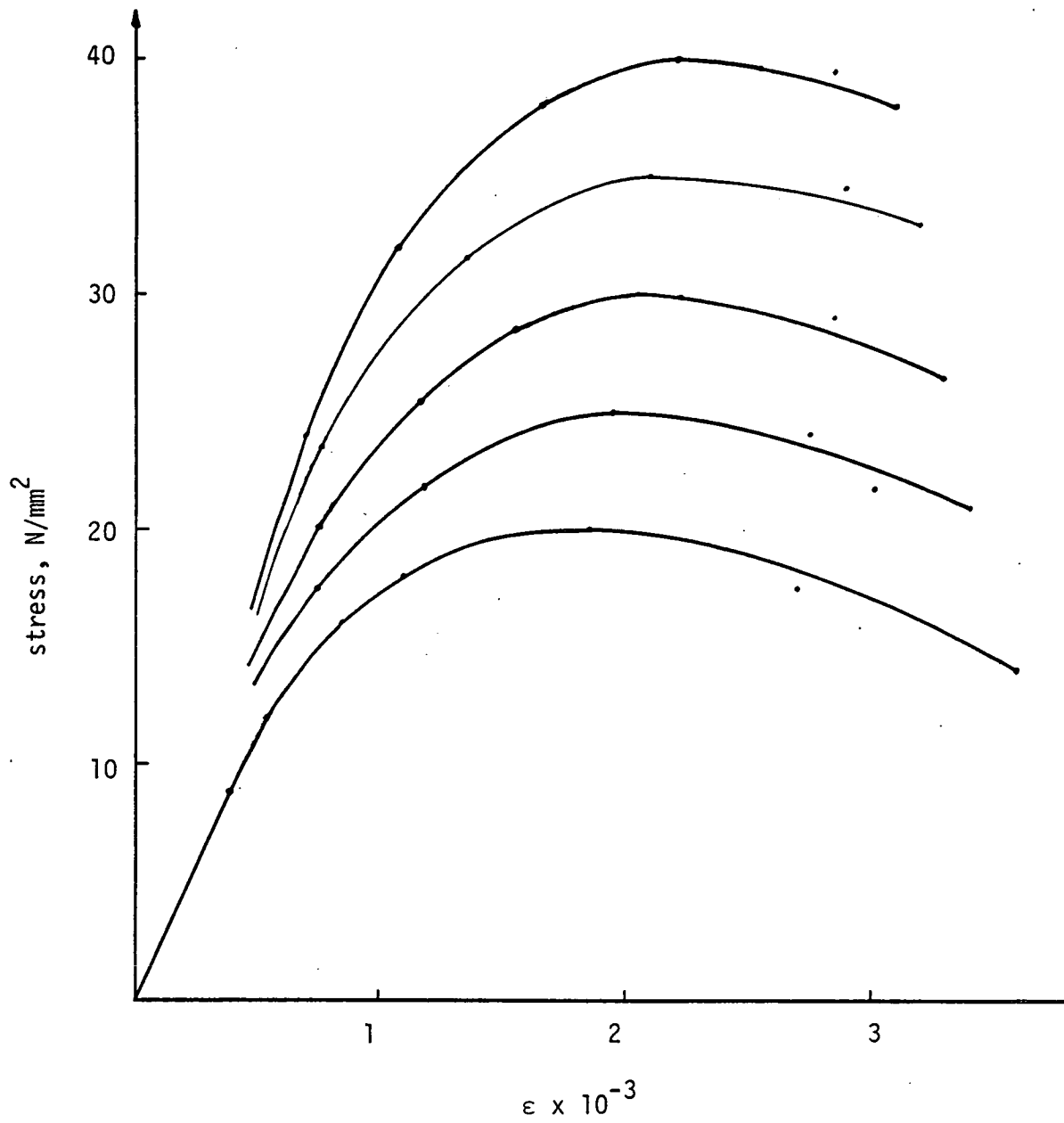


Figure 4.4 Experimental Stress-Strain Curves

Table 4.3 *Experimental Stress-Strain Relationships

$f_o = 20 \text{ N/mm}^2$		$f_o = 25 \text{ N/mm}^2$		$f_o = 30 \text{ N/mm}^2$		$f_o = 35 \text{ N/mm}^2$		$f_o = 40 \text{ N/mm}^2$	
$f \text{ N/mm}^2$	$\epsilon \times 10^{-3}$	$f \text{ N/mm}^2$	$\epsilon \times 10^{-3}$	$f \text{ N/mm}^2$	$\epsilon \times 10^{-3}$	$f \text{ N/mm}^2$	$\epsilon \times 10^{-3}$	$f \text{ N/mm}^2$	$\epsilon \times 10^{-3}$
9.0	0.40	13.6	0.5	15.0	0.5	18.0	0.55	17.4	0.5
12.0	0.55	17.5	0.75	20.0	0.75	23.5	0.77	24.0	0.71
16.0	0.85	22.0	1.20	23.0	0.95	31.5	1.35	32.0	1.07
18.0	1.10	25.0	1.95	28.5	1.55	35.0	2.10	38.0	1.65
20.0	1.85	24.0	2.75	30.0	2.05	34.5	2.90	40.0	2.20
17.5	2.7	22.0	3.0	29.0	2.85	33.0	3.2	39.5	2.85
15.0	3.2	21.0	3.4	26.5	3.3			38.0	3.10
14.0	3.6								

* Average of six concrete prism tests.

Table 4.4 Proposed Stress-Strain Relationship Equation 4.10

$\frac{\epsilon}{\epsilon_0}$	$f_o = 20 \text{ N/mm}^2$	$f_o = 25 \text{ N/mm}^2$	$f_o = 30 \text{ N/mm}^2$	$f_o = 35 \text{ N/mm}^2$	$f_o = 40 \text{ N/mm}^2$
	f	f	f	f	f
0.25	10.26	12.25	14.34	16.34	18.2
0.5	16.6	20.42	24.18	27.89	31.48
0.75	19.34	24.12	28.8	33.56	38.24
1.0	20.0	25.0	30.0	35.0	40.0
1.25	19.6	24.45	29.31	34.12	38.88
1.5	18.8	23.25	27.81	32.2	36.56
1.75	17.8	22.0	26.1	30.03	33.84
2.0	16.8	20.65	24.3	27.86	31.16

$$\frac{f'}{f_o} = \frac{\frac{E_c}{E_o} \left(\frac{\epsilon}{\epsilon_o}\right)^n}{1 + \left(\frac{E_c}{E_o} - 1\right) \left(\frac{\epsilon}{\epsilon_o}\right)^n}$$

where

$$n = \frac{\frac{E_c}{E_o}}{\frac{E_c}{E_o} - 1}$$

$$\epsilon_o = 0.875 \times 10^{-3} (f_o)^{\frac{1}{4}}$$

$$E_c = 5.5 \sqrt{f_c} \text{ kN/mm}^2$$

$$f_o = f_c' \text{ in N/mm}^2$$

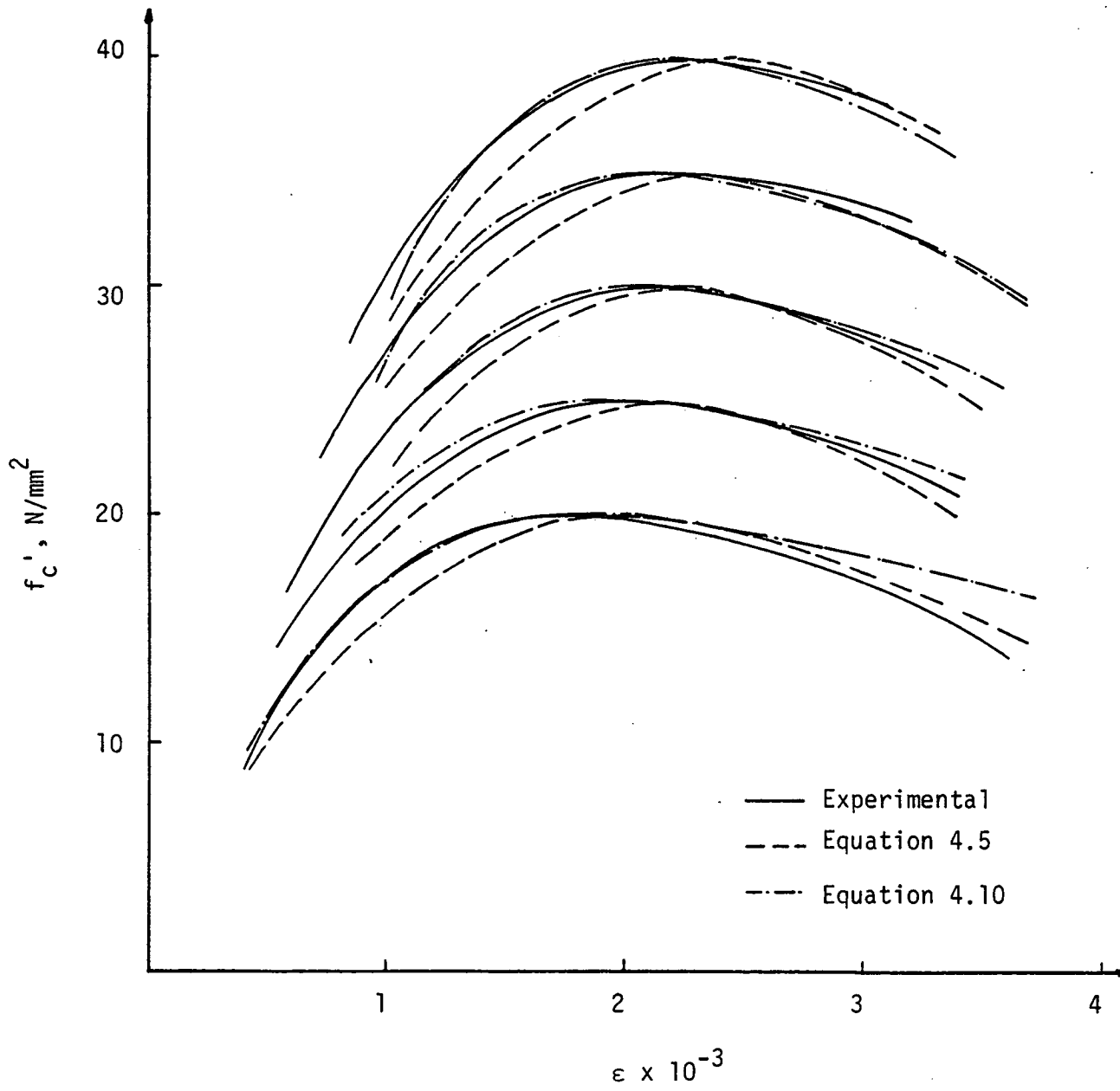


Figure 4.5 Comparison of Stress-Strain Curves

To bring a further simplification to equation 4.10, within the acceptable limits, $R (= \frac{E_c}{E_o})$ is taken as an average of $R = 2$ for all types of concrete as shown in Table 4.2. Equation 4.10 becomes:

$$\frac{f}{f_o} = \frac{2 \frac{\epsilon}{\epsilon_o}}{1 + (\frac{\epsilon}{\epsilon_o})^2} \quad (4.19)$$

which is of the same form as reported by Desayi and Krishnan [61] and Saenz [62] where $R = 2$. Furthermore good agreement was observed when compared with results obtained by the exponential expression of Smith and Young [57].

In Figures 4.6(a), (b), (c) and (d), the stress-strain curves of various types of concrete expressed by equation 4.10 and equation 4.5 are compared with experimental results.

From the reported and proposed relationships equation 4.19 is to be adopted in this study for the sectional analysis.

4.3 Stress Block Parameters for a Section Under Flexure

Jensen [22], in 1943, proposed a trapezoidal idealized stress distribution and derived the properties of this trapezoid as a function of the cylinder strength. The analysis was based on the ultimate strength of reinforced concrete beams. Whitney [23] approached the ultimate analysis by suggesting a rectangular stress distribution. Hognestad [24] reviewed many proposed idealizations for the stress distribution and then proposed a rectangular idealized stress distribution. Mattock et al [25] presented an ultimate strength design theory based on an equivalent rectangular stress distribution in the concrete compressive zone. This theory has been widely used for the ultimate analysis and

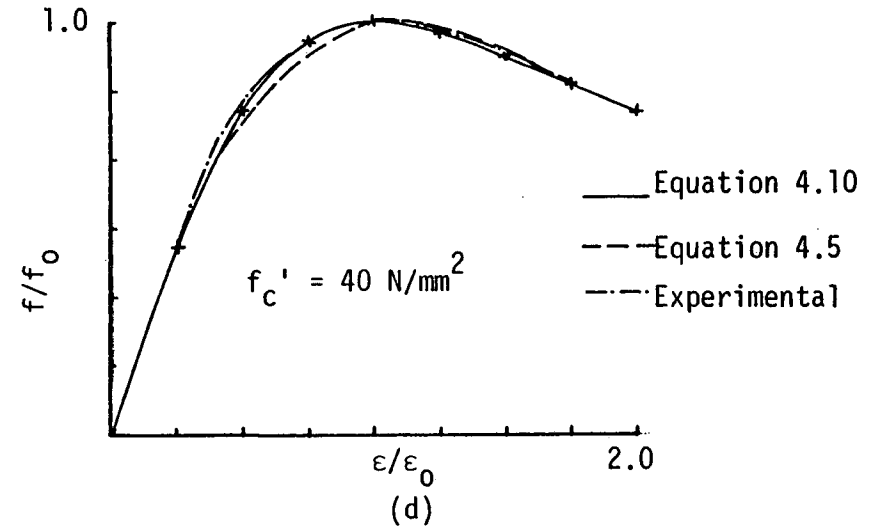
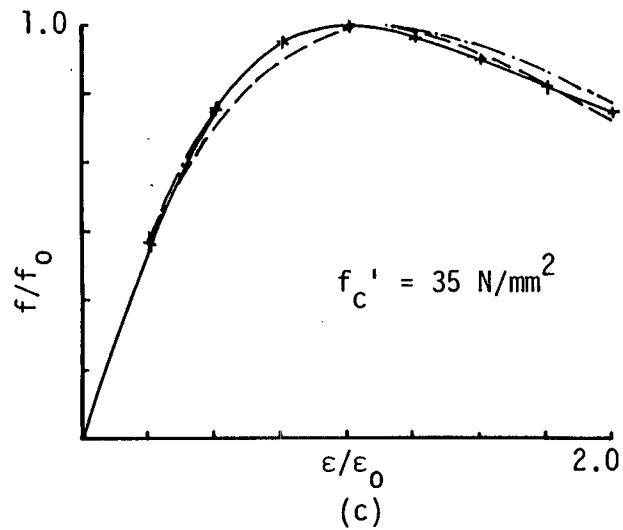
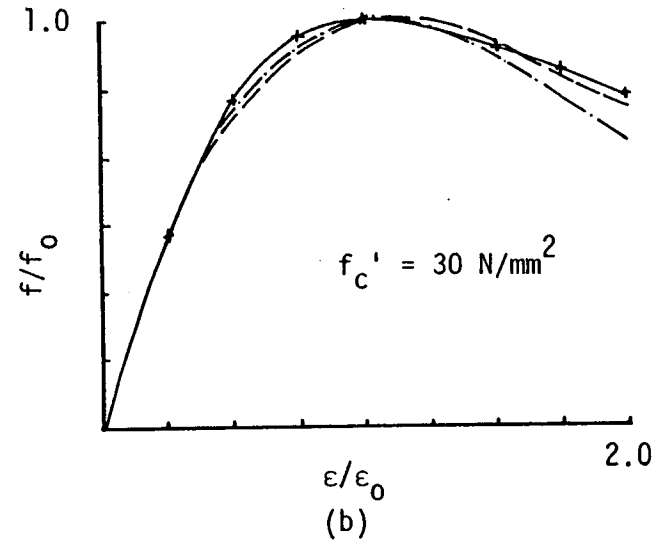
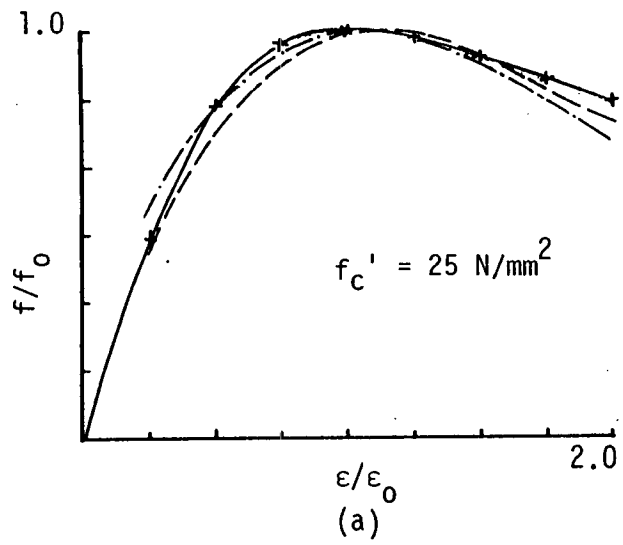


Figure 4.6 Comparison of Stress-Strain Curves of Various Types of Concrete

design of structural concrete members, and has been adopted by the ACI building code. However the following analysis to compute the theoretical ultimate moment capacity of the floor beams is more accurate and applicable to the types of floor beams tested in this study.

The section parameters, stress block and the strain distribution at ultimate stage are illustrated in Figure 4.7.

By taking moments, of the stress block shown in Figure 4.7(b) about the neutral axis:

$$(\bar{y}d) C_U = \int_0^{x_U d} y \cdot f \cdot b \cdot dy \quad (4.20)$$

where f = concrete stress at a distance y above the neutral axis,

$$f = f_0 \frac{2 \frac{\epsilon}{\epsilon_0}}{1 + \left(\frac{\epsilon}{\epsilon_0}\right)^2} \quad (4.19)$$

$x_U d$ = depth of the neutral axis from extreme compressive fibre, i.e. depth of concrete in compression,

$\bar{y}d$ = distance of the centre of the compression block from the neutral axis,

C_U = total compressive force.

The following relationship is obtained from Figure 4.7(c):

$$y = \frac{\epsilon}{\epsilon_U} (x_U d) \quad (4.21)$$

and
$$dy = \frac{x_U d}{\epsilon_U} \cdot d\epsilon \quad (4.22)$$

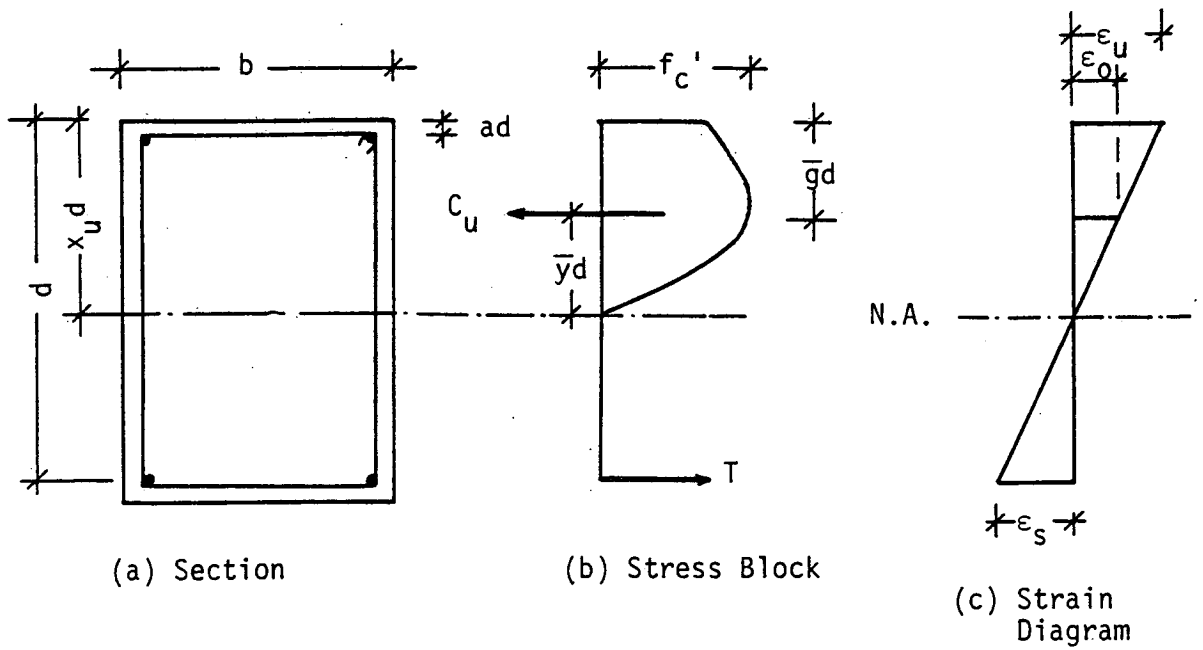


Figure 4.7 Stress Block and Strain Distribution of Reinforced Concrete Section at Ultimate

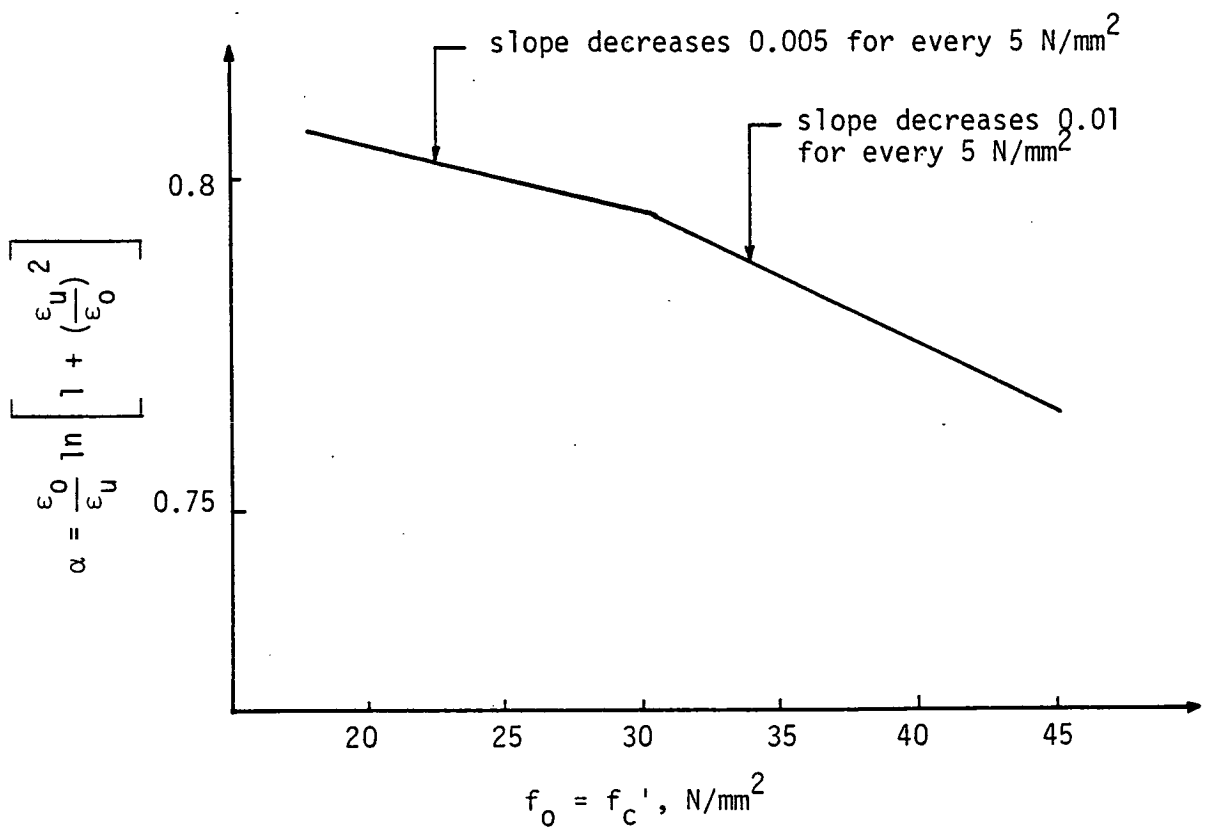


Figure 4.8 α verses f_0

Thus equation 4.20 becomes:

$$\begin{aligned}
 (\bar{y}d) C_u &= \int_0^{x_u^d} \left(\frac{\epsilon}{\epsilon_u}\right) x_u^d \cdot \left(\frac{2 \frac{\epsilon}{\epsilon_0}}{1 + \left(\frac{\epsilon}{\epsilon_0}\right)^2}\right) (f_0) b \cdot \frac{x_u^d}{\epsilon_u} \cdot d\epsilon \\
 &= \frac{2 f_0 b (x_u^d)^2}{\epsilon_u^2 \cdot \epsilon_0} \int_0^{x_u^d} \frac{\epsilon^2}{1 + \left(\frac{\epsilon}{\epsilon_0}\right)^2} \cdot d\epsilon
 \end{aligned} \tag{4.23}$$

After integrating and applying the end conditions equation 4.23 becomes:

$$(\bar{y}d) C_u = 2 f_0 b (x_u^d)^2 \left(\frac{\epsilon_0}{\epsilon_u}\right)^2 \left(\frac{\epsilon_u}{\epsilon_0} - \tan^{-1} \frac{\epsilon_u}{\epsilon_0}\right) \tag{4.24}$$

The total compressive force in concrete is given by the total area of the stress block, i.e.:

$$C_u = \int_0^{x_u^d} f \cdot b \cdot dy \tag{4.25}$$

Substituting the values of f , and dy from equation 4.22 then integrating, equation 4.25 becomes:

$$C_u = b (x_u^d) f_0 \left(\frac{\epsilon_0}{\epsilon_u}\right) \ln \left(1 + \left(\frac{\epsilon_u}{\epsilon_0}\right)^2\right) \tag{4.26}$$

Introducing f_{av} , the average stress in the compressive block, to equation 4.26 then,

$$C_u = f_{av} \cdot b \cdot x_u^d \tag{4.27}$$

where
$$f_{av} = f_c' \frac{\epsilon_0}{\epsilon_u} \ln \left(1 + \left(\frac{\epsilon_u}{\epsilon_0}\right)^2\right) \tag{4.28}$$

or
$$f_{av} = \alpha \cdot f_c' \tag{4.29}$$

where
$$\alpha = \frac{\epsilon_0}{\epsilon_u} \ln \left(1 + \left(\frac{\epsilon_u}{\epsilon_0} \right)^2 \right) \quad (4.30)$$

or
$$\alpha = \frac{f_{av}}{f_c} \quad (4.31)$$

With reference to Figure 4.8 the decrease in (α) for higher strength concretes is related to the fact that such concretes are more brittle and show sharp stress-strain curves with small strains. It is worth mentioning here, that introducing (f_{av}) and (α) as given by equations 4.28 and 4.31, is an important step as they are to be used in the evaluation of the flexural and compressive strength of concrete sections. The average stress of the compressive block (f_{av}) and the parameter (α) are also used in comparing the stress-strain relationship for confined and unconfined sections, evaluating the relationship of the moment-curvature of floor beams and to represent the failure criteria of concrete under a complex state of stress. This is discussed in the following sections.

The values of ϵ_0 and ϵ_u in equations 4.24, 4.26 and 4.28 are given by equations 4.16 and 4.17, $f_0 = f_c'$ as previously assumed.

Two types of failure are possible here, viz. tensile failure and compressive failure; in order to find the depth of the neutral axis from the extreme compressive fibre, both failures are involved, thus: For tensile failure (Figure 4.7(b)).

$$f_{av} \cdot b \cdot x_u^d = A_{st} f_{sy} \quad (\text{equilibrium condition})$$

$$\therefore x_u^d = \frac{A_{st}}{b} \left(\frac{f_{sy}}{f_{av}} \right)$$

or
$$x_u = P_s \left(\frac{f_{sy}}{f_{av}} \right) \quad (4.32)$$

For compressive failure, $\epsilon_s < \epsilon_{sy}$:

$$x_u = P_s \frac{E_s \epsilon_s}{f_{av}} \quad (4.33)$$

where A_{st} = area of tensile reinforcing steel,

P_s = tensile reinforcement ratio ($= \frac{A_{st}}{bd}$),

ϵ_s = strain in steel

ϵ_{sy} = yield strain in reinforcing steel,

f_{sy} = yield stress of the tensile reinforcing steel.

The values of f_{sy} and ϵ_{sy} can be obtained from experimental results, as shown in Table 2.7.

With reference to Figure 4.7(b), the ultimate moment capacity of flexural sections is given by:

$$\begin{aligned} M_u &= C_u (d - x_u d + \bar{y}d) \\ &= C_u (d - \bar{g}d) \\ &= f_{av} \cdot x_u (1 - \bar{g}) bd^2 \end{aligned} \quad (4.34)$$

where M_u = the ultimate moment capacity of flexural section,

$\bar{g}d$ = the distance from extreme compressive fibre to the resultant of the compressive force.

In Table 4.5 the various stress block parameters of a balanced section for different types of concretes are shown; Table 4.6 shows the stress block parameters for some specimens.

In Figure 4.9 some other parameters are shown. Figure 4.9(a) expresses (x_u) as a function of concrete strength; Figure 4.9(b) compares

Table 4.5 Stress Block Parameters of Balanced Section

f_c'	$\frac{\epsilon_u}{\epsilon_o}$	$x_u d$	$\bar{y}d$	$\bar{g}d$	$\frac{f_{av}}{f_c} = \alpha$	* P_b
20	1.99	0.724 d	0.558 $x_u d$	0.442 $x_u d$	0.805	0.582 f_c'/f_{sy}
25	1.78	0.713 d	0.566 $x_u d$	0.434 $x_u d$	0.80	0.57 f_c'/f_{sy}
30	1.62	0.704 d	0.574 $x_u d$	0.426 $x_u d$	0.795	0.56 f_c'/f_{sy}
35	1.5	0.695 d	0.581 $x_u d$	0.419 $x_u d$	0.785	0.545 f_c'/f_{sy}
40	1.4	0.688 d	0.587 $x_u d$	0.413 $x_u d$	0.775	0.533 f_c'/f_{sy}

* P_b = balanced tensile reinforcing ratio

Table 4.6 Stress Block Parameters for Some Specimens

f_c' N/mm ²	f_{av} N/mm ²	$P_s = \frac{A_{st}}{bd}$	$x_u d$	$\bar{g}d$	M_u -proposed	M_u *Hognestad et al
20	16.1	0.0134	0.236 d	0.104 d	0.17 $f_c' bd^2$	0.168 $f_c' bd^2$
25	20.0	0.0134	0.190 d	0.082 d	0.139 $f_c' bd^2$	0.138 $f_c' bd^2$
30	23.85	0.0134	0.159 d	0.067 d	0.118 $f_c' bd^2$	0.116 $f_c' bd^2$
		0.0115	0.166 d	0.071 d	0.123 $f_c' bd^2$	0.121 $f_c' bd^2$
35	27.47	0.0134	0.138 d	0.057 d	0.102 $f_c' bd^2$	0.101 $f_c' bd^2$
40	31.0	0.0134	0.123 d	0.050 d	0.090 $f_c' bd^2$	0.089 $f_c' bd^2$
		0.0115	0.128 d	0.053 d	0.094 $f_c' bd^2$	0.098 $f_c' bd^2$

$$* M_u = bd^2 f_c' (q - 0.59 q^2)$$

where $q = P_s \frac{f_{sy}}{f_c}$ = mechanical percentage of reinforcement; M_u = ultimate moment capacity of flexural sections.

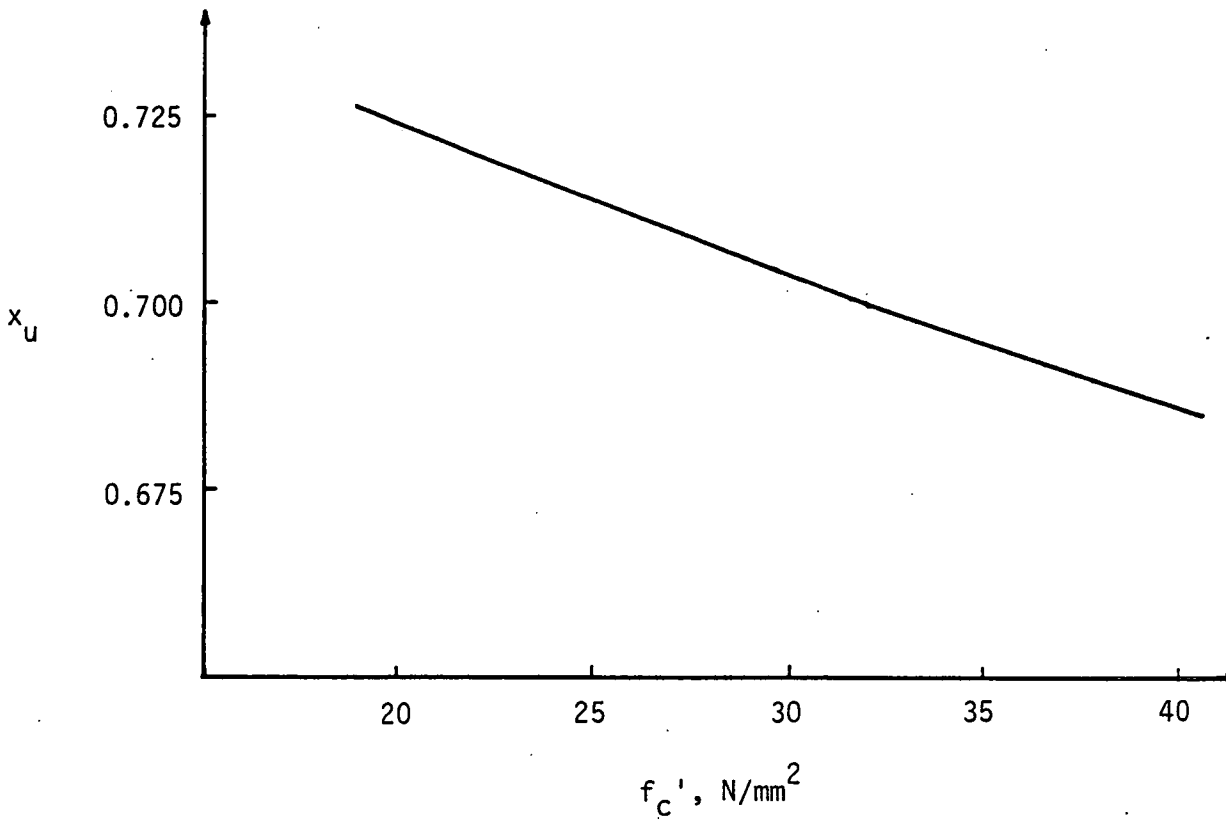


Figure 4.9(a) x_u versus f_c'

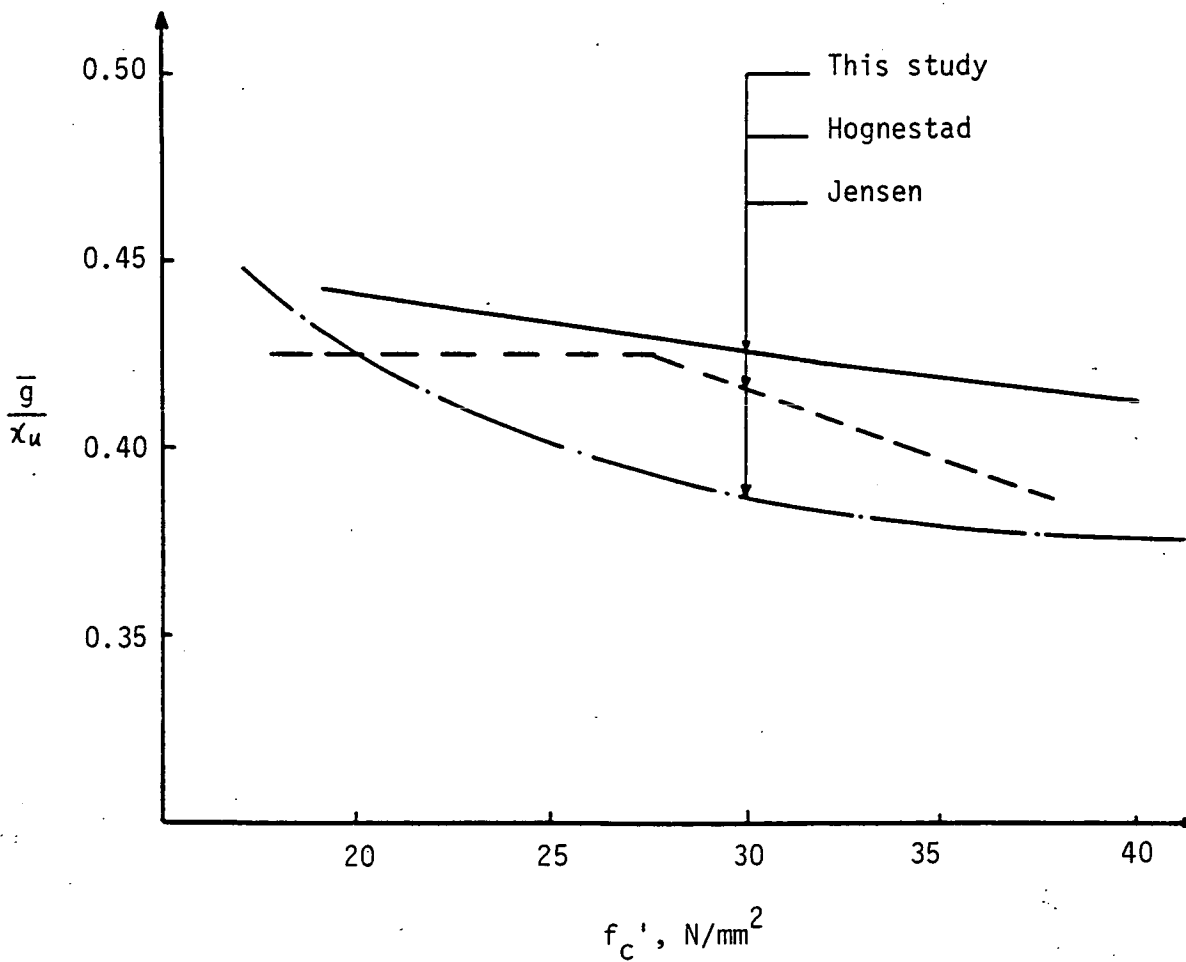


Figure 4.9(b) \bar{g} versus f_c' (balanced section).

the values of (\bar{g}) obtained from previous analysis with those obtained by Hognestad [25] and Jensen [22] using different stress blocks.

(\bar{g}) is expressed as a function of concrete strength (f_c').

The values of (M_u) obtained from equation 4.34 are compared with Hognestad et al [25] obtained from the following equation:

$$M_u = bd^2 f_c' q (1 - 0.5 q) \quad (4.35)$$

where $q = P_s \frac{f_{sy}}{f_c'}$

In fact equation 4.35 was used to design the floor beams in the first place.

4.4 Flexural Strength of Confined Section

It is evident now that the lateral confinement has a beneficial effect on the strength and deformation characteristics of reinforced concrete sections. It was believed that the main function of the transverse steel is to avoid buckling of the longitudinal reinforcement. Despite that the effect of confinement was studied by many investigators in the early days, but for instance most codes of practice [1] contain clauses to limit the size and spacing of ties only and in most recommendations, the effect of lateral reinforcement was ignored.

Richart and Brown [65] concentrated their research on spirally reinforced columns. Various experimental investigations, by King [66], Chan [32], Roy and Sozen [26], Szulczynski and Sozen [27], Bresler and Gilbert [28] and Pfister [29], were carried out to study the influence of confinement for structural concrete members subjected to different types of loading.

It may be concluded that the shape of the concrete stress-strain curve of a confined section varies with the confinement stress. The lateral reinforcement provides a confinement to the core as a result of its lateral expansion due to longitudinal deformations; this is due to Poisson's effect. The initial modulus of elasticity is not effected by the lateral reinforcement.

Though the ductility of the confined concrete is improved, it was found [27] that the increase in strength was not significant when the calculation is based on the initial gross area.

A concrete section that is laterally reinforced consists of two parts, namely core and cover. The behaviour of the cover is essentially different from that of the confined core, though they both suffer the same deformations under applied loads. Therefore it is difficult to define the cover and core by a unique approach. Logically the behaviour of a laterally confined section is based on the behaviour of both core and cover. The stress paths of the core and cover are different and unevenly distributed along the depth of the section.

The various stress-block parameters were studied by Kent and Park [67]. Expression to represent the stress and strain at different stages were derived. Soliman and Yu [68] criticised Chan's expression to evaluate the effect of transverse reinforcement on the behaviour of bound concrete under eccentric compression for being inadequate in evaluating the effect of the transverse reinforcement on the ultimate strain of which the plastic deformation of the member is a function. However, the influence of the spacing, size and type of transverse reinforcement as well as the shape of the concrete cross-section were thoroughly examined in a concrete section confined by rectangular ties under flexure. It was suggested that size and spacing of binder have

significant influence on the confinement. On the other hand, type of binders and shape of concrete cross-section have a little effect, as shown in equation 4.36. Most importantly it was observed that the ascending part of the stress-strain curve can be approximately considered the same as for unbound concrete.

The following expressions were proposed for the maximum compressive stress and average stress of the compressive block for a confined section:

$$f_c'' = 0.9 f_c' (1 + 0.05 q'') \quad (4.36)$$

$$f_{av}'' = 0.72 f_c' [1 + 0.14 (q'')^{\frac{3}{4}}] \quad (4.37)$$

where f_c'' = maximum confined concrete compressive stress,

f_{av}'' = average stress of the compressive block of bound concrete analogous to (f_{av}) for unbound concrete given by equation 4.28,

q'' = a parameter referring to the effectiveness of the transverse reinforcement

$$= 1.4 \left(\frac{A_b}{A_c} - 0.45 \right) \left(\frac{A_{sv} (S_o - S_v)}{A_{sv} S_v + 0.0028 B S_v^2} \right)$$

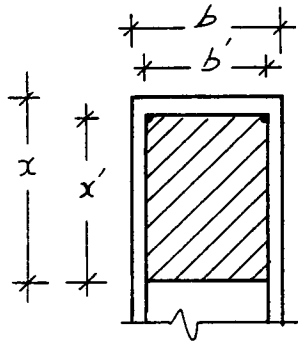
In which, A_b = area of bound concrete under compression (= $b'x'$) ... b' = smaller dimension of a stirrup,

A_c = total area of concrete under compression (= bx) ... b = breadth of section,

A_{sv} = cross-sectional area of one leg of a link,

S_v = spacing of the transverse reinforcement,

- S_0 = longitudinal spacing at which the transverse reinforcement was not effective in confining the concrete,
 $B = 0.7 x$ or b whichever is greater,
 x = depth of the neutral axis from the extreme compressive fibre,
 x' = depth of the neutral axis from the level of the compressive steel.



Chan [32] studied members which had failed due to compression of the concrete, having different amounts of confinement, and produced an expression for the ultimate properties of bound concrete. However, Chan's work was extended by Burns and Siess [69], who introduced a parameter called binding ratio (P'') to include the effect of longitudinal reinforcement which was ignored by Chan as a variable. P'' can be defined as:

$$P'' = \frac{\text{volume of stirrups}}{\text{volume of bound concrete}} + 0.1 \left(\frac{D}{S} \right)$$

where D = diameter of the compression steel,

S = spacing of the closed rectangular stirrups.

Based on Chan's tests, the following over-simplified linear expressions were suggested [32] to represent the ultimate strain in the concrete at the level of the compression steel and the average

compressive steel of bound concrete respectively in terms of the binding ratio:

$$\epsilon_{cu} = 0.011 + 0.2 P'' \quad (4.38)$$

$$f_{av}'' = f_c' (1.0 + 10 P'') \quad (4.39)$$

It may be concluded now, that confinement has an effect on the average stress of the compressive stress block of bound concrete and increases the ductility of concrete in a reinforced concrete section. The various parameters of the stress block can be evaluated in terms of the average stress of the compressive block.

The following expressions based on unbound concrete are suggested to compute the strength of a confined section:

$$C_u = f_{av}'' \cdot b \cdot x_u d \quad (4.40)$$

$$x_u = P_s \frac{f_{sy}}{f_{av}''}$$

and
$$M_u = f_{av}'' x_u (1 - \bar{g}) b d^2 \quad (4.41)$$

The ratio of the depth of the resultant compressive force from the extreme compressive fibre to the neutral axis depth, can be computed by the following expression given by Soliman and Yu [68]:

$$\frac{\bar{g}}{x_u} = \frac{0.84 + 0.5 q''}{2 + q''} \quad (4.42)$$

From equations 4.36 and 4.42 the stress block parameters for bound

concrete can be evaluated. The effect of stirrup spacing on the stress block parameters is evident in equation 4.37 and 4.42.

The effect of the confinement in the floor beams was not investigated as a variable. The stirrups in all the floor beams tested were equally spaced. Nevertheless the suggested expressions represented by equations 4.40 and 4.41 are to be adopted.

4.5 Biaxial Stress-Strain Relationship for Concrete

Early investigations were focussed on the concrete strength. Recently, a large amount of research has been done on the mechanical properties of concrete in biaxial loading. Data is now available concerning the strength, deformations and microcracking behaviour of concrete and biaxial stresses. A typical stress-strain curve for concrete under biaxial compression was shown by Kupfer et al [70]. The descending portion of the stress-strain curve in biaxial loading was achieved by Nelissen [71].

The maximum compressive strength, ductility and volumetric changes for concrete are highly affected by biaxial loading. It was found that the maximum strength envelope is largely independent of load path [71]. Despite the fact that extensive research has been carried out no general theory is yet available on the failure criteria and the concrete strength under combined loading. The concrete failure in this case is influenced by many factors such as, mix proportions, water/cement ratio, method of testing and rate of sequence of applying the stresses. A simplified failure criterion may be adopted to develop a stress-strain relationship and to evaluate the stress block parameters of concrete under biaxial stresses.

In order to develop a biaxial stress-strain relationship, the same approach discussed earlier to obtain equation 4.9 can be employed and the stress-strain curve conditions are applied.

The following proposed equation expresses the biaxial stress-strain relationship:

$$f = \frac{\epsilon}{(1 - \mu\alpha) (A' + B' \epsilon^{n'})} \quad (4.43)$$

where f = stress in direction considered,

ϵ = strain in direction of (f),

α = ratio of the principal stress in the orthogonal direction to the principal stress in direction considered,

μ = Poisson's ratio.

To find the coefficients A' , B' and n' , the stress-strain curve conditions must be satisfied, i.e. conditions at zero stress, strain and maximum strain (ϵ_0), then:

$$A' = \frac{1}{E_c}, \quad B' = \frac{R - (1 - \mu\alpha)}{\epsilon_0^{n'} (1 - \mu\alpha) E_c}$$

$$n' = \frac{R}{R - (1 - \mu\alpha)} \quad \text{and} \quad R = \frac{E_c}{E_0}$$

After substituting the values of the coefficient A' , B' and n' ; equation 4.43 becomes:

$$f = \frac{E_c \epsilon}{(1 - \mu\alpha) + [R - (1 - \mu\alpha)] \left(\frac{\epsilon}{\epsilon_0}\right)^{n'}} \quad (4.44)$$

and

$$\frac{f}{f_0} = \frac{R \frac{\epsilon}{\epsilon_0}}{(1 - \mu\alpha) + [R - (1 - \mu\alpha)] \left(\frac{\epsilon}{\epsilon_0}\right)^n} \quad (4.45)$$

Equation 4.10 for uniaxial compression is a special case of equation 4.45, where $\alpha = 0$. To simplify the use of equation 4.45 the values of f_0 , ϵ_0 and E_c may be obtained from relations established earlier. Liu [72] pointed out that the value of ϵ_0 for uniaxial compression may be different for biaxial compression.

Poisson's ratio for concrete under biaxial loading varies at different stages of loading and is influenced by many factors. The ratio (μ) remains constant until approximately 80 percent of its ultimate compressive strength. However it may be taken as equal to (0.2) in general.

Further experimental tests and further detailed study of the parameters involved in the problem are required to improve equation 4.45 and to represent the biaxial stress-strain curve of concrete more accurately. This, however is outwith the scope of the present study.

4.6 Flexural Resistance Prior to Cracking

The resistance of a reinforced concrete section in pure bending prior to cracking is dependent on the tensile strength of the concrete, therefore at this stage resistance of the concrete section depends on the nature of the stress-strain relationship in tension. The effect of reinforcement is neglected.

The theory of microcracking still can be used for the tensional states of stress. For stress levels less than 60 percent of the ultimate tensile strength (f_t), the microcracks are negligible and this stage defines the limit of elasticity. Beyond this level of

stress, bond microcracks join up and start to extend. At a stress level of about 75 percent of (f_t) crack propagation will be unstable [73]. The direction of crack propagation is transverse to the direction of stress. Growth of the cracks reduces the load-carrying area and also causes an increase in the stresses at the crack tips. Failure finally occurs due to bridging of cracks. The Modulus of Elasticity under uniaxial tension is higher than it is in compression [74], but for simplicity the values of Modulus of Elasticity is taken to be the same, i.e. $E_t = E_c$.

For the purpose of analysis the effect of the reinforcement is ignored and a semi-plastic stress distribution is adopted similar to that proposed by Cowan [75].

The following relationships can be obtained from Figure 4.10 to determine the depth of the neutral axis:

$$\frac{f_c}{f_t} = \frac{E_c \epsilon_c}{\frac{1}{2} E_t \epsilon_t} = \frac{2 \epsilon_c}{\epsilon_t} \quad (4.46)$$

$$\frac{f_c}{f_t} = \frac{x}{h - x} \quad (4.47)$$

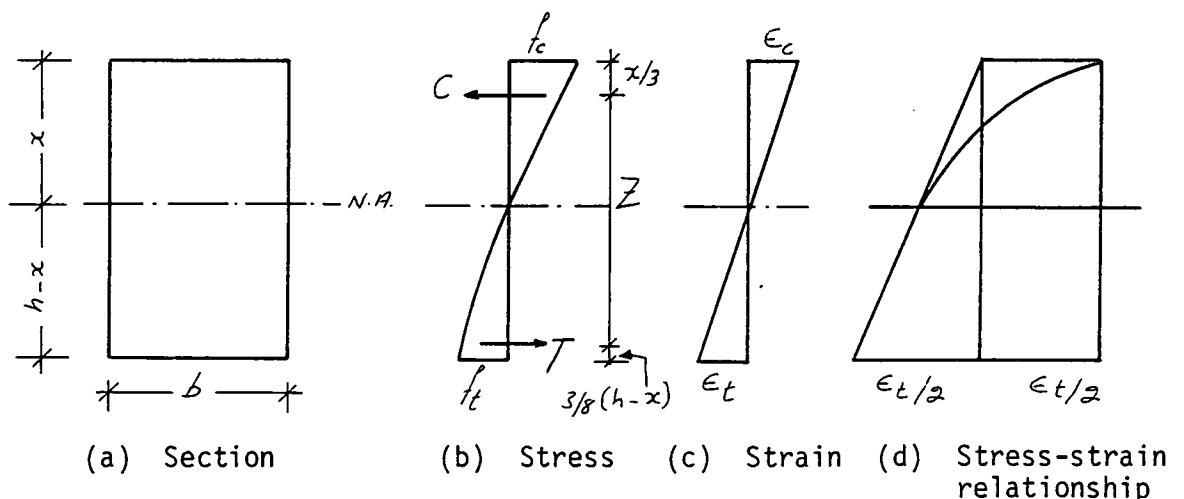


Figure 4.10 Concrete Stress-Strain Relationship in Tension

From equilibrium:

$$\frac{2}{3} f_t (h - x) b = \frac{1}{2} f_c b \cdot x$$

$$\therefore x = 0.472 h \quad (4.48)$$

With reference to Figure 4.10 the value of the lever arm (Z) can now be determined:

$$Z = h - \frac{x}{3} - \frac{3}{8} (h - x) \quad (4.49)$$

Substituting the value of x in equation 4.48 into equation 4.49, then:

$$Z = 0.645 h \quad (4.50)$$

The resistance of a concrete section under pure bending prior to cracking is given by the following equation:

$$M_u' = \frac{2}{3} f_t \cdot b \cdot (0.528 h) (0.645 h)$$

$$\text{or} \quad M_u' = f_t \frac{bh^2}{4.4} \quad (4.51)$$

$M_u' = M_{cr}$ when $f_t (= 0.6 \sqrt{f_c})$ is the ultimate tensile strength of concrete given by equation 3.5.

Equation 4.51 shows that the moment of resistance in pure bending is also a function of the geometrical properties of the section.

CHAPTER 5 : ANALYTICAL FORMULATION FOR ULTIMATE TORSIONAL STRENGTH

5.1 Torsional Strength Prior to Cracking

5.1.1 Strength of a Concrete Section in Pure Torsion

5.1.2 Strength of a Concrete Section Subjected to Bending and Torsion

5.1.3 Comparison with Test Results

5.2 Ultimate Torsional Strength of Rectangular Beams with Longitudinal and Transverse Steel

5.2.1 Analysis

5.2.2 Deformation Conditions and Failure Criteria

5.2.3 Simplified Method for Predicting the Ultimate Torsional Strength

5.2.4 Strength in Shear Compression Mode

5.2.5 Discussion

5.1 Torsional Strength Prior to Cracking

The reinforcement has a negligible influence prior to cracking and hence may be ignored. Concrete characteristics only are considered at this stage.

5.1.1 Strength of a Concrete Section in Pure Torsion

Most of the early investigators adopted the use of the elastic torsion theory for computing the torsional stresses which has been developed by St. Venant. Timoshenko and Goodier [76] illustrated Prandtl's membrane theory. The original form of those theories is too complicated for any practical use. However simplifications can only be achieved by assuming a specified stress distribution over the sides of the section and rewriting the original expressions in terms of the maximum stresses. The maximum stresses are assumed to occur at the mid-points of the sides. For example to simplify St. Venant's equations, Seely [77] assumed a parabolic distribution with maximum stress at the mid-point of the longest side of the section. Therefore the torsion moment is given as:

$$T_e = k h b^2 \cdot \tau_{\max} \quad (5.1)$$

where k is a function of h/b ; Cowan suggested an approximation to the value of k , given by:

$$k = \frac{1}{3 + \frac{2.6}{0.45 + \frac{h}{b}}} \quad (5.2)$$

From the membrane theory, Timoshenko derived the following formula similar to equation 5.1:

$$T_c = k_1 \cdot h \cdot b^2 \cdot \tau_{\max}$$

where k_1 is also a function of h/b .

Concrete in torsion exhibits plasticity, Turner and Davies [78] drew attention to this fact in 1934. This plasticity leads to a redistribution of the stresses as the load approaches its ultimate value. Turner and Davies suggested that this effect might be allowed for in calculating the ultimate torque, by multiplying the elastic torque by a factor of $(1.2 \frac{4A}{P \cdot b})$ where A = cross-sectional area, P = periphery of cross-section, and b = the shorter side of the section. Marshall [79] and the Nylander [80] both suggested that by treating concrete as an ideal plastic material, more consistent results are obtained. At failure the torsional shear stress would then be constant over the whole section and equal to the ultimate tensile strength of the concrete.

For a rectangular beam, the torsional strength is given by:

$$T_p = k_p h \cdot b^2 \cdot \tau_{\max} \quad (5.3)$$

where τ_{\max} = maximum torsional stress.

$$k_p = \frac{1}{2} \left(1 - \frac{1}{3 h/b} \right) \quad (5.4)$$

Examination of equations 5.2 and 5.4 reveals that for a wide range of

depth to breadth ratios for rectangular sections, the value of (k_p) is 1.66 ± 0.06 times greater than (k). This means for practical rectangular beams the ultimate torque calculated by the plastic theory is 1.66 ± 0.06 times the ultimate torque calculated by the elastic theory.

The plastic theory was further developed by Nadai [81] using a sand heap analogy whereby the torsional resistance of a cross-section is considered to be proportional to the volume of a sand heap over the section of constant maximum slope given by a value equal to twice the constant shear stress. The torsional resistance is then given as twice the volume confined by the surface or:

$$\tau_p = \frac{1}{2} b^2 \left(h - \frac{b}{3} \right) \tau_{\max} \quad (5.5)$$

Equation 5.5 is basically similar to equation 5.3. The practical application is to express the torsional resistance in terms of the maximum stress occurring at some specified location in the rectangular section. This is the concept of plastic behaviour.

It is universally accepted that when the magnitude of the principal tensile stress reaches the tensile strength of the concrete, the member cracks. The principal tensile stress can be determined if the shear stress caused by torsion is known, this is given by:

$$\tau = \frac{T}{S} \quad (5.6)$$

where S = the torsional section modulus. For a rectangular solid section, S , can be determined by the classical method of elasticity, thus:

$$S = k b^2 \cdot h \quad (5.7)$$

where k = is a function of h/b as mentioned earlier.

If concrete is assumed to be perfectly plastic material, S , can be determined by plastic theory thus:

$$S = k_p b^2 h \quad (5.8)$$

where k_p = is a function of h/b but has different values from k .

The torsional stress in a solid rectangular section calculated by the elastic and plastic theories are compared in Figure 5.1. The values given by the relevant codes of practice are also shown. Figure 5.1 reveals that the value of torsional stress depends upon the particular theory followed.

The principal tensile stress depends on the normal stress (σ) and the shear stress (τ). Where the normal stress (σ) equals zero then the principal stress is equal to the shear stress. Cracking occurs when $\sigma_t = f_t$ as shown in Figure 5.2. The torsional stress causing cracking can therefore be obtained by rewriting equations 5.1 and 5.5 in terms of the tensile strength of the concrete (f_t) rather than the maximum torsional stress, τ_{max} :

$$T_e = k b^2 h \cdot f_t \quad (5.9)$$

$$T_p = \frac{1}{2} \cdot b^2 (h - b/3) f_t \quad (5.10)$$

It can be seen that the cracking torsional strength (T_{cr}) depends

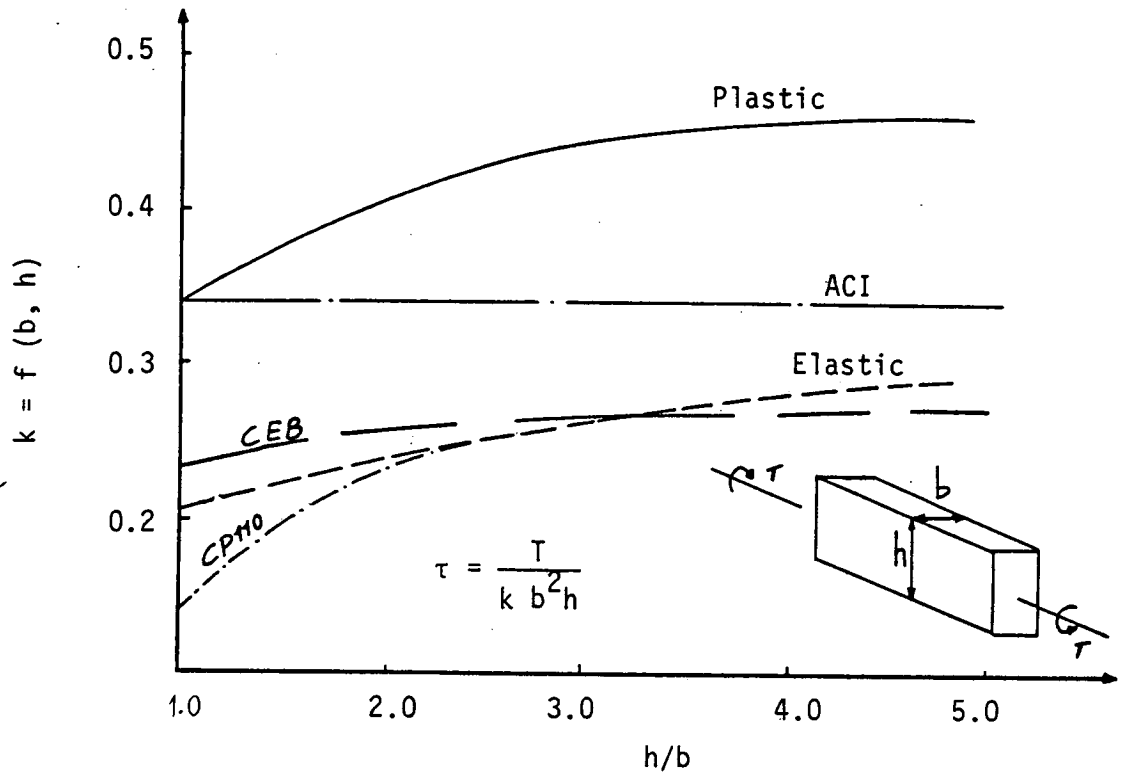


Figure 5.1 Torsional Stress Factors for Solid Rectangular Sections

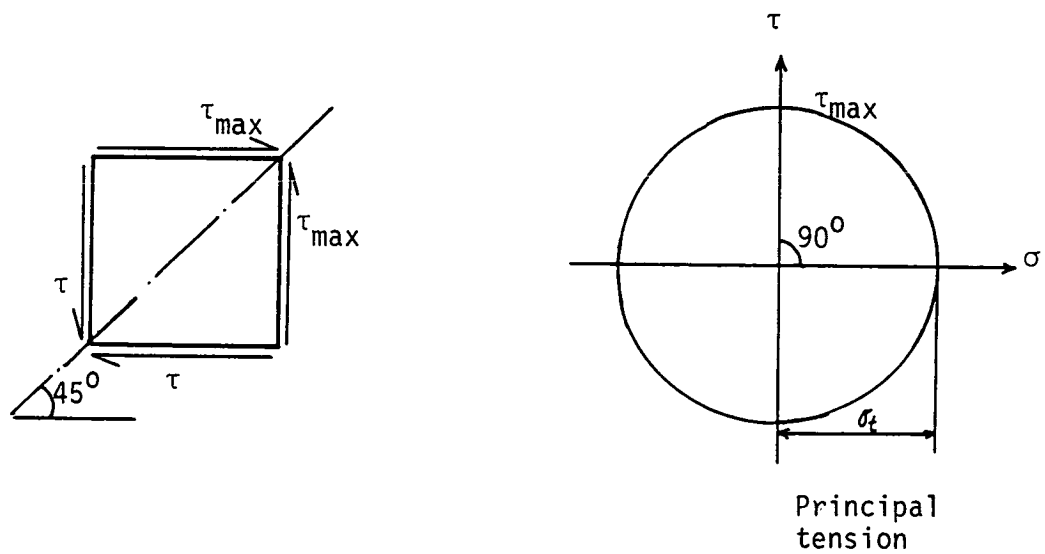


Figure 5.2 Shear Stress on an Element in Pure Torsion

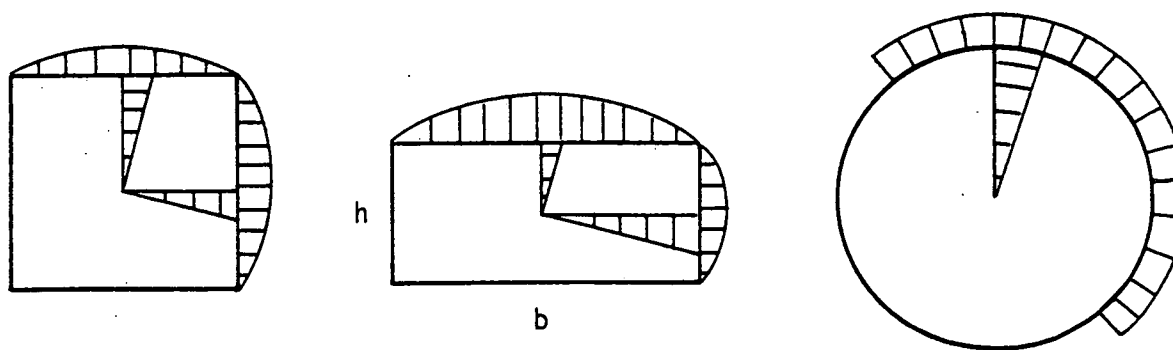
not only on the concrete properties but also on the geometry of the section and the method of loading. Figure 5.3 shows an ideal cracking stress distribution based on elastic theory for a variety of shapes and types of loading.

The theories that deal with the torsional strength of a plain concrete rectangular beam may be categorised into:

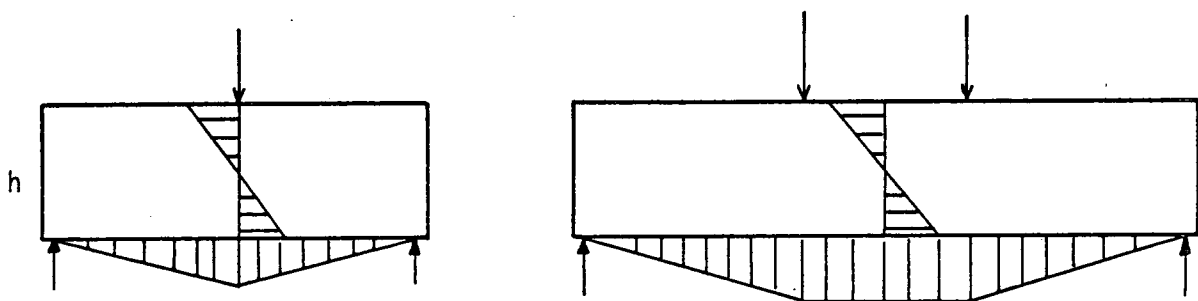
1. Elastic Theory: the procedure is to adopt St. Venant's distribution of stresses and assume concrete to be a linearly elastic material.
2. Plastic Theory: concrete is considered to be a plastic material. This theory can be expressed in two forms:
 - (a) A limited distribution of stresses is allowed for concrete in compression because of the plastic behaviour.
 - (b) The sand heap analogy; which assumes concrete to have infinite plasticity.

More details of these theories are summarised by Zia [14].

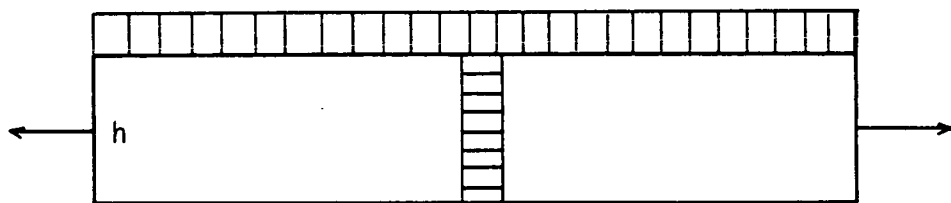
Basically these theories differ in their assumption of the concrete behaviour, although they all express the predicted failure torque of a rectangular beam in terms of the tensile stress. When the predicted torsional strengths of a rectangular beam calculated by those theories are compared with the experimental results available, the elastic theory always underestimates the torsional strength. The limited distribution of stresses allowed by the plastic theory is not enough to take into account the observed excessive strength. The sand heap analogy on the other hand takes into account the excessive strength,



Torsion



Flexure



Tension

Figure 5.3 Principal Tensile Stress at Cracking

but is theoretically unsound due to the fact that concrete shows little plastic behaviour especially in tension and the size effect is not considered. In general the plastic theory overestimates the torsional strength.

St. Venant theory has been confirmed by many investigators who adopt the view that plain concrete members fail in a spiral form. It is difficult to visualise a failure surface intersecting all four sides of a rectangular cross-section in a continuous spiral form.

The mechanism of torsion failure reported by Hsu [16] has been adopted in this study in which the failure surface for a member of a rectangular section is bounded by its four sides as shown in Figure 5.4.

Hsu, using motion picture equipment, observed the failure process very clearly. The movie showed that the first crack appeared on the front face at an angle of 45 degrees to the axis of the beam. The crack then widened and extended to the top of the section. Finally the concrete crushed on the back face. The failure process described is similar to that of a plain concrete flexural beam. The film also revealed a bending type of failure, i.e. concrete subjected to torsion fails mainly by bending. This bending mechanism of torsional failure is used to develop an equation for predicting the ultimate torsional strength of a rectangular beam.

With reference to Figure 5.5, the applied torque (T_u') can be analysed into two components acting on the failure surface i.e. the bending component (T_b), and the twisting component (T_t). The bending type of failure is therefore due to (T_b). Using classical bending theory:

$$T_b = T_u' \cos \phi \quad (5.11)$$

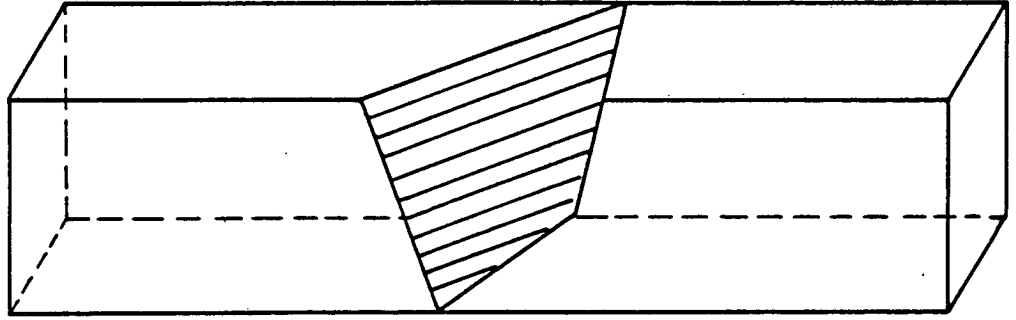
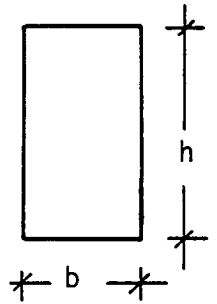
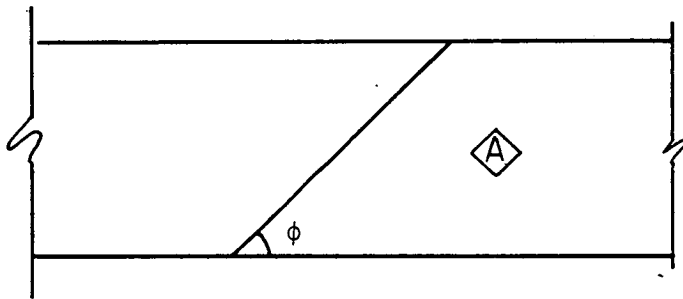
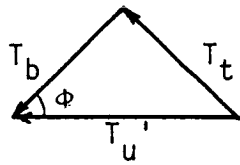


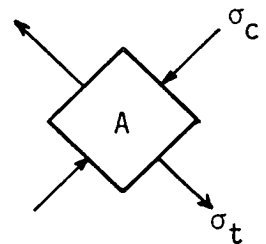
Figure 5.4 Failure Surface



beam cross-section



component of applied torque



Element A

Figure 5.5 Component of Applied Torque on the Failure Surface

$$T_b = \frac{b^2 h}{6} f_r \cos \epsilon c \phi \quad (5.12)$$

where T_b = the bending component of torque

T_u' = ultimate torsional strength

ϕ = cracking angle on the wider face, between the tensile crack and the axis of the beam

f_r = modulus of rupture of concrete

b = the shorter side of the cross-section

h = the longer side of the cross-section

From 5.11 and 5.12:

$$T_u' = \frac{b^2 h}{6} f_r (\sec \phi \cos \epsilon c \phi) \quad (5.13)$$

Differentiating equation 5.13 and equating to zero:

$$\frac{dT_u'}{d\phi} = \frac{b^2 h}{6} f_r \frac{d}{d\phi} [\sec \phi \cos \epsilon c \phi] = 0 \quad (5.14)$$

Equation 5.14 gives the minimum torsional resistance at an angle of $\phi = 45$ degrees. This is in agreement with St. Venant stress distribution. The angle ϕ coincides with the maximum principal tensile stress.

The failure torque due to the bending component of the applied torque can be expressed by:

$$T_u' = \frac{b^2 h}{3} f_r \quad (5.15)$$

Element A in Figure 5.5 is taken from the wider face of the beam and subjected to a compressive stress (σ_c) caused by the twisting

component (T_t) of the applied torque, as well as the tensile stress (σ_t). σ_c , is normal to σ_t . The compression will reduce the tensile strength of the concrete. Using the straight line simplification of Mohr's theory [82], this reduction can be obtained as:

$$f_t \text{ (reduced)} = \frac{f_c' f_t}{f_c' + f_t}$$

where f_c' = uniaxial compressive strength of the concrete

f_t = uniaxial tension strength of the concrete

f_t (reduced) = tensile strength of concrete with perpendicular compression of equal magnitude.

The value of f_t (reduced) reported by Hsu is $0.92 f_t$ whereas McHenry and Karni [83] reported this reduction factor as $0.85 f_t$. The value of the reduced tensile strength for the type of concrete used in this study varies between 0.9 to $0.91 f_t$. However the value of f_t (reduced) is taken conservatively as $(0.85 f_t)$. Bending failure, in plain concrete, is due to tension so the modulus of rupture (f_r) is reduced by the perpendicular compression in the same proportion and equation 5.15 becomes:

$$T_u' = \frac{b^2 h}{3} (0.85 f_r) \quad (5.16)$$

Equations 5.13 and 5.16 are expressed in terms of the tensile strength of the concrete (f_t) and the modulus of rupture (f_r). It is therefore advantageous to establish a relationship between (f_t) and (f_r).

Equation 5.16 can be written as:

$$\tau_{u'} = \frac{0.85}{3} b^2 h \cdot C \cdot f_t \quad (5.17)$$

where $C = \frac{f_r}{f_t}$

C , is a function of many factors which affect (f_r). Most important are the size of the specimen used and the tensile strength of the concrete. The ratio, C , therefore is a function of $[(C_1 \cdot f_t) \cdot (C_2 \cdot h)]$ or:

$$f_r = [(C_1 f_t) \cdot (C_2 \cdot h)] f_t \quad (5.18)$$

In order to determine $(C_1 f_t)$ and $(C_2 h)$ the results of Wright's [84] and Hsu's tests are used.

Figure 5.6 shows the ratio $C = \frac{f_r}{f_t}$ as a function of the tensile strength. The ratio $\frac{f_r}{f_t}$ represents the product of $[C_1 f_t \times C_2 h]$.

In order to separate the two, the type of concrete and the tensile strength must be known. Point A on the curve is assumed to represent the type of concrete used in this study. This may be used as a reference by taking $C_2 h = 1.25$. The curve in Figure 5.6 can be expressed by the following empirical equation:

$$\frac{f_r}{f_t} = \frac{1.6}{3\sqrt{f_t}} (1.25) \quad (5.19)$$

in which $C_1 f_t = \frac{1.6}{3\sqrt{f_t}}$

Wright studied the effect of the depth of the flexural beam on the modulus of rupture experimentally. Using these results and those of Hsu the effect of the flexural beam depth on $\frac{f_r}{f_t}$ can be seen in Figure 5.7.

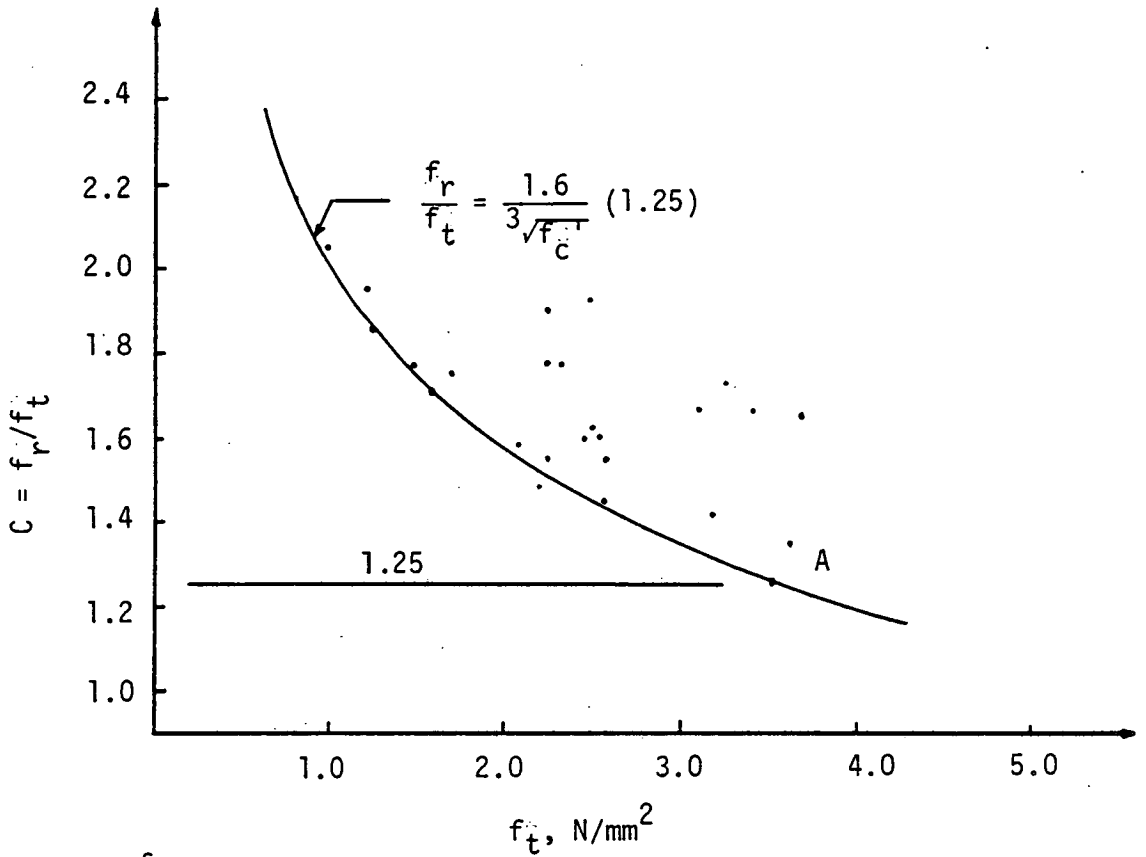


Figure 5.6 $\frac{f_r}{f_t}$ as a Function of the Tensile Strength

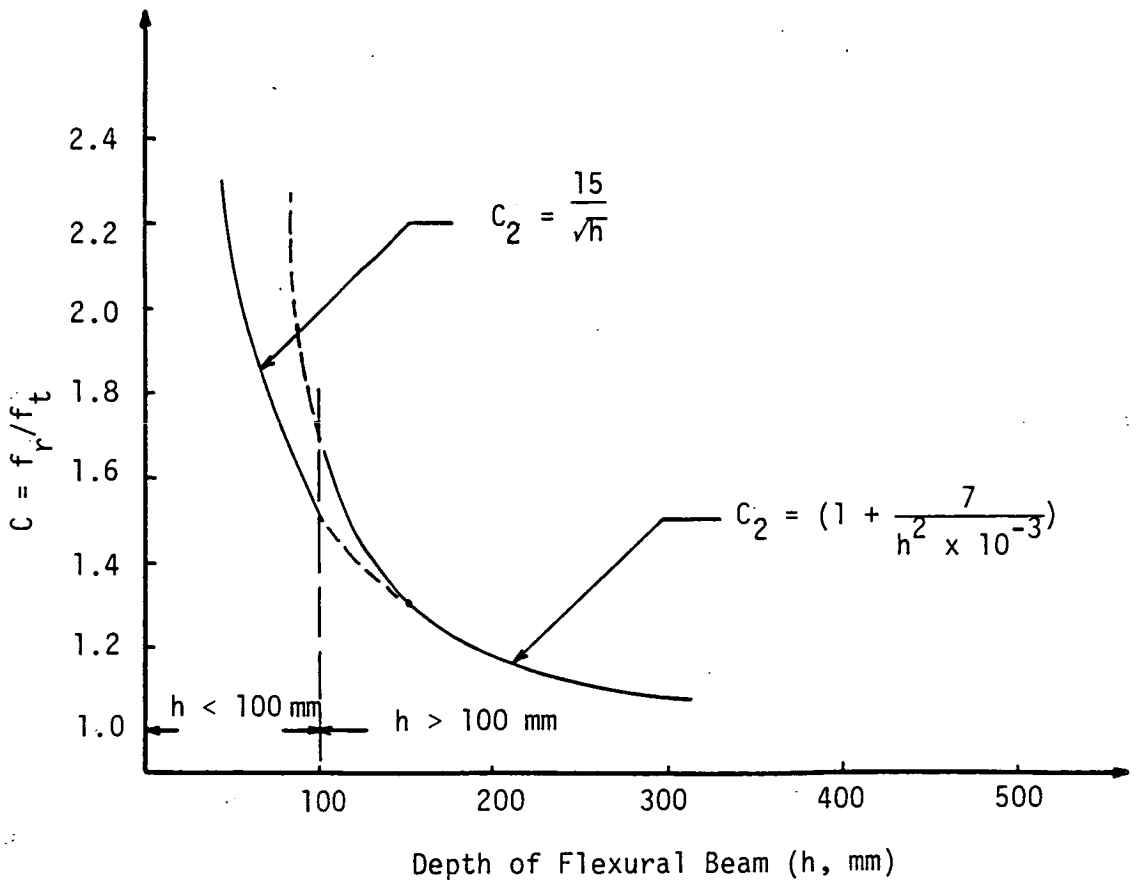


Figure 5.7 $\frac{f_r}{f_t}$ as a Function of the Beam Size

For a beam with $b > 100$ mm, the curve can be represented by:

$$C_2 h = 1 + \frac{7}{h^2 \times 10^{-3}}$$

For the concrete tested by Hsu $C_1 f_t$ is assumed = 1.0

The ultimate torque can now be calculated by substituting the value of $C_1 f_t$ and $C_2 h$ in equation 5.18:

$$C = \frac{f_r}{f_t} = \frac{1.6}{3\sqrt{f_t}} \left(1 + \frac{7}{h^2 \times 10^{-3}}\right) \quad (5.20)$$

Substituting the value of C in equation 5.17, then:

$$T_u' = \frac{0.85}{3} b^2 \cdot h \left(\frac{1.6}{3\sqrt{f_t}}\right) \left(1 + \frac{7}{h^2 \times 10^{-3}}\right) f_t$$

$$\text{or } T_u' = 0.45 b^2 h \left(1 + \frac{7}{h^2 \times 10^{-3}}\right)^3 \sqrt{f_t}^2$$

f_t is given by the following equation:

$$f_t = 0.6 \sqrt{f_c'} \quad (3.5)$$

therefore:

$$T_u' = 0.32 b^2 h \left(1 + \frac{7}{h^2 \times 10^{-3}}\right)^3 \sqrt{f_c'} \quad (5.21)$$

Similarly beams with $b < 100$ mm:

$$T_u' = \frac{0.85}{3} b^2 h \left(\frac{1.6}{3\sqrt{f_t}}\right) \left(\frac{15}{\sqrt{h}}\right) f_t$$

$$\text{or } T_u = \frac{4.8}{\sqrt{h}} b^2 h^3 \sqrt{f_c} \quad (5.22)$$

Equations 5.21 and 5.22 give the ultimate torsional strength of a rectangular beam under pure torsion. It is evident that the ultimate torsional strength of a rectangular beam is dependent on the concrete strength and section geometry.

5.1.2 Strength of a Concrete Section Subjected to Bending and Torsion

Practically speaking, reinforced concrete beams are rarely subjected to torsion only. The combined influence of bending and torsion occurs however due to asymmetrical loading and the monolithic nature of reinforced concrete frames. The influence of combined bending and torsion occurs simultaneously and this has a considerable effect on the strength of the beam. However final failure of the beam results from exceeding either the tensile or the compressive strength of the concrete depending on the ratio of bending to torsion. The exact conditions required to produce such failure are not fully understood. Nevertheless the failure criterion used to establish equation 5.21 and 5.22 is the one employed to predict the strength of a concrete rectangular section under the combined influence of bending and torsion. Figure 5.8 shows the assumed failure surface with an applied bending moment (M) and an applied torsion (T). The bending moment has a component acting about the tensile crack as shown in Figure 5.8. Also (M) is additive with (T_b) of equation 5.12.

Referring to Figure 5.8 and considering the equilibrium of the internal and external moments about the assumed failure plane, thus:

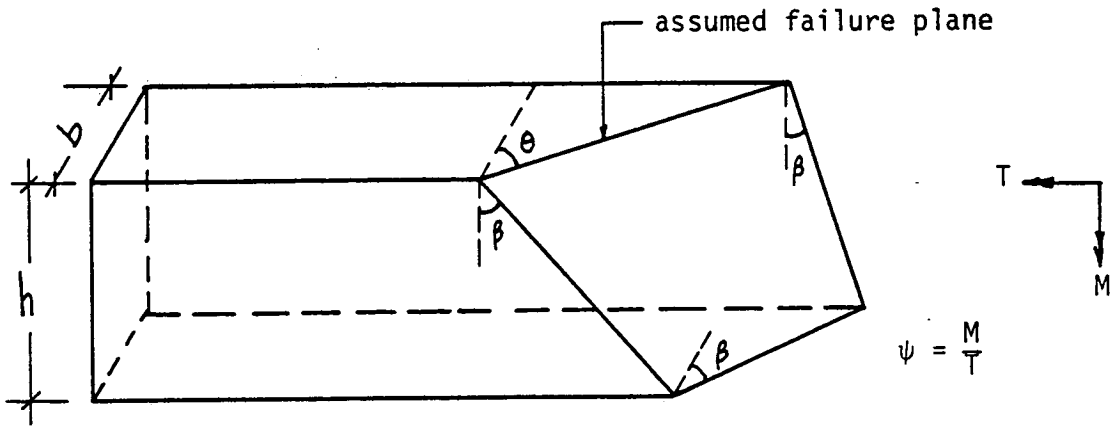


Figure 5.8 Assumed Failure Surface

Table 5.1 Values of α and λ as a function of h/b .

h/b	α	λ
1.0	0.208	0.141
1.2	0.219	0.166
1.5	0.231	0.195
2.0	0.246	0.229
2.5	0.258	0.249
3.0	0.267	0.264
4.0	0.282	0.277
5.0	0.291	0.291
∞	0.33	0.33

$$M \cos \beta + T \sin \beta = \frac{b^2 h}{6} \left(\frac{0.85 f_r}{\cos \beta} \right) \quad (5.23)$$

$$T_{un} (\psi \cos \beta + \sin \beta) = \frac{b^2 h}{6} \left(\frac{0.85 f_r}{\cos \beta} \right)$$

where $\psi = \frac{M_{un}}{T_{un}} = \frac{\text{ultimate applied bending moment}}{\text{ultimate applied torsion}}$

$$\text{or } T_{un} = \frac{0.85}{3} b^2 h f_r \left[\frac{1}{2 \cos \beta (\psi \cos \beta + \sin \beta)} \right] \quad (5.24)$$

Minimizing T_{un} by differentiation to obtain the angle β , thus

$$\frac{dT_{un}}{d\beta} = \frac{0.85}{3} b^2 h f_r \cdot \frac{d}{d\beta} \left[\frac{1}{2 \cos \beta (\psi \cos \beta + \sin \beta)} \right] = 0$$

$$\frac{d}{d\beta} \left[\frac{1}{2 \cos \beta (\psi \cos \beta + \sin \beta)} \right] = 0$$

For spandrel beams where $\psi = 2$, $\beta = 45^\circ$.

The term $\left[\frac{1}{2 \cos \beta (\psi \cos \beta + \sin \beta)} \right]$ in equation 5.24 is considered as a modifying factor to include the effect of bending moment.

The membrane analogy of Prandtl is true for both elastic conditions and beyond yield since the membrane represents stress distribution over the elastic region and the stress over the plastic area is given by a surface of constant maximum slope corresponding to the yield stress [85].

Therefore Prandtl theory can be applied, not only when the section is under torsion within the elastic limit but also when the concrete exhibits some degree of plasticity. The following proposed empirical approach is based on the experimental results of the spandrel beams tested in this project, to predict the cracking torque of reinforced concrete rectangular spandrel beams subjected to bending and torsion on

the assumption that the torsional strength is not dependent on the amount of steel provided prior to cracking.

$$T_{cr} = \alpha b^2 h \tau \quad (5.25)$$

where α = a numerical factor obtained from Table 5.1

τ = the maximum torsional shearing stress shown in Figure 5.9(a) and 5.9(b). The curves can be expressed by:

$$\tau = 0.12 \sqrt[3]{(f_c')^2} \quad \text{for } b > 100 \text{ mm}$$

$$\tau = 0.24 \sqrt[3]{(f_c')^2} \quad \text{for } b < 100 \text{ mm}$$

where f_c' = the compressive strength of concrete. Therefore equation 5.25 becomes:

$$T_{cr} = 0.12 \alpha \cdot b^2 \cdot h \sqrt[3]{(f_c')^2} \quad \text{for } b > 100 \text{ mm} \quad (5.26)$$

$$\text{and } T_{cr} = 0.24 \alpha \cdot b^2 \cdot h \sqrt[3]{(f_c')^2} \quad \text{for } b < 100 \text{ mm} \quad (5.27)$$

5.1.3 Comparison with Test Results

Hsu's expressions to calculate the ultimate torsional strength of rectangular unreinforced concrete beams under pure torsion are:

$$T_u' = 6 (b^2 + 10) h \sqrt[3]{f_c'} \dots \text{psi} \dots b > 4 \text{ in} \quad (5.28)$$

$$\text{and } T_u' = 14.3 \sqrt[3]{b^2} \cdot h \cdot \sqrt[3]{f_c'} \dots \text{psi}, 2 \text{ in} < b < 4 \text{ in} \quad (5.29)$$

The values of ultimate torsional strength of rectangular unreinforced

$$\tau = \frac{T_{cr}}{\alpha b^2 h}, \alpha = 0.246 \text{ for } h/b = 2$$

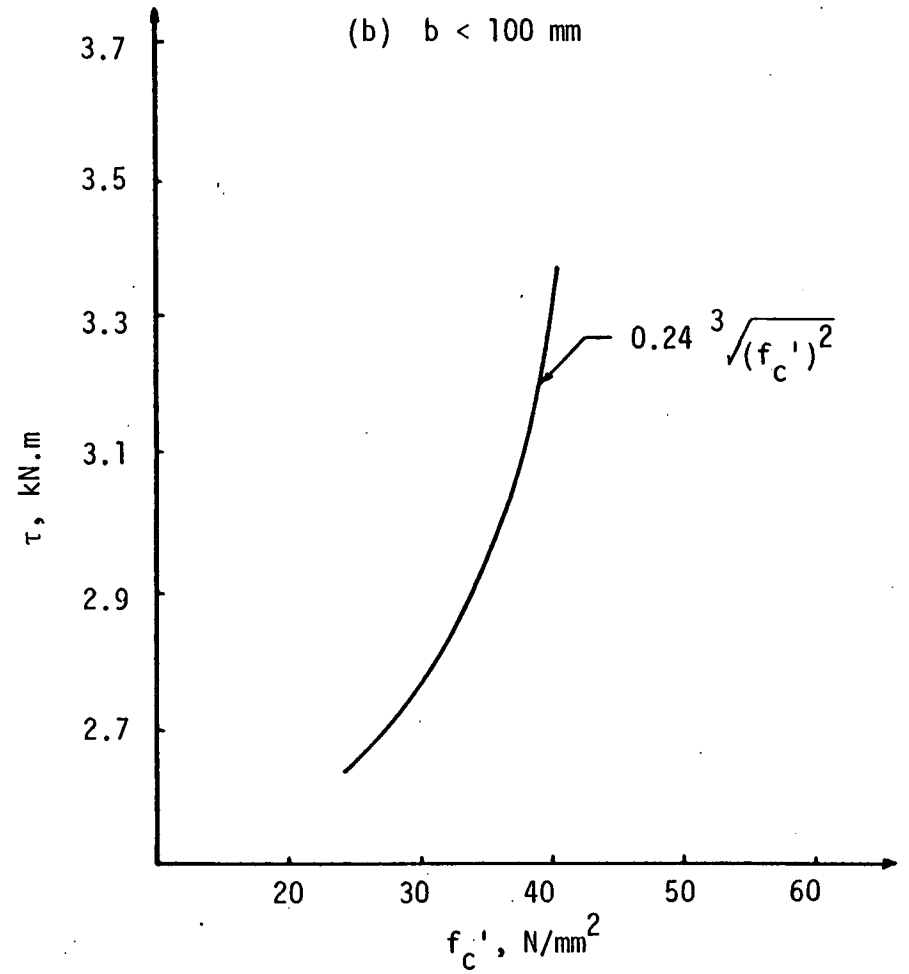
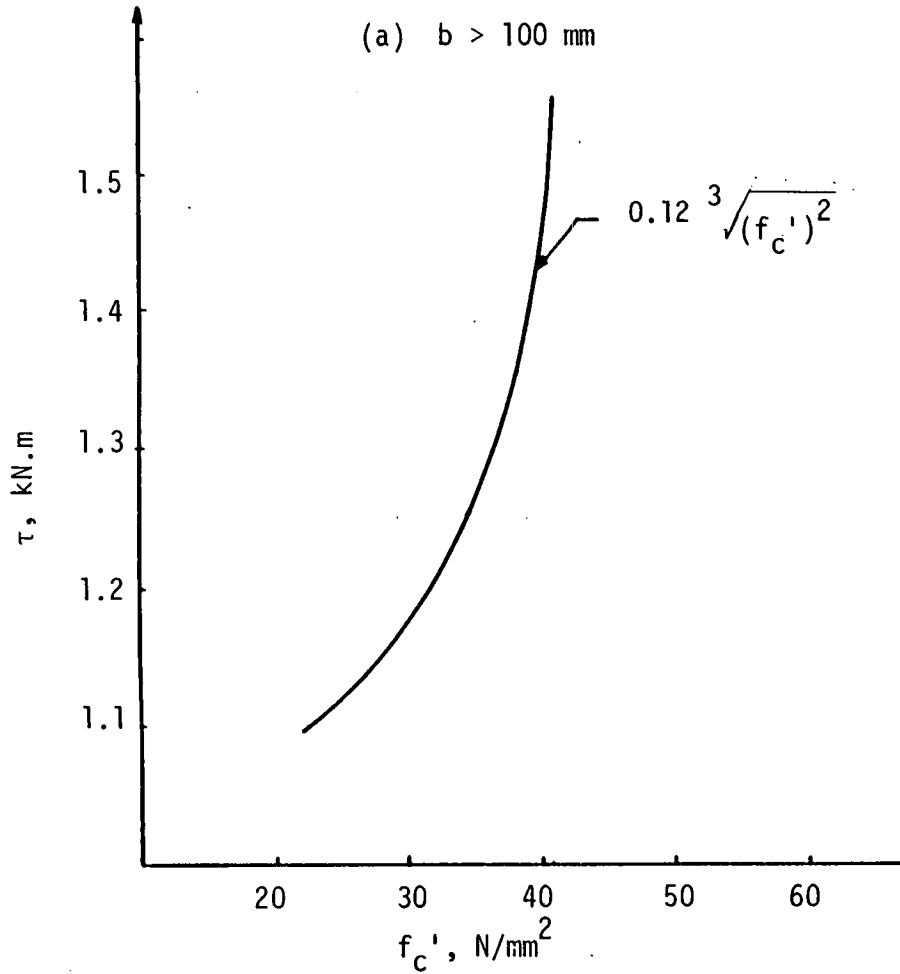


Figure 5.9 The Torsional Shearing Stress

concrete beams under pure torsion calculated by the elastic theory - equation 5.1, Hsu's expressions - equations 5.28 and 5.29 are compared in Table 5.2 for different values of (b^2h) . In Table 5.3, the values of (T_u') calculated by the various expressions are compared for varying types of concrete with the same cross-section.

It can be seen that (T_u') calculated by the proposed expression - equations 5.21 and 5.22 is between 30 to 55 percent greater than the value of (T_e) based on the elastic theory. This may explain the experimental excessive strength unaccounted ^{for} by the elastic theory.

Some consideration must be given to the effect of the reinforcement in equation 5.24. Where the beam is subjected to combined bending and torsion, Hsu suggested that the cracking torque of a reinforced rectangular beam is 1.0 to 1.3 times the failure torque of a corresponding plain concrete beam, depending on the amount of steel provided. The following equation was suggested:

$$T_{cr} = (1 + 0.04 P_t) T_u' \quad (5.30)$$

where T_{cr} = cracking torque of a reinforced concrete beam

P_t = the total volume of a reinforcement including longitudinal steel and stirrups expressed as percent of concrete volume.

Thus equation 5.24 becomes:

$$T_{cr} = (1 + 0.04 P_t) \left[\frac{0.85}{3} b^2 h f_r \left(\frac{1}{2 \cos \beta (\psi \cos \beta + \sin \beta)} \right) \right] \quad (5.31)$$

It can be seen from equation 5.31 that the cracking torque of beams under combined bending and torsion is dependent on the ratio of bending to twisting moment, concrete strength and section geometry.

Table 5.2 Ultimate Torsional Strength Calculated by Different Expressions for $f_c' = 40 \text{ N/mm}^2$

$b^2 h \times 10^6$ mm ³	T_e (elastic) kN.m	T_u' (Hsu) kN.m	T_u' (proposed) kN.m	$\frac{T_u' \text{ (proposed)}}{T_e \text{ (elastic)}}$
2.0	1.7	2.43	2.56	1.5
4.0	3.0	3.44	4.3	1.43
6.75	5.88	6.7	7.9	1.3
10.0	7.58	8.6	11.2	1.47
12.0	9.09	10.36	13.96	1.53
14.0	11.14	12.09	16.10	1.45

Table 5.3 Ultimate Torsional Strength Calculated by Different Expressions for $b \times h = 100 \times 200 \text{ mm}^2$

f_c' N/mm ²	T_e (elastic) kN.m	T_u' (Hsu) kN.m	T_u' (proposed) kN.m	$\frac{T_u' \text{ (proposed)}}{T_e \text{ (elastic)}}$
30	1.5	2.2	2.3	1.53
35	1.59	2.32	2.46	1.54
40	1.7	2.43	2.56	1.50
45	1.8	2.52	2.68	1.48

$b \times h = 150 \times 300 \text{ mm}^2$

30	5.10	6.1	7.2	1.4
35	5.5	6.4	7.6	1.38
40	5.88	6.7	7.9	1.34
45	6.24	6.97	8.26	1.32

The experimental values of the cracking torque were obtained from the cracking loads i.e. the load at which the first torsional crack appeared. During the test, beams were loaded by 5 kN or 10 kN load increments, so that cracks could be propagated while applying the load. For this reason, some of the measured cracking torques may be higher than the actual values.

In Table 5.4, the cracking torques calculated by equations 5.31, 5.26 or 5.27 are compared with the experimental results. Test results of other investigators are also shown.

The factor $(1 + 0.4 P_t)$ given by Hsu in equation 5.30 is very high for small beams of minimum dimension less than 100 mm. Also the values of cracking torque calculated by equation 5.31 are low since the reduction factor is taken conservatively as (0.85).

It can be seen that equations 5.26 and 5.27 give reasonable values and so have been adopted in this study.

5.2 Ultimate Torsional Strength of Rectangular Beams with Longitudinal and Transverse Steel

Tests concerning the combined effect of shear and bending ^{on} concrete were reported by Hsu [86]. At the PCA laboratories, Hsu developed an equation to predict the torsional strength of reinforced concrete beams under pure torsion [87]. The failure surface was assumed to be a plane perpendicular to the wider face and inclined at an angle of 45 degrees to the axis of the beam. The expression for computing torque is independent of the location of the axis of twist though the equations were based on summing moments about the axis of twist. In the case of spandrel beams, this is still valid due to the fact

Table 5.4 Comparison Between Measured and Calculated T_{cr} (kN.m)

Beam	T_{cr} (measured)	T_{cr} (eq. 5.31)	$\frac{T_{cr} \text{ (meas.)}}{T_{cr} \text{ (eq. 5.31)}}$	T_{cr} (eq. 5.26 or 5.27)	$\frac{T_{cr} \text{ (meas.)}}{T_{cr} \text{ (eq. 5.26or 5.27)}}$
GR1-B1	1.92	1.88	1.02	1.92	1.0
-B2	2.25	2.17	1.03	2.25	1.0
-B3	2.0	1.88	1.06	1.92	1.04
-B4	2.17	2.00	1.08	2.13	1.01
GR2-B5	2.30	1.88	1.2	1.92	1.19
-B6	2.25	1.88	1.19	1.92	1.17
-B7	2.2	1.88	1.17	1.92	1.14
-B8	2.2	1.88	1.17	1.92	1.14
GR3-A1	0.74	0.68	1.08	0.706	1.05
-A2	0.81	0.79	1.02	0.77	1.05
-A3	0.80	0.79	1.01	0.77	1.03
-A4	0.79	0.79	1.0	0.77	1.02
GR4-B1	0.70	0.59	1.18	0.62	1.12
-B2	0.68	0.59	1.15	0.62	1.09
-B3	0.67	0.59	1.13	0.62	1.09
-B4	0.69	0.59	1.16	0.62	1.1
		Average	1.10		1.01

Table 5.4 (continued)

Beam	T_{cr} (measured)	T_{cr} (eq. 5.31)	$\frac{T_{cr} \text{ (meas.)}}{T_{cr} \text{ (eq. 5.31)}}$	T_{cr} (eq. 5.26 or 5.27)	$\frac{T_{cr} \text{ (meas.)}}{T_{cr} \text{ (eq. 5.26or 5.27)}}$
Hsu and Burton 1974 [40]					
A1	2.8	2.02	1.38	2.13	1.3
A2	2.15	1.61	1.33	1.85	1.16
B1	3.0	2.43	1.23	2.47	1.2
B2	2.48	1.93	1.28	2.45	1.01
B3	2.30	1.90	1.2	2.25	1.02
		Average	1.28		1.13
Mansur and Rangan 1978 [46]					
SA1	3.5	2.7	1.29	3.1	1.12
SA2	3.0	2.6	1.15	2.9	1.03
SB1	4.75	3.5	1.35	3.58	1.3
SB2	5.0	3.6	1.38	4.0	1.25
SB3	3.5	3.89	0.9	3.5	1.0
SB4	4.0	3.89	1.02	3.54	1.09
SB6	4.5	2.62	1.24	3.5	1.28
		Average	1.36		1.15

that the axis of twist does not coincide with the centroid of the cross-section.

The expression for predicting the ultimate torsional strength can be divided into two terms namely:

$$T_u = T_c + T_s \quad (5.32)$$

where T_c = the torsional capacity of plain concrete also the intercept of the (T_u) vs. $(\frac{b_1 h_1 A_w f_{wy}}{s})$ curve, Figure 5.10.

For a rectangular section (T_c) may be expressed practically in terms of the concrete strength and the geometry of the cross-section, as discussed earlier. Hsu proposed the following equation:

$$T_c = \frac{2.4}{\sqrt{b}} \cdot b^2 \cdot h \sqrt{f'_c} \dots (lb.in) \quad (5.33)$$

where b = smaller dimension of the cross-section of a rectangular beam

h = larger dimension of the cross-section of a rectangular beam

f'_c = compressive strength of concrete (psi).

The second term (T_s) of equation 5.32 is the additional torsional moment due to the lateral steel:

$$T_s = \Omega \cdot \frac{b_1 h_1 A_w f_{wy}}{s} \quad (5.34)$$

where b_1 = smaller dimension of the closed stirrup

h_1 = larger dimension of the closed stirrup

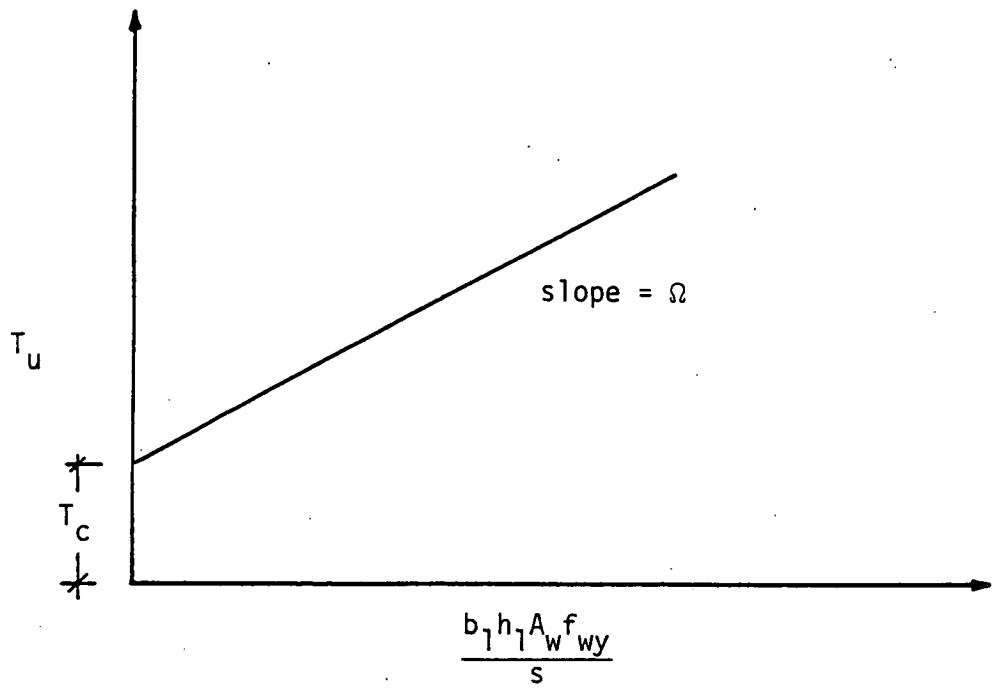


Figure 5.10 T_u Versus $b_1 h_1 A_w f_{wy}/s$

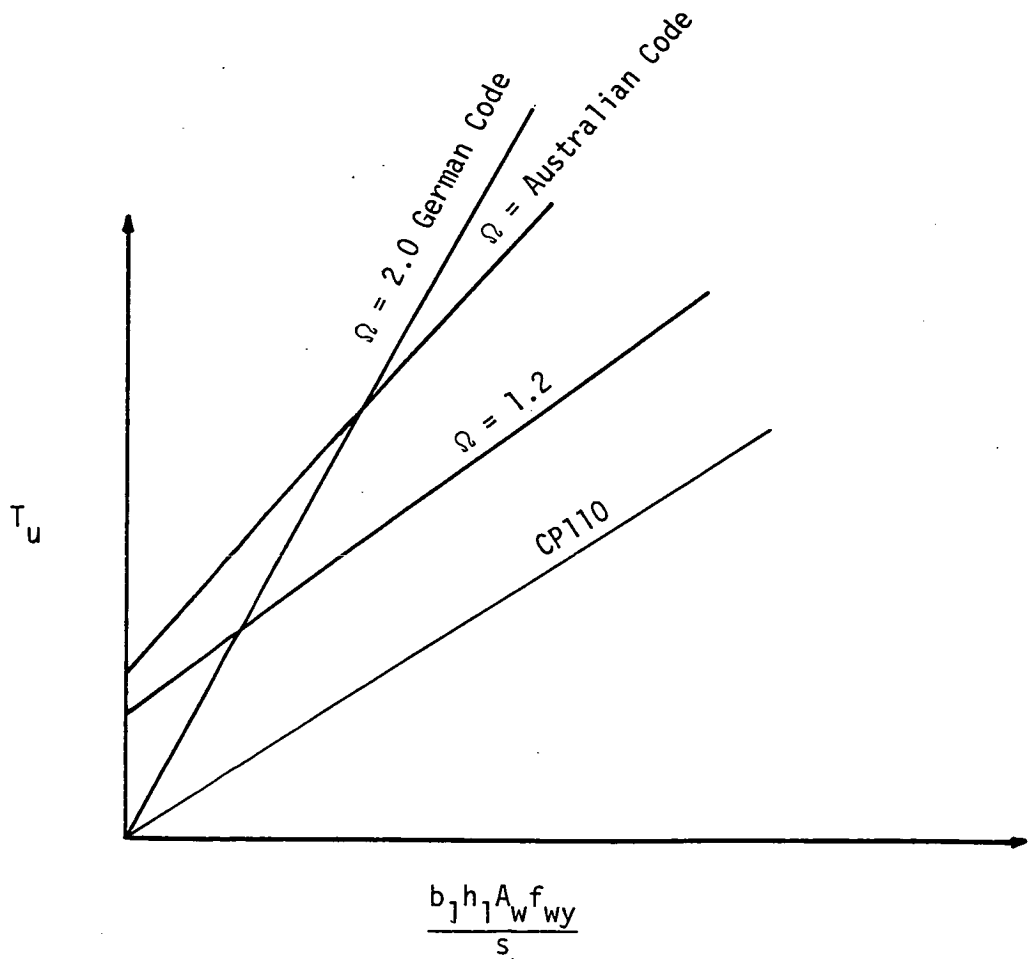


Figure 5.11 Values of Ω Compared

A_w = area of one leg of a stirrup

f_{wy} = yield stress of the web reinforcement

s = stirrup spacing

Ω = the slope of the T_u vs. $\frac{b_1 h_1 A_w f_{wy}}{s}$ curve shown in Figure 5.10.

Ω varies with the volumetric ratio (m) of the longitudinal steel to the stirrups and the h_1/b_1 ratio of the stirrup. Ω may be calculated as follows:

$$\Omega = 0.66 m + 0.33 \frac{h_1}{b_1} \quad (5.35)$$

Ω varies from a value of (1.0) for beams with square stirrups to a value of (1.5) for beams having stirrups with a ratio of $\frac{h_1}{b_1} = 2.6$. The torsional strength of narrow beams i.e. $\frac{h_1}{b_1} > 2.6$ is more accurately predicted by setting $\frac{h_1}{b_1} = 2.6$ in the calculation of Ω .

The predicted ultimate torsional strength (T_u) of an under-reinforced concrete beam under pure torsion is given by the following simplified design equation:

$$T_u = \frac{2.4}{\sqrt{b}} b^2 \cdot h \cdot \sqrt{f_c} + (0.66 m + 0.33 \frac{h_1}{b_1}) \left(\frac{h_1 b_1 A_w f_{wy}}{s} \right) \dots \quad (1b.in) \quad (5.36)$$

Equation 5.36 is similar to the equation used by the German and Australian Codes. According to the Australian and German Codes the ultimate torsional capacity may be expressed as follows:

$$T_u = T_0 + \frac{h_1 b_1 A_w f_{wy}}{s} \quad (5.37)$$

In the Australian Code (T_0) is taken as the elastic failure torque of an unreinforced concrete beam according to the maximum tensile stress

assumption. In the German Code (T_0) is taken as zero. Both Codes assume Ω to be constant;

$\Omega = 1.6$ for the Australian Code

$\Omega = 2.0$ for the German Code, as shown in Figure 5.11.

To allow for the effect of shear and flexure on the torsional strength Hsu suggested that the first term should be multiplied by a factor given as:

$$\left[\sqrt{1 + \left(\frac{3 v_0}{\tau_0} \right)^2} \right]^{-1}$$

where $v_0 = V_0/bd$ (i.e. ultimate shear stress) and $\tau_0 = 3 T_0/b^2h$ (i.e. ultimate torsional stress - $T_0 = K \frac{b^2h}{3} \cdot \sqrt{f_c}$).

This factor is included in the ACI proposed torsion specification to take into account the combined effect of torsion and shear since the calculation of (V_0) involves bending, i.e. the effect is considered indirectly. Thus equation 5.32 becomes:

$$T_u = \frac{T_c}{\sqrt{1 + (3 v_0/\tau_0)^2}} + T_s \quad (5.38)$$

All terms have been defined previously.

Most researchers agree that the ultimate strength can be divided into two terms as in equation 5.32. However the terms (T_c) and (T_s) are interpreted differently. Cowan [88] defined the terms as follows:

$$T_c = \alpha f_t \cdot b^2h \quad (5.39)$$

where f_t = tensile strength of concrete

α = a function of h/b .

For T- and L-shaped sections, equation 5.39 becomes:

$$T_c = \frac{f_t}{6} \sum \beta b^3 h$$

where b = width of the web

β = a function of h/b .

The torsional moment due to lateral steel (T_s) is given by:

$$T_s = \frac{1.6 A_w f_{wy} \cdot b_1 h_1}{s} \quad (5.40)$$

In order to develop the strength of the transverse steel (A_w), Cowan suggested that an equal volume of longitudinal torsional steel is required and this is given by:

$$A_{s1} = 2 A_w \left(\frac{b_1 + h_1}{s} \right) \quad (5.41)$$

Those expressions were based on the classical St. Venant theory assuming that the stresses are maximum at the centre of the rectangular and zero at the corners.

ACI committee 438 [2], produced expressions to determine the ultimate torsional capacity of a beam. A reduction factor (ϕ) was introduced but it is proposed not to include ϕ for the time being in order to obtain a more acceptable value for the torsional strength. A torsional shear stress ($\tau_o - \tau_{ca}$) is created by the torsional reinforcement which resists the applied torque (T_a):

$$T_a = (\tau_o - \tau_{ca}) \frac{b^2 h}{2} \quad \dots (1b.in) \quad (5.42)$$

where $\tau_o = \frac{3 T_o}{b^2 h} =$ nominal ultimate shear stress due to torsion

$$T_o = \text{total ultimate torsional moment} = K \frac{b^2 h}{3} \cdot \sqrt{f_c}$$

$$\tau_{ca} = \frac{\tau_c}{\sqrt{1 + (3 v_o / \tau_o)^2}} = \text{shear stress due to torsion}$$

$\tau_c =$ shear stress due to torsion carried by the concrete when the beam is subjected to pure torsion and is taken as $2.4 f_c' - (\text{psi})$

$v_o = \frac{V_o}{bd} =$ nominal ultimate shear stress due to shear.

The required torsional reinforcement is given by:

$$T_a = \Omega \frac{h_1 b_1 A_w f_{wy}}{s} \quad (5.43)$$

where $\Omega = 0.66 + 0.33 \frac{h_1}{b_1} -$ for $m = 1$, $\frac{f_s}{f_{sy}} = 1$. Substituting for τ_o and τ_{ca} , equating the two equations 5.42 and 5.43 and rearranging, the ultimate torsional strength (T_u) of a beam subjected to torsion and shear is given by:

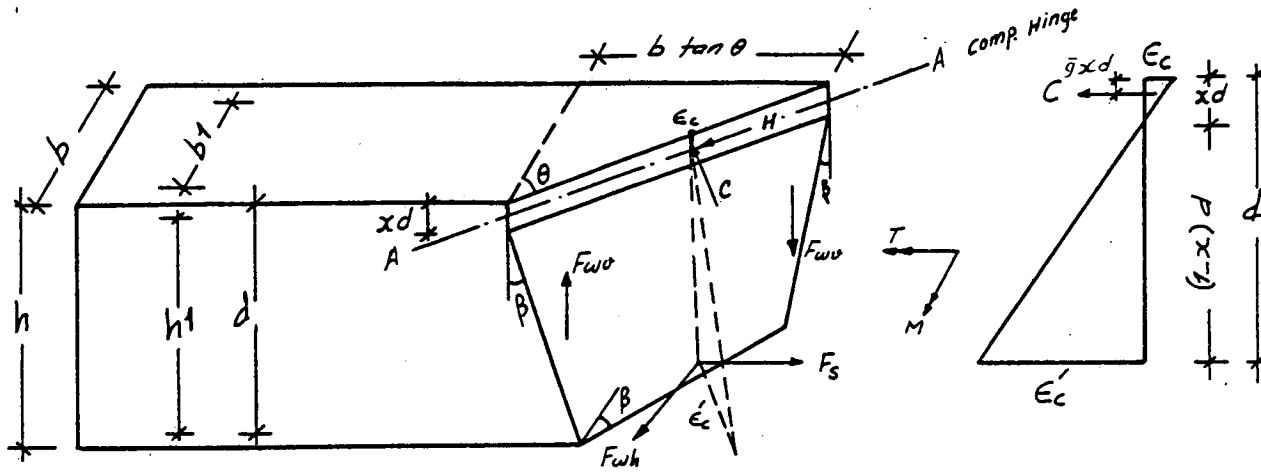
$$T_u = \frac{2.4 \sqrt{f_c}}{\sqrt{1 + (3 v_o / \tau_o)^2}} \cdot \frac{b^2 h}{3} + (0.66 + 0.33 \frac{h_1}{b_1}) \left(\frac{b_1 h_1 A_w f_{wy}}{s} \right) \quad (5.44)$$

The effect of bending is included indirectly in the computation of (v_o), (ACI 318-63).

It is evident that longitudinal and transverse steel increase the torsional strength of a beam. An intensive study of the behaviour of reinforced concrete beams subjected to the combined influence of bending and torsion has already been carried out.

Three main modes of failure have been observed in each of which the steel yields [89]:

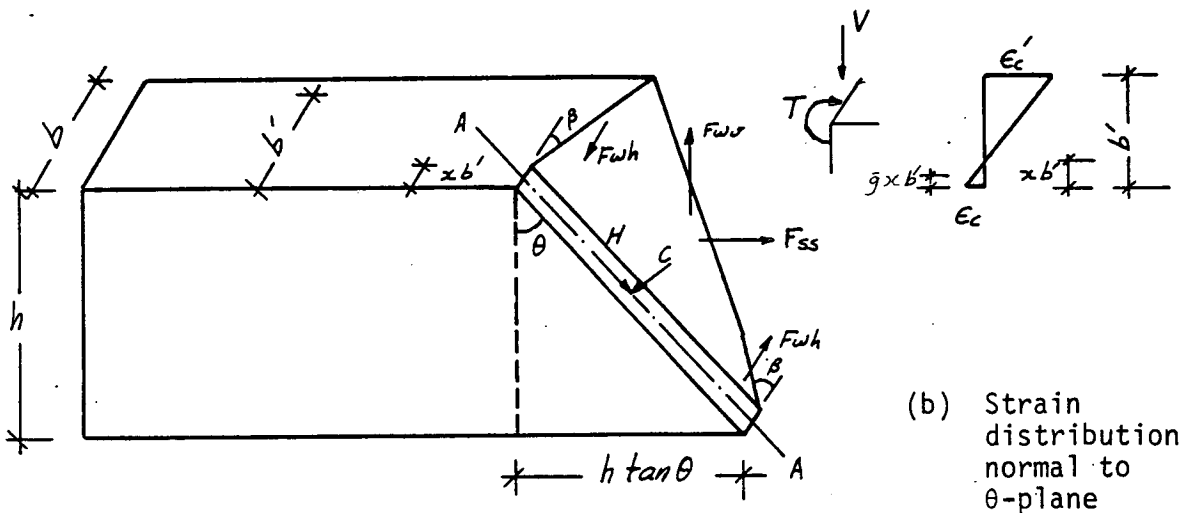
1. The first mode of failure occurs when the applied bending moment is greater than the twisting moment. Cracks form on the sides and the bottom of the beam. The cracks then widen until the reinforcement yields. The cracks continue to widen and propagate until the two sections of the beam start to rotate about an axis near the upper surface of the beam where failure finally occurs due to crushing of the concrete. The axis is inclined to ^{the} longitudinal axis of the beam. The angle of inclination depends on several factors but most importantly on the ratio of bending moment to twisting moment. This mode of failure is represented in Figure 5.12.
2. The second mode of failure occurs when the twisting moment is greater than the bending moment or when considerable shear forces are present. In this case the inclined torsion cracks are predominant on one side of the beam where tensile stresses arising from the twisting moment and the direct shear forces are additive. After yielding of the steel the two sections rotate about an inclined hinge located on the side of the beam as shown in Figure 5.13.
3. The third mode of failure was first reported by Collins et al [89]. This type of failure may occur when beams contain less top compression (longitudinal) steel than bottom tension steel. Beams which fail in this mode are those subjected to



(a) Failure surface

(b) Strain distribution normal to θ -plane

Figure 5.12 Mode 1



(a) Failure surface

(b) Strain distribution normal to θ -plane

F_{ss} = the force in top and bottom longitudinal bars in tension only.

Figure 5.13 Mode 2

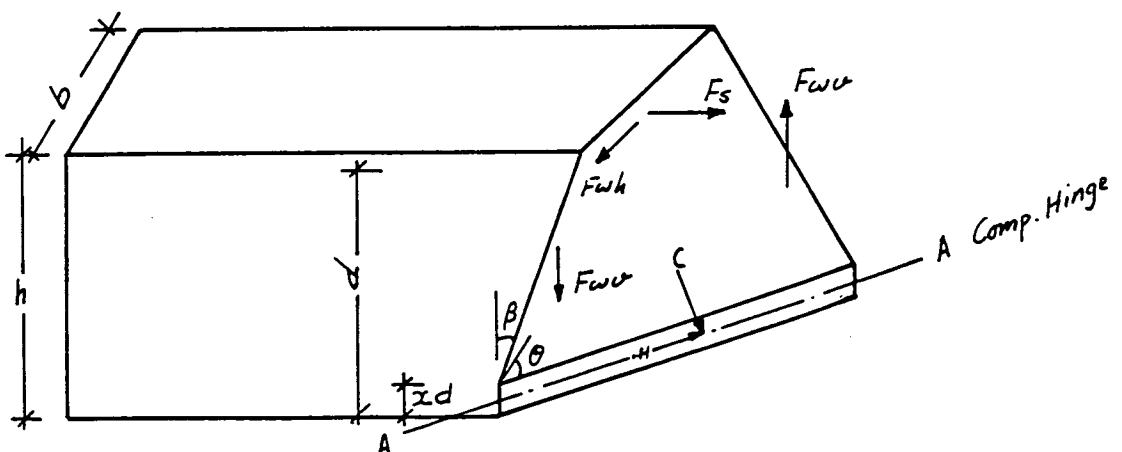


Figure 5.14 Mode 3

high ratios of twisting moment to bending moment. The tension cracks first appear in the top face of the beam and then widen. Failure occurs when rotating of the beam about a hinge located at the bottom face takes place, as shown in Figure 5.14.

5.2.1 Analysis

The skew bending theory proposed by Collins et al [89]; was subsequently modified by Rangan, Staley and Hall [21]. This modified skew bending theory has been adopted in this analysis to predict the torsional strength of spandrel beams containing longitudinal and transverse steel.

The concrete stress-strain relationships 4.10 and 4.11 proposed in section 4.2.1 are still valid. If the value of (R) taken from Table 4.2 is assumed (= 2) then equation 4.11 becomes:

$$\frac{f_c}{f_c'} = 2 \frac{\epsilon_c}{\epsilon_0} - \left(\frac{\epsilon_c}{\epsilon_0}\right)^2 \quad (5.45)$$

where ϵ_0 = concrete strain at f_c'

ϵ_c = concrete strain at f_c

f_c = stress in the concrete

f_c' = compressive strength of the concrete.

The average stress coefficient can be calculated by integration of the $\frac{f}{f_c'} - \frac{\epsilon}{\epsilon_0}$, curves shown in Figure 4.6. Integrating equation 5.45 gives:

$$k_1 = \left(\frac{\epsilon_c}{\epsilon_0}\right)^2 \left(1 - \frac{\epsilon_c}{3\epsilon_0}\right) \quad (5.46)$$

where k_1 = the average stress coefficient. Also the depth of the resultant coefficient (\bar{g}) can be calculated by:

$$\bar{g} = 1 - \frac{\frac{\epsilon_c}{\epsilon_0} (8 - 3 \frac{\epsilon_c}{\epsilon_0})}{12 - 4 \frac{\epsilon_c}{\epsilon_0}} \quad (5.47)$$

The steel stress-strain relationship is shown in Figure 2.6 and the idealized stress-strain curve is shown in Figure 6.4 in which the relation is assumed linear up to the yield stress followed by constant stress for further increase in strain.

Mode I

Satisfying the equilibrium conditions and resolving forces normal to the plane in compression, i.e. the θ -plane shown in Figure 5.12 gives:

$$C = F_s \cos \theta + F_{wh} \sin \theta \quad (5.48)$$

where $F_s = A_{st} \cdot f_s$

F_{wh} = the force in the bottom stirrup legs intersected by the tension crack and is given by:

$$F_{wh} = A_w f_w \frac{0.85 b_1}{s} \tan \beta \quad (5.49)$$

$$\text{From Figure 5.12 } \tan \beta = \frac{\tan \theta}{1 + 2 \frac{h}{b}} \quad (5.50)$$

in which $\alpha = \frac{h}{b}$

The coefficient (0.85) in equation 5.49 takes into account the fact that the horizontal web steel does not contribute to (F_{wh}) over

the whole stirrup width (b_1) because of the radii at the corners of a stirrup. Therefore the effective width of a stirrup is taken conservatively as $(0.85 b_1)$.

The compressive force can be expressed as:

$$C = k_1 f_c' (xd) b \sec \theta \quad (5.51)$$

in which k_1 = the average stress coefficient given by equation 5.46
 xd = the depth of the compression zone.

Substituting the value of C and F_{wh} in equation 5.48 then,

$$x = \frac{P_s f_s [1 + \frac{r}{1+2\alpha} \tan^2 \theta]}{f_c' k_1 \sec^2 \theta} \quad (5.52)$$

where $P_s = \frac{A_{st}}{bd}$, $P_w = \left[\frac{0.85 A_w}{bd} \right] \left(\frac{b_1}{s} \right)$ and $r = \frac{P_w f_w}{P_s f_s}$

f_s = tensile stress of the tension steel

f_w = tensile stress of the web steel.

Taking moments about a horizontal line A-A which lies in the compression zone in the θ -plane and passes through the compressive force (C), and assuming that the contribution of the force in the vertical legs of the stirrup, F_{wv} , can be neglected due to the fact that their lever arms are small, also that the bottom legs of the stirrups are at the same level as the longitudinal tensile steel, gives:

$$M \cos \theta + T \sin \theta = (F_s \cos \theta + F_{wh} \sin \theta) (1 - \bar{g}x)d \quad (5.53)$$

Dividing equation 5.53 by $\cos \theta$, then:

$$T = \frac{P_s f_s \left[1 + \left(\frac{r}{1 + 2\alpha} \right) \tan^2 \theta \right] (1 - \bar{g}x) b d^2}{\psi + \tan \theta} \quad (5.54)$$

where $\psi = \frac{M}{T}$

Differentiating equation 5.54 and equating to zero, the angle (θ) can be obtained to define the mode 1 type of failure. Therefore,

$$\tan \theta = \sqrt{\psi^2 + \frac{1 + 2\alpha}{r}} - \psi \quad (5.55)$$

In differentiating equation 5.54, the coefficient of the lever arm ($1 - \bar{g}x$) does not affect the value of (θ) significantly and thus can be neglected. Substituting the value of ($\tan \theta$) from equation 5.55 into equation 5.54, the torque (T_1) in mode 1 behaviour can be expressed by the following expression:

$$T_1 = 2 A_{st} f_s (1 - \bar{g}x) d \left(\frac{r}{1 + 2\alpha} \right) \left(\sqrt{\psi^2 + \frac{1 + 2\alpha}{r}} - \psi \right) \quad (5.56)$$

or

$$T_1 = 2 (M_{b1}) \left(\frac{r}{1 + 2\alpha} \right) \left(\sqrt{\psi^2 + \frac{1 + 2\alpha}{r}} - \psi \right) \quad (5.57)$$

where M_{b1} = pure flexural strength in positive bending and is given by

$$M_{b1} = A_{st} f_s (1 - \bar{g}x) d \quad (5.58)$$

Mode 2

In this case the applied twisting moment is greater than the

bending moment. The compression zone lies along one side of the beam cross-section. Basically the analysis and the assumptions made in mode 1 are the same. In mode 2 the external bending moment has no component about the axis parallel to the neutral axis, however the shear force exerts a moment about this axis. Equating the external and internal moments, differentiating, and substituting for the value of $\tan \theta$, the following expression for the failure torque for mode 2 is obtained:

$$T_2 = \frac{2 P_{ss} f_s \left[\sqrt{\frac{\alpha r}{\alpha + 2}} \right] (1 - \bar{g}x) b'^2 \cdot h}{[1 + \delta \left(\frac{1}{2} - \bar{g}x \right) b']} \quad (5.59)$$

where $\delta = \frac{V}{T}$

or

$$T_2 = \frac{2 A_{ss} f_s (1 - \bar{g}x) b' \left[\sqrt{\frac{\alpha r}{\alpha + 2}} \right]}{[1 + \delta \left(\frac{1}{2} - \bar{g}x \right) b']} \quad (5.60)$$

where A_{ss} = area of top and bottom steel bars in tension only.

Equation 5.60 can be written in the following form:

$$T_2 = \frac{2 (M_{b2}) \sqrt{\frac{\alpha r}{\alpha + 2}}}{[1 + \delta \left(\frac{1}{2} - \bar{g}x \right) b']} \quad (5.61)$$

where M_{b2} = pure flexural strength in lateral bending given by the following equation:

$$M_{b2} = A_{ss} f_s (1 - \bar{g}x) b' \quad (5.62)$$

Mode 3

In this mode the compression zone lies along the bottom face of

the beam. The bending moment alone causes tension. This mode of failure is likely to occur in nearly square sections where the area of top longitudinal steel is less than the area of bottom longitudinal steel. The analysis and assumptions are similar to that for mode 1. However the bending moment in this case opposes the rotation which occurs during failure. Therefore in deriving the equation for the failure torque, (M) should be taken as (- M). The failure torque for mode 3 is given by the following expression:

$$T_3 = 2 A_{sc}' f_s (1 - \bar{g}x) d \left(\frac{r}{1 + 2\alpha} \right) \left(\sqrt{\psi^2 + \left(\frac{1 + 2\alpha}{r} \right) R} + \psi \right) \quad (5.63)$$

where $R = \frac{M_{b3}}{M_{b1}}$

M_{b1} = pure flexural strength in positive bending

M_{b3} = pure flexural strength in negative bending

$$M_{b1} = A_{st} f_s (1 - \bar{g}x) d \quad (5.58)$$

A_{st} = area of bottom longitudinal bars

$$M_{b3} = A_{sc}' f_s (1 - \bar{g}x) d \quad (5.64)$$

A_{sc}' = area of top longitudinal bars.

Equation 5.63 can be written in the following form:

$$T_3 = 2 (M_{b1}) \left(\frac{r}{1 + 2\alpha} \right) \left(\sqrt{\psi^2 + R \left(\frac{1 + 2\alpha}{r} \right)} + \psi \right) \quad (5.65)$$

5.2.2 Deformation Conditions and Failure Criteria

Figure 5.15(a) shows an element of concrete (A) at depth (d). The strains experienced by this element are shown in Figure 5.15(b).

Using Mohr's circle the terms ϵ_s , ϵ_w , and angle of cracking (β) can be expressed by:

$$\epsilon_2 = \frac{\epsilon_s + \epsilon_w}{2} - \frac{\epsilon_s - \epsilon_w}{2} \cdot \frac{1}{\cos 2\beta} \quad (5.66)$$

Equation 5.66 can be simplified by assuming ϵ_2 to be zero. Using the trigonometric relations, equation 5.66 can then be expressed in terms of ϵ_s and ϵ_w , thus:

$$\epsilon_w = \epsilon_s \tan^2 \beta \quad (5.67)$$

Substituting the expression for $\tan \beta$ in equation 5.50 into equation 5.67 gives:

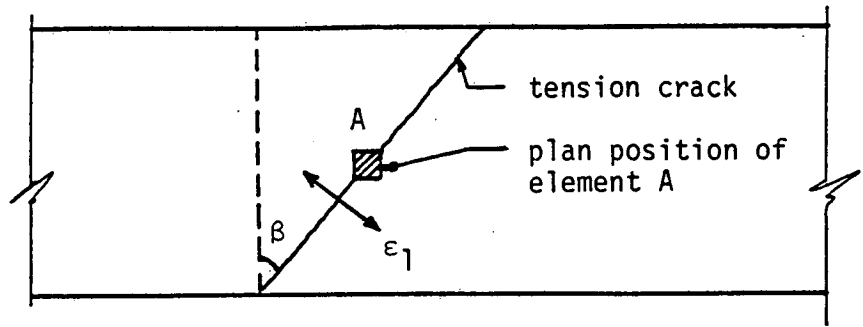
$$\epsilon_w = \epsilon_s \frac{\tan^2 \theta}{(1 + 2\alpha)^2} \quad (5.68)$$

In order to evaluate the value of (x) in Figure 5.12(b), the strains normal to the θ -plane are assumed to vary linearly with depth, therefore:

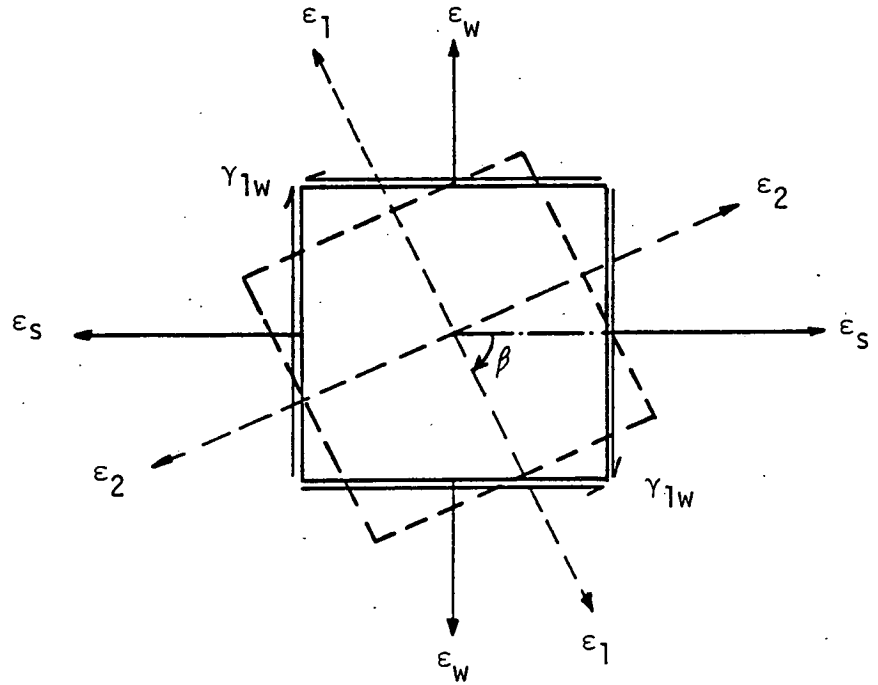
$$x = \frac{\epsilon_c}{\epsilon_c + \epsilon_c'} \quad (5.69)$$

where ϵ_c = the concrete compressive strain at the top of the beam

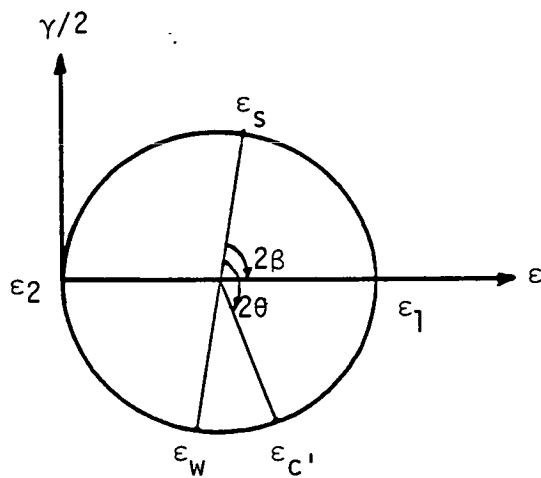
ϵ_c' = the tensile strain at depth d.



(a) Bottom surface of a beam



(b) Strains on element A at depth (d)



(c) Mohr's circle for strains on element A

Figure 5.15 Element A Taken from the Bottom Surface of a Beam at Depth (d)

ϵ_c and ϵ_c' = are measured normal to the θ -plane.

From Mohr's circle shown in Figure 5.15(c)

$$\gamma_{1W} = 2 \epsilon_W \cot \beta \quad (5.70)$$

Combining equation 5.70 with equation 5.67 then,

$$\gamma_{1W} = 2\sqrt{\epsilon_S \epsilon_W} \quad \text{or} \quad \frac{\gamma_{1W}}{2} = \sqrt{\epsilon_S \epsilon_W} \quad (5.71)$$

Acting at an angle θ from the longitudinal direction, the strain ϵ_c' can be expressed as:

$$\epsilon_c' = \epsilon_S \cos^2 \theta + \epsilon_W \sin^2 \theta + 2 \left(\frac{\gamma_{1W}}{2} \right) \sin \theta \cos \theta \quad (5.72)$$

Substituting the value of (γ_{1W}) from equation 5.71, equation 5.72 becomes:

$$\epsilon_c' = \epsilon_S \cos^2 \theta + \epsilon_W \sin^2 \theta + (\sqrt{\epsilon_S \epsilon_W}) \sin 2 \theta \quad (5.73)$$

then combining equation 5.73 with equation 5.68 gives:

$$\epsilon_c' = \epsilon_S \cos^2 \theta \left(1 + \frac{\tan^2 \theta}{1 + 2 \frac{\alpha}{\alpha}} \right)^2 \quad (5.74)$$

Substituting ϵ_c' from equation 5.74 into 5.69:

$$\epsilon_c = \left(\frac{x}{1-x} \right) \epsilon_S \cos^2 \theta \left(1 + \frac{\tan^2 \theta}{1 + 2 \frac{\alpha}{\alpha}} \right)^2 \quad (5.75)$$

The concrete was assumed to fail at a compressive strain, $\epsilon_c = 0.002$, ignoring the influence of the shear stresses and strains caused by the in-plane force H shown in Figure 5.12, in the skew compression zone, on the

value of ϵ_c . It is believed that the value of ϵ_c is significantly affected by the existing shear and strains [21], and the ultimate failure strain must be evaluated taking into account those strains.

The normal and shear strains in the skew compression zone converted using Mohr's circle, into a compressive principal ϵ_1 , and a tensile principal strain ϵ_2 , then:

$$\epsilon_c = \epsilon_1 + (-\epsilon_2)$$

or

$$\epsilon_2 = \epsilon_1 - \epsilon_c \quad (5.76)$$

From Mohr's circle:

$$\epsilon_c = \epsilon_1 \cos^2 \phi + (-\epsilon_2) \sin^2 \phi \quad (5.77)$$

where ϕ = the angle between the θ -plane and the plane on which ϵ_1 acts.

Combining equation 5.76 with equation 5.77 gives:

$$\epsilon_c = \epsilon_1 (1 - \tan^2 \phi) \quad (5.78)$$

It is shown by Kupfer et al [70] that the failure strains of concrete under biaxial compression-tension are smaller than those under uniaxial loading. The following failure criteria for the concrete strain can be used for simplicity:

$$\frac{\epsilon_1}{\epsilon_u} + \frac{\epsilon_2}{\epsilon_{tu}} = 1 \quad (5.79)$$

where ϵ_u = concrete failure strain in uniaxial compression

ϵ_{tu} = concrete failure strain in uniaxial tension.

The Modulus of Elasticity in uniaxial tension is higher than it is in compression [74]; for simplicity the value of Modulus of Elasticity is taken to be the same i.e. $E_t = E_c$. Accordingly

$$\frac{\epsilon_u}{\epsilon_{tu}} \approx \frac{f_{c'}}{f_t} \approx 12 \quad (5.80)$$

Equation 5.79 becomes:

$$\frac{\epsilon_1}{\epsilon_u} + 12 \frac{\epsilon_2}{\epsilon_u} = 1 \quad (5.81)$$

Substituting the values of ϵ_1 and ϵ_2 in terms of ϵ_c from equation 5.76, $\tan \phi$ from equation 5.78, and denoting the particular value of ϵ_c given by the failure criteria as $(\epsilon_c)_{ult}$, equation 5.81, becomes:

$$(\epsilon_c)_{ult} = \epsilon_u \frac{1 - \tan^2 \phi}{1 + 12 \tan^2 \phi} \quad (5.82)$$

where $(\epsilon_c)_{ult}$ = a particular value of ϵ_c at which the failure of a beam in combined torsion and bending is assumed to occur

ϵ_u = concrete ultimate strain at failure and can be obtained by equation 4.17.

It is assumed that the orientation of principal planes at the top surface are the same as at the bottom surface of the beam. Thus from Figure 5.15:

$$\tan \phi = \tan (\theta - \beta) \quad (5.83)$$

Substituting equation 5.50 in which θ and β are related, into equation 5.83 gives:

$$\tan \phi = \frac{2 \alpha \tan \theta}{2 \alpha + \sec^2 \theta} \quad (5.84)$$

The advantage of the modified theory is that the ultimate torsional strength of under-reinforced, partially or over-reinforced rectangular beams can be calculated and the balanced steel ratio (i.e. where the concrete crushes simultaneously with yielding of the transverse and longitudinal steel) can be derived as follows:

If the strain in the web steel ϵ_w is assumed equal to (ϵ_{wy}) the yield value and similarly the strain in the tension steel $\epsilon_s = \epsilon_{sy}$ then from equation 5.68:

$$\tan^2 \theta = \frac{\epsilon_{wy}}{\epsilon_{sy}} (1 + 2 \alpha)^2 \quad (5.85)$$

For this value of $(\tan \theta)$, equation 5.55 gives the value of r_b , the particular value of (r) to produce a balanced failure:

$$r_b = \frac{1 + 2 \alpha}{\tan \theta (\tan \theta + 2 \psi)} \quad (5.86)$$

Equation 5.86 can be further simplified by assuming $\epsilon_{wy} = \epsilon_{sy}$, then $\tan \theta = 1 + 2 \alpha$, thus

$$r_b = \frac{1}{1 + 2 \alpha + 2 \psi} \quad (5.87)$$

By taking the value of $\epsilon_c = (\epsilon_u)_{ult}$ and $\epsilon_s = \epsilon_{sy}$ and substituting the values of $\tan \theta$, r_b , x , and k_1 into equation 5.52, the balanced

tensile steel ratio P_{sb} can be obtained as:

$$P_{sb} = \frac{f_c \cdot k_1 \cdot x \sec^2 \theta (\tan \theta + 2 \psi)}{2 f_{sy} (\psi + \tan \theta)} \quad (5.88)$$

where P_{sb} = the balanced tensile steel ratio,

k_1 can be calculated from equation 5.46

x can be calculated from equation 5.52.

and $\tan \theta = (1 + 2 \alpha)$

In a similar manner, an alternative expression for calculating P_{sb} can be obtained for modes 2 and 3.

Since $r = \frac{P_w f_w}{P_s f_s}$, the balanced web steel ratio P_{wb} can be calculated

when the values of r_b and P_{sb} are known from equation 5.87 and 5.88 i.e.

$$P_{wb} = r_b P_{sb} \frac{f_{sy}}{f_{wy}} \quad (5.89)$$

5.2.3 Simplified Method for Predicting the Ultimate Torsional Strength

A simplified method for predicting the type of failure and then the ultimate torsional strength of reinforced concrete beams can now be proposed where the balanced steel ratios are known. The method given below uses a mode 1 type of failure as an example:

1. The section is under-reinforced when $P_s < P_{sb}$ and $P_w < P_{wb}$.
The torsional capacity can be calculated by equation 5.56.
The lever arm coefficient $(1 - \bar{g}x)$ can be taken approximately as (0.9), $f_s = f_{sy}$ and $r = P_w f_{wy} / P_s f_{sy}$.

2. The section is over-reinforced when $P_s > P_{sb}$ and $P_w > P_{wb}$. The excessive reinforcement is ignored and the torsional strength still can be calculated by equation 5.56 taking $P_s f_s = P_{sb} f_{sy}$, $P_w f_w = P_{wb} f_{wy}$ and $(1 - \bar{g}x) \approx 0.9$.
3. The section is partially over-reinforced when $P_s > P_{sb}$ and $P_w < P_{wb}$ or vice-versa. The excessive reinforcement is ignored and equation 5.56 can be used to calculate the torsional strength.

The method is similar for modes 2 and 3 and the torsional strength of the beam is taken as the least of the three calculated values for the three modes of failure.

5.2.4 Strength in Shear Compression Mode

It is universally accepted that high shear stresses may reduce the flexural strength predicted by the bending theory, due to the fact that the shear stresses are additive to the direct compressive stresses in the concrete in the compression zone and precipitate concrete distress prior to the steel yielding. A similar situation can be anticipated in the case of skew bending with the presence of torsion where the shear and torsional stresses are additive.

The three modes of failure discussed earlier all have flexural types of failure, although the shear force (V) is present in mode 2 but its influence is in creating a moment about the skew neutral axis.

The following approach for predicting the reduced torsional strength was originally proposed by Collins [17]. Remarkable agreement was obtained when Rangan and Hall [18] used the same approach and compared

the predicted torsional strength with the experimental results of Mukherjee and Warwaruk [19], and Henry and Zia [20].

The stirrups are assumed to yield before the longitudinal steel bars. The ultimate torsional strength at failure can be expressed by the following equation:

$$T_{us} = T_c + T_s \quad (5.90)$$

where T_c = torque carried by concrete

T_s = torque carried by stirrups

T_{us} = reduced torsional strength

The concrete must resist both shear force (V) and torsion moment (T), therefore to estimate T_c , the influence of both shear and torsion are considered. Figure 5.16 shows a linear interaction of shear and torsion. Assuming that the cracking values are equal to those for plain concrete, then

$$\frac{T_c}{T_u} + \frac{V_c}{V_u} = 1 \quad (5.91)$$

where T_c = torsional resistance of concrete

V_c = shear resistance of concrete

T_u' = resistance of the concrete in pure torsion where $V = M = 0$

V_u' = shear resistance of the concrete where $T = 0, M \neq 0$

$$T_u' = 0.32 b^2 h \left(1 + \frac{7}{h^2 \times 10^{-3}}\right) \sqrt[3]{f_c} \dots b > 100 \text{ mm} \quad (5.21)$$

$$\text{or } T_u' = \frac{4.8}{\sqrt{h}} b^2 h \sqrt[3]{f_c} \dots b < 100 \text{ mm} \quad (5.22)$$

The value of V_u' in the ACI (318-71) can be expressed as:

$$V_u' = 0.6 bd \sqrt{f_c'} + \frac{M_{cr}}{(\frac{M}{V})} \dots (1b) \quad (5.92)$$

or by definition:

V_u' = shear force causing a principal tensile stress of f_t ($= 0.6 \sqrt{f_c'}$) in an uncracked beam in flexure.

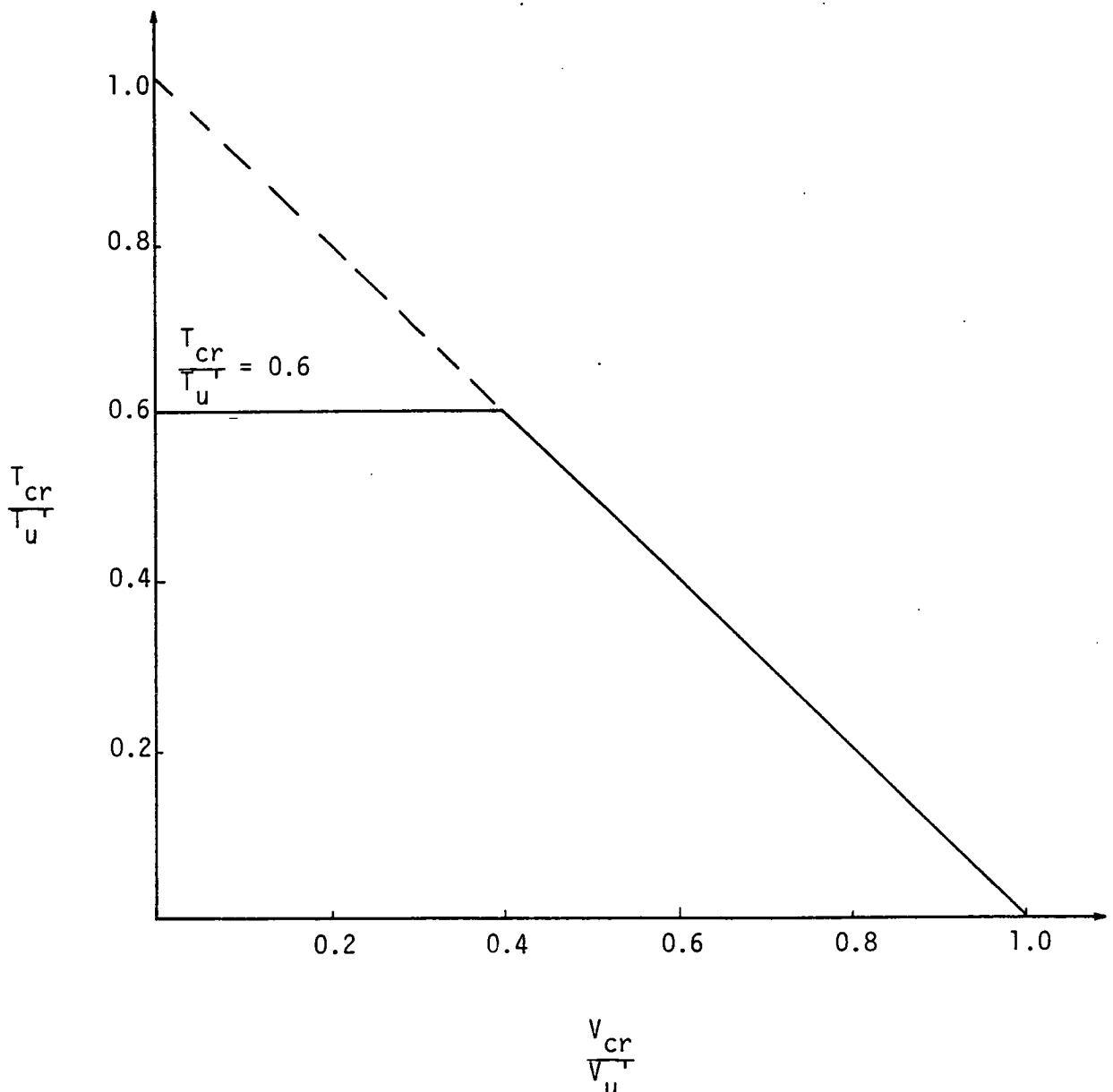


Figure 5.16 Torsion-Shear Interaction

The values of V_u' used in Figure 5.16 are calculated according to CP110-1972 i.e.:

$$V_u' = 0.75 \sqrt{f_c'} bd \leq 4.75 bd \quad (5.93)$$

where M_{cr} = the flexural cracking moment given by $M_{cr} = \frac{bd^2 \cdot f_t}{4.4}$

The ratio of applied shear to applied torsion is known; and this ratio is assumed to be the same ratio of shear to torsion resisted by the stirrups i.e.:

$$\frac{V_c}{T_c} = \frac{V_s}{T_s} = \frac{V}{T} = \delta \quad (5.94)$$

The linear interaction of equation 5.91 can now be represented by the following equation ($V_c = \delta \cdot T_c$):

$$T_c = T_u' \left(\frac{1}{1 + \delta \frac{T_u'}{V_u'}} \right) \quad (5.95)$$

The stirrup area (one leg) required to resist shear is given by the following equation as taken from ACI (318-71):

$$A_v = \frac{V_s}{2 f_{wy} \cdot d/s} \quad (5.96)$$

where A_v = area of one leg of the stirrup

s = spacing

f_{wy} = yield stress of the stirrup

V_s = shear resisted by the stirrups

$V_s = \delta \cdot T_s$

The stirrup area to resist torsion is given by the following expression which is similar to equation 5.40 given by Cowan:

$$A_{ws} = \frac{T_s}{\Omega f_{wy} \frac{b_1 h_1}{s}} \quad (5.97)$$

where A_{ws} = area of one leg of the stirrup to resist torsion only

T_s = torsion resisted by the stirrup only

Ω = the value of this factor varies between 1 and 2 as discussed in section 5.2. Therefore taking an average value of 1.5, equation 5.97 becomes:

$$A_{ws} = \frac{T_s}{1.5 f_{wy} \frac{b_1 h_1}{s}} \quad (5.98)$$

The total area of stirrups required to resist shear and torsion is then:

$$A_w = A_v + A_{ws} \quad (5.99)$$

Since V_s and T_s are related by equation 5.94, T_s can be expressed by the following expression after substituting the values of A_v , and A_{ws} into equation 5.99:

$$T_s = \left(\frac{2d}{2d + 1.5 b_1 h_1 \cdot \delta} \right) \left(1.5 A_w f_{wy} \frac{b_1 h_1}{s} \right) \quad (5.100)$$

The term in the first bracket in equation 5.100 is considered as a reduction factor since it is less than unity, and taken into account the effect of (V_s).

Substituting the value of T_c given by equation 5.95 and T_s given by equation 5.100 into equation 5.90, the value of torque (T_{us}) for failure in the shear compression mode is given by:

$$T_{us} = T_u' \left(\frac{1}{1 + \delta \frac{T_u'}{V_u}} \right) + \left(\frac{2 d}{2 d + 1.5 b_1 h_1 \cdot \delta} \right) \left(1.5 A_{wy} f_{wy} \frac{b_1 h_1}{s} \right) \quad (5.101)$$

Equation 5.101 predicts the torsional strength of a reinforced concrete beam when a combination of shear and torsion leads to a premature shear compression type of failure.

Shear was not critical in any case of loading in the spandrel beams tested in this project even for beams in group GR2 where shear was thought to be critical. Therefore values of T_{us} obtained from equation 5.101 can be expected to be higher than those obtained experimentally since the effect of shear stress in the compression zone due to bending is not included.

5.2.5 Discussion

In considering the ultimate torsional strength of a concrete beam prior to cracking, the mode of failure is dependent upon certain variables such as: ratio of the bending moment to twisting moment and concrete strength under combined stresses as discussed in deriving equation 5.31. The distribution of the longitudinal bars also has an effect. In a beam without top longitudinal steel the propagating cracks will lead to a sudden failure; on the other hand, the presence of both top and bottom longitudinal steel will lead to a s-shaped crack with the formation of a failure hinge about which the beam rotates either on top or one side of the beam.

The effect of the amount of reinforcement provided is included in equation 5.31 through a factor proposed by Hsu.

The proposed equation 5.26 and 5.27 are based on the assumption that torsional strength is not dependent on the amount of steel provided prior to cracking. This assumption was justified by Pandit [90] and by the result obtained experimentally. The strain in the reinforcement was negligible up to the cracking torque. Therefore the ultimate strength prior to cracking is not increased significantly by the reinforcement.

The empirical approach proposed to derive equations 5.26 and 5.27 is based on the fact that concrete exhibits some degree of plasticity and is based on a principal tensile stress criteria of failure. Since concrete is assumed to have plastic behaviour the shearing stress can be assumed to be constant over the cross-section.

In view of the experimental results shown in Figure 5.17 in which the ratio of cracking torque to ultimate torque calculated by equations 5.21 or 5.22 is plotted against the ratio of cracking moment to ultimate bending moment determined by equation 4.51, an empirical interaction curve relating bending moment to twisting moment is not possible. However an approximation can be made leading to conservative design by using the following criteria:

$$\frac{T_{cr}}{T_u} + \frac{M_{cr}}{M_u} = 1 \quad (5.102)$$

or by employing the criteria of the cracking torque given by equations 5.26 and 5.27.

The ACI proposal given by equation 5.44 is in fact a simplified version of Hsu's general expression given by equation 5.38. A reduction

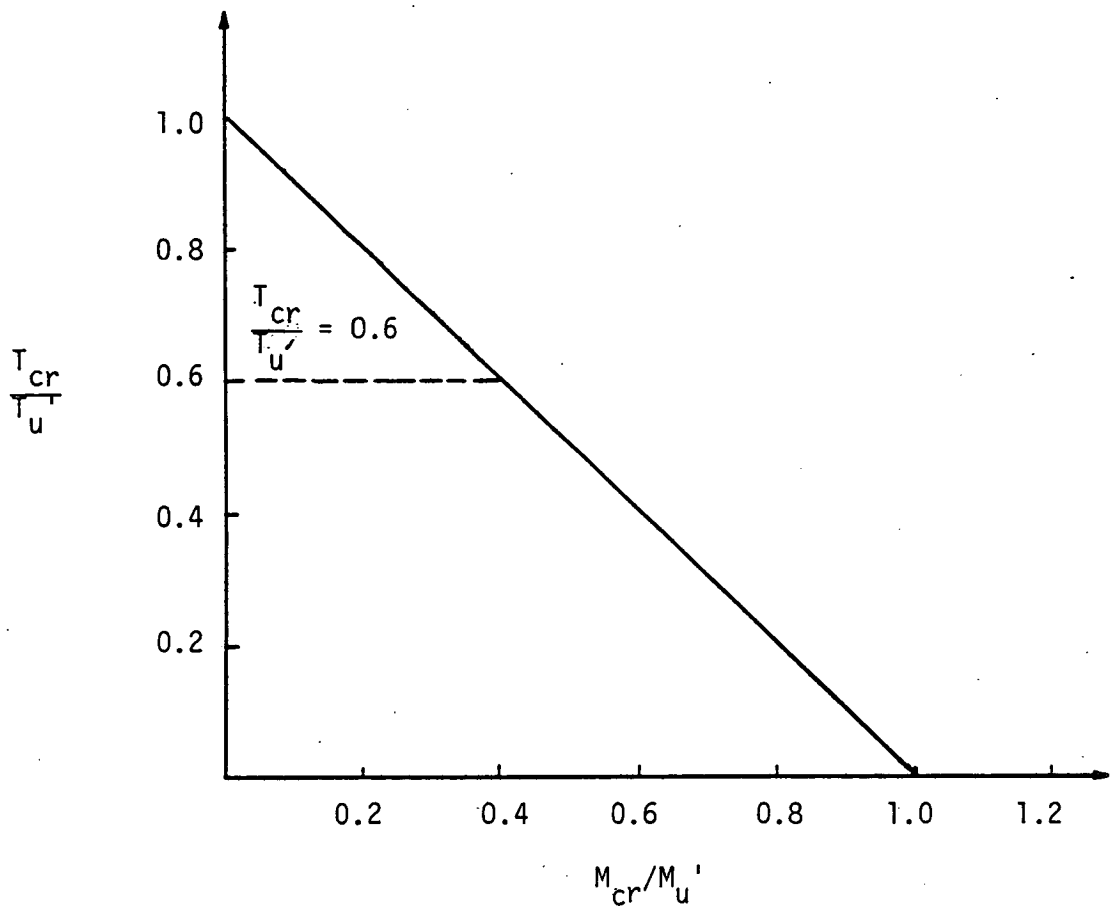


Figure 5.17 Torque-Moment Interaction

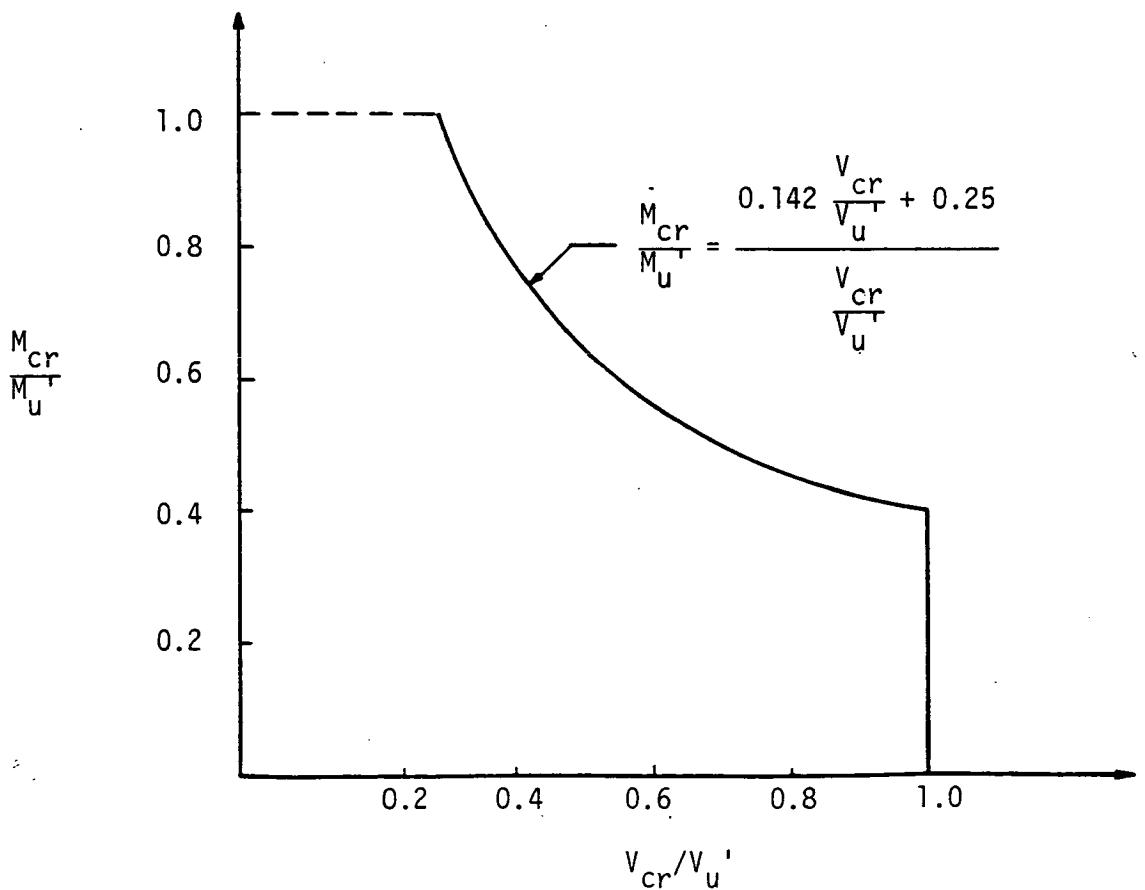


Figure 5.18 Moment-Shear Interaction

in strength for beams subjected to torsion and shear was made by replacing $\frac{1}{\sqrt{b}}$ in the first term of equation 5.36 by $\frac{1}{3}$. The volumetric ratio (m) was assumed ($= 1$). This simplifies the calculation of the shape factor (Ω) in the second term of equation 5.36 and leads to identical yield stresses for the longitudinal and web steel.

The ultimate torsional resistance of a concrete section determined by equation 5.38 of Hsu and equation 5.39 of Cowan, are compared with the experimental values in Table 5.5. Once again equations 5.26 and 5.27 predict the torsional strength of concrete more reasonably than both equation 5.38 and 5.39.

The high values of T_c given by Cowan are due to the fact that equation 5.39 considers the effect of pure torsion only. Equation 5.36 of Hsu also only considers the effect of pure torsion, so that similar values can be expected.

Hsu's modified expression given by equation 5.38 takes into account the effect of flexure in an indirect way to predict the torsional strength. The applied moment is involved in the calculation of the flexural shear stress, and this in turn will influence the torsional shear stress. Thus instead of defining the torsion-shear interaction it was proposed that a beam should be designed separately to carry torsion and bending so that the reinforcement required is the total of the steel required to resist torsion and that to resist bending. This will lead to a conservative design. In any case, shear and bending when added to torsion would decrease the torsional capacity of a beam predicted by each of the expressions.

Collins [17] considered the effect of shear and bending on the torsional capacity of reinforced concrete beam separately. The modes of failure reported were directly affected by the magnitude of

Table 5.5 Comparison Between Calculated and Measured T_c

Beam	T_c (exp.) (kN.m)	T_c (kN.m) Cowan Eq. 5.39	$\frac{T_c \text{ (exp)}}{T_c \text{ Eq.5.39}}$	T_c (kN.m) Hsu Eq. 5.33	$\frac{T_c \text{ (exp)}}{T_c \text{ Eq. 5.33}}$
GR1-B1	1.92	3.93	0.49	2.12	0.9
-B2	2.25	4.52	0.49	2.56	0.88
-B3	2.0	3.95	0.50	2.12	0.94
-B4	2.17	4.25	0.57	2.72	0.80
GR2-B5	2.30	3.93	0.585	1.90	1.2
-B6	2.25	3.93	0.57	1.90	1.18
-B7	2.2	3.93	0.56	1.90	1.15
-B8	2.2	3.93	0.56	1.90	1.15
GR3-A1	0.74	0.85	0.87	0.73	1.01
-A2	0.81	1.22	0.66	0.82	0.98
-A3	0.80	1.22	0.65	0.82	0.97
-A4	0.79	1.22	0.647	0.82	0.96
GR4-B1	0.70	0.81	0.86	0.62	1.12
-B2	0.68	0.81	0.84	0.62	1.09
-B3	0.67	0.81	0.83	0.62	1.08
-B4	0.69	0.81	0.84	0.62	1.11

the applied shear and bending moment acting on the section and the geometry of the section. The assumed failure surface was defined by a continuous tensile crack which formed a rectangular helix on three sides of the beam and a compression zone on the fourth face which joined the two ends of the helix. Failure was defined by the surface on which the compression hinge formed. Collins also considered another possible mode of failure which occurs under large direct shear forces. This however is not critical in this study as discussed in section 5.2.4.

In considering the modified skew bending theory discussed earlier in section 5.2.1, the mode of failure observed in testing the spandrel beams is mode 1. The applied bending moment is always greater than the applied twisting moment as shown in Figure 2.4. Cracks formed on the sides at the bottom of the beam. The cracks further propagated and widened then the reinforcement started to yield. The cracks then opened up and the two parts of the beam rotated about a skew axis near the top. The inclination of this axis depends on many factors such as: the ratio of the bending moment to twisting moment, distributing the reinforcement, dowel forces acting between the steel and the concrete, and the concrete strength under combined stresses.

It is interesting to note that when mode 3 of failure is likely to occur any increase in the bending moment would lead to a definite increase in the torsional capacity as shown in the following interaction equation:

$$\left(\frac{T}{T_u}\right)^2 - \frac{M}{M_u} = R \quad (5.103)$$

where $R = \frac{A_{st} f_s}{A_{sc} f_s}$ = ratio of the forces in the bottom and top steel

T_u, M_u = pure torsional and flexural capacity of the beam.

On the other hand the interaction equation for mode 1 of failure is given by:

$$\left(\frac{T}{T_u}\right)^2 + \left(\frac{M}{M_u}\right) = 1 \quad (5.104)$$

which shows that increasing the bending moment decreases the torsional capacity.

The transition between the two interaction equations occur at:

$$\frac{M}{M_u} = \frac{1}{2} (1 - R) \quad (5.105)$$

The flexural resistance of a reinforced concrete may be reduced considerably in mode 2 type of failure due to the reduction of the lever arm.

It has been proposed that the shear-torsion interaction can be satisfactorily represented by an empirical interaction relation given by equation 5.91 - for unreinforced concrete beams:

$$\frac{T_u}{T_u} + \frac{V_c}{V_u} = 1 \quad (5.91)$$

Collins [17] showed that a linear interaction between shear and torsion for reinforced concrete beams represented by the following equation gives values close to experimental results:

$$\frac{V}{V_u} + \frac{1.6 T}{b V_u} = 1 \quad (5.106)$$

in which an equivalent shear force is substituted instead of T_u' as given in equation 5.91, i.e.:

$$V + \frac{1.6 T}{b} = V_u' \quad (5.107)$$

or
$$T \left(\delta + \frac{1.6}{b} \right) = V_u' \quad (5.108)$$

After cracking the equilibrium mechanism in a reinforced concrete beam changes and the torsion which was initially carried by the concrete is then transferred to the steel which explains the sudden increase in the stresses and strains in the steel stirrups recorded experimentally as shown in Figure 3.9.

Gesund and Boston [91] tested concrete beams containing longitudinal steel only under the combined influence of bending and torsion. It was concluded that the dowel action between steel and concrete may produce a considerable torsional resistance after cracking if the cracks are of the flexural type. The contribution of the dowel action of the longitudinal bars to the torsional strength of beams under pure torsion may be as high as 40% [92].

To include the effect of shear stress due to bending in equation 5.101, the following equation is proposed to represent moment-shear interaction for a concrete beam, as shown in Figure 5.18:

$$\frac{M_{cr}}{M_u'} = \frac{0.142 \frac{V_{cr}}{V_u'} + 0.25}{\frac{V_{cr}}{V_u'}} \quad (5.109)$$

where M_u' , V_u' = concrete flexural and shear resistance

M , V = ultimate applied bending moment and shear force

M_{cr} = cracking bending moment

In the absence of more information the ultimate shear capacity as given by the ACI is taken (for reinforced concrete beams) i.e.:

$$V_u = 2 \text{ bd } \sqrt{f_c} + \frac{2 A_w f_{wy} \cdot d}{s} \leq 8 \text{ bd } \sqrt{f_c} \dots (1b) \quad (5.110)$$

CHAPTER 6 : Moment Curvature Characteristics of Flexural Sections

6.1 Introduction

6.2 Moment Curvature Relationship

6.2.1 Analysis at Cracking Stage

6.2.2 Analysis at Yield Stage

6.2.3 Analysis at Ultimate Stage

6.3 Moment Curvature Relationship for Confined Section

6.4 Experimental Evaluation of Curvature

6.1 Introduction

The evaluation of the moment-curvature relationship is an important step in the analysis of the deformation behaviour of the floor beams from which the load deformation or moment rotation characteristics are evaluated.

In this chapter analytical expressions for the moment-curvature relationship of the floor beams are derived. The properties of the material and the compatibility relationship are involved in the approach adopted.

6.2 Moment Curvature Relationship

The behaviour of the test specimen has already been discussed in terms of three significant stages which define the load-deformation response of the floor beams. It is more convenient to employ moment rather than load at each of these stages in the analysis. Once the moments are determined, the loads are easily calculated by statics.

With reference to Figure 6.1(a):

- 0-1: is the elastic uncracked region which extends up to point (2) where cracks on the tension side in the area of maximum moment start to appear. This stage is defined as the cracking stage.
- 1-2: the elastic region; yielding of the tensile steel commences in this stage and is defined as the yielding stage.
- 2-3: defines the region of non-linearity which extends until the stage of failure.

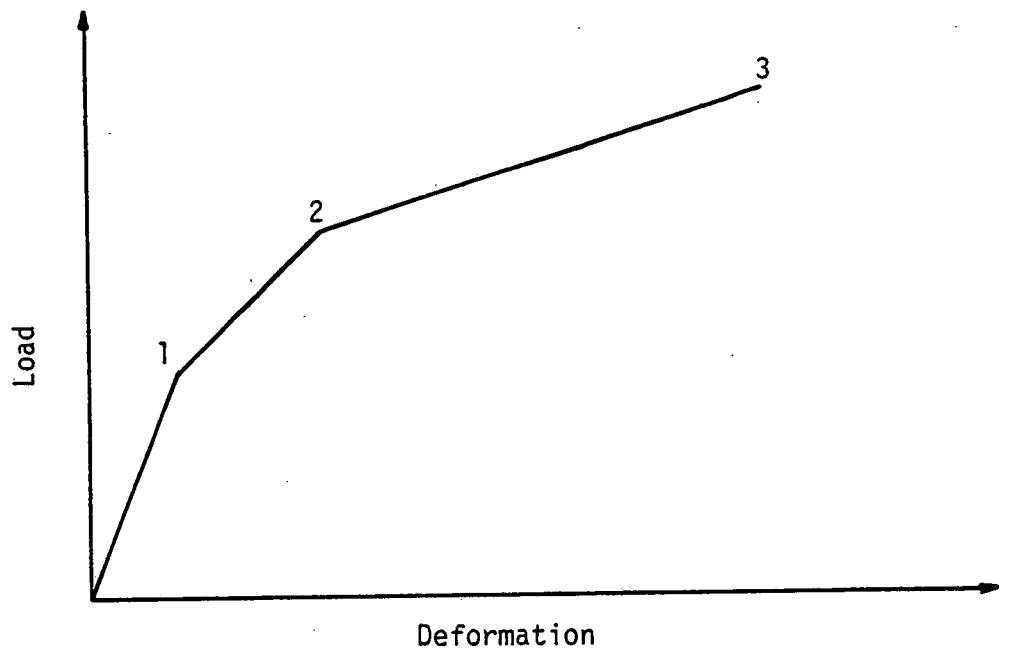


Figure 6.1(a) An Idealized Load-Deformation Diagram.

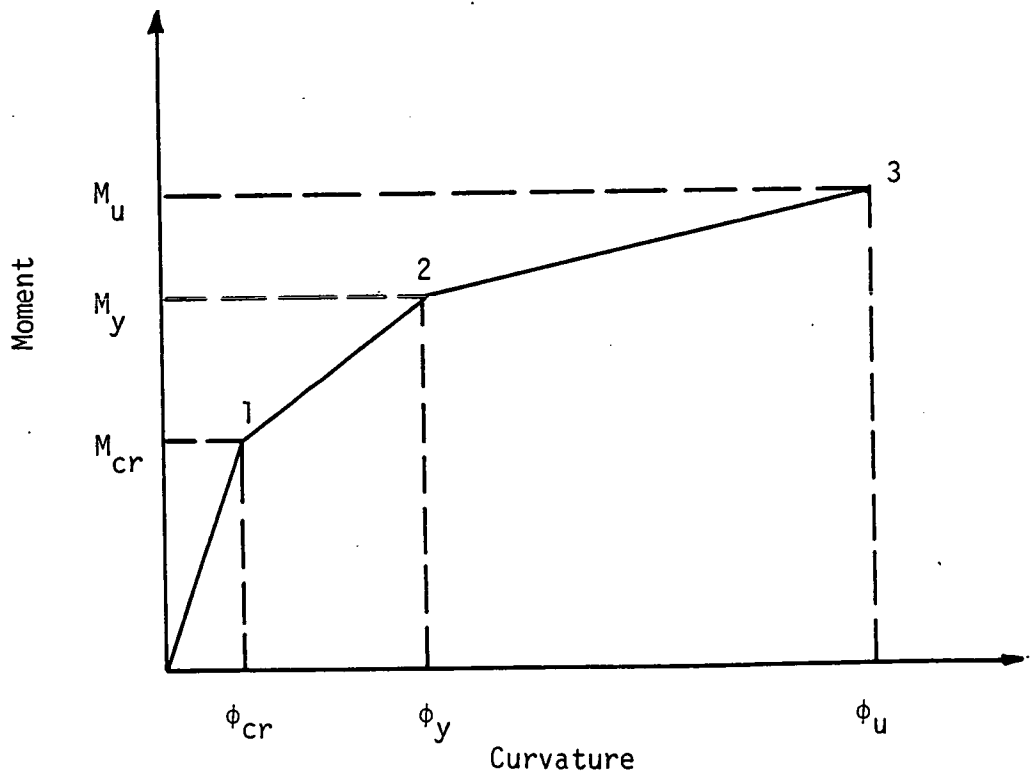


Figure 6.1(b) An Idealized Moment-Curvature Diagram

Beeby [48] discussed the pre-cracking and post-cracking flexural rigidity which can be used in the analysis of moment-curvature relationship as well as discussing some other proposed formula.

Another approach adopted for the analysis of the moment-curvature relationship, is based on a sectional analysis in which the properties of the material and compatibility are involved [30].

Any method based on the idea that curvature depends only on the bending moment at a section, underestimates the ability of a beam to take large strains in critical regions of high bending moment. Moreover prediction can not be made in a situation where the bending moment reaches a maximum value and then decreases as a function of the curvature.

The moment-curvature curve is in a form similar to the stress-strain curve for concrete in compression; that is where three separate regions can be identified, namely the elastic region (uncracked, cracked), an inelastic region and finally the falling branch, as discussed before. The falling branch, of the moment-curvature curve, where the moment decreases with considerable increase of curvature, is very difficult to assess experimentally. The difficulties involved are similar to those encountered in finding the complete stress-strain curve. However the uncertainty of the meaning of this falling branch has resulted in its omission from reported research work [93].

Figure 6.1(b) shows an idealized diagram for the moment curvature relationship for an under-reinforced concrete section. It can be seen that the diagram follows the same sequence of load-deformation response in Figure 6.1(a). Point (1) indicates the cracking of concrete in the tension zone. The commencement of the tensile steel yielding in the floor beam is represented by point (2). Beyond this point the

concrete crushes in compression since all floor beams are under-reinforced, cracking and yielding of the steel in the tension zone will always precede crushing of concrete. Then failure of the beam at ultimate occurs.

6.2.1 Analysis at Cracking Stage

This is determined by the first significant break marked as (1) in the moment curvature diagram. Prior to cracking the section is uncracked and the beam behaves essentially elastically. When the tensile stress in the tension zone at the critical section is equal to the tensile strength of concrete, the concrete cracks thus reducing the flexural stiffness of the section. The curvature (ϕ) of an uncracked section may be expressed by:

$$\phi = \frac{M}{E_c I} \quad (6.1)$$

where M = the applied moment,

E_c = concrete modulus of elasticity,

I = moment of inertia of the gross section about its centroidal axis in the plane of bending.

The modulus of elasticity for the concrete is taken from experimental results given in the test programme. A good approximation can be adopted by considering the gross moment of inertia rather than the moment of inertia of the transformed section in determining the flexural rigidity ($E_c I$). Using the value of the uncracked flexural rigidity, the deflection at mid-span can also be determined at this stage prior to cracking. Cracking of concrete will result when the tensile stress

in the extreme fibre of the concrete in the tension zone produced by the applied moment, is equal to the tensile strength of the concrete expressed by the modulus of rupture (f_t). This criteria is suitable for calculating the cracking moment, thus:

$$M_{cr} = f_t \cdot \frac{I}{C} = f_t \cdot Z = \frac{f_t (b h^2)}{4.4} \quad (4.51)$$

where Z = section modulus,

h = gross depth of beam section,

f_t = tensile strength of concrete expressed as the modulus of rupture and can be determined using equation 3.5 viz:

$$f_t = 0.6 \sqrt{f_c}$$

A comparison between the computed cracking moment and the measured cracking moment for the floor beams of the test specimens is shown in Table 6.1. The behaviour of the floor beams is not influenced by the development of the cracks at this stage. Though the results do not show a definite trend, in general the cracking moment of the floor beams varies between 30% to 55% of the maximum measured moment.

6.2.2 Analysis at Yield Stage

The second break in the moment-curvature diagram is also indicated (2). This stage is defined by yielding of the tension steel and a continuous increase in deflection at a point where the applied load becomes nearly constant. Yielding of the tension steel is reached before the strain in the concrete is high enough to produce crushing as long as the section is under-reinforced. This region extends between (1) and (2) on the idealized moment-curvature diagram. The

Table 6.1 Comparison Between Measured and Calculated M_{cr}

Specimen	Cracking Moment (kN.m)		M_{cr} (cal.)	M_{max} Measured (kN . m)	$\frac{M_{cr}}{M_{max}}$ (meas.) %
	Measured	Calculated	$\frac{M_{cr}}{M_{cr}}$ (meas.)		
GR1-B1	24.79	7.39	0.30	31.41	78.9
-B2	23.87	8.54	0.35	44.25	54
-B3	23.65	7.39	0.31	46.0	51.4
-B4	23.95	8.0	0.33	49.75	48.1
GR2-B5	17.05	7.39	0.43	47.0	36.2
-B6	19.88	7.4	0.37	46.6	42.6
-B7	19.62	7.4	0.38	51.12	38.3
-B8	16.68	7.4	0.44	52.37	31.8
GR3-A1	3.78	1.64	0.43	8.3	45.5
-A2	2.23	1.9	0.85	7.41	30.0
-A3	2.02	1.9	0.94	7.63	26.5
-A4	2.48	1.9	0.766	7.5	33.06
GR4-B1	1.52	1.07	0.70	3.85	39.4
-B2	1.26	1.07	0.85	3.22	39.1
-B3	1.75	1.07	0.61	3.46	50.0
-B4	1.49	1.07	0.72	4.28	34.8

analysis of this stage requires the following assumptions:

1. Linear distribution of strains over the depth of the section. This assumption has been proved experimentally to be reasonably accurate and universally accepted in most analyses of reinforced concrete sections; the average strains are measured on adequately long gauge lengths.
2. Linear stress-strain relationship for concrete at the commencement of the tensile reinforcement yielding, i.e. zero at the neutral axis and maximum at the compressive face as shown in Figure 6.2.
3. Concrete tensile strength is negligible.
4. The stress-strain curve for the reinforcement obtained experimentally and shown in Figure 2.6 can be approximated to the tri-linear form shown in Figure 6.4.

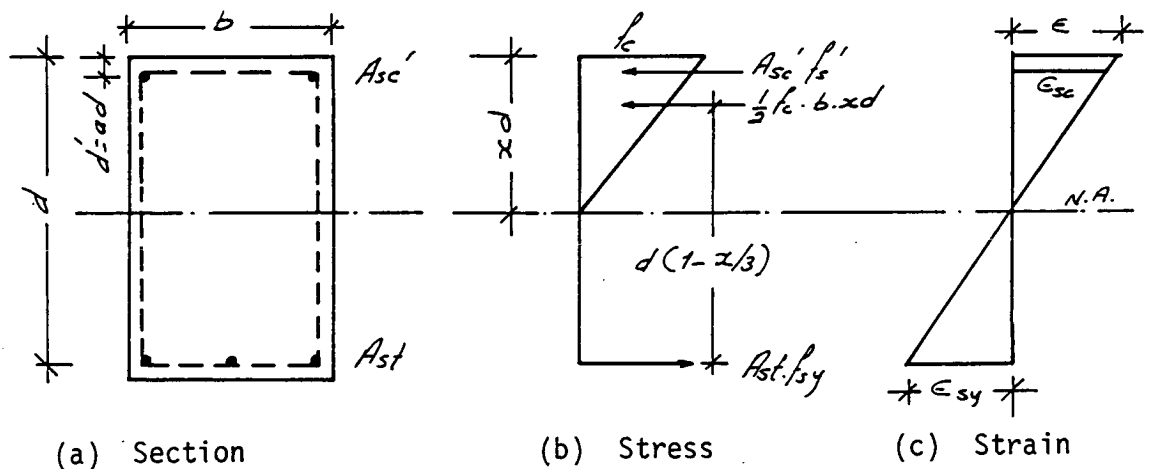


Figure 6.2 Conditions of Yielding of Tension Reinforcement

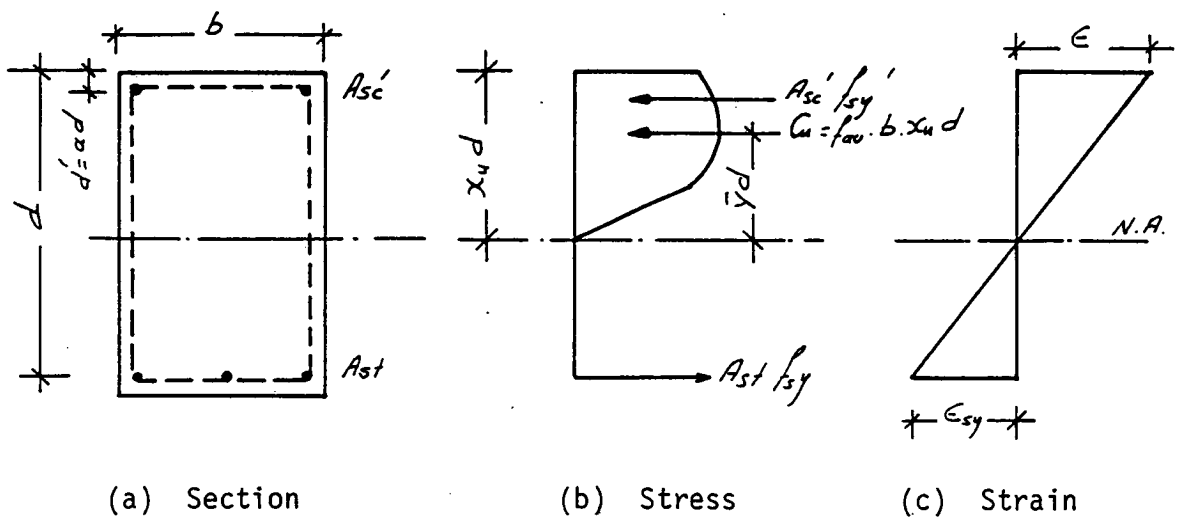


Figure 6.3 Conditions at Ultimate Stage

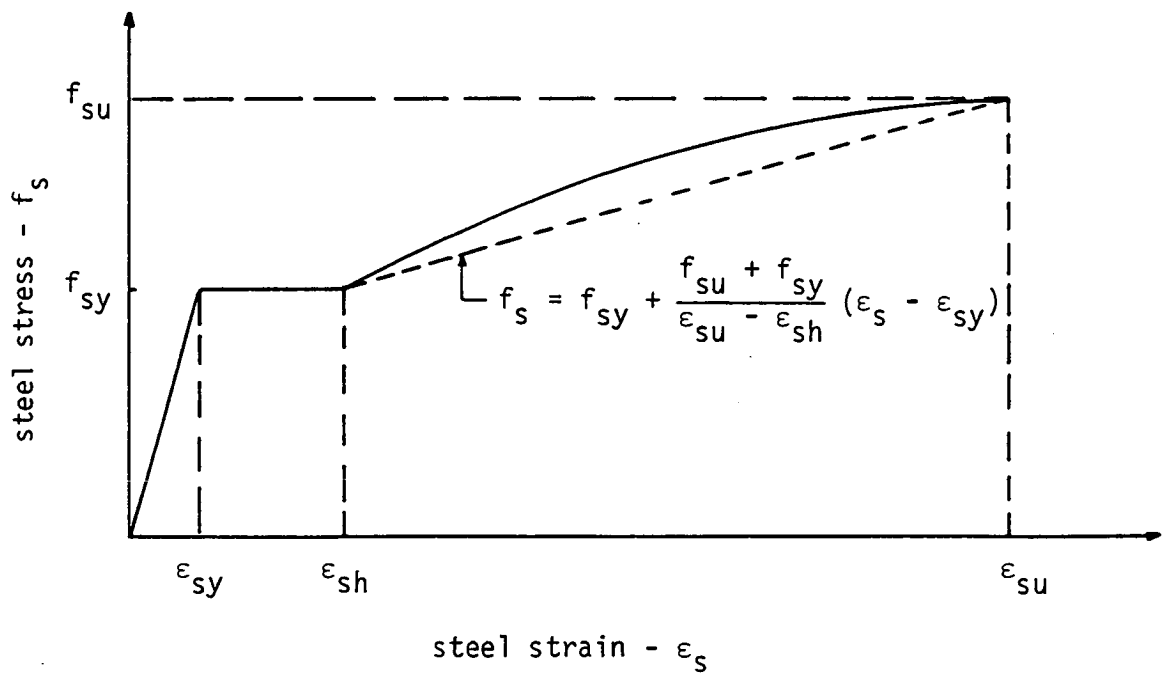


Figure 6.4 Idealized Steel Stress-Strain Curve

The yield strain of the steel can be determined accurately from the stress-strain curve and since up to the yielding strain, ϵ_{sy} , the stress is linearly proportional to the modulus of elasticity E_s ; the yield curvature is thus:

$$\phi_y = \frac{\epsilon_{sy}}{d - xd} = \frac{f_{sy}}{d E_s (1 - x)} \quad (6.2)$$

where xd = depth of the neutral axis from the extreme compressive fibre of the section.

The beams are assumed to have compression steel as well as tension steel. Using the following general expression, the ratio (x) can be obtained:

$$x = -m (P_s + P') \left[1 - \sqrt{1 + \frac{2 (P_s + a P')}{m (P_s + P')^2}} \right] \quad (6.3)$$

where $P_s = \frac{A_{st}}{bd}$, $P' = \frac{A_{sc}'}{bd}$

$a = \frac{d'}{d}$, $m = \text{modular ratio, } \frac{E_s}{E_c}$

$ad = d'$: depth of the compression steel from the top fibre of the section under compression.

Combining equations 6.2 and 6.3, the yield curvature becomes:

$$\phi_y = \frac{f_{sy}}{d E_s \left[1 + m (P_s + P') \left(1 - \sqrt{1 + \frac{2 (P_s + a P')}{m (P_s + P')^2}} \right) \right]} \quad (6.4)$$

The internal moment at the critical section at the yield stage

can be computed by establishing the depth of the neutral axis and the magnitude and distribution of the strain over the section.

The strain in the compression steel is:

$$\epsilon_{sc} = \phi_y (xd - ad) = \phi_y d (x - a) \quad (6.5)$$

when $\epsilon_{sc} < \epsilon_{sy}$, the compressive force in the compression steel, C_{sc} , is:

$$C_{sc} = \epsilon_{sc} \cdot E_s \cdot A_{sc}' \quad (6.6)$$

when $\epsilon_{sc} \geq \epsilon_{sy}$, then:

$$C_{sc} = A_{sc}' \cdot f_s' \quad (6.7)$$

where f_s' = the stress in compression steel.

By satisfying the equilibrium condition i.e. the compressive forces must equal the tensile force in the tension steel, at yield, in the section then:

$$T = C$$

$$A_{st} \cdot f_{sy} = C_c + C_{cs} \quad (6.8)$$

$$\text{or} \quad C_c = A_{st} \cdot f_{sy} - C_{cs} \quad (6.9)$$

where C_c = is the compressive force in the concrete. The moment at the critical section at this stage is thus:

$$M_y = C_c \left(d - \frac{xd}{3} \right) + C_{sc} (d - ad) \quad (6.10)$$

By substituting for C_c and C_{sc} in equation 6.10, M_y becomes:

$$M_y = (A_{st} \cdot f_{sy} - A_{sc}' \cdot f_s') \left(d - \frac{xd}{3}\right) + A_{sc}' \cdot f_s' (d - ad) \quad (6.11)$$

The stress in the compression steel (f_s') can be determined from Figure 6.2:

$$\begin{aligned} f_s' &= E_s \cdot \epsilon_{sc} \\ &= E_s \cdot \epsilon_{sy} \left(\frac{x-a}{1-x}\right) \end{aligned} \quad (6.12)$$

when the compression steel has also yielded:

$$F_s' = A_{sc}' \cdot f_{sy}' \quad (6.13)$$

where f_{sy}' = yield strength of compressive reinforcement.

For beams without compression steel, the depth of the neutral axis, the yield curvature and the yield moment can still be computed using more simplified expressions by reducing equations 6.3, 6.4 and 6.11 respectively to:

$$x_d = (\sqrt{(mp_y)^2 + 2 mp_s} - mp_y) d \quad (6.14)$$

$$\phi_y = \frac{f_{sy}}{d E_s (1 + mp_y) - \sqrt{(mp_y)^2 + 2 mp_s}} \quad (6.15)$$

and
$$M_y = (A_{st} \cdot f_{sy}) \left(d - \frac{xd}{3}\right) \quad (6.16)$$

The load_displacement response can be evaluated if the distribution and magnitude of the curvature can be computed. The factors that influence the theoretical prediction of the curvature at the yield stage therefore must be investigated. The assumed linear distribution of concrete may be different from the actual distribution. The error is negligible if the maximum stress at the top fibre of the beam is less than approximately half the ultimate compressive strength of concrete. Since the floor beams investigated in this programme are under-reinforced, this assumption is satisfied. The reinforcement ratios (P_y) provided in the beams are well below the value of the balanced reinforcement ratio required to produce a balanced failure by simultaneous crushing of the concrete and yielding of the tension steel. A better evaluation can be obtained by employing the actual stress-strain curve of the concrete in the beam.

The curvature at yielding given by equation 6.2 is very sensitive to the yielding strain, ϵ_{sy} , in the tensile steel. Computations on the basis of carefully measured values of ϵ_{sy} are more preferable than adopting an assumed theoretical value.

The depth of the neutral axis given by equation 6.3 is also involved and influences the magnitude of the curvature. The effect of the approximation in equation 6.3 may not be significant as long as the beams are under-reinforced as discussed earlier. The effect may disappear in equation 6.14.

The value of the steel modulus of elasticity E_s , is obtained from experimental results and the value of the concrete modulus of elasticity E_c , is also obtained from experimental results measured at 0.5×10^{-3} strain as shown in Table 2.6. Table 6.2 shows the moment_curvature values for the floor beams.

Table 6.2 Moment_Curvature at Yield Stage

Specimen	f'_c N/mm ²	P_s	P'	$\phi_y \times 10^{-4}$	Yield Moment (kN.m)		$\frac{M_y \text{ (meas.)}}{M_y \text{ (comp.)}}$
					Computed	Measured	
GR1-B1	30	1.345	0.24	0.837	30.85	31.00	1.0
-B2	40	"	"	0.832	30.86	33.52	1.09
-B3	30	"	"	0.837	30.70	31.80	1.04
-B4	35	"	"	0.833	30.85	32.00	1.03
GR2-B5	30	"	"	0.837	30.85	34.00	1.1
-B6	30	"	"	0.837	30.85	34.25	1.102
-B7	30	"	"	0.837	30.85	34.3	1.11
-B8	30	"	"	0.837	30.85	35.75	1.16
GR3-A1	30	1.2	0.43	1.48	5.29	6.0	1.13
-A2	40	"	"	1.249	5.31	5.5	1.04
-A3	40	"	"	1.249	5.31	5.3	0.994
-A4	40	"	"	1.249	5.31	5.35	1.0
GR4-B1	40	1.1	"	1.598	2.59	2.8	1.08
-B2	40	"	"	1.598	2.59	2.75	1.06
-B3	40	"	"	1.598	2.59	2.75	1.06
-B4	40	1.2	"	1.598	3.80	3.9	1.03

6.2.3. Analysis at Ultimate Stage

This is the third significant break in the moment-curvature curve prior to failure. This region extends between 2-3 on the idealized diagram and is defined by yielding of the tensile steel, propagation of the cracks and crushing of the concrete in the compression zone.

In order to analyse this stage, the following assumptions have to be made in addition to those referred to in the yield stage.

1. The properties of the concrete stress block at maximum moment and the characteristics of the complete stress-strain curve are required. The inelastic stress distribution and the strain distribution over the section are shown in Figure 6.3. The shape of the stress block adopted is the stress-strain curve represented by equation 4.19 as discussed in Chapter Four.
2. Steel in the compression zone has yielded at ultimate stage.
3. The stress-strain curve for the reinforcement is idealized to a tri-linear form in order to consider any effect of strain hardening of the steel at this stage.
4. The assumed stress distribution in the compression zone, the ultimate strain of the concrete in the compression zone, the average stress and other stress block parameters are computed on the basis of experimental results and represented by expressions adopted in Chapter Four.

With reference to Figure 6.3 and due to the equilibrium condition of the internal forces, the following relationship is true:

$$T = C$$

$$f_s \cdot A_{st} = C_u + f_{sy}' A_{sc}' \quad (6.17)$$

where C_u is the ultimate compressive force and given by the following equation in terms of the average stress of the compression zone:

$$C_u = (f_{av}) (b) (x_u d) \quad (4.27)$$

Thus equation 6.17 becomes:

$$f_s \cdot A_{st} = f_{av} \cdot b \cdot x_u d + A_{sc}' \cdot f_{sy}'$$

or

$$x_u = \frac{f_s \cdot A_{st} - A_{sc}' \cdot f_{sy}'}{f_{av} \cdot b \cdot d}$$

or

$$x_u = \frac{P_s f_s - P' f_{sy}'}{f_{av}} \quad (6.18)$$

Having located the neutral axis using equation 6.18, the ultimate moment of the internal forces is given as:

$$\begin{aligned} M_u &= C_u (d - x_u d + \bar{y}d) + A_{sc}' f_{sy}' (d - ad) \\ &= bd^2 [f_{av} \cdot x_u (1 - \bar{g}) + P' f_{sy}' (1 - a)] \quad (6.19) \end{aligned}$$

where $\bar{g} = x_u - \bar{y}$

From Figure 6.3(c), the curvature at this stage is

$$\phi = \frac{\epsilon_s + \epsilon_u}{d} \quad (6.20)$$

also
$$\frac{x_u d}{d} = \frac{\epsilon_u}{\epsilon_s + \epsilon_u} \quad (6.21)$$

Substituting the value of x_u from equation 6.18 in equation 6.21 gives:

$$\frac{P_s f_s - P' f_{sy}'}{f_{av}} = \frac{\epsilon_u}{\epsilon_s + \epsilon_u}$$

$$\therefore f_s = \frac{1}{P_s} \left(\frac{f_{av} \cdot \epsilon_u}{\epsilon_s + \epsilon_u} + P' f_{sy}' \right) \quad (6.22)$$

Equation 6.22 defines the tensile stress in the tension steel and with the help of the idealized stress-strain curve in Figure 6.4, the strain in the steel at any stage can be evaluated according to the following three conditions:

1. $f_s < f_{sy}$, then $\epsilon_s = \frac{f_s}{E_s}$
2. $f_s = f_{sy}$, then $\epsilon_s = \epsilon_{sy}$
3. $f_s > f_{sy}$, then $\epsilon_s = \epsilon_{sy} + \frac{f_s - f_{sy}}{E_s'}$

$$\text{where } E_s' = \frac{f_{su} - f_{sy}}{\epsilon_{su} - \epsilon_{sh}}$$

It can be seen that the ultimate moment and the ultimate curvature are dependent on the condition of stress in the tension steel (f_s). For beams without compression steel equations 6.18 and 6.19 are reduced to:

$$x_u = \frac{P_s \cdot f_s}{f_{av}} \quad (6.18a)$$

and
$$M_u = f_{av} \cdot b d^2 x_u (1 - \bar{g}) \quad (6.19a)$$

It may be noted that this equation is similar to the expression obtained in Chapter Four, equation 4.34. Furthermore the reinforced ratio (P_s) corresponding to a particular strain condition must be known to determine the stress in the tension steel at the ultimate stage. This can be done by applying the conditions of strain compatibility and forces equilibrium then:

$$x_u = \frac{\epsilon_u}{\epsilon_s + \epsilon_u} = \frac{P_s \cdot f_s}{f_{av}}$$

or
$$P_s = \frac{1}{f_s} \left(\frac{\epsilon_u \cdot f_{av}}{\epsilon_s + \epsilon_u} \right)$$

In the case of balanced failure, i.e. yielding of the tensile steel and crushing of the concrete take place simultaneously, the balanced steel ratio P_b is:

$$P_b = \frac{1}{f_{sy}} \left(\frac{\epsilon_u \cdot f_{av}}{\epsilon_{sy} + \epsilon_u} \right) \quad (6.23)$$

For the case of strain hardening commencement, i.e. $\epsilon_s = \epsilon_{sh}$, then steel ratio P_{sh} is

$$P_{sh} = \frac{1}{f_s} \left(\frac{\epsilon_u \cdot f_{av}}{\epsilon_{sy} + \epsilon_u} \right)$$

in this case $f_s > f_{sy}$.

There are three possible conditions:

1. When $P_s > P_b$ then $f_s < f_{sy}$, i.e. the stress in the tension steel is below yielding stress.

2. When $P_b > P_s > P_{sh}$, then $f_s = f_{sy}$, i.e. the stress in the tension steel is equal to the yielding stress.
3. When $P_{sh} > P_s$, then $f_s > f_{sy}$ at ultimate.

The ultimate curvature is given by equation 6.20:

$$\phi_u = \frac{\epsilon_s + \epsilon_u}{d}$$

The value of ϵ_s can be evaluated by considering the following three conditions:

For the first condition where $f_s < f_{sy}$

$$\epsilon_s = \frac{f_s}{E_s}$$

For the second condition where $f_s = f_{sy}$, $\epsilon_s = \epsilon_{sy}$

$$\phi_u = \frac{\epsilon_u}{x_u d} \quad (6.24)$$

where $x_u = \frac{P_s f_{sy}}{f_{av}}$

For the third condition where $f_s > f_{sy}$

$$\epsilon_s = \epsilon_{sy} + \frac{f_s - f_{sy}}{E_s}$$

for beams without compression steel (f_s) can be obtained from equation 6.22.

The values of ϵ_o , ϵ_u and f_{av} adopted in this section for the computation of the moment and the curvature at various stages are

obtained from the expressions given in Chapter Four viz:

$$\begin{aligned}\epsilon_o &= 0.875 \times 10^{-3} (f_c')^{\frac{1}{4}} \\ \epsilon_u &= \frac{7.8 \times 10^{-3}}{(f_c')^{\frac{1}{4}}} \\ f_{av} &= f_c' \frac{\epsilon_o}{\epsilon_u} \ln \left(1 + \frac{\epsilon_u}{\epsilon_o} \right)^2\end{aligned}$$

Using the relationships developed in this section, the moment curvature characteristics and the load-deformation response can be evaluated by establishing the distribution of curvature along the member.

Table 6.3 shows the moment-curvature values for the floor beams. Figure 6.5 shows idealized distributions of moment and curvature at different stages.

6.3 Moment Curvature Relationship for Confined Section

The effect of confinement has been discussed in detail in Chapter Four. However the most significant effect of the confinement is on the strength and deformation characteristics of the specimens. The ultimate strain of the concrete is highly influenced by the confinement of the section. Chan [32] proposed the following expression to calculate the ultimate strain of a section confined by rectangular ties:

$$\epsilon_u' = \epsilon_u + \frac{(P'')^{1/3}}{24.44} \quad (6.25)$$

where ϵ_u' = ultimate strain of bound concrete

Table 6.3 Moment-Curvature at Ultimate Stage

Specimen	$\phi_u \times 10^{-4}$	Ultimate Moment (kN.mm)		$\frac{M_u \text{ (meas.)}}{M_u \text{ (comp.)}}$
		Computed	Measured	
GR1-B1	5.0	41.6	31.41	0.75
-B2	4.99	42.3	44.25	1.04
-B3	4.99	41.98	46.0	1.1
-B4	5.00	41.6	49.75	1.19
GR2-B5	5.0	41.6	47.0	1.12
-B6	5.0	41.6	46.6	1.12
-B7	5.0	41.6	51.175	1.2
-B8	5.0	41.6	52.37	1.27
GR3-A1	8.88	8.47	8.3	0.98
-A2	8.57	8.6	7.41	0.86
-A3	8.57	8.6	7.63	0.89
-A4	8.57	8.6	7.5	0.88
GR4-B1	9.57	4.0	3.85	0.96
-B2	9.57	4.0	3.22	0.8
-B3	9.57	4.0	3.46	0.87
-B4	9.57	4.0	4.28	1.07

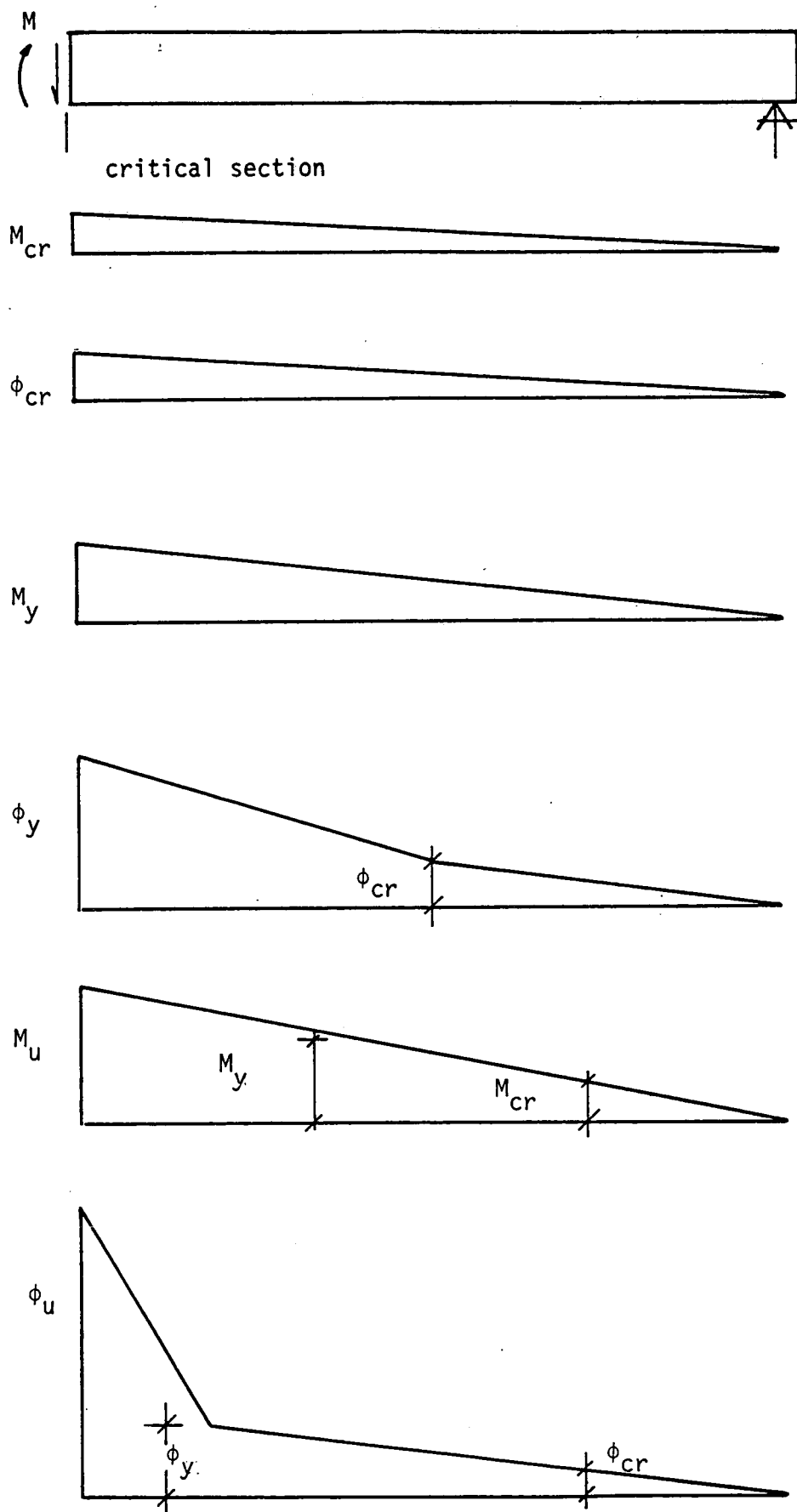


Figure 6.5 Idealized Distribution of Moment and Curvature at Cracking, Yield and Crushing

$$P'' = \frac{\text{volume of stirrups}}{\text{volume of bound concrete}} + 0.1 \frac{D}{s}$$

D = diameter of the compression steel,

s = spacing of the closed rectangular stirrups.

Corley [31] included a parameter to define the size-effect and strength of the lateral reinforcement on the ultimate strain given by the following expression:

$$\epsilon_u' = 0.003 + 0.02 \frac{b}{Z} + \left(\frac{P_C'' f_{wy}}{140} \right)^2 \quad (6.26)$$

where Z = distance between points of zero and maximum moments,

f_{wy} = the yield stress of the lateral reinforcement expressed in N/mm^2 ,

P_C'' = ratio of volume of binding steel (one stirrup plus compression steel between stirrups) to volume of concrete bound (product of stirrup spacing and area enclosed by stirrup).

It is evident that the ultimate strain of concrete depends on the following factors:

1. The depth of the neutral axis at failure ($x_u d$).
2. Volume of stirrups.

Indeed equations 6.25 and 6.26 take into consideration only the second factor. Another approach proposed by Baker and Amarakone [94] to take into consideration the influence of the stirrups and the neutral axis depth at failure on, ϵ_u , for bound concrete, and is given by the following empirical equation where $\epsilon_u < 0.01$:

$$\epsilon_u' = 0.0015 [1.0 + 1.5 P_v + \frac{1}{x_u d} (0.7 - 0.1 P_v)] \quad (6.27)$$

where $P_v = \frac{\text{volume of stirrups per unit length}}{bd}$

The results of Soliman and Yu's experimental investigations [68] on the confined concrete stress-strain relationship to define the ultimate strain is given by the following expression:

$$\epsilon_u' = 0.003 (1 + 0.8 q'') \quad (6.28)$$

The parameter q'' is defined in section 4.4.

It can be seen that the ultimate strain of a confined section is given by the total of the ultimate strain of the unconfined section plus a value due to confinement. Therefore it is more convenient to rewrite equations 6.26 and 6.28 in the following form since the ultimate strain of the unconfined concrete section is dependent on the concrete strength and never constant:

$$\epsilon_u' = \epsilon_u + 0.02 \frac{b}{Z} + \left(\frac{P_c'' f_{wy}}{140} \right)^2 \quad (6.29)$$

$$\epsilon_u' = \epsilon_u (1 + 0.8 q'') \quad (6.30)$$

The value of ϵ_u is given by equation 4.17.

The expressions derived earlier to compute the ultimate flexural strength of the unbound section can be modified to include the effect of confinement, so that equation 6.19 can be rewritten as:

$$M_u = bd^2 [f_{av}'' x_u (1 - \bar{g}) + P' f_{sy}' (1 - a)] \quad (6.31)$$

f_{av}'' = the average stress of the compressive block for the confined section

$\bar{g}d$ = the distance of the centroid of the compressive block from the extreme compressive fibre.

Both terms are defined in section 4.4. Equation 6.31 is also valid for beams without compression steel and becomes:

$$M_u = f_{av}'' \cdot x_u (1 - \bar{g}) b d^2$$

which is similar to equation 6.19(a) obtained earlier. Similarly the curvature of a confined section can be calculated by the following expression:

$$\phi = \frac{\epsilon_u'}{x_u d} \quad (6.32)$$

where $x_u d = \frac{P_s f_{sy}}{f_{av}''}$

Table 6.4 shows the values of the ultimate strain for the confined section proposed by Chan, Corley and Soliman and Yu. It is evident that the values computed by the expressions proposed by those investigators differ considerably and the values of the curvature of a confined concrete section differ accordingly since the ultimate strain (ϵ_u') is the main parameter for computing the curvature as given by equation 6.32. This is illustrated in Table 6.5 where the values of curvature of specific specimens are compared. Undoubtedly, Chan's expression gives considerably higher values than the other two. The values of the other parameters involved in Tables 6.4 and 6.5 are computed by expressions given in Chapter Four.

Table 6.4 Ultimate Strains of a Confined Section

ϵ_u	Chan Eq. 6.25	Corley Eq. 6.26	Soliman and Yu Eq. 6.28
	ϵ_u'	ϵ_u'	ϵ_u'
0.00368	0.0126	0.0062	0.0047
0.00348	0.0124	0.0060	0.0045
0.00333	0.0123	0.0058	0.0043
0.0032	0.0121	0.0057	0.0041
0.00310	0.0120	0.0056	0.0040

Table 6.5 Values of Curvature

Specimen	Chan	Corley	Soliman and Yu
	$\phi \times 10^{-4}$	$\phi \times 10^{-4}$	$\phi \times 10^{-4}$
GR1-B1	2.76	1.3	0.962
-B2	3.131	1.47	1.06
-B3	3.48	1.63	1.16
-B4	2.76	1.3	0.962
GR3-A1	4.11	1.94	1.44
-A2	5.2	2.43	1.736
GR4-B1	7.2	3.36	2.4

6.4 Experimental Evaluation of Curvature

The strain measurements were recorded over the depth of the floor beam section at midspan i.e. at the critical section using Demec points. Demec points were fixed at six levels from the extreme compression side to the level of the tension reinforcement. Electrical resistance type strain gauges were also fixed on the bottom tensile steel in the beams. More details regarding instrumentation are discussed in the test programme.

The assumption of a linear distribution of strain is not valid at higher loads, i.e. in the inelastic region and strains measured at the surface can no longer be regarded as a true measure of the internal behaviour of the concrete.

At this stage the strain in the tension steel is considered more reliable assuming that the steel-concrete bond remains perfect which is not true for all loading stages.

CHAPTER 7 : TORQUE-TWIST CHARACTERISTICS

7.1 Torsional Stiffness

7.1.1 Precracking Stiffness

7.1.2 Postcracking Stiffness

7.1.3 Comparison and Discussion

7.2 Deformation Response

7.2.1 Rotational Behaviour

7.2.2 Ductility

7.1 Torsional Stiffness

The behaviour of concrete members subjected to torsion is well understood and the torsional stiffness can be predicted reliably. When the applied torsion is increased until the principal tensile stresses at the critical section are equal to the tensile strength of the concrete, the concrete cracks. This reduces the stiffness of the section. Following formation of the first crack, crack propagation continues well into the member changing the section properties from uncracked stiffness to the lower stiffness drastically. The decrease in torsional stiffness after cracking is generally greater than the decrease in flexural stiffness. Accordingly two types of stiffness are recognized:

1. Precracking stiffness.
2. Postcracking stiffness.

The torsional stiffness can be defined as the twisting moment required to produce a unit angle of twist per unit length,

$$\text{i.e. } S = \frac{T}{\theta} \quad (7.1)$$

where S = torsional stiffness,

T = twisting moment,

θ = angle of twist.

7.1.1 Precracking Stiffness

The torsional stiffness of a reinforced concrete beam prior to cracking is considered to be the same as the stiffness of a plain

concrete beam.

Hsu [7,16] proposed the following equation to predict the cracking torque (T_{cr}) of a reinforced concrete beam:

$$T_{cr} = (1 + 0.04 P_t) T_u' \quad (5.30)$$

By definition the torsional stiffness may be expressed as the ratio of torque/twist, where T_u' in equation 5.30 is the failure torque of an unreinforced concrete beam. The failure rotation of an unreinforced beam or the cracking rotation (θ_{cr}) is given by:

$$\theta_{cr} = \frac{0.43 \times 10^{-3}}{\sqrt{bd}} \left(1 + \frac{10}{b^2}\right) \dots \text{rad/in} \quad (7.2)$$

therefore according to Hsu's expressions the stiffness is given by:

$$S = \frac{T_{cr}}{\theta_{cr}}$$

The value of the torsional stiffness (S) in equation 7.1 can be expressed as:

$$S = K \cdot G \quad (7.3)$$

where G = shear modulus of elasticity,

K = a torsion constant dependent on the section geometry.

$$K = \frac{2}{G \cdot \theta} \iint \phi_e \, dx \, dy \quad (7.4)$$

ϕ_e = elastic stress function.

GK can be calculated using the classical method of elasticity by considering the material to be homogenous and ignoring the steel i.e.:

$$GK = G \cdot \lambda \cdot b^3 \cdot h \quad (7.5)$$

where λ = a function of b/h as given in Table 5.1.

$$G = \frac{E}{2(1 + \mu)} \quad (7.6)$$

G in the ACI Code is taken as $0.5 E_c$ on the assumption that $\mu = 0$, and G in CP110-72 is taken as $0.4 E$. Also in the British Code K is taken as $\frac{1}{2} (\lambda b^3 \cdot h)$ to ensure that the stiffness is underestimated.

Equation 7.1 can not be applied to concrete because the stress-strain relationship is non-linear hence the difficulty involved in measuring the value of G. The torque-twist relationship is therefore considered to be non-linear and represented by a curve rather than a straight line as shown in Figure 7.1. If the torsional stiffness is assumed analogous to the modulus of elasticity [13] the parameter (S_i), secant (S_s) and tangent torsional stiffness (S_t) can be defined as shown in Figure 7.1. Pandit [13] showed that:

$$\theta = \frac{T}{S_s} = \frac{T}{S_i} \left(1 + \beta \frac{T}{T_{cr}} \right) \quad (7.7)$$

where T_{cr} = cracking torque in pure torsion,

β = a dimensionless constant taken as 2.3.

From equation 7.7, the secant torsional stiffness may be expressed as:

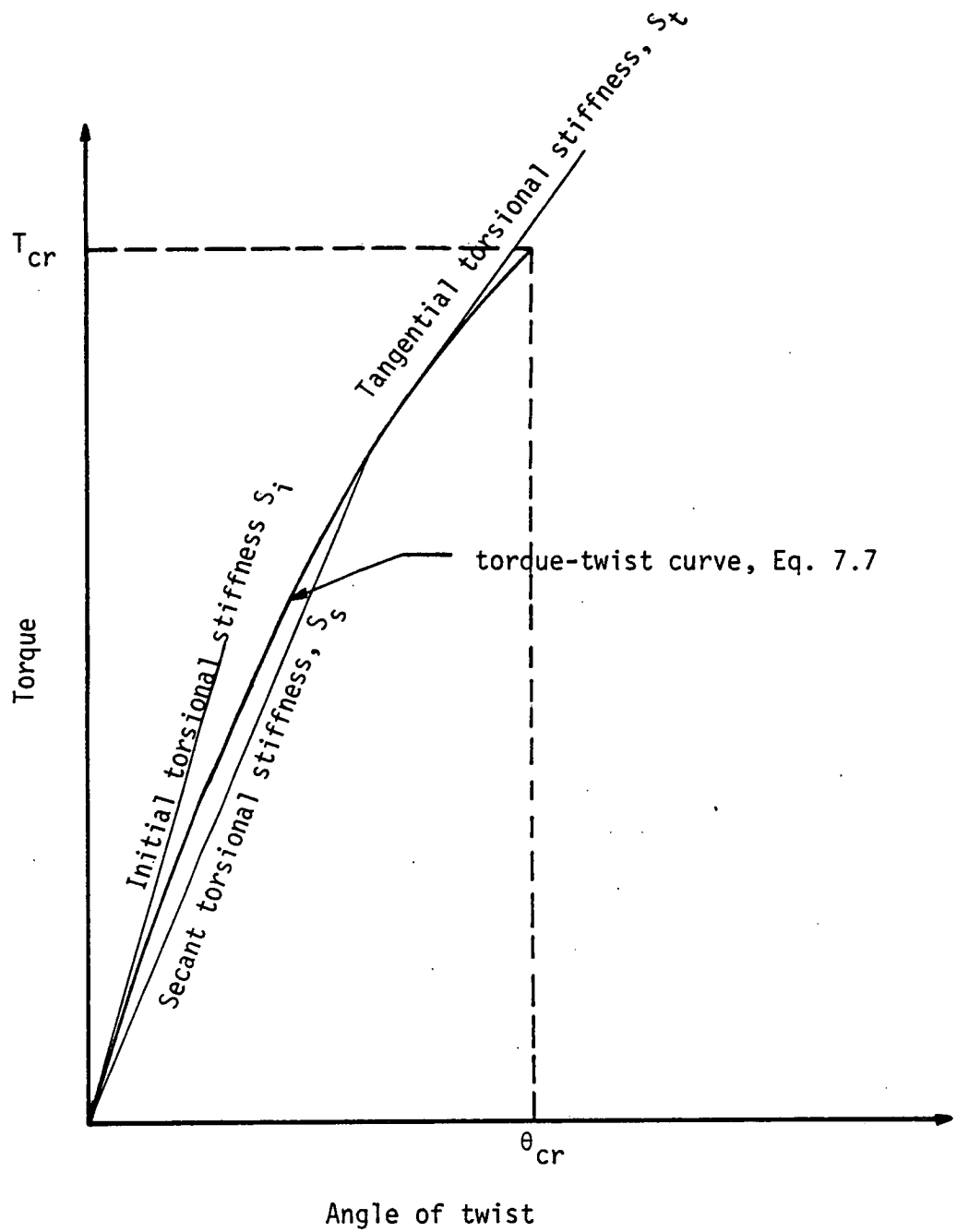


Figure 7.1 Torque-Angle of Twist Characteristics

$$S_s = \frac{S_i}{1 + \beta \frac{T}{T_{cr}}} \quad (7.8)$$

The reduction in the torsional stiffness given by the factor $(1 + \beta \frac{T}{T_{cr}})^{-1}$ is due to the reduction in the shear Modulus of Elasticity and micro-cracking of the concrete. The lower limit of equation 7.8 validity is when $T = 0$, and the upper limit when $T = T_{cr}$.

For beams under combined torsion and bending, it was found [11] that the initial torsional stiffness is reduced by the factor $(1 + \frac{M}{M_u})^{-1}$ due to the effect of bending therefore equation 7.7 becomes:

$$\theta = \frac{T}{S_i} (1 + \beta \frac{T}{T_{cr}}) (1 + \frac{M}{M_u}) \quad (7.9)$$

where M = flexural moment (applied),

M_u = ultimate flexural resistance in pure bending.

Equation 7.9 is valid when $T_{cr} > T$ and $M_u > M$.

The presence of flexural shear tends to reduce the torsional capacity of the beam, as discussed earlier, because the shear stress due to torsion is additive to the flexural shear on one side of the beam's cross-section. Accordingly, the angle of twist in the presence of the flexural shear can be expected to be increased. Pandit suggested the following equation to include the effect of flexural shear:

$$\theta = \frac{T}{S_i} (1 + \beta' \frac{T}{T_{cr}}) (1 + \frac{M}{M_u}) \quad (7.10)$$

where $\beta' = \beta / (1 - \sqrt{T_{eq}/T_{cr}})$

T_{eq} = equivalent torque necessary to produce the same shearing stress as that produced by the flexural shear at the critical section.

Equation 7.10 is again valid when $T_{cr} > T$, $T_{cr} > T_{eq}$, and $M_u > M$. The limiting case of combined bending and shear is for, $T_{eq} = 0$ and $\beta' = \beta$; the limiting case of pure torsion is therefore $T_{eq} = M = 0$.

In order to calculate the angle of twist of the spandrel beams subjected to bending and torsion, equation 7.9 can be expressed in the following form:

$$\theta = \frac{T}{S_i} \left(1 + \beta \frac{T}{T_u} \right) \left(1 + \frac{M}{M_u} \right) \quad (7.11)$$

The upper limiting values of T and M are T_{cr} and M_{cr} respectively. T_u is given by equation 5.21 or 5.22. The cracking angle of twist can be calculated by the following proposed expression as a special case of equation 7.11:

$$\theta_{cr} = \frac{T_{cr}}{S_i} \left(1 + \beta \frac{T_{cr}}{T_u} \right) \left(1 + \frac{M_{cr}}{M_u} \right) \quad (7.12)$$

where $\beta = 2.0$.

T_{cr} , M_{cr} = cracking torsion and bending respectively. The cracking angle of twist when shear and bending are acting in addition to torsion is given by the following expression:

$$\theta_{cr} = \frac{T_{cr}}{S_i} \left(1 + \beta' \frac{T_{cr}}{T_u} \right) \left(1 + \frac{M_{cr}}{M_u} \right) \quad (7.13)$$

where $\beta' = \beta \sqrt{1 + \frac{T_{ceq}}{T_{cr}}}$

T_{ceq} = torque necessary to produce the same shearing stress as that produced by the flexural shear in the concrete.

$$T_{ceq} = \alpha b^2 h v_c \quad (7.14)$$

α = is given in Table 5.1,

and $v_c = \frac{V_c}{bd}$ = maximum shear stress resisted by the concrete.

7.1.2 Postcracking Stiffness

When the cracking stage is reached, the torsional stiffness is no longer a constant quantity and reduces at different levels of loading.

In statically indeterminate structures a considerable reduction in the stiffness occurs at the cracking stage resulting in a significant redistribution of internal forces. At this stage it may be difficult to estimate the torsional stiffness and therefore the torsional moment.

Many methods of analysis and design have been suggested to deal with this problem. Collins and Lampert [39] have assumed zero torsional stiffness of the spandrel beam so that the conventional elastic method can be used for the analysis. Hsu and Burton [40], Pillai and Bharganan [43] and Hsu and Hwang [44] suggested a limit design with assumed torsional stresses.

Using the uncracked stiffness in the cracking stage proved to give unrealistic results and a high estimation of the postcracking torsion. The ratio of flexural stiffness to torsional stiffness increases when using the cracked stiffness, hence different values of moment distribution are obtained. In fact a more accurate prediction of the moment distribution can be obtained when using cracked stiffness than that based on gross stiffness as can be seen from equation 2.1.

This has led investigators to use postcracking stiffness to obtain a more reasonable correlation. Hsu [7,16] proposed the following

equation to predict the cracking stiffness:

$$S_{cr} = (0.021 P_t) S_i \quad (\text{kip.in}) \quad (7.15)$$

where S_{cr} = cracking stiffness,

S_i = initial stiffness,

P_t = the total volume reinforcement percentage.

The calculated ultimate rotation (θ_u) is a function of the cracking rotation (θ_{cr}) and the reinforcement percentage (P_t), given by:

$$\theta_u = (28 + 3.2 P_t) \theta_{cr} \quad (\text{rad}) \quad (7.16)$$

where θ_{cr} = is given in equation 7.2

Lampert [8] derived the following expression for the postcracking torsional stiffness:

$$GK_{cr} = \frac{E_s (b_o h_o)^2 A_h}{2 (b_o + h_o) s} (1 + m) \quad (2.2)$$

Hsu [9] derived the following equation for the cracking stiffness:

$$G_{cr} C_{cr} = \frac{T - \eta T_o}{\theta} \quad T > T_{cr} \quad (7.17)$$

where

$$G_{cr} = \frac{E_s}{(4 \eta + \frac{U h_{eff}}{A_c P_l} + \frac{U h_{eff}}{A_c P_h})} \quad (7.18)$$

$$C_{cr} = \frac{4 A^2 h_{eff}}{U} \quad (7.19)$$

where G_{cr} = shear modulus of the concrete,

C_{cr} = St. Venant torsional constant,

$h_{eff} = 1.4 (P_l + P_h) b$,

$\eta = 0.57 + 2.86 \frac{h}{b}$ (for solid section $\eta = 2$),

A_c = solid cross-sectional area within the outer perimeter of the concrete,

A = cross-sectional area within the centre line of the stirrup,

U = length of the centre line perimeter of a stirrup,

P_h, P_l = volume of ratio of stirrup steel and longitudinal steel respectively with respect to the solid cross-section, A_c ,

T_0 = contribution of the concrete to the ultimate strength in pure torsion = $\frac{2.4}{\sqrt{b}} b^2 \cdot h \cdot \sqrt{f_c}$.

It can be seen that the stiffness calculated by equations 2.2 and 7.17 is a function of the amount of transverse steel, accordingly large values of GK_{cr} can be expected using the conventional elastic method.

Ramakrishnan and Rangan [10] proposed the following expression for the torsional rigidity at any stage in terms of initial torsional rigidity of the uncracked section:

$$GJ = \frac{G_i J_i}{(1 + \beta \frac{T}{T_u})} \quad (7.20)$$

where $G_i J_i$ = torsional rigidity of transformed uncracked section,

T_u = ultimate torsional moment in pure torsion,

β = constant.

The angle of twist is given by the following expression:

$$\theta = \alpha [1 + (\frac{h}{b})^2] \frac{T}{G_i J_i} (1 + \beta \frac{T}{T_u}) \quad (7.21)$$

The values of α and β in equation 7.21 are obtained experimentally and tabulated in reference [10].

As mentioned earlier, the torsional stiffness is reduced due to the presence of the flexural moment [11] and the reduction factor given by Pandit, $(1 + \frac{M}{M_b})^{-1}$ is still applicable, where M_b in this case is the ultimate flexural resistance of a reinforced concrete beam in pure bending.

Shear modulus and modulus of elasticity of concrete are related by equation 7.6:

$$G_i = \frac{E_c}{2(1 + \mu)} \quad (7.6)$$

where μ = Poisson's ratio = 0.2 as assumed in section 4.5.

Therefore

$$G_i = 0.4 E_c \quad (7.22)$$

E_c can be calculated by equation 4.15, i.e.:

$$E_c = 5.5 \sqrt{f_c} \quad (4.15)$$

then $G_i = 2.2 \sqrt{f_c} \quad (7.23)$

K_i from equation 7.5 is equal to:

$$K_i = \lambda b^3 . h$$

λ is a function of h/b and given in Table 5.1.

$$S_i = G_i K_i \quad (7.3)$$

or
$$S_i = (2.2 \sqrt{f_c}) \lambda \cdot b^3 \cdot h \quad (\text{kN}\cdot\text{mm}^2) \quad (7.24)$$

similar to equation 7.11 the following expression is proposed to predict the ultimate angle of twist:

$$\theta_u = \frac{T}{S_i} \left(1 + \beta \frac{T}{T_u}\right) \left(1 + \frac{M}{M_b}\right) \quad (7.25)$$

where T, M = the ultimate torsion and bending moment respectively,

S_i = is given by equation 7.24,

β = constant = 2.0,

T_u = ultimate torsional resistance of a reinforcement concrete beam in pure torsion and can be calculated by the following equation:

$$T_u = T_u' + 1.5 \frac{A_w \cdot f_{wy} \cdot b_1 h_1}{s} \quad (7.26)$$

T_u' = is given by equation 5.21 or 5.22,

M_b = the ultimate flexural resistance of a reinforced concrete beam in pure bending and can be calculated by equation 4.34 or by the more simplified expression:

$$M_b = 0.9 A_{st} \cdot f_{sy} \cdot d \quad (7.27)$$

on the assumption that $(1 - \bar{g}x)$ is taken as 0.9.

The ultimate angle of twist of a reinforced rectangular beam subjected to shear, bending and torsion can be calculated by the following proposed expression similar to equation 7.13:

$$\theta_u = \frac{T}{S_i} \left(1 + \beta' \frac{T}{T_u}\right) \left(1 + \frac{M}{M_b}\right) \quad (7.28)$$

where $\beta' = \beta \left(\sqrt{1 + \frac{T_{eq}}{T_u}}\right)$

T_{eq} = torque necessary to produce the same shearing stress as that produced by the flexural shear at the critical section.

T_{eq} in this case can be expressed by:

$$T_{eq} = T_{ceq} + T_{seq} \quad (7.29)$$

$$T_{ceq} = \alpha b^2 \cdot h \cdot v_c \quad (7.14)$$

T_{seq} is calculated by equation 5.98 for an equivalent area of one leg of a stirrup required to resist a shear stress of $(v_u - v_c)$ i.e.:

$$T_{seq} = 1.5 A_v f_{wy} \frac{b_1 h_1}{s} \quad (7.30)$$

$$A_v = \frac{(v_u - v_c) b \cdot s}{2 f_{wy}} \quad (5.96)$$

where v_u = ultimate shear stress

v_c = the ultimate shear stress resisted by concrete.

$v_u - v_c = v_s$ = shear stress resisted by stirrup steel.

Substituting A_v from equation 5.96 into equation 7.30, T_{seq} becomes:

$$T_{seq} = 0.75 (v_u - v_c) b \cdot (b_1 h_1)$$

or
$$T_{seq} = 0.75 v_s \cdot b \cdot (b_1 h_1) \quad (7.31)$$

Substituting the values of T_{ceq} and T_{seq} into equation 7.29, T_{eq} becomes:

$$T_{eq} = \alpha b^2 h v_c + 0.75 v_s b \cdot (b_1 h_1) \quad (7.32)$$

7.1.3 Comparison and Discussion

From the torque-twist curves shown in Figure 3.3 and since the flexural cracking took place before the torsional cracking, it would appear that spandrel beams maintain their initial torsional stiffness longer than their flexure stiffness. This may be illustrated by the initial part of the torque-twist curves; which may be considered as curve (12) as shown in Figure 7.1.

Hsu's expression for the cracking torque, stiffness and angle of twist were derived to satisfy data obtained from tests carried out on isolated beams subjected to pure torsion. The spandrel beams, however are subjected to combined torsional moment and bending moment and may also be subjected to high shear forces. Therefore a direct comparison under these circumstances can not be made.

Applying equation 2.2 to spandrel beams may result in underestimated values for the cracked stiffness because spandrel beams do not uniformly crack. Extra stiffness is expected in the region of low tensile stresses and where the concrete is still uncracked.

The factors $(\sqrt{1 + \frac{T_{ceq}}{T_{cr}}})$ in the case of uncracked stiffness and $(\sqrt{1 + \frac{T_{eq}}{T_u}})$ in the case of cracked stiffness have been proposed to include the effect of shear; however the increase in the value of (β) due to those factors is considered to be low. Indeed Lampert [8] proved that

the torsional stiffness can be regarded as being independent of the shear force. In addition the effect of the shear force on the deflection is not significant if a substantial amount of torsion is present.

The measured angle of twist can be obtained either from the torque-twist curves shown in Figure 3.3 or from the applied load at different stages, i.e. cracking or ultimate and then the corresponding measured value of angle of twist as shown in Figure 3.8.

The calculated cracking angles of twist are compared with the measured values in Figure 7.2. Equation 7.13 is used for beams in group GR2 where shear is relatively high, and equation 7.12 for the remainder of the beams.

Three beams in group GR2 reached their ultimate torsional strength. The calculated angle of twist with the measured values are compared in Figure 7.3. On Figure 7.3 four beams reported by Rangan [46] to have reached their ultimate strength, are also compared to show the validity of equations 7.25 and 7.28.

It can be seen that the proposed equations 7.12 and 7.13 for the cracking angle of twist and equations 7.25 and 7.28 for the ultimate angle of twist, give good agreement with the test results.

7.2 Deformation Response

The evaluation of localized deformations of reinforced concrete members is necessary to ascertain the maximum moment distribution to ensure that the structure does not collapse prior to the formation of a mechanism. This requires the evaluation of the angles of rotations at individual sections as well as over plastic hinging regions. Reinforced

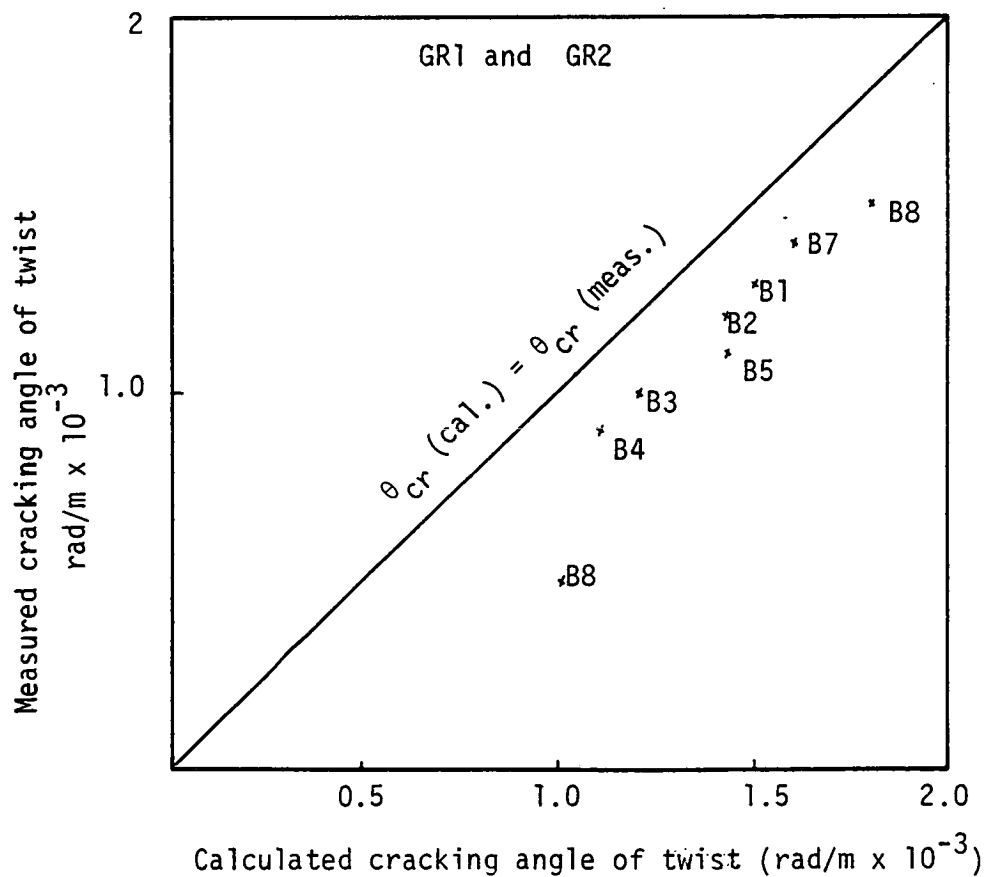
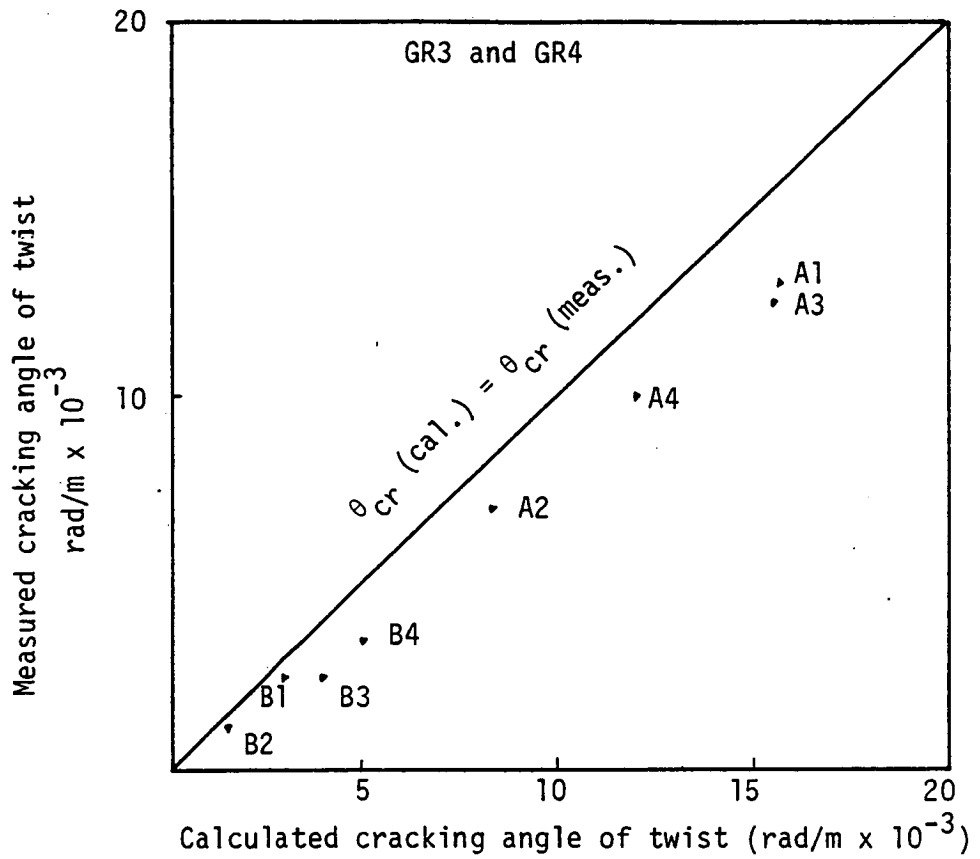


Figure 7.2 Measured Cracking Angle of Twist Against the Calculated Values

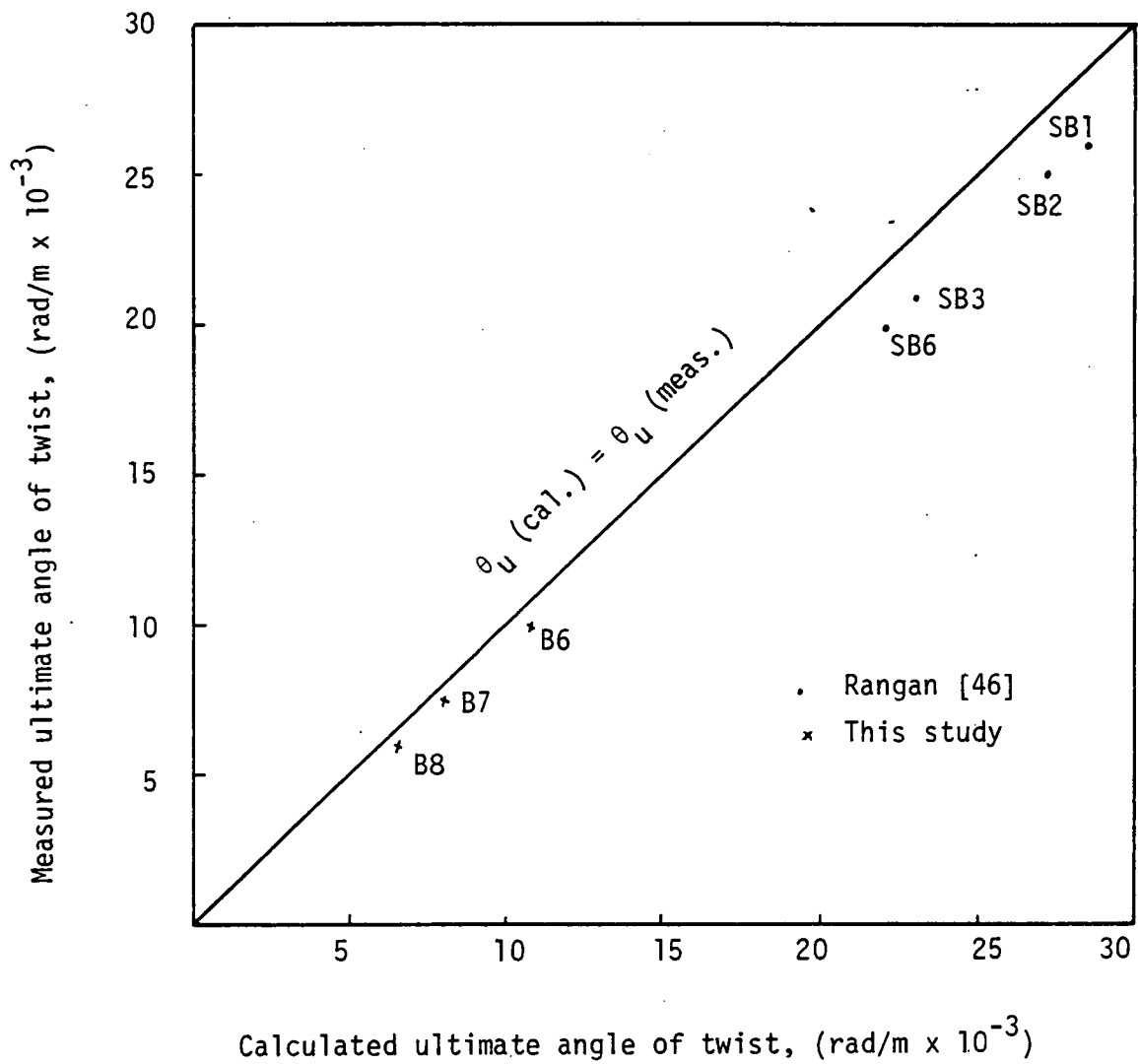


Figure 7.3 Measured Ultimate Angle of Twist Against the Calculated Values

concrete structures can be designed in such a way that a member fails in a particular manner by ensuring that the member between selected hinges resists the bending moment without yielding of the steel or crushing of the concrete until the formation of the last hinge required to convert the structure into a mechanism [95].

The plastic hinges are assumed to form at points of maximum bending moment. The deformation however extends on the sides of the points where the plastic hinges are to develop.

Mattock [30] observed that a more realistic evaluation of the moment-curvature relationship for a concrete section can be made by taking into account strain-hardening of the reinforcement. The depth of the neutral axis is highly influenced by the amount and distribution of longitudinal steel. An increase in the compression steel will reduce the depth of the neutral axis and therefore the curvature.

The moment-curvature relationship at various stages has been discussed in detail in Chapter 6.

7.2.1 Rotational Behaviour

The rotational capacity of the hinging region is a function of the load-deformation response, which in turn can be represented by the moment-rotation behaviour. Rotation of the member can be obtained from the displacements, i.e. by measuring midspan deflection as shown in Figure 7.4 in which:

$$\Delta_t = \Delta_e + \Delta_p \quad (7.33)$$

where Δ_t = total deflection,

Δ_e = elastic deflection,

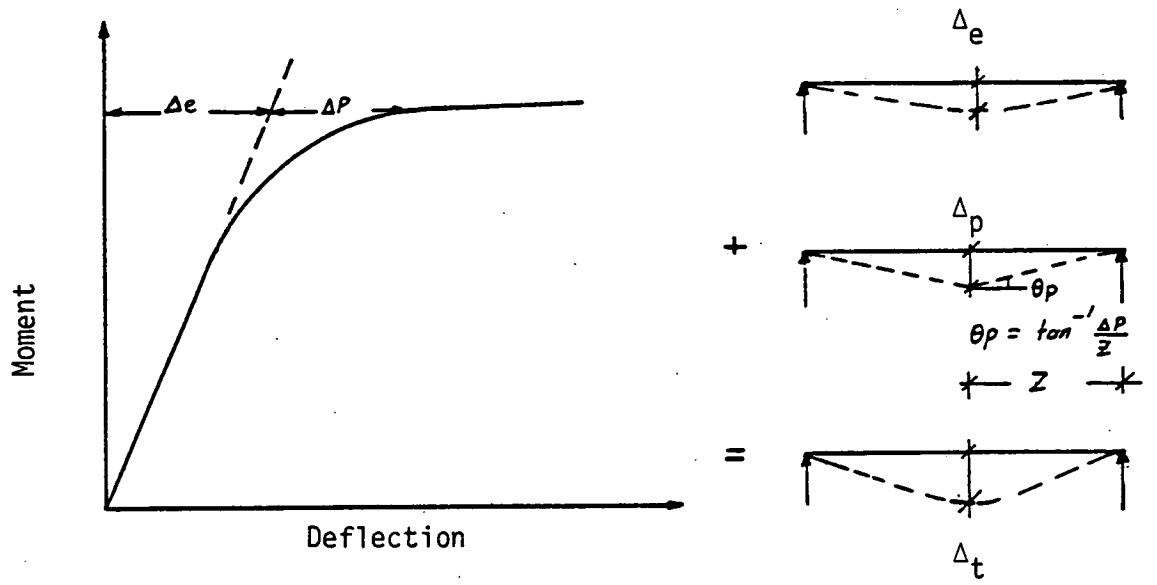


Figure 7.4 Moment-Deflection

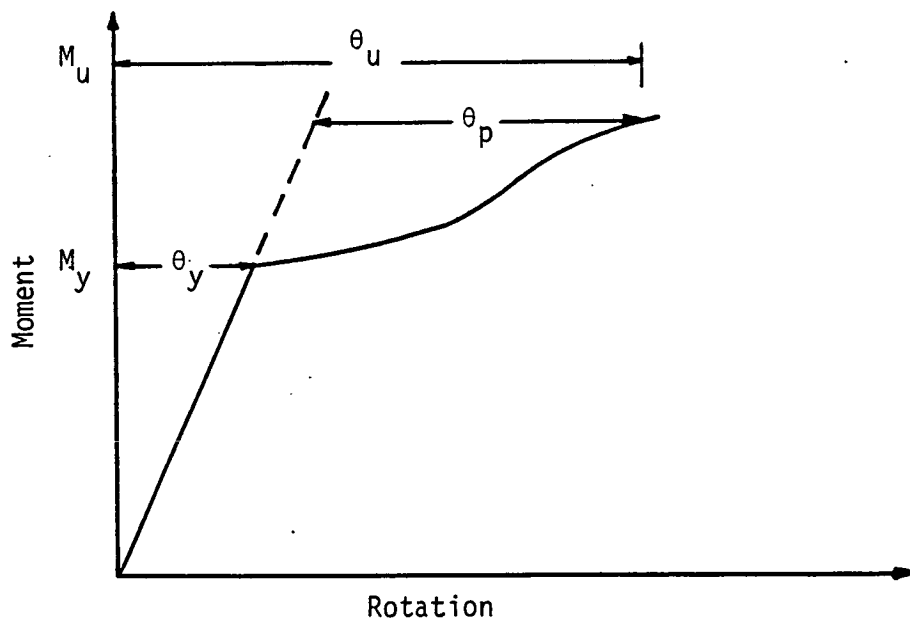


Figure 7.5 Moment-Rotation

Δ_p = inelastic deflection.

Δ_e is taken as the deflection corresponding to the cracking load.

Δ_p is taken as $(\Delta_t - \Delta_e)$.

Several parameters were investigated by Mattock [30] to show their influence on the spread of plasticity at the critical section in a flexural member. Parameters such as: concrete strength, yield stress of the reinforcement, beam effective depth, and amount of the reinforcement provided. It was found that a considerable quantity of inelastic deformation occurs beyond the distance $d/2$ on each side of the midspan where the maximum moment is expected. It was also concluded that the extent to which the plasticity spreads along the beam depends on the geometry of the member as expressed in terms of the effective depths (d), the distance (Z) from the point of maximum moment to the point of zero moment, and on the amount of flexural reinforcement. Mattock expressed the spread of plasticity by the following equation in terms of the ratio $\frac{\theta_{tp}}{\theta_p}$:

$$\frac{\theta_{tp}}{\theta_p} = 1 + (1.4\sqrt{\frac{Z}{d}} - 1) \left(1 - \left(\frac{q - q'}{q_0}\right) \sqrt{\frac{d}{16.2}}\right) \quad (7.34)$$

where θ_{tp} = total inelastic rotation at ultimate capacity occurring between a section of maximum moment and an adjacent section of zero moment,

θ_p = inelastic rotation at ultimate capacity occurring with a length $d/2$ to one side of the section of maximum moment,

$$\theta_p = \phi_p \cdot d/2$$

Z = distance between the section of maximum moment and an adjacent section of zero moment,

$$q = \text{tension reinforcement index} = \frac{P_s f_{sy}}{f_c}$$

$$q' = \text{compression reinforcement index} = \frac{P'_s f_{sy}}{f_c}$$

$$q_0 = \text{tension reinforcement index for balanced condition} = \frac{P_b f_{sy}}{f_c}$$

With reference to Figure 7.5, the following relationship can be obtained:

$$\theta_p = \theta_u - \theta_y \frac{M_u}{M_y} \quad (7.35)$$

in which $\theta_u = \phi_u \cdot d/2$

$$\theta_y = \phi_y \cdot d/2$$

ϕ_u, ϕ_y are the curvature at the ultimate and yield stage respectively.

Corley [31] conducted extensive tests concerned with the prediction of the rotational capacity of a hinging region. The following expression was suggested to define the spread of yielding as a function of the geometry of the member.

$$\frac{\theta_{tp}}{\theta_p} = 1 + \frac{0.4}{\sqrt{d}} \cdot \frac{Z}{d} \quad (7.36)$$

The ACI-ASCE joint committee 428 recommended the calculation of the plastic hinge rotation, θ_p , in the region of maximum moment in a flexural member, as the difference between the curvature ϕ_u at the ultimate design moment and ϕ_y , the curvature at yielding stage,

$$\text{i.e.} \quad \theta_p = (\phi_u - \phi_y) L_p \quad (7.37)$$

where L_p = the spread of peak curvature or plastic length over which plastic rotation occurs with constant curvature.

In the case of spandrel beams where bending exists in addition to torsion, Syamal, Mirza and Ray [96] noted that as the ratio of the applied bending moment to twisting moment was increased, the beams appeared to show a considerable improvement in ductility and as a result better redistribution of stresses at values of torque approaching ultimate due to large angles of twist can be obtained.

Very little research on the development of hinging regions in the case of combined bending and torsion has been carried out to date. Mattock, Corley and ACI-ASCE expressions to evaluate the rotational capacity of hinging regions in reinforced concrete beams are only applicable to flexural members.

Bishara et al [97] introduced a reduction factor, η , and the flexural plastic hinge, θ_{tp} , under combined bending and torsion may be obtained by the following equation:

$$\theta_{tp} = \eta \cdot \theta_p \quad (7.38)$$

where $\theta_p = (\phi_u - \phi_y) L_p \quad (7.37)$

$$\eta = \frac{1}{1 + \left(\frac{T_u}{T_o} / \frac{M_u}{M_{uo}} \right)^2} \quad (7.39)$$

where T_u, M_u = applied torque and moment respectively,

T_o, M_{uo} = pure torsional and flexural capacity.

It was suggested that the rotational capacity of the hinging region

under combined bending and torsion is less than that under pure flexure.

7.2.2 Ductility

One of the main factors affecting the rotational capacity of hinging regions and therefore the redistribution of moments in a structure is ductility [34]. Ductility can be defined after Cohn and Ghosh [36] as follows:

"Ductility is taken to be the ability to sustain deformation beyond the elastic range without a significant variation of the resistance capacity."

The major factors affecting the ductility of a reinforced concrete section can be categorised as follows [36]:

1. Material variables:

- (a) Concrete quality
- (b) Grades of tension and compression steel
- (c) Grade of lateral steel
- (d) Bond
- (e) Tensile strength of concrete

2. Geometrical variables:

- (a) Shape and size of section
- (b) Amount of tension steel
- (c) Amount of compression steel
- (d) Amount and spacing of lateral steel
- (e) Cover thickness

3. Loading variables:
- (a) Axial loading
 - (b) Duration of loading
 - (c) Prestressing
 - (d) Repetition of loading
 - (e) Loading reversal

Ductility in flexural members is well understood, however very little attention has been drawn to the ductility of reinforced concrete members under combined bending and torsion. The behaviour of the spandrel beams has been discussed in detail in Chapter 3, and the sequence of the steel yielding also has been discussed with reference to Figure 3.9 which shows that the bottom longitudinal steel in the spandrel beam yielded before the stirrups.

A measure of the ductility can be expressed by the Ductility Index, i.e. the ratio of beam deflection at ultimate load to the beam deflection at the stage of steel yielding, i.e.:

$$U = \frac{\Delta_u}{\Delta_y} \quad (7.40)$$

Δ_u = maximum measured deflection,

Δ_y = deflection at stage of steel yielding.

From Table 7.1 it can be seen that the ductility of the spandrel beams is less than that for the floor beams. This loss of ductility is due to torsion.

Also in Table 7.1 the values of end rotation are compared for yield and ultimate stage.

Table 7.1 Ductility Index and End Rotation

Beam	Floor Beam			Spandrel Beam		
	Ductility Index	End Rotation (Rad)		Ductility Index	End Rotation (Rad)	
		Yield Stage	Ultimate Stage		Yield Stage	Ultimate Stage
GR1-B1	3.0	5.1×10^{-3}	11.5×10^{-3}	1.53	2.9×10^{-3}	4.5×10^{-3}
-B2	3.9	4.0	19.4	2.09	2.3	6.0
-B3	3.5	4.2	22.2	2.07	2.5	8.8
-B4	3.8	4.5	23.6	2.01	2.5	7.7
GR2-B5	4.1	3.4	29.6	2.8	2.2	9.9
-B6	4.26	3.6	26.8	3.3	1.4	8.0
-B7	4.4	3.6	30.0	3.3	1.83	7.4
-B8	4.6	3.2	32.0	3.5	2.0	12.2
GR3-A1	3.69	2.7	10.2	2.09	2.4	5.1
-A2	2.97	2.4	6.7	2.5	1.4	3.0
-A3	2.7	2.9	8.1	1.9	2.0	4.0
-A4	2.3	4.0	12.7	2.1	1.0	5.4
GR4-B1	2.9	4.9	14.9	2.0	1.87	4.9
-B2	2.7	3.3	15.0	2.5	1.85	6.0
-B3	3.2	3.9	19.9	2.7	2.3	6.6
-B4	3.0	4.7	20.0	2.30	3.4	7.0

CHAPTER 8 : DISCUSSION AND CONCLUSIONS

- 8.1 Introduction
- 8.2 Effect of Variables
 - 8.2.1 Longitudinal Steel
 - 8.2.2 Transverse Steel
 - 8.2.3 Concrete Strength
 - 8.2.4 The Joint
 - 8.2.5 Behaviour at Service Load
- 8.3 Conclusions
- 8.4 Suggestion for Further Research

8.1 Introduction

The general behaviour and the observed effect of certain variables on the behaviour and failure mechanism of the specimens tested in this study have been described in Chapter 3. The various parameters discussed have a significant influence on the strength and the deformation response of the test specimens. The general conclusions drawn from this study are discussed in this chapter as well as the author's proposals for further investigation which would reveal some of the other factors that might affect the behaviour and strength of reinforced concrete spandrel beams or to substantiate some of the evidence produced by this study.

8.2 Effect of Variables

8.2.1 Longitudinal Steel

The function of the longitudinal steel in bending is well understood. However the observed behaviour and test measurements of the spandrel beams tested indicated that the contribution of the longitudinal steel to the torsional strength is not significant.

Three spandrel beams in group GR2 namely B6, B7 and B8 did reach their ultimate strength without provision for longitudinal steel due to torsion. Although the remaining beams in the other groups did not reach their ultimate strength, they all reached their design strength except for beams B1 and B2 of group GR1, where failure of the floor beams occurred in flexure.

Table 2.2 shows a comparison between the amount of longitudinal steel required for the spandrel beams when torsional moment is considered

and the amount of longitudinal steel provided when torsional moment is not considered. A large saving can therefore be achieved by not allowing for the effect of torsion in designing the longitudinal steel. Also the ductility index decreases by increasing the amount of longitudinal steel. The longitudinal steel was observed to be effective in controlling the crack width and counteracting the tendency for the spiral cracks to widen.

In the author's opinion, a nominal amount of longitudinal steel must be provided not in addition to the bottom longitudinal steel, but at mid depth on both sides of the spandrel beam cross-section to avoid the type of failure observed in the beams of groups GR2, GR3 and GR4, due to the large angle of twist, as shown in Plate 8.1. The type of failure referred to can be recognised in Plate 8.1, by the cracks at the far ends of the cracked zone and tended to propagate towards the joint i.e. a cleavage crack. The nominal amount of longitudinal steel to be provided for this purpose is proposed to be:

$$A_1 = 0.03 A_c \left(\frac{d}{L_s}\right) \leq 2 A_s \quad (8.1)$$

where: A_c = the concrete cross-sectional area,

A_1 = area of longitudinal steel to be provided at mid depth
on both sides of the beam cross-section,

A_s = the area of main longitudinal bar.

The relative amounts of negative and positive longitudinal steel provided in the floor and spandrel beam due to negative and positive bending moment, is very effective in determining the final position and formation of the plastic hinges. Test measurements show that no

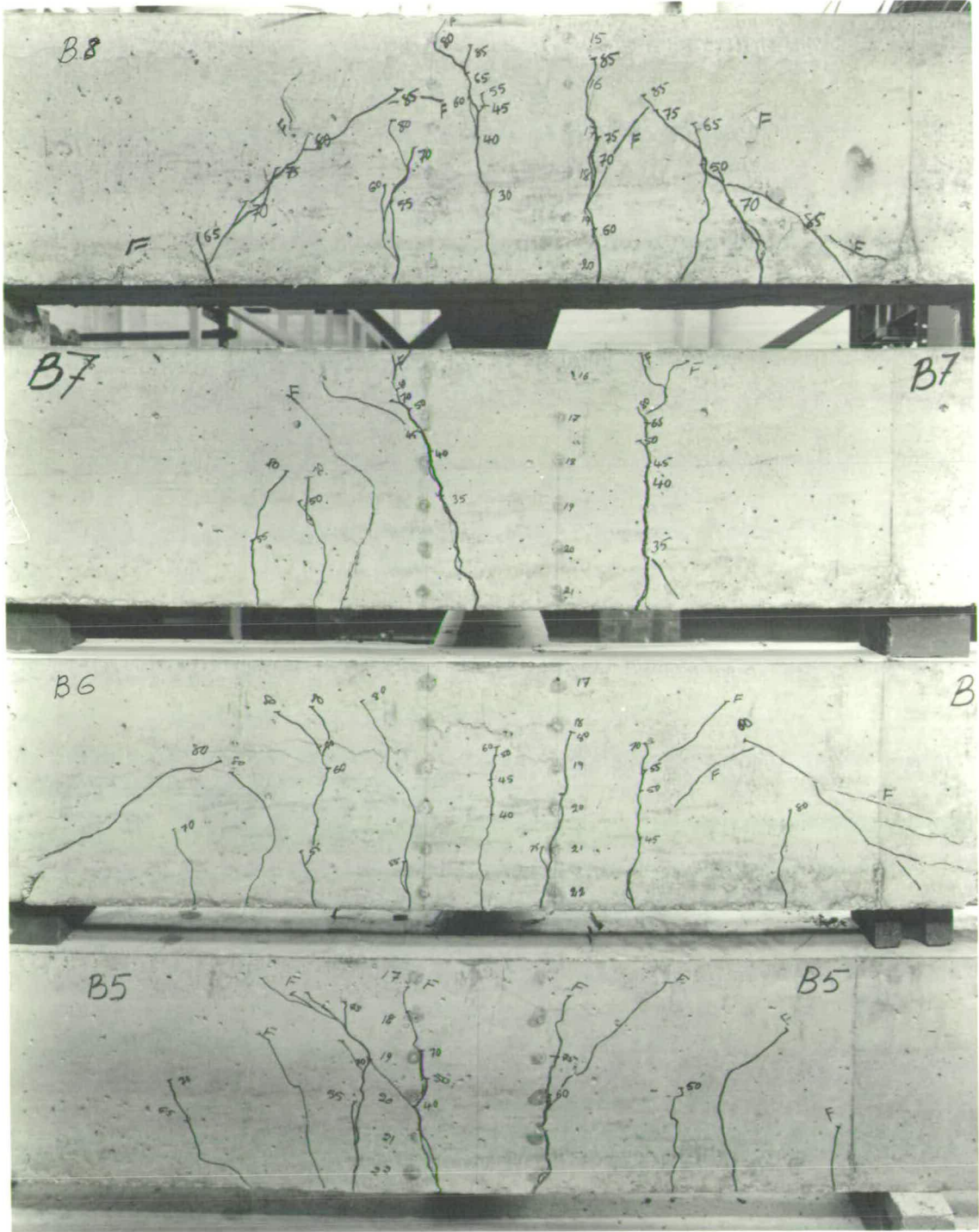


Plate 8.1 Specimens of Group GR2 (back view)

yield was recorded in the negative steel of the floor beams at failure because the floor beams were adequately reinforced in the area of the negative moment, and the reaction of the floor beam will produce an opposite moment of value equal to the reaction times the eccentricity of the reaction. The value of this eccentricity is equal to half the width of the spandrel beam as shown in Figure 1.1(e). This induced moment was not accounted for in the design process because the design is based on the assumption that the spandrel beam is a straight line of zero width.

8.2.2 Transverse Steel

Test data shows that the strength of the beam and its behaviour are greatly affected by the amount of stirrups provided.

Transverse steel is very effective in resisting the shear stresses due to torsion and shear, and preventing the sudden and explosive type of failure caused by torsion. Sufficient transverse steel should be provided for the beam to exhibit adequate ductility. Test measurements show that the stirrups have no significant effect prior to cracking. It is therefore only after the formation of cracks that the stirrups are effective in carrying the applied torsion. Also transverse steel displays an effective role in resisting the growth of the diagonal cracks thereby reducing their propagation into the compression area.

Test measurements in Figure 3.9 and Figure 8.1 show that at the failure stage of the floor beam, the stirrups did not develop their ultimate strength, however when the spandrel beam failed due to twist, the stirrups reached their yield stress.

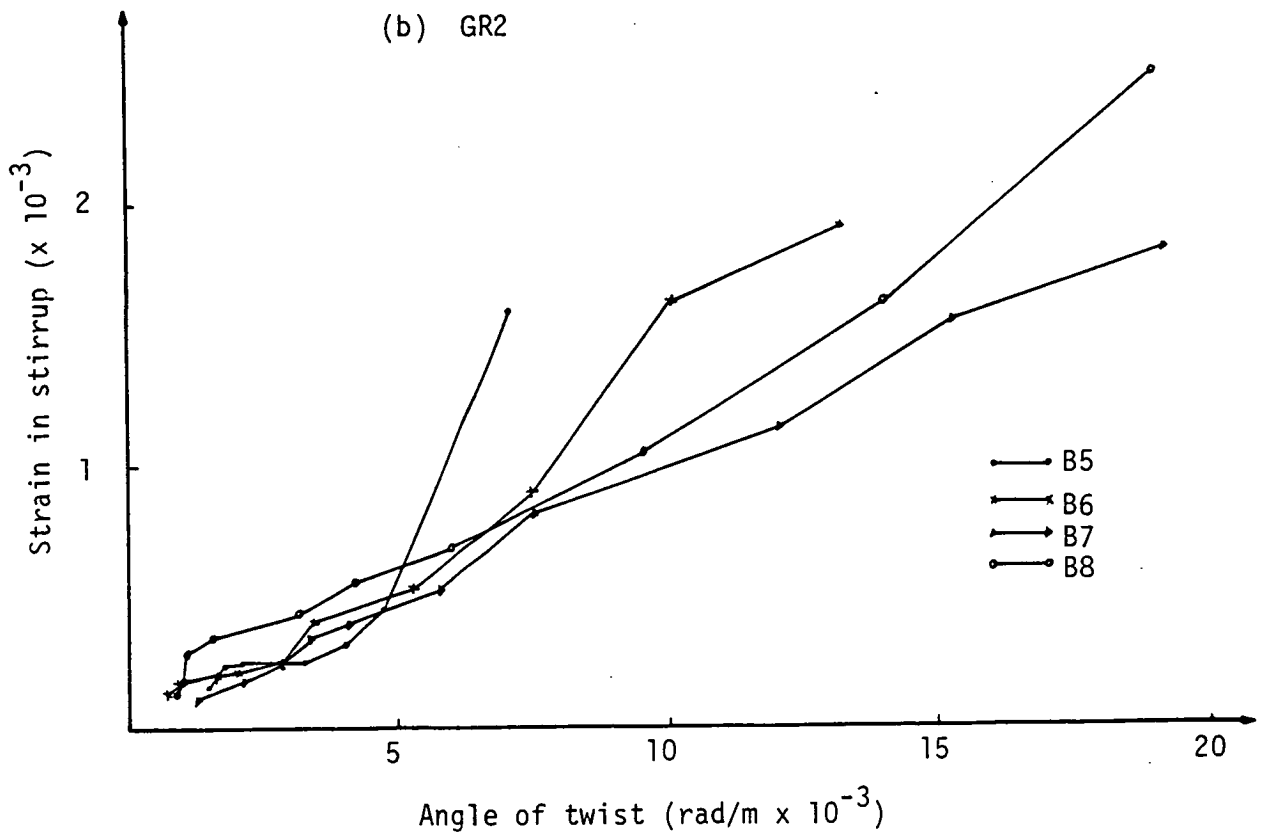
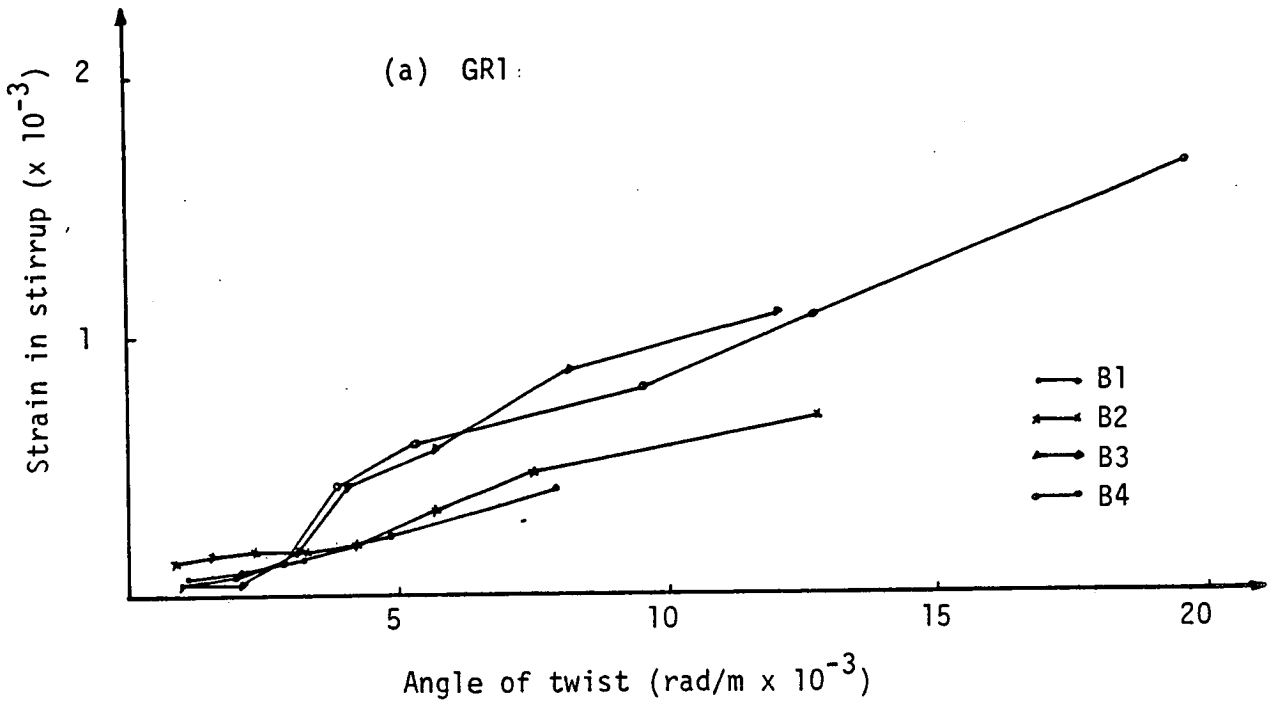


Figure 8.1 Strain in Stirrup - Angle of Twist Curves

Yield stress and spacing of the stirrups have a great influence on the location of the plastic hinges in the spandrel beams as shown in Plate 3.1. Therefore any parameter incorporating these two factors would affect the behaviour and strength of the spandrel beam.

The effect of confinement is discussed fully in Chapters 4 and 6. The ductility of the beams is also influenced by the amount of transverse steel provided.

On the basis of the author's test results, it becomes obvious that designing the stirrups from a strength consideration is doubtful, since the behaviour of the spandrel beams reveals that the strength and efficiency of the test specimens are not greatly influenced by any variation in the transverse reinforcement as long as they are governed by the strength and rotation of the floor beam. Therefore design of the stirrups should be governed by limiting the angle of twist which is in turn dependent on the rotation of the floor beam. Nevertheless stirrups should be provided to resist any torsional and shear stresses which are ⁱⁿexcessive of those resisted by the concrete as well as to provide adequate anchorage for the longitudinal steel.

The amount of transverse steel is determined either by the bar diameter or by the spacing of the stirrups. Practically speaking it is preferable and more effective to reduce the spacing between the stirrups to achieve a better crack control so that any possible failure surface will intersect a sufficient number of stirrups. In addition it is more effective from ductility considerations.

8.2.3 Concrete Strength

Three grades of concrete were used for the test specimens (30,

35 and 40 N/mm²). The effect of concrete strength has been widely discussed elsewhere in this thesis. The behaviour and strength of the test specimen are significantly influenced by the concrete strength as demonstrated by the load-deformation relationships. Ductility, and spread of plasticity are also affected by concrete strength.

8.2.4 The Joint

The forces and deformations are transferred through the joint from the floor beam to the spandrel beam as well as any redistribution of forces from the spandrel beam to the floor beam or vice versa.

The nature of the stresses in the joint is very complex, nevertheless two conditions must be satisfied in designing and detailing the reinforcement:

1. The longitudinal steel in the floor beam must be placed on top of the spandrel beam longitudinal steel.
2. Equation 3.6 must be satisfied. No joint failure was observed in any of the test specimens except in beams C1 and C2 of group GR5.

8.2.5 Behaviour at Service Load

In Table 8.1 the measured values of deflection and crack width at service load are shown. The service load is taken as the design load divided by 1.8. The allowable limit of deflection given by the ACI code is $\frac{L}{360}$ and by the Australian AS 1480-74 is $\frac{L}{375}$, however

Table 8.1^x Deflection, Maximum Crack Width and Angle of Twist at Service Load^{xx}

Specimen	Deflection (mm)		Max. crack width (mm) [†]		Angle of twist (10 ⁻³ rad/m)
	F.B.	S.B.	F.B.	S.B.	
GR1 - B1	6.5	3.5	0.05	0.02	4.8
B2	5.2	3.0	0.04	0.035	3.0
B3	5.3	3.1	0.05	0.035	4.0
B4	6.0	3.1	0.08	0.06	3.8
GR2 - B5	4.5	1.5	0.03	0.04	2.2
B6	4.2	0.83	0.06	0.06	1.5
B7	4.0	1.1	0.07	0.095	2.8
B8	3.6	1.0	0.08	0.09	1.5
GR3 - A1	0.65	0.69	- *	0.06	7.0
A2	0.6	0.17	-	0.05	4.5
A3	0.73	0.6	-	0.03	12.3
A4	1.7	0.3	-	0.05	8.25
GR4 - B1	1.5	0.5	0.05	0.01	1.55
B2	0.7	0.3	0.01	0.03	2.09
B3	0.85	0.6	0.01	0.04	2.55
B4	1.1	0.8	0.01	0.04	2.2

[†] Flexural cracks measured at mid span where max. B.M.

* No visible cracks were observed.

^{xx} The service load is taken as the design load divided by (1.8).

^x The measured values of deflection and crack width at the service load are all within the allowable limits.

the tabulated values are all within the allowable limits given by the three codes of practice, ACI, AS 1480 and CP110. Similarly the flexural crack widths are all within the permissible limit of 0.3 mm. In Figures 8.2 the maximum torsional cracks measured at mid depth of the wider face of the critical sections are plotted against the angle of twist for beams of groups GR1 and GR2.

8.3 Conclusions

The floor-spandrel beam assembly is a very important part of the whole structure. A more acceptable design process will be achieved when the behaviour of the spandrel beam is better understood and thus more fully employed. The general conclusions drawn from this study may be summarized as follows:

1. The concrete and steel stress-strain relationships have been defined and employed in designing the floor beams and the spandrel beams.
2. The flexural resistance of a reinforced concrete floor beam can be determined using the expressions proposed by the author, where two stages are recognized: (i) prior to cracking and (ii) ultimate. The flexural resistance of a reinforced concrete floor beam prior to cracking is dependent on the section properties and the concrete stress-strain relationship in tension. The ultimate flexural resistance of a reinforced concrete beam is dependent on the concrete stress-strain relationship, the type of concrete, section parameters, steel stress-strain relationship, amount of steel and strain

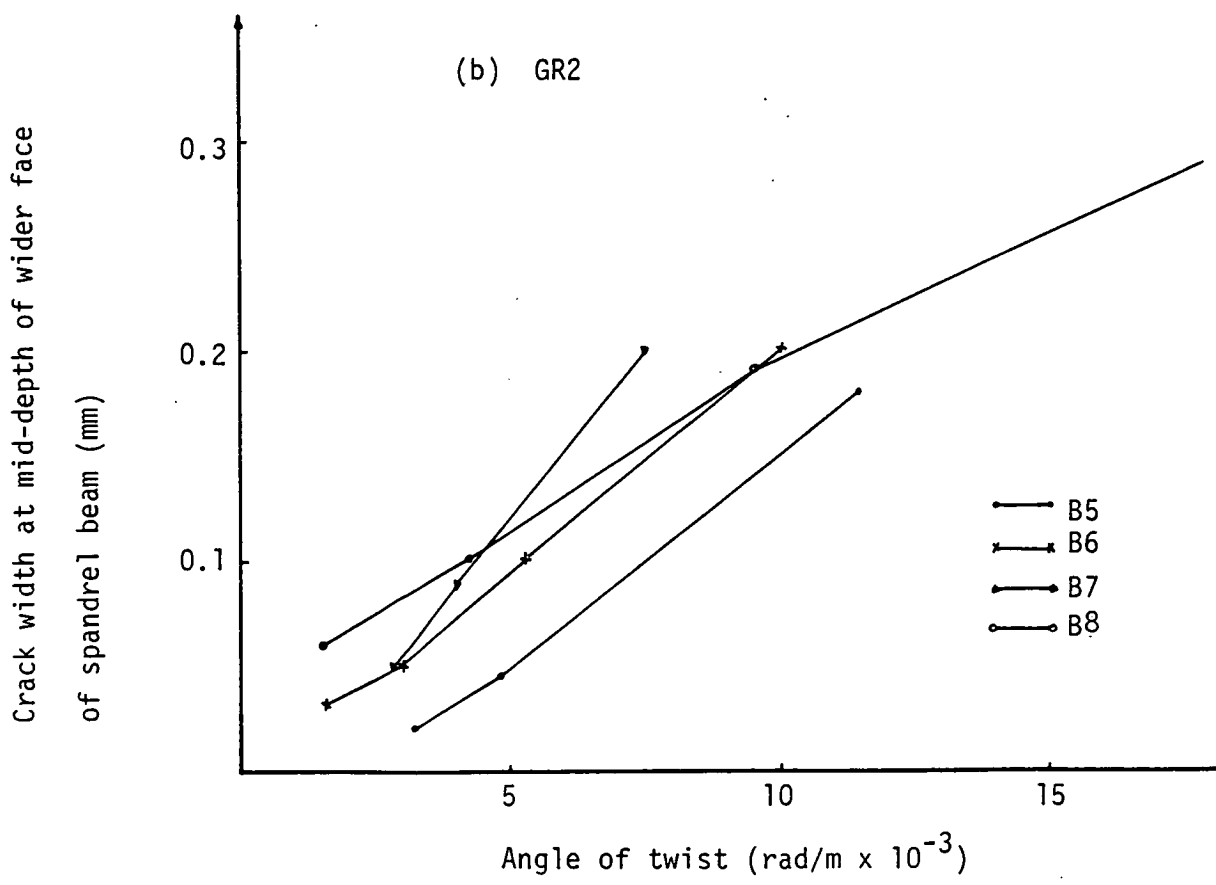
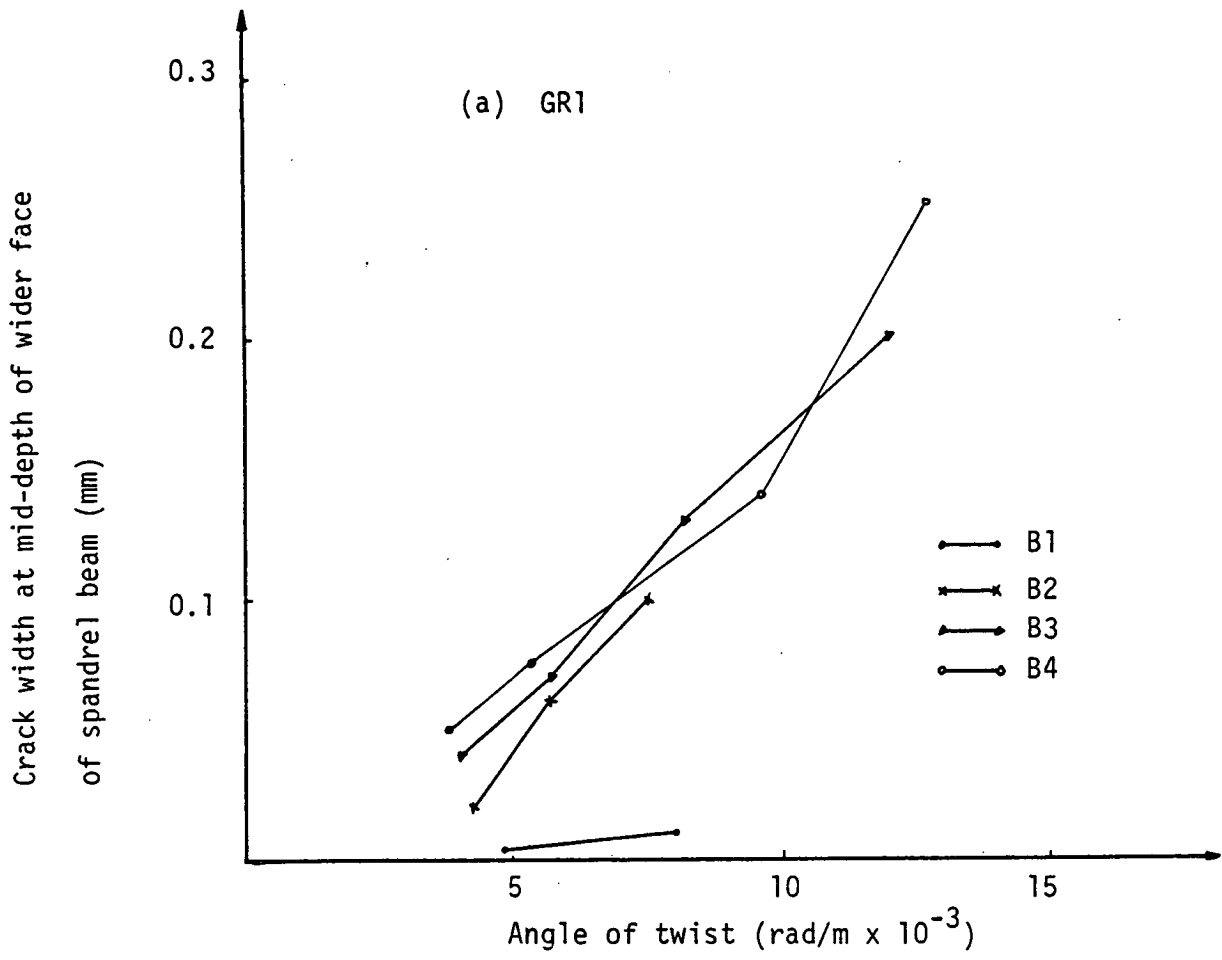


Figure 8.2 Crack Width - Angle of Twist

distribution. Moment-curvature relationships at cracking, yield, and ultimate stage have been defined in Chapter 6.

3. The torsional resistance of reinforced concrete members can be considered to consist of the concrete resistance and the steel resistance. Equations have been derived to determine the torsional strength of reinforced concrete beams prior to cracking and after cracking under pure torsion and are given in Chapter 5.
4. Spandrel beams are subjected to combined loading and two stages can be recognised viz prior to cracking and ultimate. For both stages the torsional strength of spandrel beams subjected to bending moment and torsion can be determined by the proposed expressions given in Chapter 5. The torsional resistance prior to cracking is influenced by the ratio of bending moment to twisting moment, section geometry and the tensile strength of the concrete. The ultimate torsional strength based on the skew bending theory is dependent on the concrete and steel stress-strain relationships, ratio of the bending moment to twisting moment, section properties and amount of steel provided. When shear is present the torsional strength in addition to the above factors is also affected by the ratio of shear to torsion.
5. The skew bending theory has been employed to determine the ultimate torsional strength of the spandrel beam. Accordingly three modes of failure have been defined. A fourth mode of failure has been defined to include the effect of shear stress.

6. The torsional stiffnesses of the spandrel beam prior to cracking and after cracking have been defined. Modified expressions have been derived to determine the torsional stiffnesses and the corresponding angles of twist. An initial torque-twist curve has been adopted to define the initial, secant and tangential stiffness. Precracking stiffness is influenced by the applied bending moment and shear forces, type of concrete and section properties. Post-cracking stiffness is also influenced by the applied bending moment and shear forces, as well as being influenced by the type of concrete, section properties and the amount of steel provided. The angles of twist are similarly affected at different stages.
7. The location of the torsional plastic hinge is determined by the amount of steel provided in the spandrel beam.
8. The amount of tensile reinforcement provided in the beams and the concrete strength have an effect on the inelastic deformation and spread of plasticity in the hinging regions.
9. The longitudinal steel is not significantly effective in resisting torsion. Therefore no provision for longitudinal steel to resist torsion is required in the spandrel beam. However a nominal amount of longitudinal steel should be provided at mid-depth of the spandrel beam section on both sides to avoid the type of failure caused by the large angle of twist.

10. A spandrel beam should not be designed from a strength consideration - but by limiting the angle of twist which in turn is dependent on the rotation of the floor beam. Rotation of the floor beam is influenced by many factors including type of loading and construction.
11. Joint failure should not occur before floor or spandrel beam failure.

8.4 Suggestion for Further Research

The scope of this study was limited to spandrel beams subjected to a static type of loading. A limited number of variables were investigated to provide information on the behaviour and strength of the floor-spandrel beam assembly. Information and data are not available for specimens subjected to dynamic and reversible loadings.

Further investigations are also required to investigate the behaviour and strength of a floor-spandrel beam assembly constructed using light weight concrete.

The joint between the floor and spandrel beam is a very important element in the assembly. Further studies into the strength and behaviour of this joint would also provide substantial information that would be of relevance to the design process.

Since only one type of joint detailing was used in this study, it is possible that the efficiency of the joint can be increased by varying the type of detailing under different types of loading.

Furthermore, more realistic information would be obtained if the effect of the floor slab could be included in the study of the joint assembly.

Finally, the author is also of the opinion that a Finite Element Method can be utilised to provide an alternative theoretical approach up to some specified limit of accuracy.

REFERENCES

1. American Concrete Institute:
"Building Code Requirements for Reinforced Concrete"
ACI 318-63, Detroit, June 1963.
2. ACI Committee 438:
"Tentative Recommendations for the Design of Reinforced
Concrete Members to Resist Torsion"
Journal of the ACI, Vol.66, No.1, January 1969.
3. ACI Committee 318-71:
"Building Code Requirements for Reinforced Concrete"
ACI Pubs., Detroit, 1971.
4. Marshall, W.T.:
"Torsion in Concrete and CP110-1972"
The Structural Engineer, March 1974, No.3, Vol.52.
5. Goode, C.D.:
"Torsion CP110 and ACI 318 Compared"
Concrete, March 1974, pp.36-40.
6. Hsu, T.T.C. and Kemp, E.L.:
"Background and Practical Application of the Tentative Design
Criteria for Torsion"
Journal of the ACI, Vol.66, No.1, January 1969.
7. Hsu, T.T.C.:
"Torsion of Structural Concrete - Behaviour of Reinforced
Concrete Rectangular Members"
Special Publications SP18, ACI, Detroit, 1968.
8. Lampert, P.:
"Postcracking Stiffness of Reinforced Concrete in Torsion and
Bending"
Torsion of Structural Concrete, SP35, ACI, Detroit, 1971.
9. Hsu, T.T.C.:
"Postcracking Torsional Rigidity of Reinforced Concrete Section"
Journal of the ACI, May 1973, pp.352-360.
10. Ramakrishnan, V. and Rangan, B.V.:
"The Torque-Twist Relationship for Rectangular Beams"
Concrete, November 1967, pp.383-386.
11. Pandit, G.S. and Warwaruk, J.:
"Effect of Flexure on the Initial Torsional Stiffness of
Reinforced Concrete Beams of Rectangular Cross-Section"
Indian Concrete Journal, September 1967, pp.355-358.
12. Pandit, G.S.:
Discussion on Paper by Behera, V. and Ferguson, Phil, M.:
"Torsion, Shear and Bending on Stirruted L-Beams"
ASCE Proc., Journal of the Struct. Div. ST4, April 1971.

13. Pandit, G.S.:
"Torsional Stiffness of Reinforced Concrete Bridge Girders"
Proc. of the Second International Symposium on Concrete
Bridge Design, Chicago, Ill., March-April 1969.
14. Zia, P.:
"Torsion Theories for Concrete Members"
Special Publications, SP18, ACI, 1968.
15. Zia, P.:
"What Do We Know About Torsion in Concrete"
ASCE Proc., Journal of the Struct. Div., ST6, June 1970,
pp.1185-1199.
16. Hsu, T.T.C.:
"Torsion of Structural Concrete - A Summary on Pure Torsion"
Special Publications, SP18, ACI, Detroit, 1968.
17. Collins, M.P.:
"The Ultimate Strength of Rectangular Reinforced Concrete
Beams Subjected to Combined Torsion, Bending and Shear"
Ph.D. Thesis, University of New South Wales, 1967.
18. Rangan, B.V. and Hall, A.S.:
"Strength of Rectangular Pre-Stressed Concrete Beams in
Combined Torsion, Bending and Shear"
Journal of the ACI Proc., April 1973.
19. Mukherjee, P. and Warwaruk, J.:
"Torsion, Bending and Shear in Pre-Stressed Concrete Beams"
Proc. ASCE, Vol.97, ST4, April 1971.
20. Henry, R.L. and Zia, P.:
"Behaviour of Rectangular Pre-Stressed Concrete Under Combined
Torsion, Bending and Shear"
Department of Civil Eng., North Carolina State University at
Raleigh, April 1971.
21. Rangan, B.V., Staley, R.F. and Hall, A.S.:
"Behaviour of Concrete Beams in Torsion and Bending"
Proc. of ASCE, Struct. Div., No.ST4, April 1977, pp.759-772.
22. Jensen, V.P.:
"The Plasticity Ratio of Concrete and Its Effects on the
Ultimate Strength of Beams"
Journal of the ACI, Vol.14, No.6, June 1943.
23. Whitney, C.S.:
"Plastic Theory in Reinforced Concrete Design"
Transactions, ASCE Vol.107, 1942, pp.251-326.
24. Hognestad, E.:
"A Study of Combined Bending and Axial Load in R.C. Members"
Bulletin 339, Engineering Experiment Station, University of
Illinois, Urbana, November 1951.

25. Mattock, A.H., Kriz, L.B. and Hognestad, E.
"Rectangular Concrete Stress Distribution in Ultimate Strength Design"
Journal of the ACI, Vol.57, February 1961, pp.875-928.
26. Roy, H.E. and Sozen, M.A.:
"A Model to Simulate the Response of Concrete to Multi-Axial Loading"
Struct. Research Series No.268, Civil Eng. Studies, Univ. of Illinois, Urbana, June 1963.
27. Szulczynski, T. and Sozen, M.A.:
"Load-Deformation Characteristics of Reinforced Concrete Prisms with Rectilinear Transverse Reinforcement"
Struct. Research Series, No.224, Civil Eng. Studies, Univ. of Illinois, Urbana, September 1961.
28. Bresler, B. and Gilbert, P.H.:
"The Requirement for Reinforced Concrete Columns"
Journal of the ACI, Proc. Vol.58, No.5, November 1961.
29. Pfisher, J.F.:
"Influence of Ties on the Behaviour of Reinforced Concrete Columns"
Journal of the ACI, Proc., Vol.61, No.5, May 1964.
30. Mattock, A.H.:
"Rotation Capacity of Hinging Regions in R.C. Beams"
Proc. ASCE-ACI, International Symposium on Flexural Mechanics of Reinforced Concrete, Miami, Florida, November 1964, pp.143-182.
31. Corley, G.W.:
"Rotational Capacity of R.C. Beams"
Proc. ASCE, Journal of the Struct. Div. Vol.92, October 1966.
32. Chan, W.W.L:
"The Ultimate Strength and Deflection of Plastic Hinges in Reinforced Concrete Frameworks"
Mag. of Concrete Research, London, Vol.7, No.21, November 1955.
33. Pfrang, E.O., Siess, C.P. and Sozen, M.A.:
"Load-Moment-Curvature Characteristics of Reinforced Concrete Cross-Sections"
Journal of the ACI, July 1964.
34. Roy, H.E. and Sozen, M.A.:
"Ductility of Concrete"
Proc. ASCE-ACI International Symposium on Flexural Mechanics of Reinforced Concrete, Miami, Florida, 1964.
35. Shah, S.P. and Rangan, B.V.:
"Effects of Reinforcements on Ductility of Concrete"
ASCE Proc. Journal of the Struct. Div. ST6, June 1970.

36. Cohn, M.Z. and Ghosh, S.K.:
"The Flexural Ductility of Reinforced Concrete Sections"
University of Waterloo, Waterloo, Ontario, Canada, June 1972.
37. Jirsa, J.O.:
"Cast in Place Joints for Tall Buildings"
State of Art Report No.3, Tech. Committee 21, Proc. Intern.
Conference on Tall Buildings, Lehigh University of Bethlehem,
1973.
38. Nilsson, I.H.E. and Losberg, A.:
"Reinforced Concrete Corners and Joints Subjected to Bending
Moment"
ASCE Proc. Journal of the Struct. Div. ST6, June 1976.
39. Collins, M.P. and Lampert P.:
"Redistribution of Moments at Cracking - The Key to Simpler
Torsion Design"
Civil Eng. Publications, 71-21, Univ. of Toronto, Toronto,
Canada, February 1971.
40. Hsu, T.T.C. and Burton, K.T.:
"Design of R.C. Spandrel Beams"
Proc. ASCE, Journal of the Struct. Div. Vol.100, ST1, January
1974.
41. Saether, K. and Prachand, N.M.:
"Torsion in Spandrel Beams"
Journal of the ACI, January 1969.
42. Onsongo, W.M. and Collins, M.P.:
"Longitudinal Restrained Beams in Torsion"
Pub. No.72-07, May 1972, Univ. of Toronto, Dept. of Civil
Eng., Canada.
43. Phillai, S.U. and Bhargavan, K.K.:
"Bending-Moment-Torque Redistribution in Reinforced Concrete
Frames"
Proc. of a Conference on Tall Buildings, Kuala Lumpur, December
1974.
44. Hsu, T.T.C. and Hwang, C.:
"Torsional Limit Design of Spandrel Beams"
Journal of the ACI, February 1977.
45. "Building Code Requirements for Reinforced Concrete"
ACI-318-77, ACI, Detroit, 1977.
46. Mansur, M.A. and Rangan, B.V.:
"Torsion in Spandrel Beams"
ASCE Proc., Journal of the Struct. Div. ST7, July 1978,
pp.1061-1075.

47. Discussion by Hsu, T.T.C. and Hwang, C.:
 "Torsion in Spandrel Beams"
 ASCE Proc., Journal of the Struct. Div. ST9, September 1979,
 pp.1858-1862.
48. Beeby, A.W.:
 "Short Term Deflections of R.C. Members"
 C&Ca (London), Tech. Report, TRA 408, March 1968.
49. ACI Committee 435:
 "Deflection of R.C. Flexural Members"
 ACI Journal, Proc. Vol.63, No.6, June 1966, pp.637-673.
50. Comite Européen Du Béton:
 "Recommendations for an International Code of Practice for
 Reinforced Concrete"
 ACI and C&Ca, 1965, pp.156.
51. Warwaruck, J. et al:
 "Strength and Behaviour in Flexural of Pre-Stressed Concrete
 Beams"
 Civil Eng. Studies, Struct. Research Series 205, Univ. of
 Illinois, September 1960.
52. Teychenne, D.C.:
 "Discussion on: The Design of Concrete Mixes on the Basis of
 Flexural Strength"
 Proc. of a Symposium on Mix Design and Quality Control of
 Concrete, p.153 (London, C&Ca, 1954).
53. Hanson, N.W. and Kurvits, O.A.:
 "Instrumentation for Structural Testing"
 PCA, Development Bulletin, D-91, Chicago.
54. Kotsovos, M.D. and Newman, J.B.:
 "Behaviour of Concrete Under Multi-Axial Stresses"
 ACI Journal, Proc. Vol.74, No.9, 1977, pp.443-446.
55. Karl, M., Romstad, Michael, Taylor, A. and Herrmann, Leonard, R.:
 "Numerical Biaxial Characterization for Concrete"
 ASCE Proc., Journal of the Eng. Mechanics Div. EM5, October
 1974, pp.935-948.
56. Sahlin, S.:
 "Effect of Far-Advanced Compressive Strains of Concrete in
 R.C. Beams Submitted to Bending Moments"
 Library Translation No.65, C&Ca, London, 1955.
57. Smith, G.E. and Young, L.E.:
 "Ultimate Theory in Flexure by Exponential Function"
 ACI Journal, Proc. Vol.52, No.3, November 1955, pp.349-360.
58. Rüsck, H.:
 "Research Towards a General Theory for Structural Concrete:
 ACI Journal, Proc. Vol.57, July 1960, pp.1-28.

59. Levi, F.:
"The Work of the European Concrete Committee"
ACI Journal, Proc. Vol.57, No.9, March 1961, pp.1041-1070.
60. Kabaila, A.:
"Discussion of Equation for the Stress-Strain Curve of Concrete - by Desayi and Krishnan"
ACI Journal, Proc. Vol.61, September 1964, pp.1227-1229.
61. Desayi, P. and Krishnan, S.:
"Equation for the Stress-Strain Curve of Concrete"
ACI Journal, Proc. Vol.61, No.3, March 1964, pp.345-350.
62. Saenz, L.P.:
"Discussion of Equation for the Stress-Strain Curve of Concrete - By Desayi and Krishnan"
ACI Journal, Proc. Vol.61, No.9, September 1964, pp.1227-1235.
63. Tulin, L.G. and Gerstle, K.H.:
"Discussion of Equation for the Stress-Strain Curve of Concrete - by Desayi and Krishnan"
ACI Journal, Proc. Vol.61, No.9, September 1964, pp.1227-1235.
64. Popovics, S.:
"A Review of Stress-Strain Relationship for Concrete"
ACI Journal, Proc. Vol.67, March 1970, pp.243-248.
65. Richart, F.E. and Brown, R.L.:
"An Investigation of Reinforced Concrete Columns"
Bulletin No.267, Engg. Experiment Station - Univ. of Illinois, Urbana, June 1934.
66. King, J.W.H.:
"Further Notes of Reinforced Concrete Columns"
Structural Engineer, London, Vol.24, Nov.1946, pp.609-616.
67. Kent, D.C. and Park, R.:
"Flexural Members with Confined Concrete"
ASCE Proc., Journal of the Struct. Div. ST7, July 1971.
68. Soliman, M.T. and Yu, C.W.:
"The Flexural Stress-Strain Relationship of Concrete Confined by Rectangular Transverse Reinforcement"
Mag. of Concrete Research, Vol.19, December 1967.
69. Burns, N.H. and Siess, C.P.:
"Load-Deflection Characteristics of Beam-Column Connection in Reinforced Concrete"
Univ. of Illinois, Structural Research Series, No.234, January 1962.
70. Kupfer, H., Hilsdorf, H.K. and Rüsçh, H.:
"Behaviour of Concrete Under Biaxial Stresses"
ACI Journal, Proc. Vol.66, No.8, August 1969.

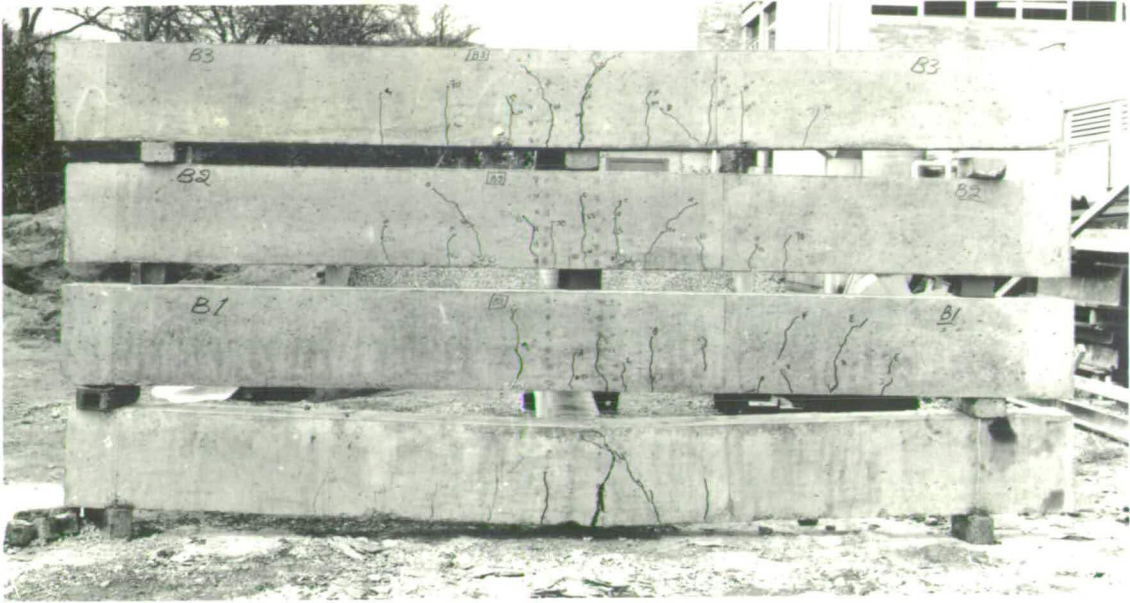
71. Nelissen, L.S.M.:
"Biaxial Testing of Normal Concrete"
Heron-Delft, Vol.18, No.1, 1972.
72. Liu, T.C.Y., Nelson, A.H. and Slate, F.O.:
"Biaxial Stress-Strain Relations for Concrete"
ASCE Proc., Journal of the Struct. Div. ST5, May 1972.
73. Evans, R.H. and Marathe, M.S.:
"Microcracking and Stress-Strain Curves for Concrete in Tension"
Material Construction, No.1, 1968, pp.61-64.
74. Welch, G.B.:
"Tensile Strains in Unreinforced Concrete Beams"
Mag. of Concrete Research, Vol.18, No.54, 1966.
75. Cowan, H.J.:
"The Strength of Plain and Reinforced Concrete Under the Action of Combined Stresses with Particular Reference to Combined Bending and Torsion of Rectangular Sections"
Mag. of Concrete Research, Vol.5, No.14, 1953.
76. Timoshenko, S. and Goodier, J.N.:
"Theory of Elasticity"
McGraw-Hill, New York, 1951.
77. Seely, F.B.:
"Advanced Mechanics of Materials"
Wiley and Sons, New York, 1932.
78. Turner, L. and Davies, V.C.:
"Plain and Reinforced Concrete in Torsion"
Proc. Inst. Civil Engrs. No.165, 1934.
79. Marshall, W.T.:
"The Torsional Resistance of Plastic Materials with Special Reference to Concrete"
Concrete Construction Engineering, 39, 4, 1944.
and
80. Nylander, H.:
"Torsion and Torsional Restraint of Concrete Structures"
Statens Kommitte för Buggnadsforsk, Stockholm, 1945.
81. Nadai, A.:
"Theory of Flow and Fracture of Solids"
Vol. II, McGraw-Hill, N.Y., 1951.
82. Timoshenko, S.:
"Strength of Materials"
Part II, Van Nostrand Co., In., 1956.
83. McHenry, D. and Karni, J.:
"Strength of Concrete Under Combined Tensile and Compressive Stress"
ACI Journal, Proc. Vol.54, April 1958.

84. Wright, P.J.F.:
 "The Effect of the Method of Test on the Flexural Strength of Concrete"
 Mag. of Concrete Research, No.11, October 1952.
85. Fairbairn, D.R.:
 "An Experimental and Analytical Investigation of the Behaviour of Reinforced Concrete Beams Subjected to Combined Bending and Torsion"
 Ph.D. Thesis, Univ. of Edinburgh, 1967.
86. Hsu, T.T.C.:
 "Torsion of Structural Concrete - Interaction Surface of Combined Torsion, Shear and Bending in Beams Without Stirrups"
 ACI Journal, Proc. Vol.65, No.1, January 1968.
87. Hsu, T.T.C.:
 "Ultimate Torque of Reinforced Rectangular Beams"
 ASCE Proc., Journal of the Struct. Div. Vol.94, No.ST2, February 1968.
88. Cowan, H.J.:
 "Design of Beams Subjected to Torsion, Related to the New Australian Code"
 ACI Journal Proc. Vol.31, No.7, January 1960.
89. Collins, M.P., Walsh, P.F., Archer, F.E. and Hall, A.
 "Ultimate Strength of Reinforced Concrete Beams Subjected to Combined Torsion and Bending"
 ACI, SP-18, Detroit, 1968, pp.379-402.
90. Pandit, G.S.:
 Discussion on "A New Approach to the Ultimate Strength of Concrete in Pure Torsion" by Navaratnarajah
 ACI Journal, Proc., August 1968.
91. Gesund, H. and Boston, L.A.:
 "Ultimate Strength in Combined Bending and Torsion of Concrete Beams Containing Only Longitudinal Reinforcement"
 ACI Journal, Proc. Vol.61, November 1964.
92. Youssef, M.A.R. and Bishara, A.G.:
 "Dowel Action in Concrete Beams Subjected to Torsion"
 ASCE Proc., Journal of the Struct. Div., No.ST6, June 1980.
93. "Report of the Committee on Ultimate Load Design of Concrete Structures"
 Proc. London, Vol.21, February 1962, pp.400-442.
94. Baker, A.L.L. and Amarakone, A.M.N.:
 "Inelastic Hyperstatical Frames - Analysis and Application of International Correlated Test"
 Hyperstatic Symposium, European Concrete Committee, 1964.

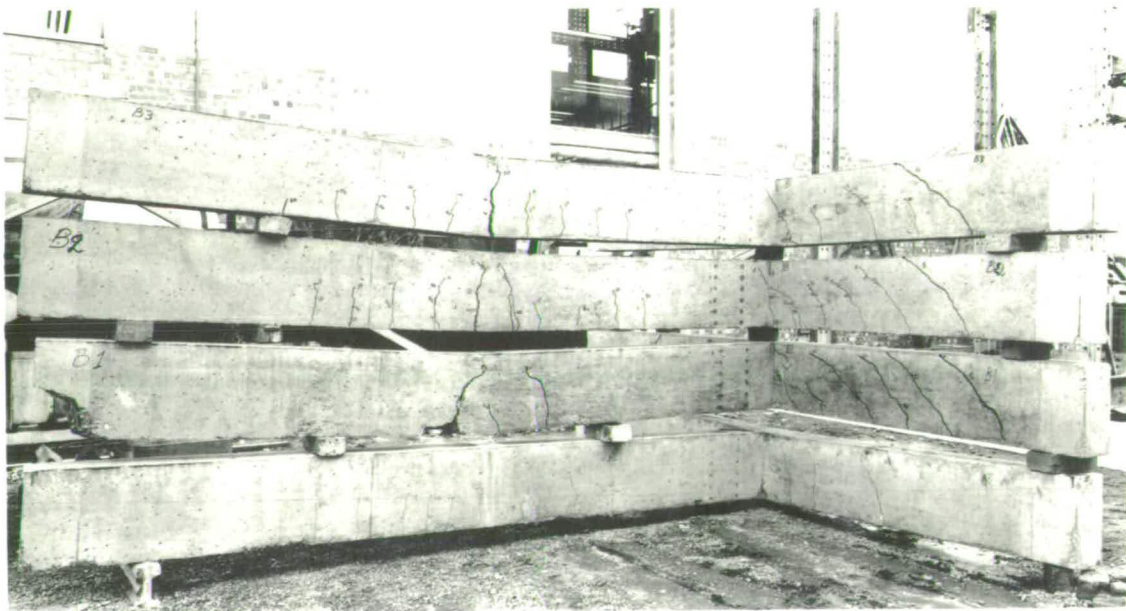
95. Baker, A.L.L.:
"The Ultimate Load Theory Applied to the Design of Reinforced and Pre-Stressed Concrete Frames"
Concrete Publications Limited, 1956.
96. Syamal, P.K., Mirza, M.S. and Ray, D.P.:
"Plain and Reinforced Concrete L-Beams Under Combined Flexure, Shear and Torsion"
ACI Journal, Proc. Vol.68, No.11, November 1971.
97. Bishara, A.G., Londot, L., Au, P. and Sastry, M.:
"Flexural Rotational Capacity of Spandrel Beams"
ASCE Proc., Journal of the Struct. Div., No.ST1, January 1979.

APPENDIX : PHOTOGRAPHS

This appendix contains photographs of the floor-spandrel beam specimens tested in this investigation as well as the testing rig and the equipments used for testing measurements. Crack propagation are marked with numbers. These numbers indicate the applied load in kN.

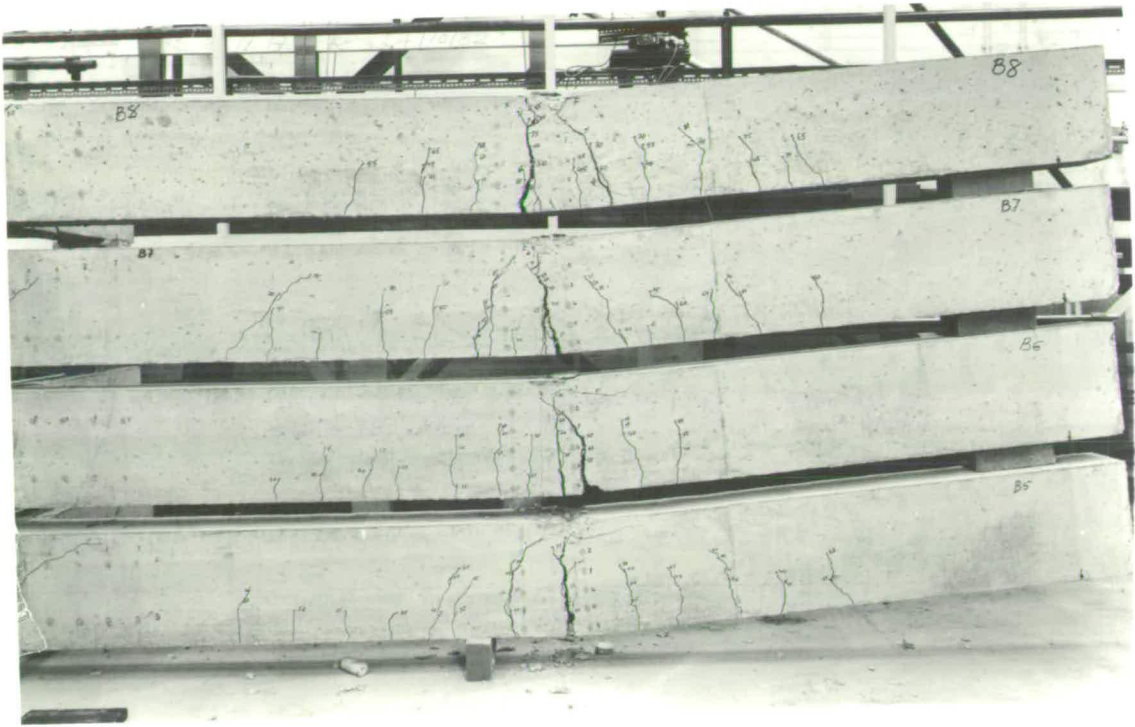


(a) Back View



(b) Side View

Plate 1A1 Specimens of Group GR1

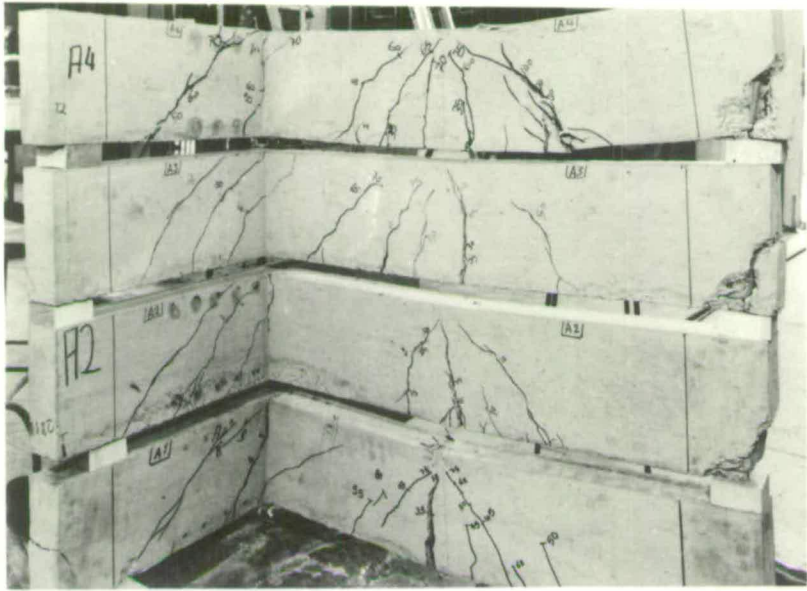


(a) Floor Beams

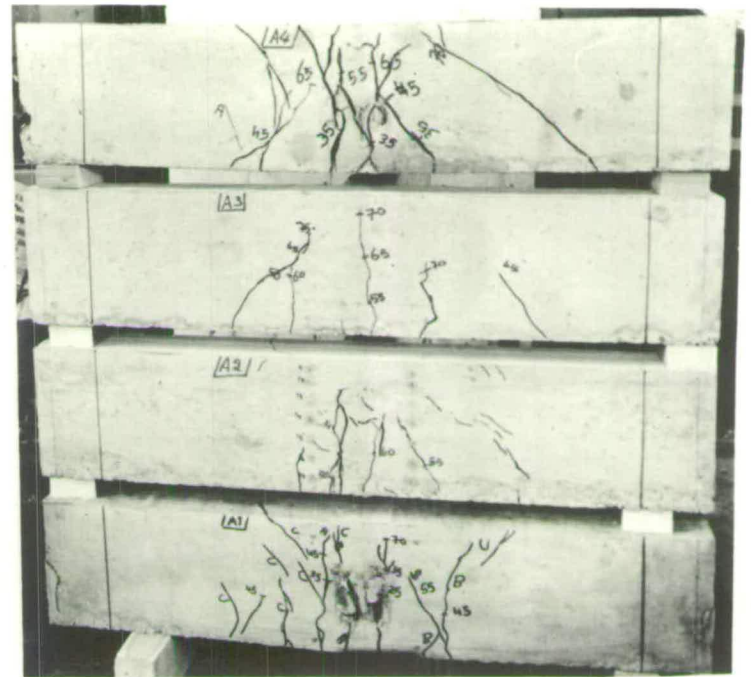
Plate A2 Specimens of Group GR2



(b) Spandrel Beams



(a) Side View



(b) Back View

Plate A3 Specimens of Group GR3

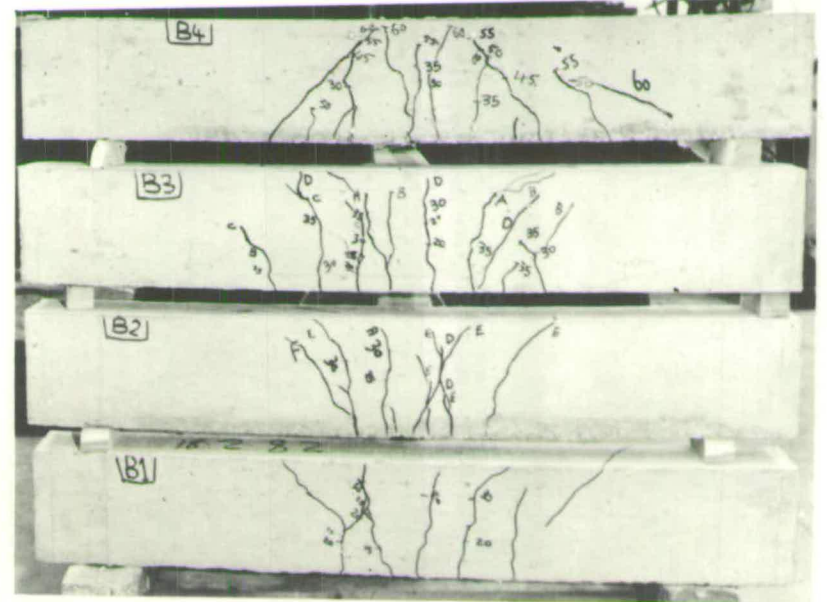
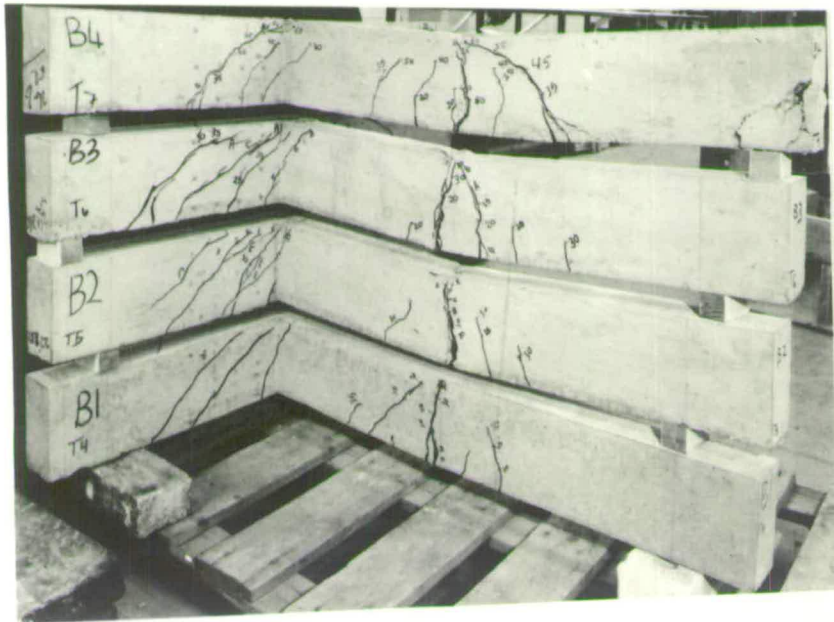


Plate A4 Specimens of Group GR4

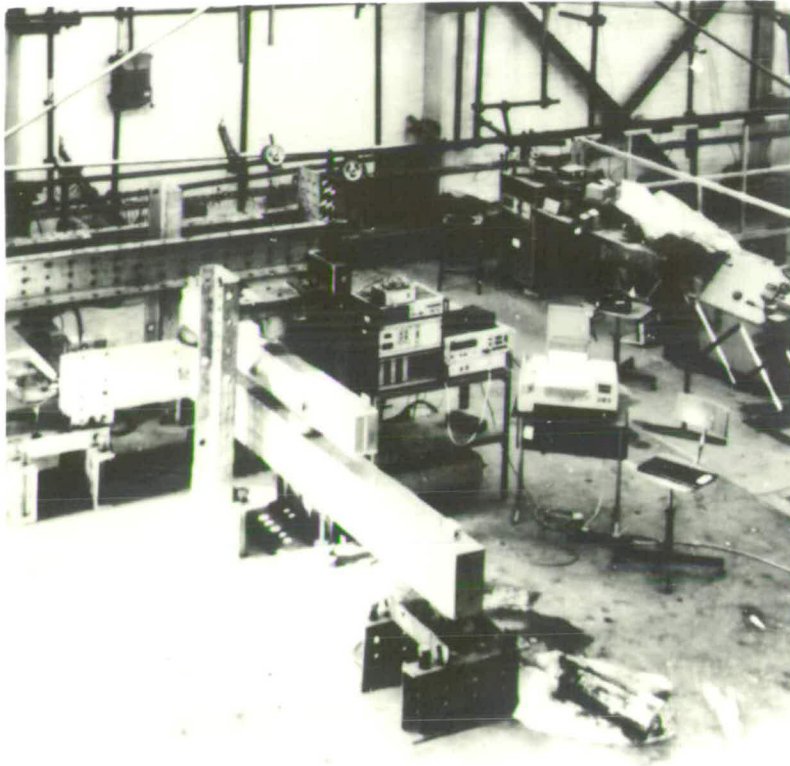


Plate A5 General View of Test Rig (GR1 and GR2)

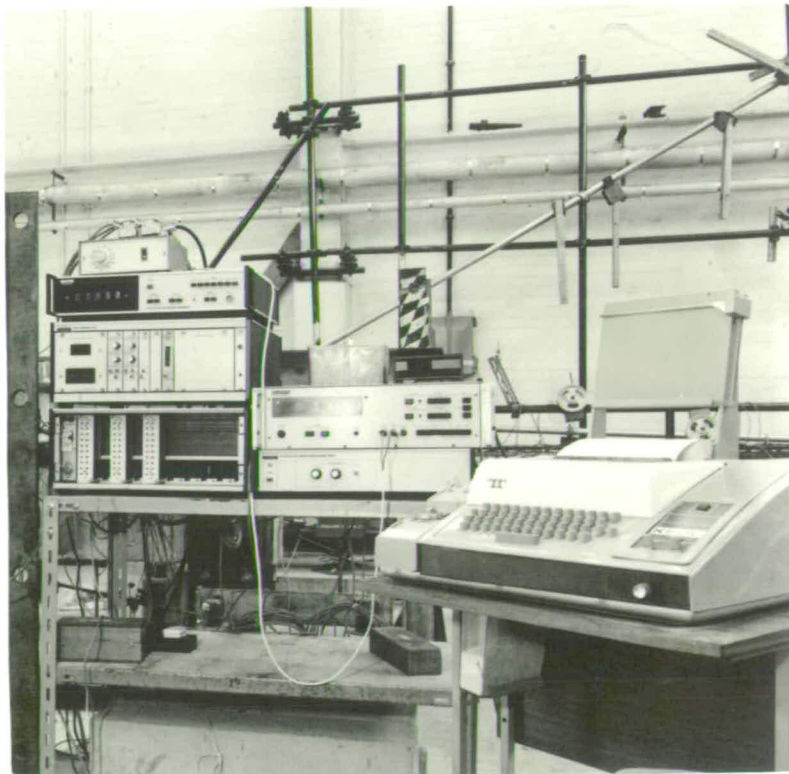


Plate A6 View of the Equipments Used for Test Measurement (GR1 and GR2)

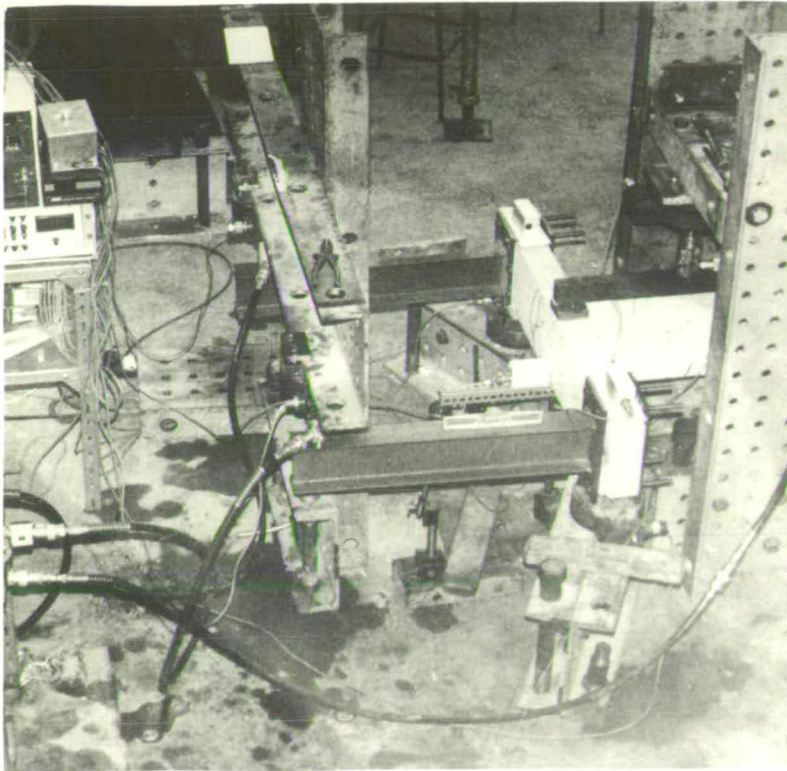


Plate A7 General View of the Test Rig (GR3, GR4 and GR5)

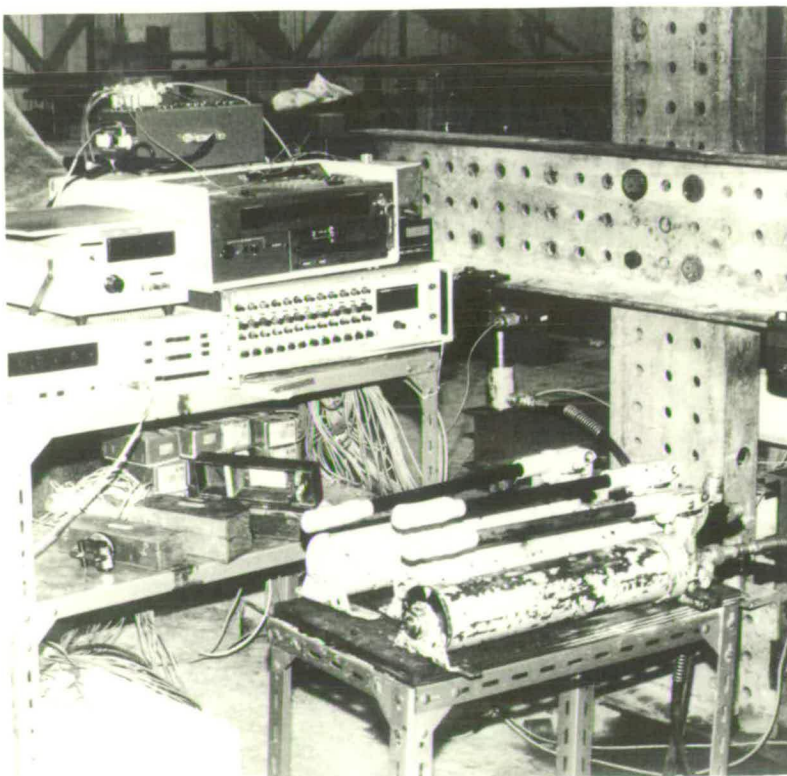


Plate A8 View of the Equipment Used for Test Measurement (GR3, GR4 and GR5)